MODELING AND ANALYSIS OF EXTRUSION PRESSURE AND DIE LIFE FOR COMPLEX ALUMINUM PROFILES

BY

Sayyad Zahid Qamar

A Dissertation Presented to the

DEANSHIP OF GRADUATE STUDIES

KING FAHD UNIVERSITY OF PETROLEUM & MINERALS

DHAHRAN, SAUDI ARABIA

In Partial Fulfillment of the
Requirements for the Degree of

DOCTOR OF PHILOSOPHY

In

MECHANICAL ENGINEERING

June 2004

KING FAHD UNIVERSITY OF PETROLEUM AND MINERALS
DHAHRAN 31261, SAUDI ARABIA

DEANSHIP OF GRADUATE STUDIES

This dissertation, written by **Mr. Sayyad Zahid Qamar** under the direction of his dissertation advisor and approved by his dissertation committee, has been presented to and accepted by the Dean of Graduate Studies, in partial fulfillment of the requirements for the degree of **DOCTOR OF PHILOSOPHY IN MECHANICAL ENGINEERING.**

Dissertation Committee

Prof. Dr. Anwar Khalil Sheikh
Dissertation Committee Chairman

Dr. A. F. M. Arif
Dissertation Committee Co-Chairman

Dr. Faleh A. Al-Sulaiman, **Member**

Dr. Zafarullah Khan, **Member**

Dr. Faleh A. Al-Sulaiman
Chairman, Mechanical Engineering

Dr. Yaqoub N. Al-Nasser, **Member**

Prof. Dr. Osama A. Jannadi
Dean, College of Graduate Studies

Dr. Zuhair Gasem, **Member**

Date: ٩/٤٢٥/٥/٢٥
13 July 2004

Dr. Anwarul Hamid, **Member**

ACKNOWLEDGEMENT

Acknowledgement is due to the King Fahd University of Petroleum & Minerals for supporting this research.

I wish to express my profound gratitude and appreciation for the continued guidance, help and support extended by the Chairman of my dissertation committee, Prof. Dr. Anwar Khalil Sheikh, and the Co-Chairman, Dr. A.F.M. Arif. I also wish to sincerely thank all the other committee members for their helpful comments and reviews from time to time.

My special thanks go out to the Chairman, Mechanical Engineering Department for help in all matters academic and administrative. I wish to extend my appreciation to all the staff members at the department for their assistance and cooperation, especially the engineers and technicians in the labs and workshops where I performed the numerous experiments. I would also like to acknowledge the support provided by the Aluminum Products Company Ltd, Dammam (ALUPCO) regarding hot extrusion experimentation and access to industrial data. Thanks to all my friends at KFUPM for their encouragement and support.

This work could not have been completed without the unreserved devotion and caring, the steadfast sacrifice and support, and the continued prayers and supplications of my family members. They deserve my heartfelt and most sincere thanks.

TABLE OF CONTENTS

LIST OF TABLES

LIST OF FIGURES

DISSERTATION ABSTRACT

Name: Sayyad Zahid Qamar
Title of Study: Modeling and Analysis of Extrusion Pressure and Die Life for Complex Aluminum Profiles
Major Field: Applied Materials and Manufacturing
Date of Degree: June 2004

Extrusion is a very popular manufacturing technique, especially as it can produce a large variety of complicated shapes with no requirement for downstream machining or finishing. Aluminum extrusion finds extensive application in the construction, automobile and aerospace industries. The thermo-mechanical process is complex in nature. In cold extrusion, heat is generated due to friction and deformation. In hot extrusion, high temperatures are involved since billet, die and deformation chamber are preheated. Irregularities in metal flow add to this complexity, especially in multi-cavity production and in extrusion of complex solid and hollow profiles. High pressures, elevated temperatures, and intricate section geometries also lead to repeated mechanical and thermal stresses in the die and affiliated tooling. Moreover, process aberrations and tooling related problems directly contribute to extrusion defects and affect product quality. A comprehensive investigation of the entire operation can thus be divided into three distinct yet inter-related areas: deformation process, dies and tooling, and product defects.

The focus of the current work is on two major issues of aluminum extrusion: extrusion process and extrusion tooling. Some aspects of extrusion product defects have also been explored to complete the picture. Study-A (Extrusion Process) is an investigation into the variation of extrusion pressure and how it is affected by different process parameters (Chapter-2), relationship between extrusion pressure and profile complexity (Chapter-3), and interaction of various extrusion parameters in the deformation chamber (Chapter-4). In Study-B (Extrusion Tooling), modes and mechanisms of die failure are examined (Chapter-5), a probabilistic study of die life is undertaken (Chapter-6), a complexity-based die-life prediction scheme has been formulated (Chapter-7), fracture toughness evaluation of extrusion die materials has been carried out in order to develop an optimum heat treatment strategy (Chapter-8), and a simulation scheme has been worked out to forecast die failures due to fracture and wear (Chapter-9). Study-C (Product Defects) covers defect morphology, defect mechanisms and causes, and remedial measures for various defects encountered in aluminum extrusion (Chapter-10), along with a brief statistical analysis of product defects in a typical large-size aluminum extrusion plant (Chapter-11).

ملخص رسالة الدكتوراة

الإسم: سيد زاهد قمر

عنوان الرسالة: نمذجة الضغط الطردي و عمر قوالب السكب لأشكال الألمنيوم المعقدة

التخصص الرئيسي: علوم المواد التطبيقية والتصنيع

تاريخ الشهادة: يونيو ٢٠٠٤

عملية الطرد من تقنيات التصنيع الشائعة و خصوصاً عند إنتاج الأشكال المعقدة و بدون الحاجة إلى المكننة الآلية. تركيز هذه الدراسة على موضوعين متعلقين بطرد الألمنيوم: عملية الطرد و أدوات الطرد. لقد تم استكشاف عدة أوجه لعيوب عملية الطرد لإكمال الدراسة. الدراسة – أ (عملية الطرد) يتم فيها دراسة التغير في الضغط الطردي و كيفية تأثره بعوامل عملية الطرد (الجزء الثاني), العلاقة بين ضغط الطرد و الشكل التعقيدي (الجزء الثالث), تفاعل عوامل الطرد المختلفة في غرفة التشكيل (الجزء الرابع). في الدراسة- ب (أدوات الطرد), يتم دراسة نماذج و آليات فشل القوالب (الجزء الخامس), و يتم إجراء دراسة إحتمالية على فشل القوالب (الجزء السادس), أوجد ت صيغة لمخطط توقعي لعمر القالب على أساس الشكل التعقيدي (الجزء السابع), لتطوير استراتيجية المعالجة الحرارية المثلى, تمت عملية تقويم لمتانة التهتك لمواد القوالب (الجزء الثامن), تم إجراء محاكاة مخططية لتوقع فشل القوالب بسبب التهتك و الإحتكاك (الجزء التاسع). الدراسة -ج (عيوب المنتج) تغطي العيوب التشكيلية, عيوب الآليات و المسببات, والإقتراحات التصحيحية لعيوب مختلفة بسبب عملية طرد الألمنيوم (الجزء العاشر), بالإضافة إلى تحليل إحصائي لعيوب المنتج في مصنع ألمنيوم طردي (الجزء الحادي عشر).

دكتوراة في الفلسفة

قسم الهندسة الميكانيكية

جامعة الملك فهد للبترول والمعادن

الظهران, المملكة العربية السعودية

CHAPTER 1
INTRODUCTION AND LITERATURE REVIEW

1.1 MOTIVATION AND SIGNIFICANCE

With the invention of the hydraulic extrusion press by S Bramah in 1810, extrusion has an industrial history of almost 200 years. As a result of spectacular technological advances in the later half of the twentieth century, the process has gained much wider application and economic significance. Because of its wide-ranging and abundant application in the automobile, aircraft, and especially the construction industry, aluminum has been called the *metal of the millennium*. As extrusion is the primary manufacturing process for aluminum alloys, the popularity and importance of extrusion has increased even more. The main reasons for this popularity are:

1. Large versatility
    (a) Light, strong, good manufacturability, good aesthetic appeal
    (b) Complex, refined, thin-walled, massive, strong, flexible shapes
2. Relatively modest prototyping costs due to less expensive dies compared to other metalforming operations
3. High benefit/cost ratio
    (a) No extra metal required for finishing operations
    (b) Easy formability
    (c) Savings in assembly
4. High strength and excellent corrosion resistance, requiring no maintenance and minimum protective coating.

Though aluminum extrusion has been an area of active investigation for quite long, complexity and diversity of the process have restricted researchers from exploring many critical issues in detail. Most of the research effort has been targeted only at specific aspects of the process. Hot extrusion being a difficult and costly commercial activity, laboratory-based research has been confined mostly to cold extrusion and lacks real-world experimentation. An overall and global research view is therefore needed, covering the entire set of operations, and presenting a comprehensive outlook of all aspects of the process.

The work presented here adopts an integrated approach, which aims to cover some critical aspects of metal extrusion. The work involves simultaneous studies of extrusion process, tooling, and product. Real-world data for hot and cold extrusion have been collected and experiments conducted both in the industry and in the laboratory. Statistical, probabilistic and numerical techniques are used for modeling and analysis of aluminum extrusion.

1.2 Extrusion Process and Tooling

Derived from the Latin word *extrudere* (meaning 'to thrust out'), the process of extrusion consists of forcing a workpiece (generally a round billet) through a *die* opening while it is supported in a *container*. As the workpiece is in compression, heavy deformations are possible, and the result is a wide range of extruded sections. Due to the nature of the process, downstream finishing operations are not required. Because of this large variety and commercial viability, extrusion is one of the most widely used bulk deformation processes, especially in the building construction sector.

1.2.1 Extrusion Plant Layout

The sequence of operations in commercial hot extrusion of aluminum is outlined schematically in Fig 1.1 [Arif et al. Sep 2001]. Round billets of aluminum alloy, of a diameter compatible with the size of the container in the extrusion press, are brought from the billet yard and stacked in front of the billet preheat ovens. Billets are then stage-wise heated to the desired temperature in a series of ovens. Next, they are sheared to the exact

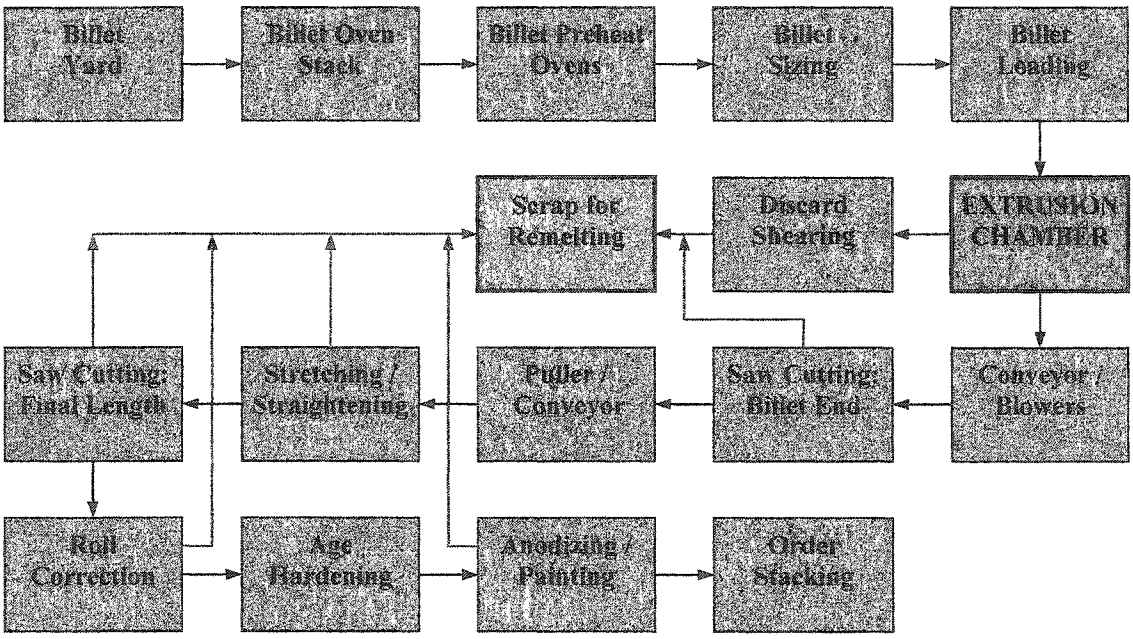

Figure 1.1 Sequence of operations in a typical commercial hot extrusion plant

billet size required for each profile, and subsequently loaded into the extrusion chamber. Meanwhile, properly preheated die set is loaded into the chamber, to be replaced by another one after the completion of one order. Once the ram pushes the entire billet through the die opening, a small remaining portion called the *discard* is sheared and sent to scrap. The extruded profile is gripped into the jaws of a puller, again discarding a small initial portion of the extrudate by saw cutting, and pulled over an air-cooled (through blowers) conveying system. This extruded length is stacked in the *stretching* area for straightening, and then cut to pieces of desired final length by a saw-cutting machine. The pieces may go to a *roll correction* station to remove any shape distortions, if required. Stacked batches go through an *age hardening* process in large furnaces, for prescribed temperature-time cycles, to improve the strength and hardness characteristics of the metal. They are then sent to painting and anodizing shops, as per customer requirements, and are later stacked for shipment.

1.2.2 Direct and Indirect Extrusion

Figure 1.2 [TALAT 2004, Kalpakjian 2003] illustrates the essential principle of the process, and the distinction between the two major working methods. In *direct* or *forward extrusion*, the die is located at one end of the container and the metal to be extruded is pushed towards it, hence moving relative to the container. In the case of *indirect* or *backward extrusion*, the die is placed on the end of the ram, which is bored out to allow passage of the extruded section, and moves through the container from one end, the opposite end being closed. It is generally more convenient for the container to travel and for the die (die assembly, nowadays) to be attached to a stationary ram. Direct extrusion is the more widely utilized method, due to the difficulties in ram construction for the indirect process.

1.2.3 Die and Related Tooling

The die and tooling arrangement employed in direct extrusion of soft and medium grade aluminum alloys is shown in Fig 1.3 [AEC 2004, Arif et al. Mar 2003]. Functions of various components shown are listed in Table 1.1. The feeder plate, die, and die backer

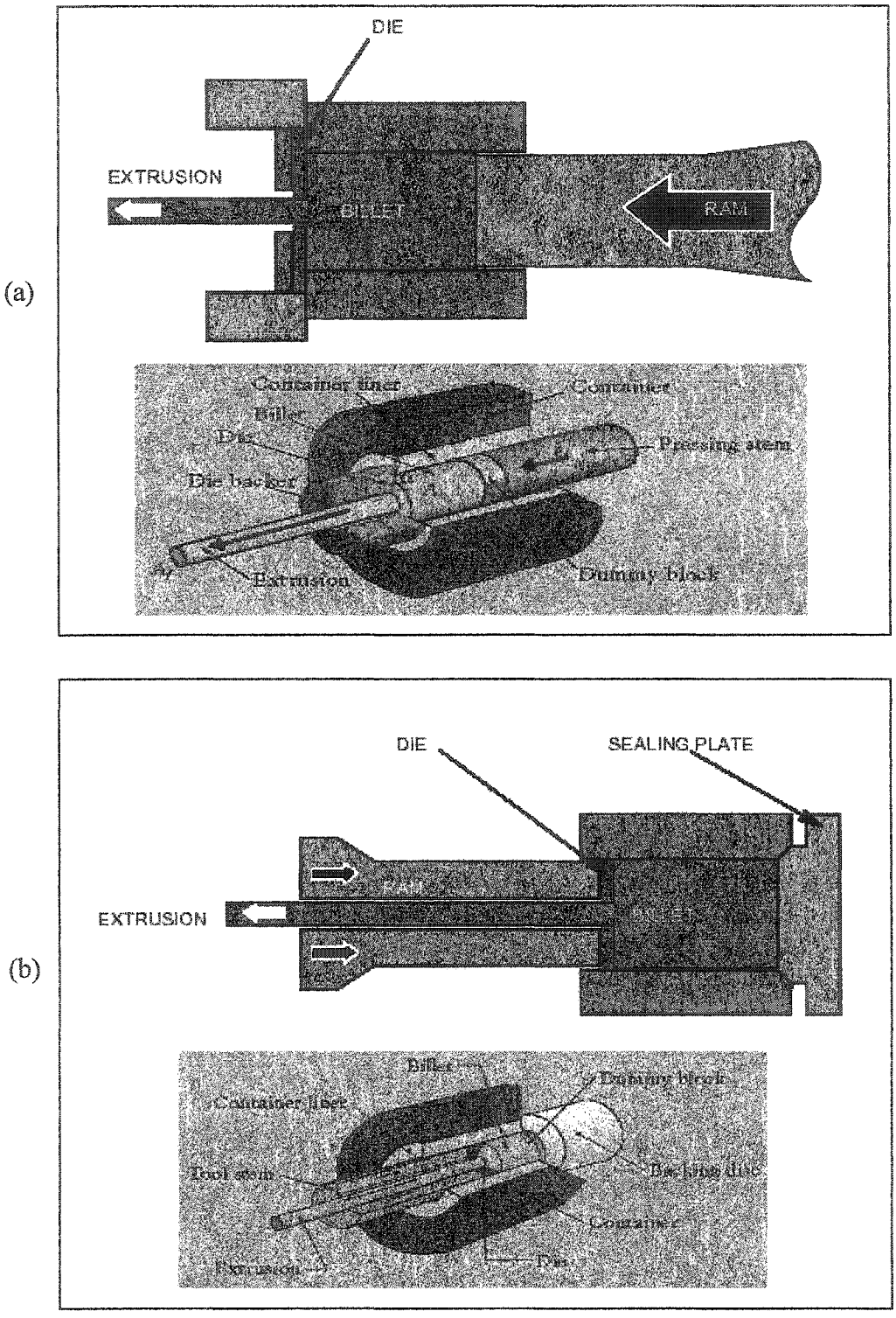

Figure 1.2 The two major working methods: direct extrusion (a), and indirect extrusion (b) [TALAT 2004, Kalpakjian 2003]

(a)

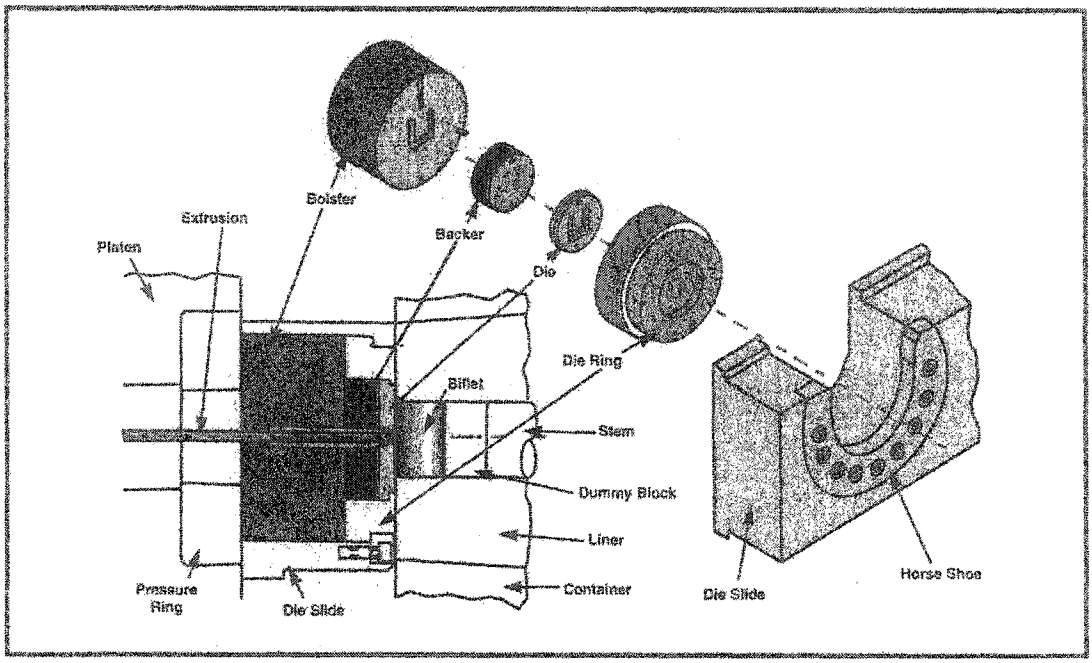

(b)

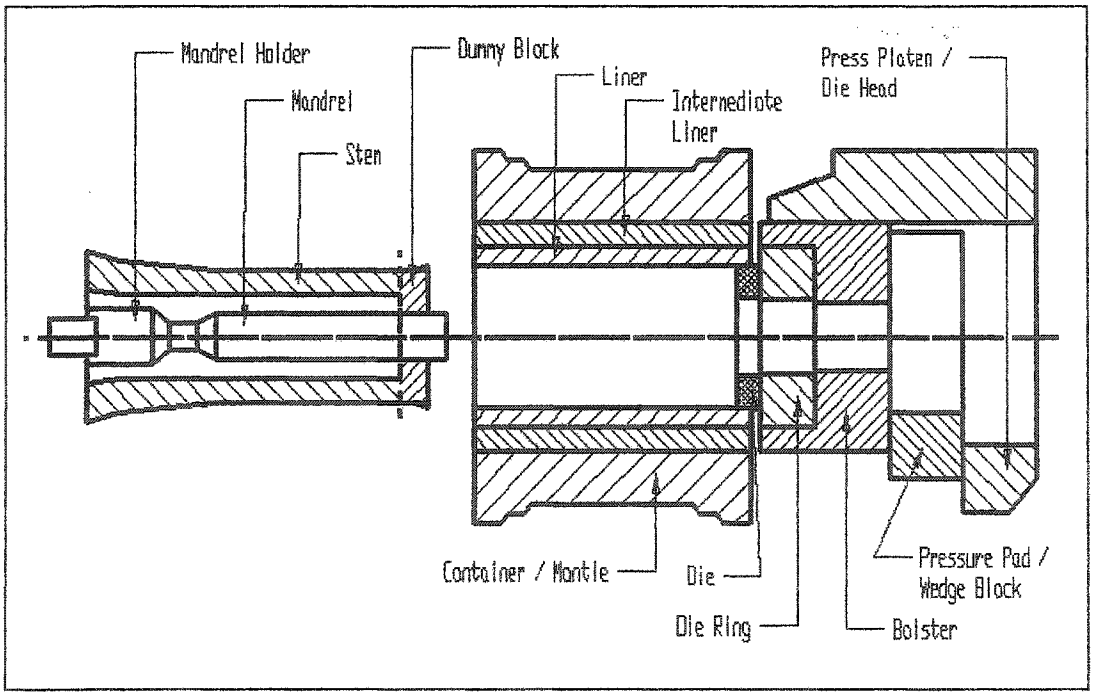

Figure 1.3 Exploded view (a) [AEC 2004] and 2D view (b) of typical die and tooling arrangement in direct hot aluminum extrusion

Table 1.1 Aluminum extrusion press and tooling

Component	Function
Die	Produces the extrusion shape/profile
Die Holder / Ring	Holds the die, the feeder plate and the die backer together
Die Backer	Provides support to the die against collapse or fracture
Bolster	Transfers the extrusion load from the die to the pressure ring/pad
Pressure Ring/Pad	Transfers the extrusion load from the bolster to the press platen and also guards against bolster deflection
Die Carrier/Slide	Holds together the complete die set (bolster and die ring)
Feeder Plate	Placed in front of the die, it balances the metal flow and allows continuous extrusion without breaks
Liner	Provides protection against thermal and mechanical stresses to the large and expensive container
Stem	It is fitted with the main ram to force the billet through the container
Dummy Pad	Floating or fitted in front of the stem, it protects the life of the costly stem

are fitted inside a die ring. This assembly, together with the bolster, rests on the die slide. A feeder plate is used in a solid die designed to produce a shape larger than the billet size, and may not be used in all applications. To produce a hollow shape, an additional component called a *mandrel* is used in conjunction with the die, as shown in Fig 1.4 (a) [TALAT 2004].

1.2.4 Solid, Hollow, and Semihollow Dies

Solid dies may have one or more openings (cavities), and produce "open" extrusions without any enclosed internal voids. The die cavity has the exact cross sectional profile of the extruded shape. Solid dies are used primarily for the production of bars, channels, angles, and a variety of custom shapes. Hollow dies turn out "closed" profiles; shapes that include an entirely enclosed internal void. The desired hollow shape requires two die components: a mandrel and a cap. Hollow dies are used to produce tubes, boxes, and many custom hollow shapes. Semihollow dies produce shapes that include partially enclosed voids with "open" profiles. The void has an area which is generally in a ratio of 3-to-1 larger than the tongue of the die. Semihollow dies are used most often in the production of atypical channels and other custom shapes. Types and components of the die used in the three cases are shown in Fig 1.4 (b) [AEC 2004].

Hollow sections of softer metals (such as the aluminum alloy Al-6063) are usually produced by the use of dies having a *welding chamber*. Some of the advantages of the welding chamber process are:

(a) Longer length can be extruded in hollow sections.

(b) Extrusion can be done for very thin hollow sections.

(c) Complicated hollow sections, finding wide application in the industry and the construction sector, can be more easily and reliably extruded than other methods.

The three common welding-chamber type dies are bridge, porthole, and spider dies. The first two types are shown in Fig 1.5 [TALAT 2004, AEC 2004]. Metal is forced to flow into separate ports and around the bridges, which support the mandrel. These separate streams of metal flowing through the ports come back into contact in a welding chamber that surrounds the mandrel. Metal finally exits the die through the space between the

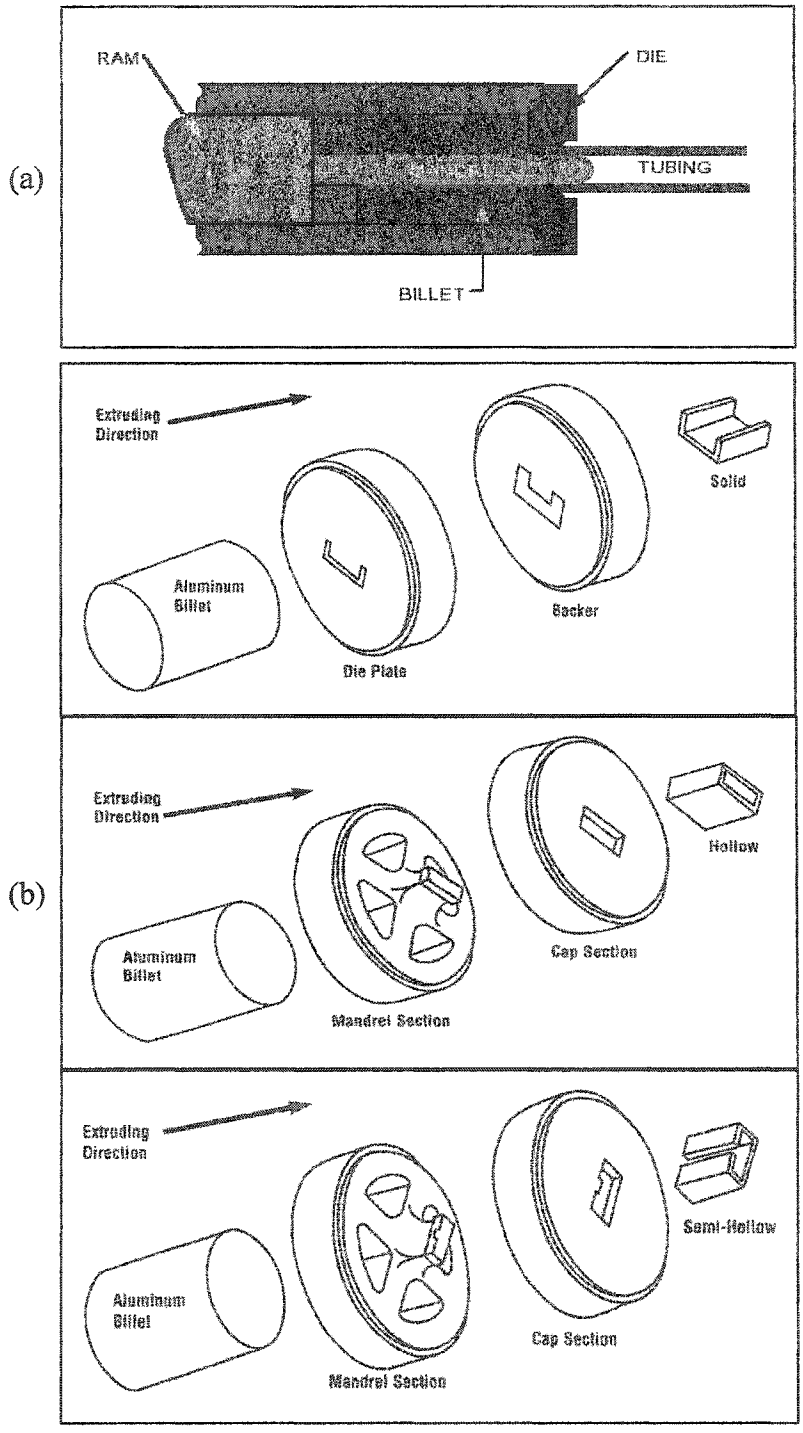

Figure 1.4 Schematic illustration of the use of a die and mandrel for the generation of a hollow shape (a) [TALAT 2004], and die components used to produce solid, hollow, and semihollow profiles (b) [AEC 2004]

(a)

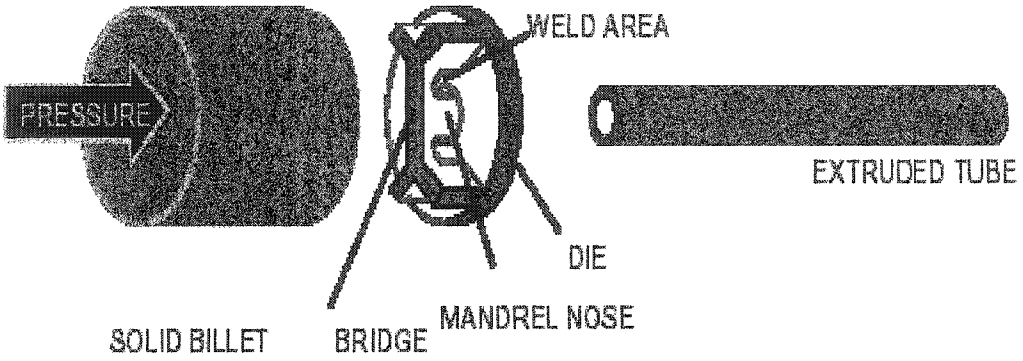

(b)

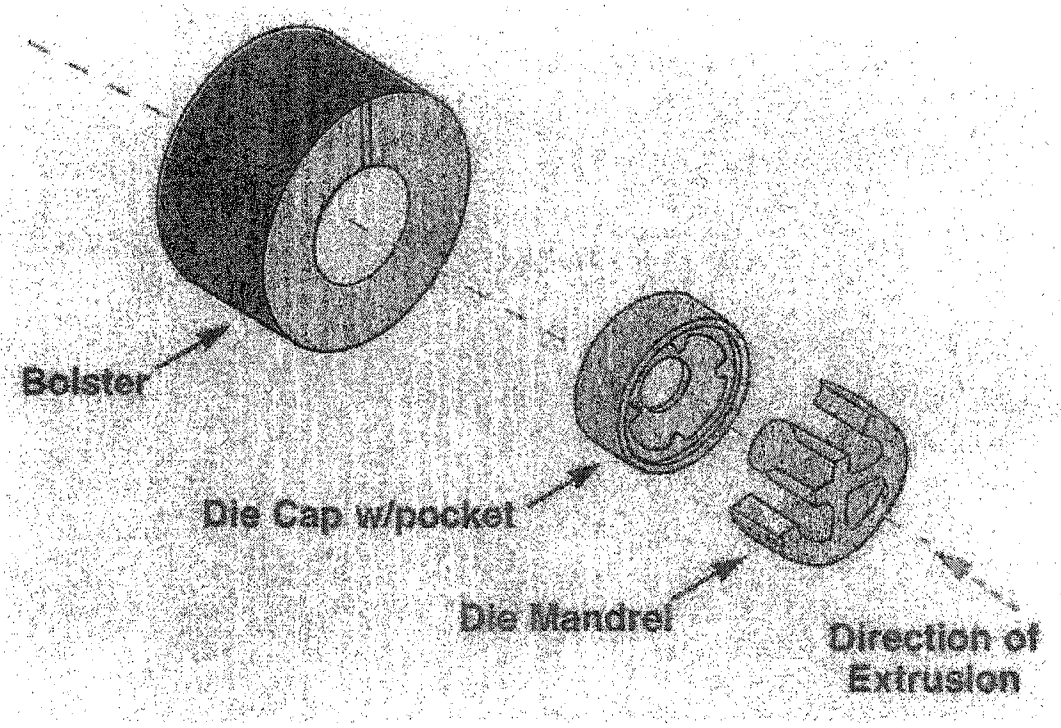

Figure 1.5 Two of the common die types used for extrusion of hollow shapes: bridge die (a) [TALAT 2004], and porthole die (b) [AEC 2004]

mandrel and the die cap in the form of a hollow profile. A high quality weld is formed because the metal streams are joined inside the die without any atmospheric contamination. Working principle of a porthole die is shown schematically in Fig 1.6 [Saha 2000].

1.2.5 Flat Face Dies

Flat-face dies (die cone semi-angle of 90°) are generally used in hot extrusion of aluminum alloys. Configuration of a solid flat-face die is shown schematically in Fig 1.7 [Saha 2000]. The most crucial part of any die is the *bearing* used to control the dimensions, profile, surface finish and speed of extrusion. It also plays a vital part in determining the die life. Friction at the die land (bearing surface) retards and thus controls the metal flow.

1.3 Extrusion Parameters

Prediction or calculation of important physical quantities of the process, such as extrusion force or pressure, depends upon various factors. These *process parameters* include material properties of the workpiece, billet geometry (billet diameter, billet length), die geometry (die or container diameter, bearing length, die cone half-angle, extrusion ratio, profile perimeter, profile area, minimum section thickness, circumscribing circle diameter, etc), ambient conditions (billet preheat temperature, die preheat temperature, container temperature, billet-container friction coefficient, billet-die friction coefficient), ram speed, strain rate, complexity of die shape, etc. Some of the more relevant of these *extrusion parameters* are listed in Table 1.2 and shown in Fig 1.8.

1.4 Metal Flow in Extrusion

Many aspects of product quality are directly affected by metal flow during extrusion, including material homogeneity, internal defects, surface finish, etc. *Metal flow pattern* thus becomes an important process consideration. Characteristic patterns in direct extrusion using a square die are shown in Fig 1.9 [Laue 1981]. Flow pattern *S* is found in

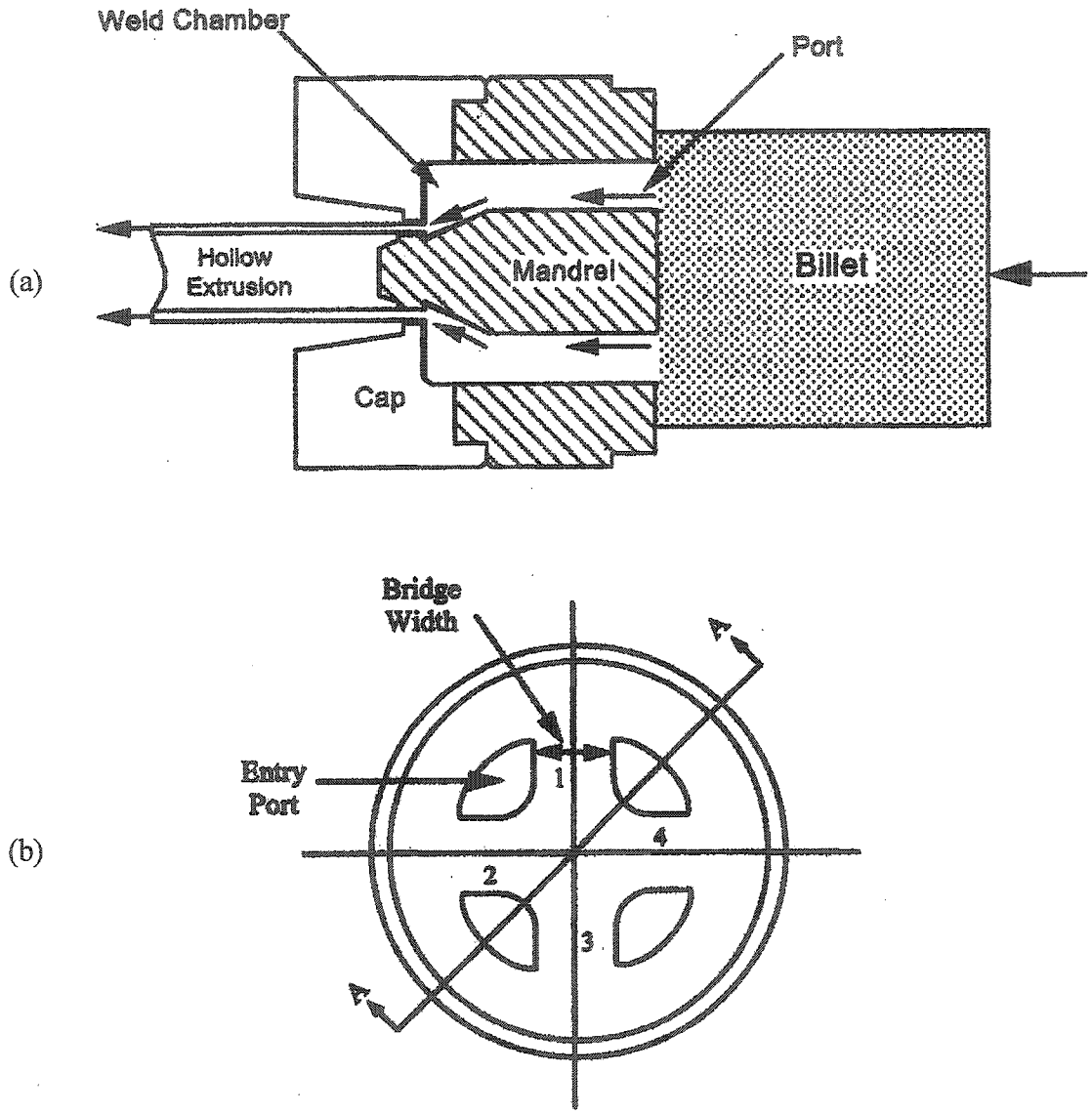

Figure 1.6 Working principle of a porthole welding-chamber die: Cross-sectional view showing metal flow into port streams and around mandrel (a); view of the die face where the billet enters the die set (b) [Saha 2000]

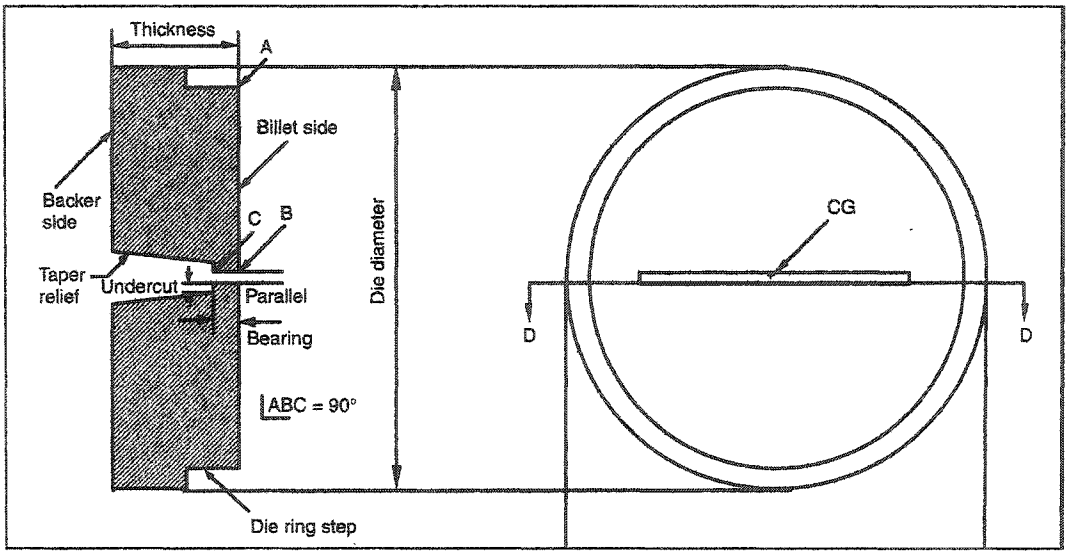

Figure 1.7 Configuration of a solid flat-face die [Saha 2000]

Table 1.2 Terminology used for description of die profiles and extrusion pressure

Symbol	Term	Description	Unit
P_s	Section or profile perimeter	Outside perimeter of die profile (mm)	mm
A_s	Section or profile area	Cross-sectional area of die profile (mm^2)	mm^2
P_0	Equivalent circle perimeter	Circumference of a solid circular profile having same cross-sectional area as profile under study	mm
W_s	Weight per unit length	Weight of extruded section per unit length	g/m
T_m	Minimum section or wall thickness	Minimum section thickness of die profile	mm
CCD	Circumscribing circle diameter	Diameter of circle that contains the die profile	mm
N	Number of cavities	Number of same profiles in a die	Number
R	Extrusion ratio	Ratio of billet or container area to extruded section area	mm^2
p_s	Section or extrusion pressure	Actual maximum extrusion pressure	MPa
p_0	Equivalent circle pressure	Maximum extrusion pressure for an equal-area circular profile, calculated analytically	MPa

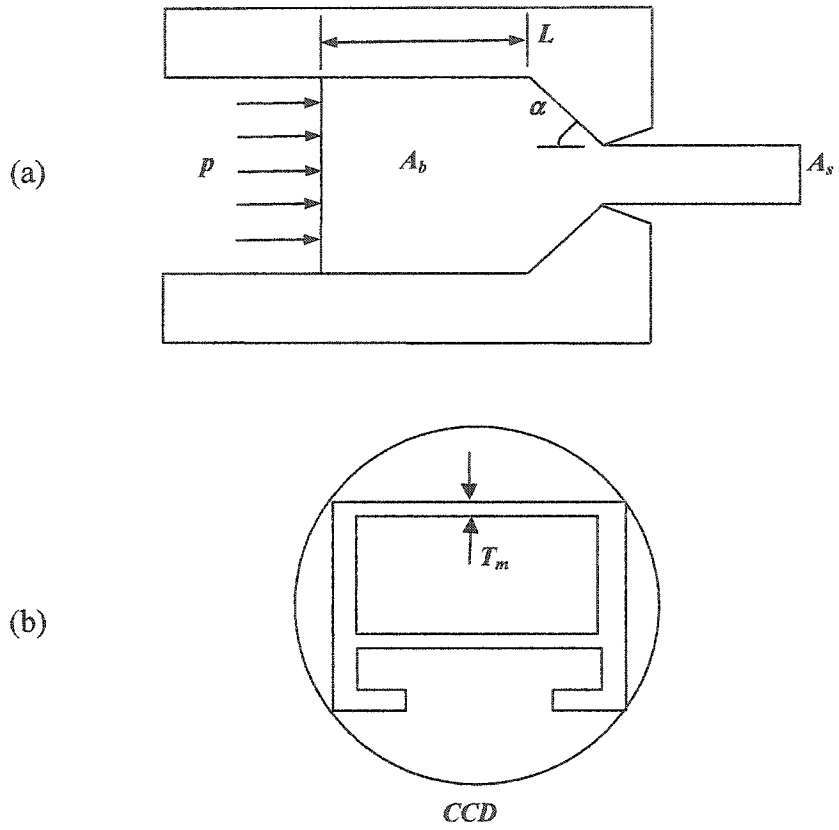

Figure 1.8 Schematic illustration of some of the basic variables (a) and profile parameters (b) in direct extrusion

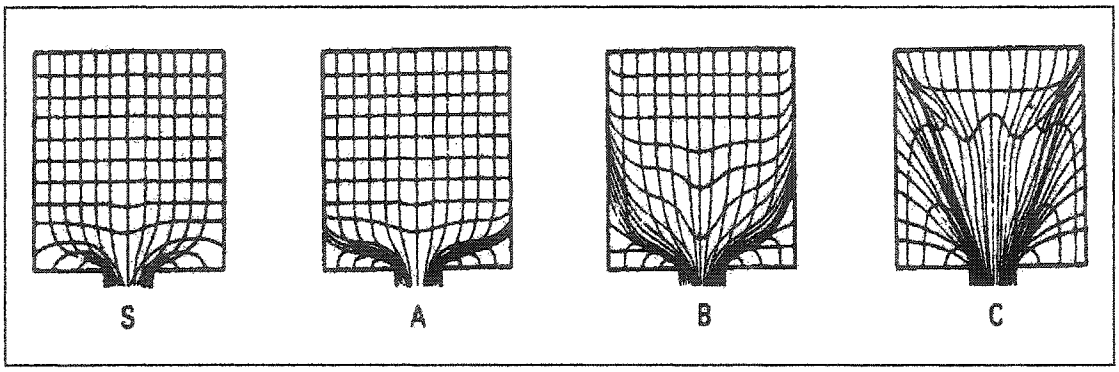

Figure 1.9 Different types of metal flow in direct extrusion [Laue 1981]

the absence of friction at the container and die interfaces, during extrusion of homogeneous materials. This can be achieved by using a very effective lubricant or in indirect extrusion. Flow pattern *A* is obtained in extrusion of homogeneous materials in the presence of friction at the die interface only. A *dead-metal zone* (*DMZ*) is formed, creating a funnel-shaped high-shear area near the die exit, as seen in Fig 1.10 [TALAT 2004]. When billet surfaces, together with their oxide layer and lubricant, are extruded through this high-shear zone, defects can occur. Flow pattern *B* is obtained in homogeneous materials when there is friction at both die and container interfaces. An extended dead metal zone is formed. If the container wall friction is considerably high (slowing down the flow of the billet), or if we have a material in which flow stress drops steeply with rising temperature, the high-shear zone extends quite farther back, giving flow pattern *C*. Such a flow pattern can also be observed with billets having inhomogeneous material properties or with nonuniform temperature distribution in the billet. In hot extrusion, where material near the container walls cools at a faster rate, material in the inner region can flow more easily. Such a flow pattern can lead to a defect called *pipe* or *extrusion defect*. The two most dominant factors influencing extrusion flow pattern are billet-container-die friction, and billet thermal gradients. Studies also show that for die cone semi-angles under 45°, the dead metal zone does not form.

1.5 Extrusion Pressure

Referring to Fig 1.8 (a), let us assume the simplest case of the extrusion of a solid round bar. The process is cold extrusion of a strain-hardening material (neglecting strain-rate sensitivity of material properties, etc). The *extrusion ratio* or the *reduction ratio* is defined as

$$R = \frac{A_b}{A_s}, \tag{1.1}$$

where A_b is the cross-sectional area of the billet, and A_s is the final cross-sectional area of the extruded section.

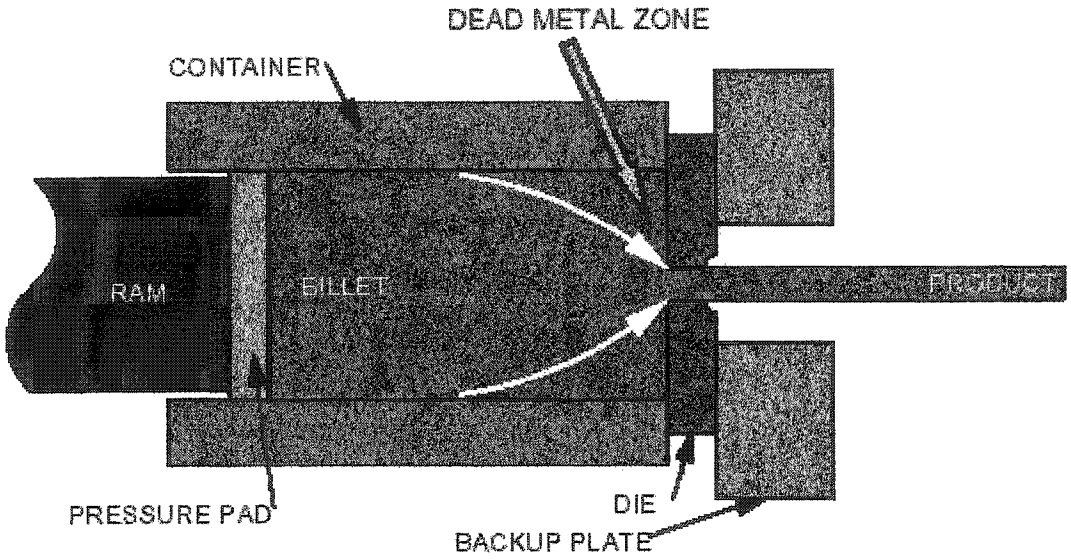

Figure 1.10 Metal flow and dead metal zone formation in extrusion [TALAT 2004]

The ram force in direct extrusion has to account for three contributing factors: *ideal work* (for energy dissipated in plastic work), *frictional work* (to overcome friction at billet-container and billet-die interfaces), and *redundant work* (caused by inhomogeneous deformation). For the case of ideal deformation, with no redundant work and no friction, the true strain in extrusion is

$$\varepsilon = \ln R . \tag{1.2}$$

Ram pressure for ideal deformation is then given by

$$p_i = \overline{Y}_f \varepsilon = \overline{Y}_f \ln R , \tag{1.3}$$

where $\overline{Y}_f$ is the average flow stress during deformation. *Flow stress*, defined as the instantaneous value of stress required for continued deformation of the material, is the yield strength of the metal as a function of true strain:

$$Y_f = K\varepsilon^n , \tag{1.4}$$

where K is the strength coefficient, and n is the strain-hardening exponent. In the case of hot working, flow stress is given by

$$Y_f = C\dot{\bar{\varepsilon}}^m , \tag{1.5}$$

where C is the strength coefficient, $\dot{\bar{\varepsilon}}$ is the average strain rate, and m is the strain rate sensitivity exponent.

In a metal forming situation such as extrusion, flow stress is a function of both the strain rate applied and the temperature. Temperature in hot extrusion depends on billet preheating and container temperature as well as on the heat generated due to friction and deformation. Determination of flow stress for a particular metal is thus a complicated task. Fortunately, some researchers have conducted extensive experimental work and have developed correlations for flow stress in terms of temperature-compensated strain rate, especially for commercial aluminum alloys [Sheppard 1999]. If we know the average temperature during extrusion, the average flow stress $\overline{Y}_f$ can be found from these correlations or charts for the given metal alloy.

Due to friction between the billet and the container walls, the additional ram force required to overcome friction is

$$\frac{p_f \pi D_b^{\,2}}{4} = \mu p_c \pi D_b L, \tag{1.6}$$

where p_f is the additional pressure required to overcome friction, $A_b = \pi D_b^2/4$ is the billet cross-sectional area, μ is the coefficient of friction at the billet-container interface, p_c is the pressure of the billet against the container wall, L is the billet length remaining to be extruded, and $\pi D_b L$ is the area of the billet-container interface.

Assuming the worst case where sticking occurs at the container wall, the friction stress equals the shear yield strength of the work material (τ_s):

$$\mu p_c \pi D_b L = \tau_s \pi D_b L. \tag{1.7}$$

Assuming that $\tau_s = \bar{Y}_f/2$, and combining (1.5) and (1.6), we get

$$p_f = \bar{Y}_f \frac{2L}{D_b}. \tag{1.8}$$

Total extrusion pressure is now the sum of ideal and friction pressures ($p = p_i + p_f$):

$$p = \bar{Y}_f\left(\varepsilon + \frac{2L}{D_b}\right) = \bar{Y}_f\left(\ln R \frac{2L}{D_b}\right). \tag{1.9}$$

It should be noted that extrusion pressure p goes down as the remaining billet length L decreases during the process. Typical plots of ram pressure as a function of ram stroke for direct and indirect extrusion are shown in Fig 1.11 [Groover 1999]. Obviously, the higher values in direct extrusion result from friction at the container wall. The shape of the initial pressure buildup at the beginning of the plot depends on the die angle, and is steeper for higher die angles. The pressure increase at the end of the stroke is related to butt (or discard) formation.

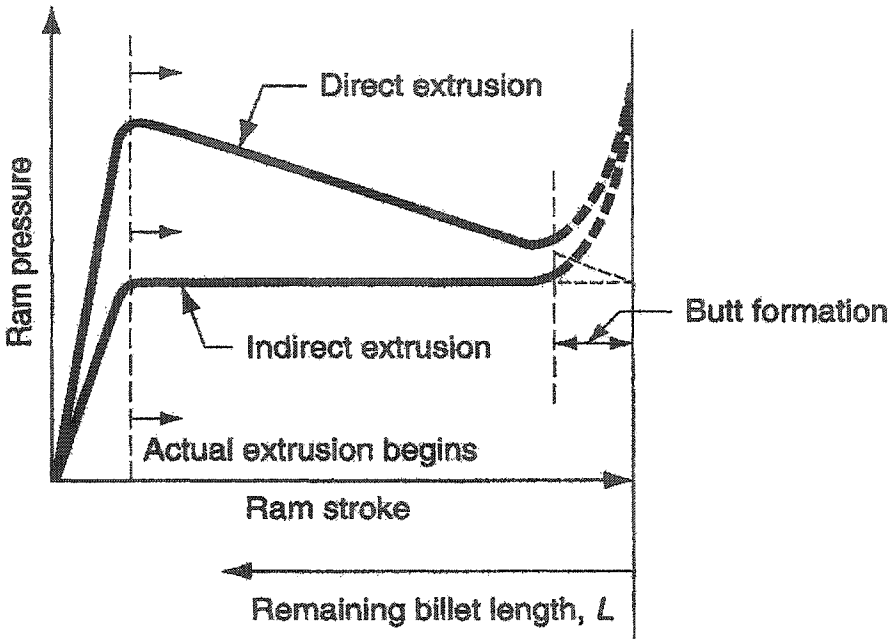

Figure 1.11 Variation of ram pressure with ram advance along the container [Groover 1999]

1.6 Solution Methodologies

There are several methods of analysis for theoretical determination of various quantities such as stresses, strains, forces and pressures in bulk deformation processes (forging, rolling, extrusion, etc).

1.6.1 Slab Method

The *slab*, *freebody*, or *equilibrium* method is one of the simpler methods of analyzing the stresses and loads in extrusion and other deformation processes. It requires the selection of an element of the workpiece and identification of all normal and frictional stresses acting on that element (similar to the *block-diagram* technique utilized in design problems). Homogenous deformation is assumed throughout the deformation zone. External friction effects are included but internal shear losses are neglected. Predicted extrusion pressures may thus be lower than those actually required, and represent *lower-bound* solutions.

Figure 1.12 [Mielnik 1991] shows a cylindrical rod being extruded through a conical die, and the free body equilibrium diagram of an element of the billet in the process of being reduced. For the free body to be in static equilibrium, the axial components of the forces in the x direction are those due to (a) longitudinal stress σ_x, (b) die pressure p (normal pressure at the die surface), and (c) frictional drag μp along the length of billet being extruded L. Coulomb coefficient of friction μ is assumed to be the same at the billet-container and billet-die interfaces. By combining the yield criterion with the equilibrium equation, integrating the resulting differential equation, and simplifying, we get

$$\frac{\sigma_x}{\bar{Y}_f} = \left(\frac{1+B}{B}\right)\left[1-\left(\frac{D_s}{D_b}\right)^{2B}\right]. \tag{1.10}$$

B is a constant depending upon various factors. As applied to hot forward extrusion through conical dies, the above equation can be converted after expansion and simplifications to

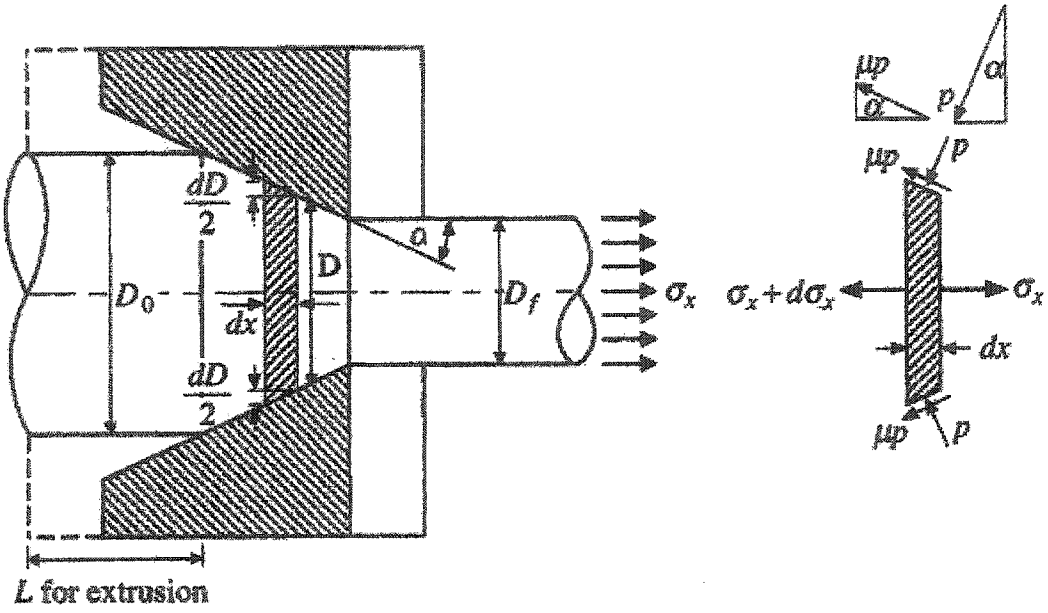

Figure 1.12 Slab method representation of a cylindrical billet being drawn through a conical die, and free body equilibrium diagram at an element in the reduction section [Mielnik 1991]

$$-\sigma_{x0} = \bar{Y}_f \ln\left(\frac{A_b}{A_s}\right) + \frac{\tau \ln(A_b / A_s)}{\sin\alpha\cos\alpha}, \tag{1.11}$$

where $-\sigma_{x0}$ is pressure at the extrusion end of the die, and $\ln(A_b/A_s) = 2\ln(D_b/D_s)$.

1.6.2 Upper-Bound Method

These solutions assume a velocity field that is kinematically acceptable, and predict extrusion forces that are expected to be above those actually required (as opposed to the lower-bound solution just presented, which gives a value equal to or less than the stress). The technique requires breaking down the overall deformation zone into a number of smaller ones within which velocity of a particle remains constant. Adjacent zones, however, may have different velocities. Because of the practical need to satisfy power requirements, this is a preferred theoretical approach as it yields a more conservative solution. As reported by Mielnik [1991], Avitzur derived the following equation for forward extrusion stress of round sections for a constant frictional shear factor with no forward tension:

$$\frac{\sigma_x}{\bar{Y}_f} = -2f(\alpha)\ln\frac{R_b}{R_s} - \frac{2}{\sqrt{3}}\left[\frac{\alpha}{\sin^2\alpha} - \cos\alpha + m(\cos\alpha)\ln\frac{R_b}{R_s} + m\frac{L}{R_L}\right]. \tag{1.12}$$

In this equation, σ_x is the back push stress, $\bar{Y}_f$ is the flow stress of a perfectly plastic metal under von Mises yield criterion, m is constant frictional shear factor, and $f(\alpha)$ is a complex function involving $\sin^2\alpha$ and $\cos\alpha$ terms, varying from 1 to 1.666 as α varies from 0° to 90°.

Derivation of this equation involves minimizing the energy or power consumed in (a) causing the reduction in cross-section, (b) shearing at the surfaces of tangential velocity discontinuity, and (c) overcoming friction at the interfaces. The first term represents the *internal energy of deformation*, which is slightly angle-dependent. The first two terms in the square brackets represent the *shear losses* at the spherical surfaces of the tangential velocity discontinuities. The third term in the brackets represents the *external friction loss*

over the conical die surface. The last term in the brackets represents the *external frictional loss* of the cylindrical surface of length L at die entry.

1.6.3 Slip-Line Field Method

The method of *slip-line analysis* is more readily applicable to plain-strain conditions. It is assumed that the billet is rigid, perfectly plastic, and isotropic. A family of straight (or curvilinear) lines known as *slip-line field* is constructed, intersecting orthogonally, corresponding to directions of maximum shear stress; Fig 1.13 [Lange 1985]. Requiring time consuming graphic representation, the method can yield solutions for stress and strain rate in a few cases of plane-strain problems.

With the advent of fast and efficient numerical procedures, methods such as upper-bound technique and slip-line analysis have lost most of their former importance.

1.6.4 Finite Element Method (FEM)

The *finite-element method* is a numerical technique and divides the elastic-plastic body into a number of elements that are interconnected at a finite number of nodal points [Kalpakjian 2003]. A set of simultaneous equations is then developed and solved for actual velocity and stress distributions. The technique can incorporate friction conditions at interfaces and actual material properties, and can be applied to relatively complex geometries. Accuracy is influenced by the number and shape of finite elements, the deformation increment, and the methods of calculation. A detailed picture of the actual stress and strain distributions throughout the workpiece or die can be obtained. The technique can also be used to predict microstructural changes in the material during hot working, temperature distribution throughout the workpiece, and the onset of defects without actual experiments. Inputs required may be stress-strain characteristics of the material as a function of strain rate and temperature, and heat transfer characteristics of the die and workpiece. Figure 1.14 is a sample of stress distribution obtained from FEM simulation of extrusion through a solid circular die.

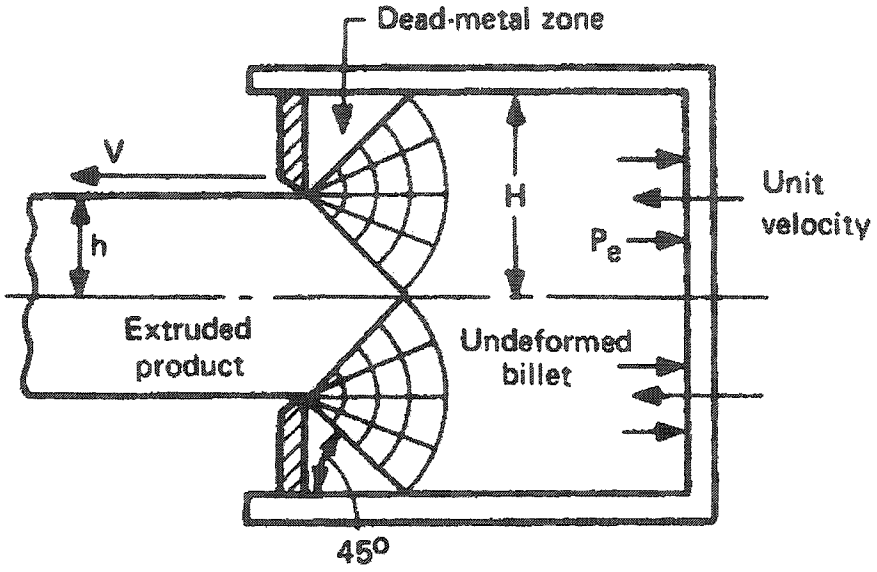

Figure 1.13 Slip-line field for backward extrusion with unlubricated die [Lange 1985]

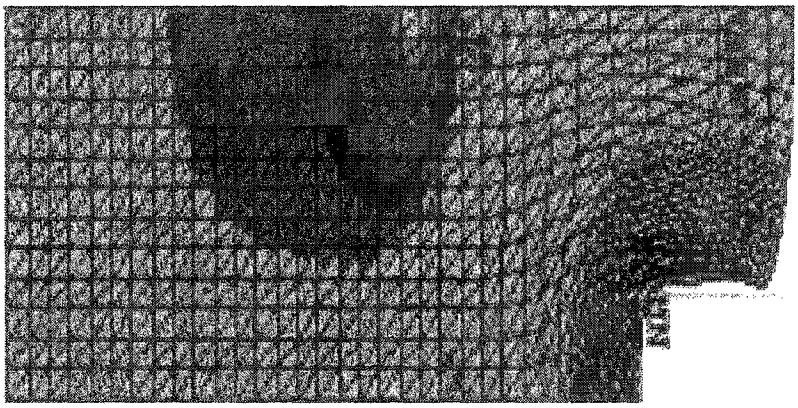

Figure 1.14 Finite element solution of stress distribution in extrusion of a symmetrical profile

1.6.5 Empirical and Statistical Methods

Empirical solutions, utilizing statistical and probabilistic techniques, are primarily based on experimental (laboratory) and production (industrial) data. An equation is generally fitted to the data by regression or some other curve-fitting procedure. The larger the data set, the higher the accuracy of the regressed model. Depending on the type of the problem, and the behavior and spread of the data set, different regression models can be more suitable (such as linear, quadratic, cubic, logarithmic, etc). Some problems are nonlinear in nature, but can be linearized through the use of appropriate strategies. Simple linear regression may be sufficient in some specific cases, but the majority of linearized actual problems require multiple linear regression. For instance, many physical quantities such as force, pressure, energy, and power have been found to naturally behave in an Arhenius manner. Assuming that extrusion pressure also follows this Arhenius trend, the pressure for a complex profile may be expressed as

$$p_c = p_0 X_1^{a1} X_2^{a2} \ldots X_N^{aN}, \tag{1.13}$$

where p_c is the pressure for a complex profile, p_0 is a reference pressure (for a circular solid profile, say), $(X_1, X_2, \ldots, X_N)$ are the geometrical parameters of the complex profile (such as billet diameter, billet area, profile perimeter, profile area, etc), and $(a_1, a_2, \ldots, a_N)$ are constants to be determined by regression performed on a reasonably large set of experimental data. The model may be linearized by taking natural log on both the sides:

$$\ln p_c = \ln p_0 + a_1 \ln X_1 + a_2 \ln X_2 + \ldots + a_N \ln X_N. \tag{1.14}$$

The power-law format of the problem expressed by equation (1.13) has been reduced to the linear form by equation (1.14). The problem can now be solved by performing multiple linear regression on available experimental data. As an illustration of an empirical solution, Figure 1.15 gives two types of regression models fitted to a set of experimental extrusion data. Cold extrusion (at room temperature) is performed inhouse on a lead billet, and variation of extrusion force is recorded as the ram advances along the container. Linear curve fitting will yield a rather poor model of the process, while a cubic polynomial fit will yield a much more accurate regression model.

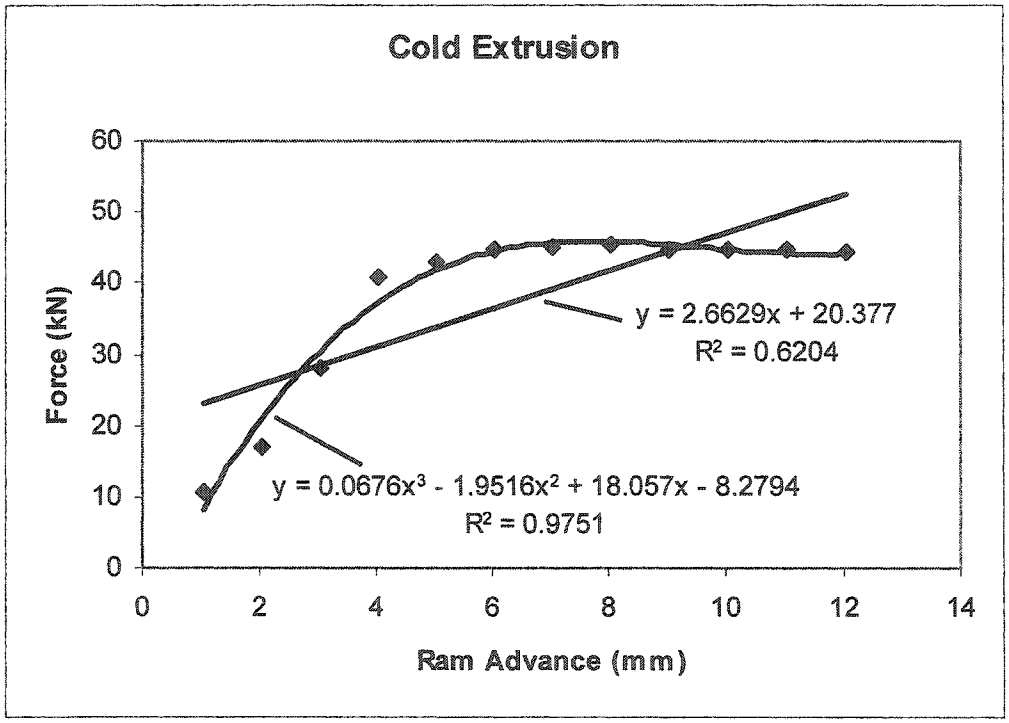

Figure 1.15 Linear and cubic (polynomial) regression models fitted to data from a cold extrusion experiment performed inhouse on lead

1.7 Shape Complexity

Equation (1.9) given above for extrusion pressure is valid for the simple case when both the billet and the die have a solid circular cross section, and when only billet-container friction has been taken into account, billet-die friction being neglected. What if the extrusion profile is a complex one? As the word *shape complexity* implies, complexity is a measure of how complicated the *geometry* or *shape* or *form* of an extrusion die is. The simplest shape is a solid circular section. Even a solid square or rectangular profile is more complicated because it has four corners or sharp bends that act as stress raisers. In general, a hollow shape has a higher complexity than a solid one, since hollows cannot be extruded without the inclusion of an additional component in the die set called the mandrel. Semi-hollows are shapes that are not completely hollow, but still require a mandrel for extrusion. Figure 1.16 [Schey 2000] demonstrates how complexity progressively increases in solid, semi-hollow, and hollow die profiles.

When we say that one die is more *complex* than the other, it is intuitively implied that it will require a larger amount of extrusion force or pressure than that required for the simpler profile. That is why one fundamental definition of extrusion shape complexity is that it is the *ratio of the pressure required to extrude a complex profile as against the pressure required for a solid circular profile of equal area.* Based on this higher complexity-higher pressure premise, various definitions for shape complexity of extrusion dies have been proposed in published literature.

If the perimeter of a profile is larger than the perimeter of another profile of the same area, it would definitely involve more twists or turns. More shearing would thus be required in the deformation zone, adding to the complexity. This led to one of the earliest definitions of complexity index [Schey 2000] of an extrusion profile:

$$C_1 = P_s / A_s \tag{1.15}$$

A modified form of the above is

$$C_2 = P_s / W_s. \tag{1.16}$$

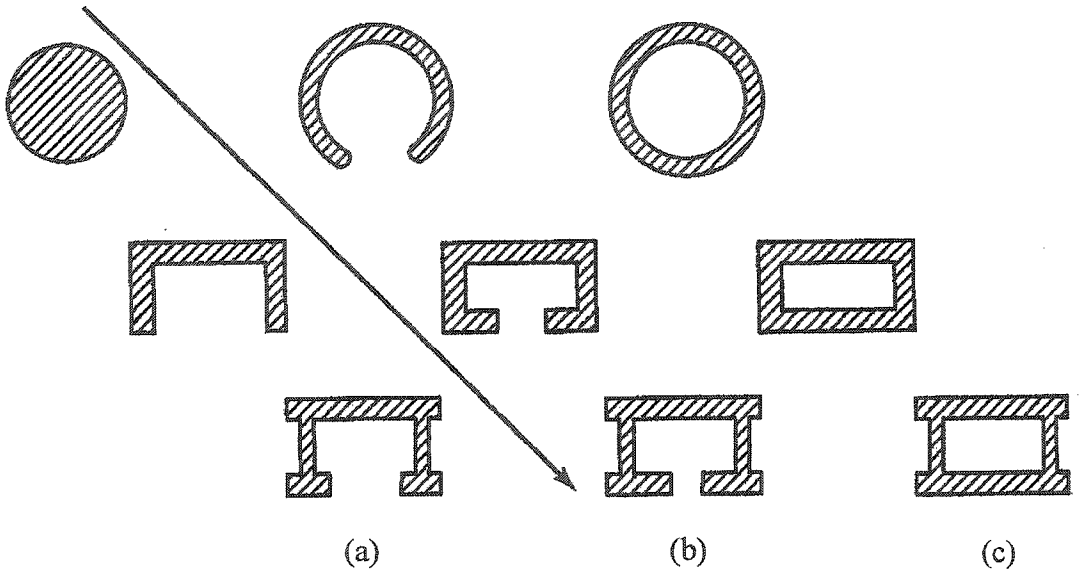

Figure 1.16 Increasing order of complexity in solid (a), semi-hollow (b), and hollow (c) extrusion die profiles [Schey 2000]

P_s, A_s, and W_s are the perimeter, area, and weight per unit length of the extruded section respectively.

It has been observed that larger diametral size of the die requires a higher pressure. Also, extrusion pressure increases as the wall thickness of the section is reduced. These observations resulted in another complexity index known as the *form factor* [Laue 1981]:

$$C_3 = CCD / T_m, \tag{1.17}$$

where CCD is the circumscribing circle diameter and T_m is the minimum wall thickness of the extruded section.

Going back to the fundamental definition (solid circular die being considered the least complex), Mielnik [1991] describes *shape factor* as a function of the perimeter ratio P_s/P_o:

$$C = f(P_s / P_0). \tag{1.18}$$

Perimeter of the extruded section under consideration is P_s, while that of a round shape of the same cross-sectional area is P_o. The definition based on such a shape factor, proposed by Altan et al. [1983] and reported by Groover [1999], is

$$C_4 = 0.98 + 0.02\left(\frac{P_s}{P_o}\right)^{2.25}. \tag{1.19}$$

The relationship may be invalid beyond a P_s/P_o range of 1.0 to 6.0 [Groover 1999].

1.8 Failure of Extrusion Dies

Some samples of die failures are shown in Fig 1.17. Any failure analysis of extrusion dies must include their manufacturing and service history. Improper die material composition, presence of quench cracks, scales or inclusions, can all lead to premature die failure. A large percentage of die failures can be traced back to heat treatment problems. Other sources can be distortion during heat treatment, machining or service, erosion and/or pitting, corrosion, etc [Laue 1981, ASM 1986]. Once a die is passed after some trial runs, the most common modes of in-service failure are *fatigue* (brittle failure through crack

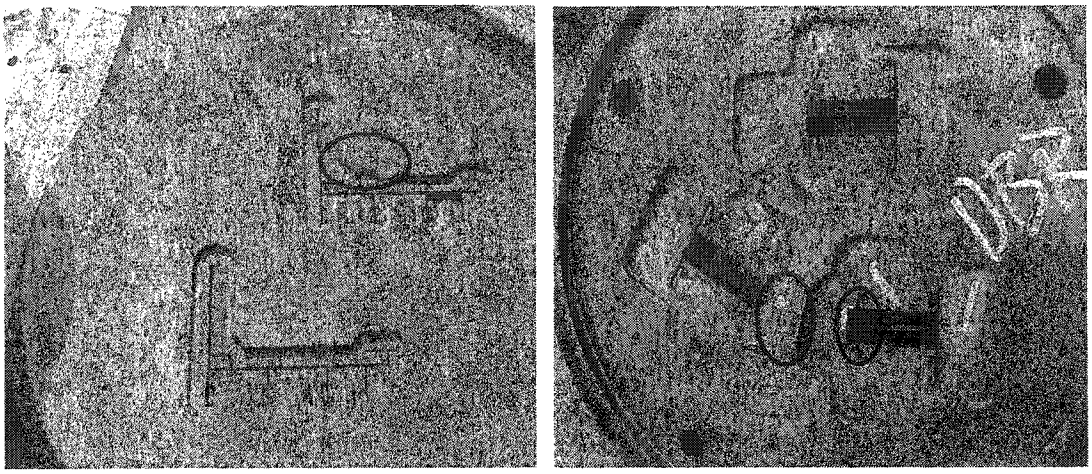

(a) (b)

(c)

Figure 1.17 Samples of actual die failures in hot aluminum extrusion: corner broken (a) and chip-off (b) are categories of fracture failure, while bearing washout is a wear-type failure.

propagation), *wear* (gradual wearing out of the bearing surface), and *deflection* (plastic deformation) [Arif et al. Mar 2003, Jul-Aug 2001].

Fracture failures are generally located at a section change, sharp corner, stamp marks, etc. Large cyclic stresses, combined with regions of high stress concentration in cavities, lead to crack growth. The high-strength hardened material (H-13 steel) generally results in fatigue failure.

Aluminum oxide (Al_2O_3) is formed on the billet surface during preheating, its hardness comparable to diamond. Similarly, iron oxides form on the die bearing surface. Friction between the billet and the die land results in accumulation of wear with use. The die cavity is often unevenly worn out due to higher wear at stress concentration locations.

Preheating of the billet and die, together with the heat of deformation and friction during extrusion, create high temperatures (400-470°C). High pressure is required to force the billet through the die opening; frictional forces at the container-billet and die-billet interfaces are the contributing factors. Unsymmetrical profiles can create force imbalance. Coupled with the high temperature, this can lead to plastic deformation (deflection) of the mandrel which, in turn, creates extra stresses on the bearing surface. Deflection or fracture of the mandrel or die is the usual outcome.

1.9 Product Defects

The quality of any extruded product is a function of various factors, such as chemical composition, geometric dimensions, appearance and regularity of microstructure, variation of mechanical properties over the extruded length and cross section, and surface finish. Extrusion defects may arise in extruded products from the starting material or billet, the deformation process itself, or from other post-processing corrective measures. An extruded profile may be deemed to be a reject (unacceptable product that does not fulfill standard or customer specifications), owing to any of the following reasons:

(i) Defective billets (slag/impurity inclusion, scales/flakes, internal cracks, undissolved oxides, etc)

(ii) Faulty or unsuitable tooling (billet and die preheat furnaces, dies/mandrels, dimensional correction equipment, etc)

(iii) Defects arising during extrusion (inappropriate extrusion pressure, chamber temperature, friction, ram speed, etc)

(iv) Flaws resulting in the course of post-extrusion operations (saw cutting, stretching/straightening, roll correction, age hardening, anodizing, painting, etc)

1.10 Review of Related Literature

1.10.1 Extrusion Pressure: Solution Methodologies

Axman and Mannl [1998] used a modified **slab method**, modifying the basic slab method by introducing a new 'relative density' variable, to study axisymmetric forward extrusion of metals. Material is modeled as rigid-plastic. Wifi et al. [1998] used an incremental slab method to obtain the shape of the optimum curved die profile for minimum extrusion load in hot forward rod extrusion. Results were verified using FEM. Lo [1996] presented a method for the design of streamlined extrusion dies based on some prescribed strain-rate variation, and applied it to plane-strain and axisymmetric extrusions. Use of the technique for hydrostatic extrusion was also briefly touched upon. Reddy et al. [1997, 1995] employed a combined upper bound-slab method for the determination of extrusion power for various die shapes, claiming significant saving of computational time over FEM, and similar accuracy.

Basavaraju [1998] presented **upper-bound** estimates for extrusion pressure in cold forward axisymmetric extrusion of lead for lubricated dies with varying extrusion ratios and die cone angles. Minimum upper-bound values under plane-strain conditions were deduced analytically for perfectly smooth and perfectly rough dies. Yang and Yeh [Feb 1997, Apr 1997] used the 'variational upper bound (VUB) method,' deriving an upper-bound solution through variational calculus, for plane strain tube extrusion. They claimed

a better solution than the conventional UB approach due to 'natural boundary conditions' (NBCs) for frictional effect. Sheppard et al. [1998] presented a review of methods to determine pressure requirement for both hollow and solid shape extrusions in the aluminum industry. Upper bound and finite element methods were reviewed as regards pressure prediction and flow characteristics. Monaghan [1998] presented an experimental upper-bound analysis, coupled with an elasto-plastic finite-element analysis of the plane-strain lateral extrusion process. Sahoo et al. [1998, 1999] analyzed extrusion of bars of channel section from square or rectangular billets through rough dies using the upper-bound method, utilizing it to determine the lowest upper-bound extrusion pressure for various area reductions. Ulysse and Johnson [1998] used analytical and semi-analytical expressions for a plane-strain upper-bound analysis of eccentric single-hole and unsymmetrical multi-hole extrusions. Analytical and numerical optimization was also attempted. Lin and Wang [1997] introduced an improvement of the upper-bound elemental technique (UBET) for complex geometries, especially in forgings. Curve fitting property of FEM was utilized together with flexible tolerance method for constrained optimization. Kim et al. [1997] proposed a simple upper bound solution for final-stage extrusion load and average length of extruded products in square die extrusion of non-axisymmetric bars from round billets. Regular polygonal-shaped, trochoidal gear-shaped and rectangular-shaped bars were investigated. Profile function was used for various shapes.

Reddy et al. [1995, 1997] employed a combined **upper bound-slab method** for the determination of extrusion power for various die shapes, claiming significant saving of computational time over FEM, while having similar accuracy. Reddy, Dixit and Lal [1997] discussed a comprehensive finite element model for temperature distribution of the workpiece or tooling in hot and warm extrusion. A combined thermo-mechanical finite-element method (TMFEM) and combined upper bound/finite element method (UBFEM) were used for extrusion power and temperature distribution prediction. UBFEM, claimed to be significantly faster, was used to obtain optimal die profile. Sahoo

et al. [1998, 1999] developed an upper bound solution for steady state extrusion of asymmetric polygonal section bars through rough square dies.

Chitkara and Butt [1999] presented a numerical method for construction of axisymmetric **slip-line fields** and their associated velocity fields for some cases of forward tube extrusion through smooth, rigid conical and cosine dies, and over a smooth rigid conical mandrel. Chitkara and Butt [1997] earlier used a similar slip-line field method for combined rod and tube extrusion and for axisymmetric tube extrusion through smooth and rough flat-faced circular dies. Wang [1998] established a new procedure for viscoplasticity method through a numerical approach. First, finite flow-line regions were produced by the least-square method, and then velocity and strain-rate fields were obtained. Slip-line field lines were drawn for plane-strain extrusion through a cosine-curved die. Yang and Yeh [Feb 1997, Apr 1997] discussed the centered-fan slip-line field solution of plane-strain extrusion problems in comparison with variational upper-bound method analysis.

Zuyan and Zhongjin [1999] described a method in which load-displacement curves during equal-cross-section lateral extrusion were measured and calculated using the **finite element method**. Influences of various factors were analyzed. Lu and Lo [1999] presented an advanced model for design of streamlined plane-strain extrusion dies based on prescribed strain-rate variation. Workpieces had mechanical properties sensitive to strain-rate distribution. Accurate prediction of die shape was claimed, based on velocity field and die angularity. Influence of interfacial friction and ram velocity on die geometry was studied. The elasto-plastic finite element program was based on an updated Lagrangian formulation. Gadal and Wang [1999] pointed out inherent difficulties in simulation of metal forming processes with traditional Lagrangian and Eulerian formulations. A more general method, 'arbitrary Lagrangian-Eulerian' (ALE) was adopted for large deformation effects. Liu et al. [1999] analyzed equal cross section lateral extrusion (ECSLE) for ultra-fine grain materials. Structural change and properties were found to be strongly dependent on process stress-strain history. Stress distribution was simulated by FEM and influencing factors were discussed. Gouveia et al. [1999]

focused on large nonlinear finite element systems, using the combined Eulerian-Lagrangian formulation to study stress and strain fields in cold forward extrusion of rods. Lu et al. [1998] used FEM technique for analysis of continuous forming extrusion process (Conform**T**M, trademark owned by BWE International, Ashford, Kent, UK). The model predicts stress, strain, strain rate, temperature fields. Hsiang and Liao [1997] developed a numerical simulation model for forward hot extrusion of tube. A combination of upper bound and finite difference methods was employed for prediction of deformation behavior and forming load. Sheppard et al. [1998] investigated extrusion of aluminum alloy 6063 through bridge dies for hollow shapes based on FEM. Monaghan [1998] presented an experimental upper-bound analysis, coupled with an elasto-plastic finite-element analysis of the plane-strain lateral extrusion process. Reddy et al. [1995, 1997] discussed a comprehensive finite element model for workpiece and tooling temperature distribution in hot and warm extrusion. A combined thermo-mechanical finite-element method (TMFEM) and combined upper bound/finite element method (UBFEM) were used for extrusion power and temperature distribution prediction. UBFEM, claimed to be significantly faster, was used to obtain optimal die profile.

1.10.2 Die Shape

Elkholy [1997] developed an optimization scheme to achieve a better product, minimum power consumption and small frictional losses in hydrostatic extrusion through an analytical model, investigating the effects of various extrusion parameters including **die shape**. Chung and Hwang [1997] used a genetic algorithm coupled with finite element analysis to determine extrusion die shapes that are optimal with regard to various objective functions. Joun and Hwang [1998] formulated extrusion die design problem as an optimization problem, incorporating a 3D FEA model, for various cross-sections including polygons and T-sections. Wifi et al. [1998] used an incremental slab method to obtain the shape of the optimum curved die profile for minimum extrusion load in hot forward rod extrusion. They found that shape depends on extrusion ratio and Coulomb friction coefficient, and not on the extrusion velocity. Lee and Kwan [1997] proposed an upper-bound analysis of generally non-axisymmetric hollow shapes. They determined

extrusion load and average extruded height for internally elliptic-shaped tubes from rectangular-shaped billets, internally regular polygon-shaped tubes from similar billets, and internally trochoidal gear-shaped tubes from similar billets. Reddy et al. [1995, 1997] employed a combined upper bound-slab method for the determination of extrusion power for various die shapes (third and forth-order polynomial, cosine, elliptical, hyperbolic, conical, etc), claiming significant saving of computational time over FEM, while having similar accuracy. Lu and Lo [1999] introduced an advanced model for design of streamlined plane-strain extrusion dies based on prescribed strain-rate variation, highlighting accurate prediction of die shape based on velocity field and die angularity. Sahoo et al. [1998, 1999] used the spatial elementary rigid region (SERR) technique for analyzing extrusion of sections having re-entrant corners. Circular cross section of round billet was approximated by a regular polygon of equal area. Number of sides was increased progressively until convergence of extrusion pressure was achieved. Sheppard et al. [1998] investigated extrusion of aluminum alloy 6063 through bridge dies for hollow shapes. A new method of pressure requirement determination was presented besides assessment of shaped extrusion difficulties. Lo [1996] presented a method for the design of streamlined extrusion dies based on some prescribed strain-rate variation, and applied it to plane-strain and axisymmetric extrusions. Accurate prediction of die shape was claimed. Wang [1998] established a new procedure for viscoplasticity method through a numerical approach. Slip-line field lines were drawn for plane-strain extrusion through a cosine-curved die. Kim et al. [1997] proposed a simple upper bound solution for final-stage extrusion load and average length of extruded products in square die extrusion of non-axisymmetric bars from round billets. Regular polygonal-shaped, trochoidal gear-shaped and rectangular-shaped bars were investigated. Profile function was used for various shapes.

1.10.3 Die Failure and Die Life

Very little published work is available in the area of die failures, especially in the aluminum extrusion industry. Kortmann [2000] studied some causes that lead to failure of extrusion tooling, and suggested possible methods to avoid these failures. Thedja et al.

[1992] described and analyzed the progressive wear damage at the bearing surface during extrusion. Saha [1998] restricted his study of die land wear to aluminum extrusion dies. Some authors, such as Guobin et al. [1998] investigated failure modes and mechanisms of tool steels, based on laboratory experiments, but the data does not relate specifically to die failures, and especially not in the thermo-mechanical context of aluminum extrusions.

Domblesky [2001] looked into the causes of die failures occurring in cold heading operations through FEM analysis. Reduction in fatigue failure and improvement in die life was reported to be achieved by die redesign aimed at reducing stress levels in critical areas.

Pederson [2000] performed a numerical study of low cycle fatigue in forward extrusion dies. His inference was that accumulation of plastic strain in the critical region can be controlled through a pre-stressing system or by changing the geometry of the die insert. Ahn et al. [1997] presented some results on fatigue behavior of a typical axi-symmetric forward extrusion die. Their simulated fatigue crack propagated in a zigzag path along the radial direction, and they estimated the fatigue life of the die by using the computed crack growth rate. Sonsoz and Tekkaya (May 1996) and Tekkaya et al. [1995] presented an analytical investigation of the fatigue behavior of cold extrusion dies. Fatigue cracks and highest stress concentrations occurred at the inlet radius of die shoulders. Service life of the extrusion die was estimated from the crack growth rate.

Navinsek et al. [2001] explored physical vapor deposition (PVD) coatings and duplex treatment for improved die and tool design in pressure die casting, hot extrusion and hot forging. They concluded that an improvement in die life is not as critical in overall analysis as reproducibility of extrudate surface quality, increase in manufacturing reliability, and decrease in manufacturing interruption contributing to downtime. Jeong et al. [2001] explored the effects of surface treatments and lubricants on die life in warm forging. They reasoned that repeated warm operations reduce the surface hardness of the die, while the temperature increase causes thermal softening leading to plastic deformation. They performed various experiments by changing surface treatment, lubricant, initial billet temperature, and applied load to investigate the resulting amount of

thermal softening and heat transfer. Sheljaskow [2001] reported the development of an environmentally friendly tool lubricating system for optimal tool life in forward or backward extrusion. He concluded that the best combination is a graphite-based slug coating and an oil-graphite-free die lubricant. Schruff et al. [1998] asserted that lifetime of the tool in hot working operations such as pressure die casting and extrusion is influenced by tool design, steel quality and to a high degree by heat treatment. They reported the development of a new rating chart for correct evaluation of the quality of a hot-work tool steel through microscopic examinations. Iwama and Morimoto [1997] reported that die life of backward extrusion punch is reduced under conventional processing conditions due to heat cracks and softening of the surface layer. Their suggested solution was a dry lubrication adhesion layer that binds strongly to the die. Die temperature for appropriate adhesion was 200-300°C.

Zhong et al. [2000] developed a thermo-mechanical elasto-plastic FEM system (ANSYS based) to simulate various extrusion processes and die design parameters for deep extrusion of a thin-walled cup. Apart from other things, cause of failure at the die was also included in the analysis. Good agreement with experimental results was claimed. Geiger and Haensel [1993] used FEM simulation of tool loading and fatigue crack initiation in extrusion dies to suggest methods of tool optimization and tool life improvement. They also presented some considerations about tool life prediction.

Arif et al. [Mar 2003, Jul-Aug 2001] gave detailed descriptions of die failure mechanisms encountered in commercial aluminum extrusion, categorized them into failure modes such as fracture, wear and plastic deformation, and presented a statistical analysis of die failure modes and mechanisms based on actual industrial data.

1.10.4 Product Defects

It is rather difficult to find comprehensive and in-depth investigations of product defects in metal extrusion in published literature. Lotzenheiser [2001] described extrusion defects such as cross section defects, linear defects, and surface finish defects, and discussed their relationship with material specifications and chemistry, material homogenization, and operating practices. Ko and Kim [2000] tried to predict conditions that lead to central

burst defects in extrusion and wire drawing. Minoda et al. [2000] investigated the effect of iron content on surface defects such as pick-up in aluminum extrusion. Bryant et al. [1999] presented a classification of metallurgical defects in aluminum extrusion, together with an attempt at a cause-effect relationship. Berezhnoy et al. [1999] reviewed some extrusion defects (metal flow related) and suggested preventive measures through improved direct extrusion process control. Zhang et al. [1992] used numerical simulation to study extrusion defect phenomena such as formation and tear of dead metal zone, and formation and development of central cavity. Somewhat more detailed treatment of extrusion product defects can be found in Laue [1981], Sheppard [1999], and Alum Assoc [1993].

Arif et al. [Dec 2002] and Qamar et al. [Sep 2003] presented descriptions of various of product defects encountered in metal extrusion, categorized them into major classes, investigated their causes and suggested practical remedial measures, and statistically analyzed industrial data (covering 10 years) on product defects in aluminum extrusion.

1.10.5 Dead Metal Zone and Metal Flow in Extrusion

Misiolek and Kelly [1992] reported experiments on 6105 aluminum alloy billet through a 2-cavity solid round profile. In a later work [Misiolek and Kialka, 1996] they identified three zones of interest regarding metal flow: dead metal zone, intensive shear zone, and main deformation zone. They also concluded that the dead metal and shear zones are not the same at the beginning and end of the extrusion cycle. Kusiak et al. [1992] used a commercial finite element package FORGE-2 and their own rigid-plastic steady-state program to investigate dead metal zone formation in axisymmetric aluminum extrusion through different die shapes. They found that the angle of dead zone increases with increasing die angle and with decreasing coefficient of friction. They compared their observations with experimental results published earlier.

Misiolek [1996, 1997] stated that the final microstructure of extruded metal is a result of billet microstructure, history of metal deformation, and post-processing treatment. He used electron backscatter diffraction (EBSD) technique to perform crystallographic characterization of deformation zones and recrystallization zone at the billet-container

interface in aluminum extrusion. Van Geertruyden at al. [2002] reported results of EBSD analysis regarding preferred grain orientations or textures in extrusion of 6xxx series aluminum alloys. They concluded that grain textures depend upon metal flow, which in turn is influenced by the state of stress, temperature, strain, and strain rate during metal deformation.

Thackray et al. [2000] performed extrusion experiments on gridded billets of Al-5083 and Al-6061 to study the effect of friction, die temperature, container temperature and pad temperature on bulk metal flow. They took into account variations in friction factor and strain rate sensitivity with temperature. The commercial package FORGE2 was used for metal flow simulation, and very good agreement was found with experimental results. The model was then extended to investigate effect of tooling conditions and material properties on billet surface layer flow. Incorporation of billet surface layer into metal flow was found to be reduced by increasing die temperature, decreasing pad temperature, and increasing container temperature. Surface layer inclusion was also reduced by reducing billet-tooling friction and by decreasing material strain rate sensitivity. Heat transfer coefficient of the alloy interestingly had no effect.

Chanda et al. [2000] used the DEFORM code to carry out 3D FEM analysis on Al-6061 extrusion through three different die shapes. Modeling the material as visco-plastic, their metal flow simulations for a channel shaped die (unequal wall thickness) revealed velocity inhomogeneities across the extrudate, which can be reduced by adjustment of the die bearing length. They concluded that corners are the most vulnerable regions as they can lead to speed cracking and hot shortness. Their work is yet to be experimentally verified. Lof et al. [2000] used DiekA, an Arbitrary Lagrangian Eulerian (ALE) code developed in-house by Huetnik at al., to simulate metal flow in the bearing area. They found that geometry of the bearing determines the shape and, to a large extent, the exit velocity of the profile. As material deformations are very small and elastic effects are dominant inside the bearing channel, they used an elasto-viscoplastic material model. Simulations were used to investigate the influence of bearing parameters such as profile

thickness, friction coefficient, bearing length, and bearing angle. Validation through experiments on flat dies was encouraging.

Xie at al. [1995] analyzed the deformation behavior during extrusion of pipes (tubes) through a porthole die by employing an upper-bound approach (UBA). Their predictions about extrusion pressures were within 10% of experimental results, but their forecast of flow velocities and shape and size of the dead metal zone yielded significant discrepancies with the actual scenario. Gasiorczyk and Richert [2000] investigated metal flow in the welding chamber of two porthole dies used for hollow extrusion of Al-6063. Pressure, temperature, strain rate and gradual material filling were simulated by the use of FORGE3 software package. They concluded that improper metal flow creates an increasingly larger dead metal zone in the welding chamber, which does not participate in the formation of the required metal joint. This also generates friction of metal against metal, leading to deterioration of weld quality, and nonuniform metal outflow from the die.

Flitta and Sheppard [2000] used the commercial package FORGE3 for 3D simulation of Al-6063 extrusion through bridge dies to produce hollow shapes, using a viscoplastic material model. Metal flow was found to be more distorted in the welding chamber than in the container. Simulation results, based on velocity fields, had good agreement with earlier experimental findings. An interesting observation was that empirical equations giving reasonable pressure predictions cannot be used to forecast metal flow or final temperatures.

Van Rens [1999] modeled the aluminum extrusion process as a Stokes flow problem, coupled with a thermal convection-diffusion problem. He stressed that it is important to incorporate the temperature dependence of viscosity, and that the Coulomb friction coefficient has a substantial influence on the flow and temperature fields. Caloska et al. [2002] used CFD technology for 3D simulation of aluminum extrusion through a hollow square die. They treated the material as a Newtonian fluid with high viscosity, and the process as steady state laminar fluid flow. The numerically obtained exit velocity profiles had a good match with experimental values. Sibilla and Baron [2000] employed a 3D

finite volume scheme to solve fluid dynamics equations for numerical simulation of flow of plastic aluminum through container and die. Material was modeled as a highly viscous non-Newtonian fluid with temperature-dependent physical properties. Velocity, temperature and pressure fields obtained were validated to some extent by experimental results published earlier for axisymmetric extrusion of Al-6060. Authors claimed good applicability to determination of optimal bearing length.

Arif et al. [Jul 2004] investigated (experimentally and numerically) metal flow and formation and development of dead metal zone (DMZ) in cold extrusion, discussing the influence and interaction of important factors such as billet material, ram speed, extrusion ratio, and profile complexity on metal flow and DMZ.

1.11 Major Contributions of Current Work

1.11.1 Solution Methodologies

Due to a multitude of reasons, analytical solutions for extrusion pressure and other parameters are restricted to very simple geometries. *Slip-line field* method has generally been applied only in the case of indirect or backward extrusion. Also, it yields solutions for just a few plain-strain problems. *Slab method* and *upper-bound* method provide quite rigorous analytical solutions, but only for relatively simple shapes in metalworking processes. In real-world extrusion (whether solid, hollow, or semi-hollow sections), the profiles are generally quite complex. The resulting complicated boundary conditions are almost impossible to be handled analytically. The necessity of assuming homogenous force and pressure distributions also make the two methods untenable. Elevated temperatures involved in hot extrusion, and temperature variation with ram advance (due to heats of deformation and friction) add to the difficulty. Material properties, friction coefficients, etc become temperature-dependent. Analytical solutions are therefore restricted to rather simple geometries. Moreover, a tedious and time-consuming solution has to be carried out for each profile geometry separately, making it impossible to cover even a few of the tens of thousands of extruded sections.

FEM provides a more realistic and workable solution technique, as it has the capability of handling somewhat complicated and irregular geometries, nonlinear material properties, and non-homogenous load distributions. However, due to the prohibitive size and cost of hot extrusion equipment, most of the reported research based on FEM is restricted to cold extrusion. This leaves out most of the commercial extrusion work, especially in the burgeoning aluminum extrusion sector, which is performed in hot working conditions.

Some simple empirical models have been developed in literature to predict extrusion pressure. However, extensive *empirical* or *statistical* studies of metal extrusion are almost nonexistent in the published domain. Similarly, very few instances of investigations based on *probability theory* can be cited.

The **current work** uses experimental-empirical, statistical-probabilistic, and 2D-3D FEM methods to investigate various issues involved in extrusion process, extrusion tooling, and extrusion product defects. This approach of utilizing different solution techniques to study metal extrusion is expected to provide a better understanding of the process. As each method has its own limitations, individual-solution attempts are restricted in their scope, and this multi- methodology approach gives a comprehensive understanding of the field of aluminum extrusion.

1.11.2 Comprehensive Treatment

Most of the published research work targets specific individual aspects of extrusion. The process of metal extrusion, on the other hand, is a large and integrated activity. Interrelationships between various components of equipment and tooling, and among numerous process variables, thus become critically important.

The uniqueness of the current work lies in its comprehensive research approach, wherein the process, the tooling, and the product are simultaneously investigated. This global view provides a much better understanding of the entire process of extrusion. For instance, the way that product defects are linked with certain process aberrations on the one hand and with die and tooling problems on the other, could not be explored satisfactorily without this comprehensive approach.

1.11.3 Experimental Data

A thorough investigation of metal extrusion, especially with a view to addressing process, tooling and defects together, is possible only if a large amount of real world data is available for analysis. Unfortunately, published literature is seriously lacking in this regard. Laboratory-based studies are mostly restricted to cold extrusion. On top of that, many studies are based on experiments using model materials (such as plasticine) instead of actual metals. The resulting lack of real material properties can contribute to inconsistencies with actual metal behavior. Even in the laboratory setup, generation of reasonably large experimental data sets is difficult and often cost-prohibitive due to the high cost of real tool materials and specialized manufacturing techniques required. On the other hand, the only viable source for hot extrusion data is the industry, which is obviously reluctant in sharing it openly with researchers. There is thus a serious dearth of experimental data.

In collaboration with a commercial die manufacturing plant, laboratory data for the ***current work*** *was generated using actual die (H13 steel) and billet (aluminum and Al-6063) materials used in commercial extrusion. Also, a large number of experiments were conducted and data sets obtained for pressure and other process variables, die and tooling failures, and a variety of product defects in hot extrusion, as a result of collaboration with one of the largest extrusion facilities in the region. Availability of large sets of experimental data for both hot and cold extrusion, and for all pertinent issues, gives the current work a distinct advantage over the mostly laboratory-based published literature.*

1.11.4 Shape Complexity

Published work has not explored in detail the correlation between shape complexity of an extrusion profile and the various process parameters. There is no unique definition of complexity, and the ones available in literature do not satisfactorily correlate with process parameters in metal extrusion. Moreover, no work has been done in relating die life to profile complexity, and the available definitions do not yield the natural trend of earlier failures for more complex shapes.

*The **current work** meticulously investigates how profile complexity is related to extrusion pressure, and to die and tooling failure. Attempts are then made to develop more reliable and consistent definitions of shape complexity, both from a pressure prediction viewpoint, and from a die reliability angle.*

1.11.5 Die Failure and Reliability

Because of the high degree of precision and finishing required, dies and related tooling require special materials and advanced manufacturing techniques. Their repair and replacement thus add greatly to the product cost. However, little work is reported in this important area of extrusion die failures. Die life and reliability is another critical issue which has been scantily researched. Optimum maintenance and replacement strategies for extrusion dies and tooling are not possible without reasonably accurate life prediction models. Once again, the problem has not been thoroughly investigated.

*A distinctive feature of the **current work** is the detailed classification, description, and analysis of die failure modes and mechanisms. Another important contribution is the study of the probabilistic behavior of die life, and regression-based models for failure prediction in terms of geometric parameters of a die profile.*

1.11.6 Product Defects

Product quality and cost, and thus the viability of a commercial extrusion setup, are directly linked to product defects. Some researchers have attempted to analyze a few of the process defects encountered in extrusion. However, no exhaustive and systematic study has yet been reported in this area. Also, very few references are available on properly categorizing extrusion related flaws.

*Some of the salient features that differentiate the **current work** from hitherto published material are*

1. *Exhaustive definition, together with visual exhibits in most of the cases, of all defects arising in aluminum extrusion,*
2. *Scientific and systematic classification of extrusion related defects into logical categories*

3. *Investigation into the causes (mechanical, metallurgical, equipment or process related) of all the defects, and description of practical remedies and precautionary measures generally carried out in the industry, and*
4. *Statistical analysis of product defects in a typical extrusion plant, to serve as a benchmarking tool for plant efficiency.*

1.12 Problem Statement and Work Breakdown

The overall process of extrusion (outlined in Fig 1.1) consists of many complicated processes and stages that are apparently disjointed but are actually fully integrated and interrelated. The heart of the entire process is the *extrusion chamber*, where the deformation of the workpiece into the desired profile takes place. Figure 1.18 schematically illustrates the four sets of contributing factors involved: *input variables, tooling*, *process parameters*, and *output variables*. In a nutshell, the current work can be described as an ***investigation of the deformation process, tooling, and the input and output parameters governing the extrusion chamber***. The dominant role players during this deformation stage are *process parameters* and *die and tooling*. However, since cost and quality determine the commercial viability of the operation, *product defects* (extrusion output) cannot be neglected. Consequently, the proposed work is divided into the three separate yet inter-related studies shown in Fig 1.19.

1.12.1 Study-A: Extrusion Parameters

The most significant process parameter in extrusion is the **extrusion pressure** (or extrusion force). For *equipment selection* (in terms of press capacity, billet size, container size, etc), for *die design* (material toughness, bearing surface design, heat treatment and surface hardening, etc), and for *product costing* (in terms of energy costs related to work of deformation, frictional work, and redundant work), extrusion pressure is probably the most critical parameter. First part of the current work, *Study-A* (Fig 1.20), focuses on extrusion pressure, its relationships with other process parameters, and the development of a pressure-prediction model. The role of profile complexity in pressure variation is given special attention.

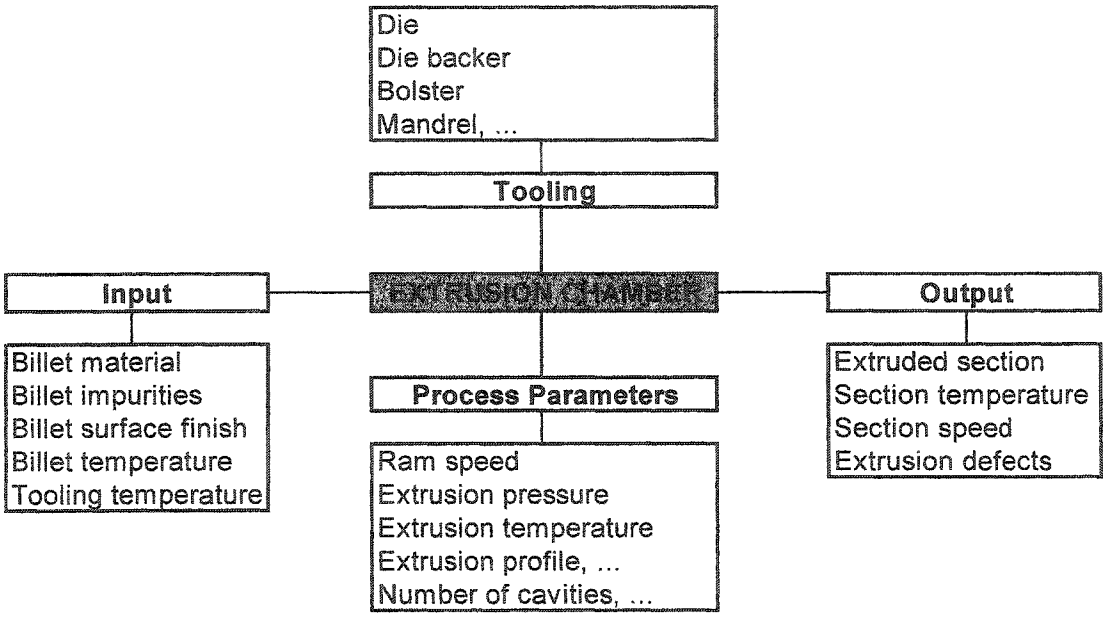

Figure 1.18 Components and parameters playing active role in the extrusion chamber

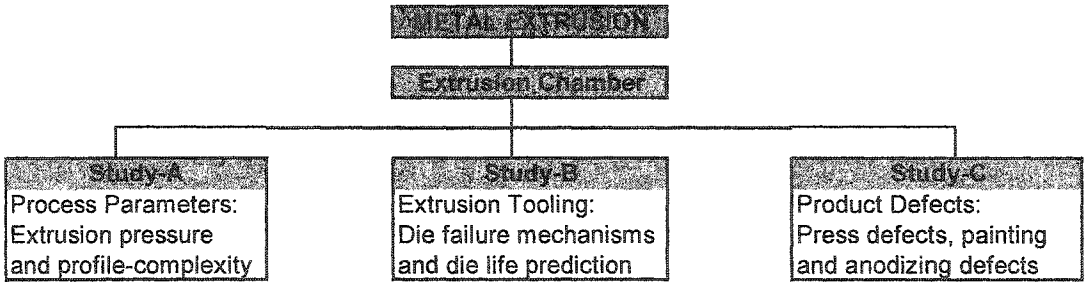

Figure 1.19 Investigation focusing on the extrusion chamber can be broken down into three distinct studies

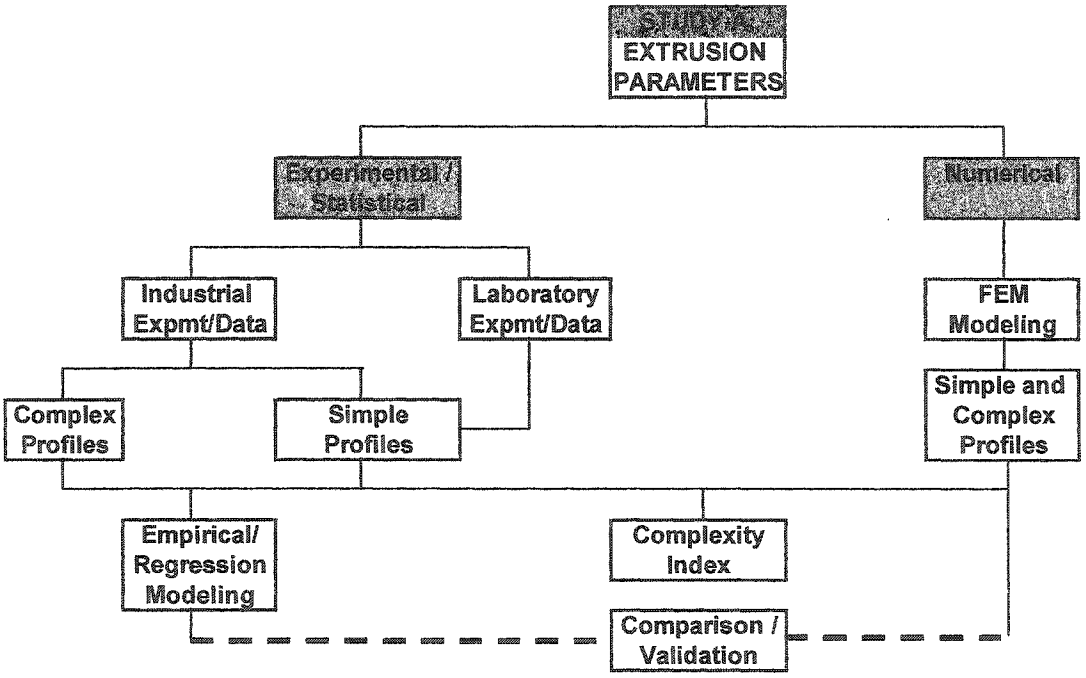

Figure 1.20 Study-A consists of empirical/statistical and numerical investigation of extrusion pressure and die shape complexity.

1.12.2 Study-B: Extrusion Tooling

A very large number and a wide variety of tooling and equipment are employed during various production stages in commercial extrusion. The deformation chamber forms the hub of the entire process, and the die and die-set is at the heart of this production stage. The second part of the current work, *Study-B* (Fig 1.21), concentrates on two significant aspects of extrusion tooling: *die failure* modes and mechanisms, and *die life* prediction. Process parameters and shape complexity are considered to be major role-players.

1.12.3 Study-C: Product Defects

From a customer-satisfaction viewpoint (quality and cost), the main concern in any manufacturing operation is product defects. The amount and the frequency of defective output can be a clear indication of the shortcomings in design, operation and maintenance of the process and the equipment and tooling. In terms of rework and rejection, it can also directly quantify the additional cost of the product. The third element of the current work, *Study-C* (Fig 1.22), attempts at a comprehensive scheme for classification, description and characterization, remedial measures, and statistical analysis of extrusion product defects. The study covers defects generated in all the three main activity centers in a commercial extrusion plant: extrusion press, anodizing, and painting. The main thrust of the work is on studies A and B, while study C is of a secondary nature.

1.12.4 Work Breakdown

As the work comprises of several in-depth studies, and as each study in turn involves various sub-investigations, a modular approach has been employed. Following is the work breakdown in a summarized form.

(A) ***Investigation of Extrusion Process***

- Extrusion Pressure Variation and Prediction: influence of process parameters and shape complexity
  - Empirical study
    - Industrial data collection
    - Hot extrusion experiments (industry)

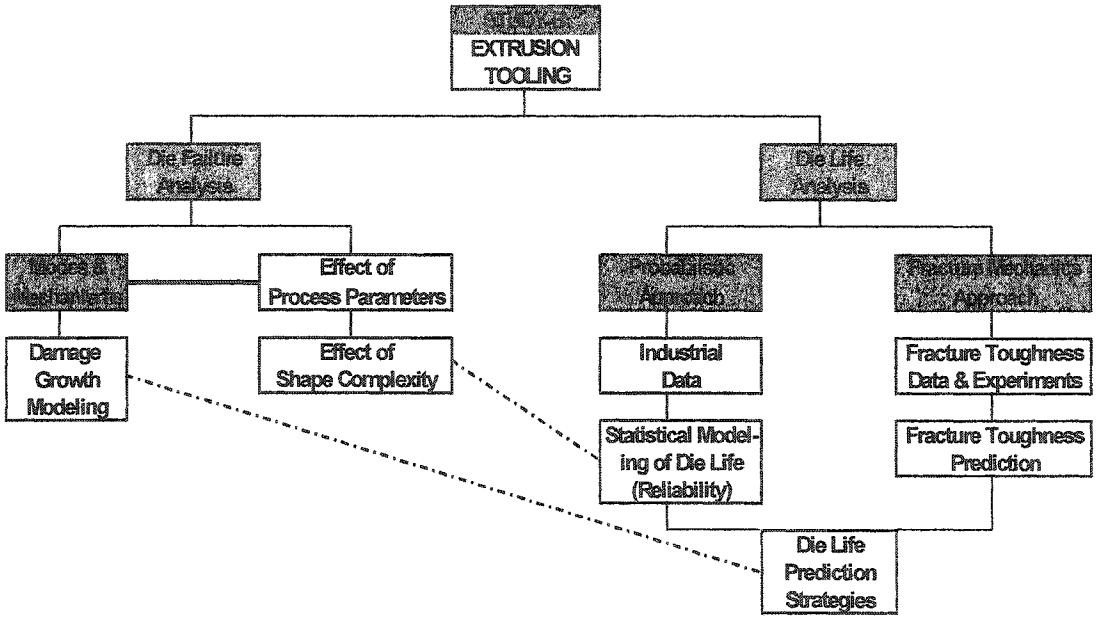

Figure 1.21 Study-B covers die failure analysis and die life analysis.

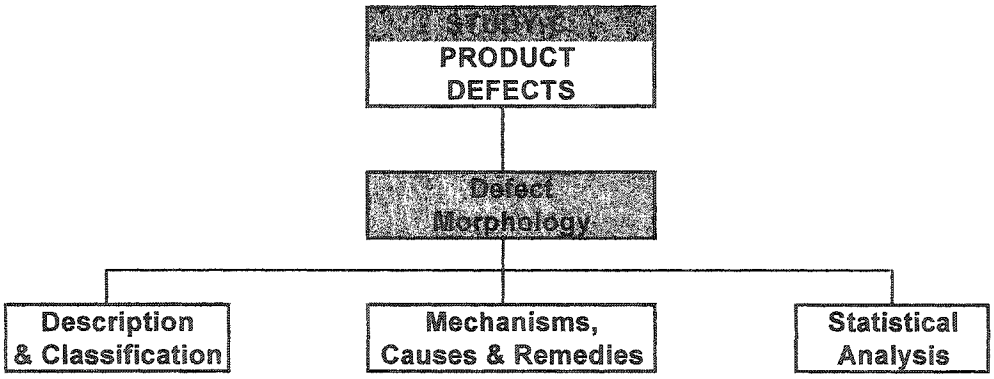

Figure 1.22 Study-C covers the morphology of product defects in metal extrusion.

Design/manufacture of cold extrusion dies, and fabrication of split billets

- Cold extrusion experiments (in-house)
- Empirical/statistical inferences from hot and cold extrusion experiments

- Semi-analytical/numerical study
  - Numerical modeling using commercial software (ANSYS and ANSYS-LSDYNA)
  - Simulation runs for various process parameters under various conditions
  - Model validation against experimental results

- Evaluation of Shape Complexity
  - Analysis of complexity index definitions found in published literature
  - Empirical/Statistical study
    - Collection of geometrical data (industry) for dies of varying complexities
    - Hot extrusion experiments (industry) for determination of maximum extrusion force/pressure
    - Regression modeling to correlate pressure and shape complexity
    - New and improved definition of complexity index for extrusion die profiles

(B) *Dies and Tooling Study*

- Die Failure Study
  - Collection of die-failure history and data/samples from industry
  - Effect of extrusion parameters
  - Effect of shape complexity
  - Failure mechanisms
  - Failure classification
  - Failure modeling
  - Failure analysis
- Die Life Study
  - Probabilistic analysis of die failures
    - Collection of die-failure data/samples from industry
    - Die failure probability and reliability

- Regression of industrial data to generate reliability models
- Shape complexity and die reliability

- Determination of facture toughness of tool steels
  - Examination and collection of published data
  - Preparation of samples (tool-steel material) for testing of mechanical properties
  - In-house experimentation on tool-steel material under varying conditions
  - Development of CVN-K_{IC} correlations
    - For different tempering temperatures
    - For different operating temperatures
- Die life prediction model
  - Collection of die-failure histories for various complexities (industry)
  - New shape complexity definition
  - Complexity based die-life prediction model
  - Fracture mechanics based die-life prediction model

(C) ***Product Defects Study***

- Defect Morphology
  - Defect information/sample collection from industry
  - Classification of defects
  - Study of defect mechanisms and causes
  - Remedies and preventive measures
- Defect Analysis
  - Defect information/sample collection from industry
  - Determination of defect probabilities
  - Defect analysis
    - Overall breakdown
    - Annual rejection behavior
    - Breakdown of press, anodizing, and painting defects

CHAPTER 2
EXTRUSION PROCESS: PRESSURE VARIATION

2.1 INTRODUCTION

As mentioned earlier, the single most important process parameter in extrusion is the **extrusion pressure**. It plays a significant role in decisions regarding equipment selection, die design, and product costing, and it contributes directly to product defects and quality. It is therefore important to investigate the relationship of extrusion pressure with other process parameters.

Prediction of extrusion pressure, especially in the case of complex die geometries, is an area of continued research interest. It is natural to expect that die complexity would significantly affect the flow of metal and the pressure required to extrude a given product. Applied strain rate (related directly to the ram speed of the extrusion press) also alters the product quality significantly. Results are presented in this chapter from a study about effects of ram speed and profile complexity on extrusion pressure. Experiments were conducted using dies of different complexity to track the effects of ram speed variation and changing die profiles on extrusion pressure. Al-6063, the most popular commercial variety of structural aluminum, was used as the billet material for all experiments.

The focus of this study was the interrelationship of three basic parameters: *ram pressure* (force with which the ram/plunger pushes the billet through the die profile, divided by the billet or container area), *ram speed* (speed at which the ram pushes the billet along the container), and tool complexity (shape complexity of the die profile, measured by a factor called *complexity index*). Instead of actual ram speed, *puller speed* (speed at which the extruded sections are pulled out of the extrusion chamber) has been

recorded for this study. As puller speed is directly proportional to ram speed, the conclusions are synonymous.

Most of the work discussed here has been reported in Arif et al. [Sep 2001, Feb 2001].

2.2 Profile Complexity

As described in the preceding chapter, the simplest extrusion shape is considered to be a solid round bar. Complexity usually increases from solid to semi-hollow to hollow profiles. The four definitions of extrusion shape complexity readily found in published literature were described in section 1.7 of chapter-1. For the purpose of this study, the first two definitions have been chosen due to their popularity and ease of calculation (equations 1.15 and 1.16).

2.3 Experimental Work

Various experiments in direct (forward) hot extrusion were conducted in collaboration with a local industrial setup, Aluminum Products Company (ALUPCO), Dammam, Saudi Arabia. Figure 2.1 and Fig 2.2 show various details of the hot extrusion setup. The same die material (H-13 steel) and the same billet material (Al-6063) were used in all experiments, under almost similar conditions (temperature range of about 425-475 °C, without the use of any lubricants). A fully computerized 3500-ton capacity SMS-Hasenclever press was utilized, on-line real-time data being directly available through the CADEX (Computer-Aided Direct Extrusion) software package. Experimental runs were carried out to record the following two major data sets:

1. Variation of extrusion pressure against increasing die complexity at constant ram speeds.
2. Variation of extrusion pressure against increasing ram speed for constant complexity (fixed die profile).

(a)

(b)

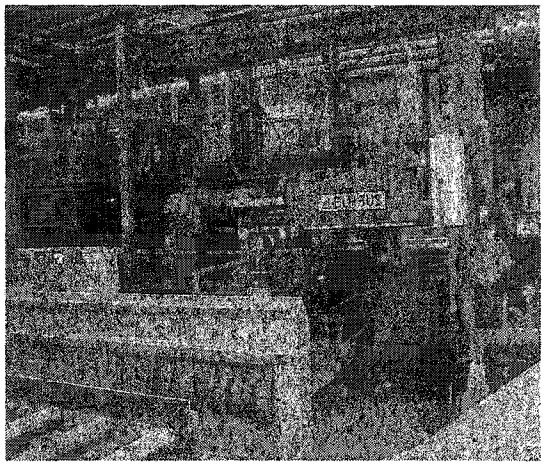

(c)

Figure 2.1 Overall view of the aluminum extrusion press and its CADEX system (a), together with top view (b) and front view (c) of the facility; also seen is the die stack, ready to be loaded into the container [ALUPCO].

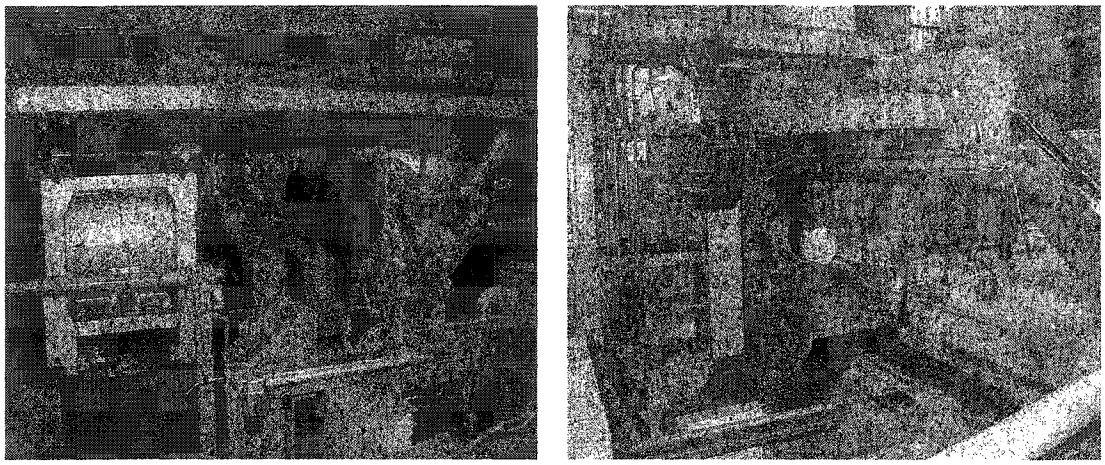

(a) (b)

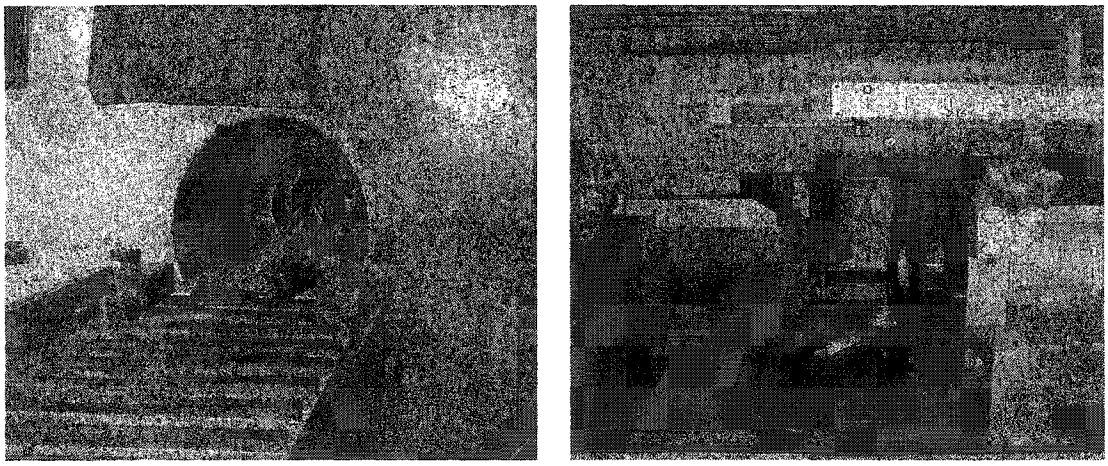

(c) (d)

Figure 2.2 Different stages of the hot extrusion cycle: billet loading mechanism (a), billet being loaded into the container (b), extruded product coming out of the extrusion chamber(c), and discard being sheared (d) [ALUPCO]

Figure 2.3 shows the solid, hollow, and semi-hollow profiles on which the experiments were conducted, while Table 2.1 lists indices giving their shape complexity (based on the first two definitions of complexity index given above). Profile names start with a letter indicating profile type (*S* for solid, and *H* for hollow) followed by a number indicating its complexity index rating in an ascending order ('1' for lowest complexity, '2' for next higher *C*, and so on). There are often multiple cavities in the same die to give a higher production rate, depending on the size of the extruded profiles and the die size. The table also lists the number of cavities against each profile, to give a better understanding of the process. Also given for each die is another very important process parameter, *extrusion ratio* (*R*), the ratio of billet or container area to the extruded area.

2.4 Results and Discussion

All observations are summarized in the form of graphs showing variation of extrusion pressure as the ram advances along the container. Billet lengths may be different for different profiles, so the starting and ending ram positions may not be the same in all graphs. Minor fluctuations and deviations from smoothness in the plots are expected, and are due to experimental aberrations inherent in a real production setup. Depending on whether the profile is solid or hollow (requiring a mandrel in the die set), and on the complexity of the profile, the initial pressure buildup (known as *upsetting*) can be quite different for different sections. This small initial part of the graph has been omitted in all cases, giving the behavior after maximum pressure has been achieved. Similarly, the very small ending part of each extrusion stroke (known as *discard*) has not been included in the graphs, wherein pressure suddenly drops to a minimum.

2.4.1 Pressure Variation against Ram Position

Pressure gradually and rather smoothly drops down as the plunger moves forward along the container. However, against the popular belief that extrusion (especially hot extrusion) is a steady state process, all graphs exhibit a gradual decrease in pressure with ram advance. This behavior would be readily understandable in cold extrusion, where billet-container friction has a significant influence on extrusion pressure. As the

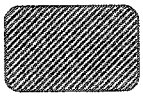

S1: 30 x 25

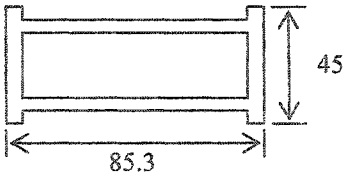

H2: t = 3

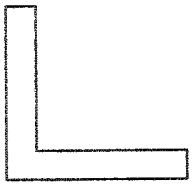

S3: 40 x 40 x 4

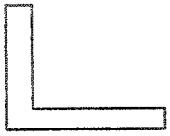

S4: 38 x 38 x 3.8

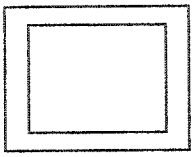

H5: 40 x 40 x 1.1

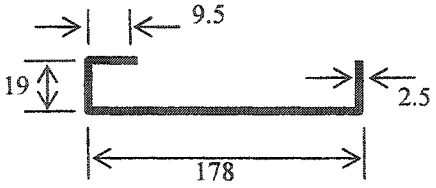

S6: t = 2

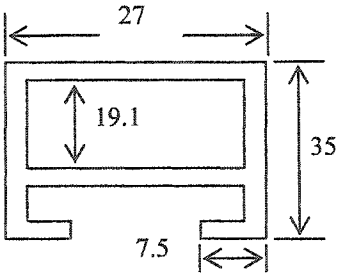

H7: t = 13

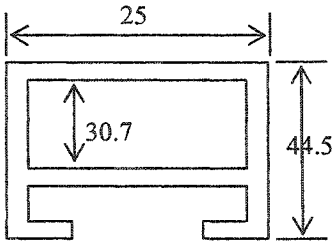

H8: t = 1.15

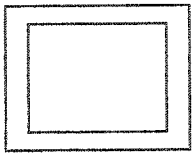

H9: 40 x 40 x 0.9

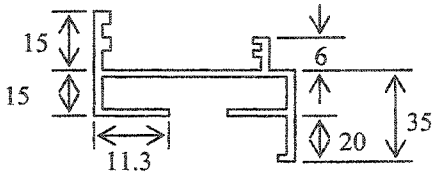

H10: t = 1.1

Figure 2.3 Sketches of profiles of different complexity used for experimental investigation in hot extrusion of Al-6063

Table 2.1 Details of tool profiles used in the pressure variation experiments

Die Number	Profile Number	Profile Type	P_s	A_s	W_s	N	R	C_1	C_2
1988	S1	Solid	107	746	2014	2	36	0.143	0.053
9898	H2	Hollow	279	763	2060	1	71	0.366	0.135
1187	S3	Solid	156	304	820	3	60	0.513	0.19
8133	S4	Solid	152	272	734	3	67	0.559	0.207
9330	H5	Hollow	160	171	462	4	79	0.936	0.346
B399	S6	Solid	436	461	1245	2	59	0.946	0.35
9834	H7	Hollow	174	170	459	4	80	1.023	0.379
A560	H8	Hollow	181	165	445	4	82	1.097	0.407
F030	H9	Hollow	160	141	380	4	96	1.135	0.421
9363	H10	Hollow	294	169	456	4	80	1.739	0.645

remaining billet length decreases, friction force goes down due to reduction in the contact surface, and pressure in turn also decreases. In hot extrusion however, friction plays only a marginal role. Higher plasticity of aluminum (in comparison with other metals and alloys, such as steel) appears to be the cause for the pressure drop. With sustained application of pressure at the high temperatures involved, metal flow improves due to the increase in plasticity, resulting in a steadily lowering pressure requirement. Moreover, all recorded data show that the billet, initially preheated to 425-475°C, exits the extrusion chamber at a temperature of around 500-530 °C. This increase in temperature during the process (caused by added heats of friction and deformation during extrusion) is another reason for the improved metal flow and the decreasing pressure.

2.4.2 Pressure v/s Shape Complexity at Constant Ram Speed

A batch of four profiles was first selected for experiments at constant ram speeds of 15, 20, 25, and 30 m/min. There were two solid dies (S4 and S6) and two hollow dies (H8 and H9). Another set of six different profiles (a simple symmetric pure solid S1, an unsymmetrical solid S3, three hollows H2, H5, and H7, and a somewhat complex semi-hollow H-10) was run at one fixed speed (20 m/min) to corroborate results from the first group. The findings appear to be:

1. At a fixed ram speed, there is a general trend of higher pressure curves for profiles of larger shape complexity values, as exhibited by all figures from Fig 2.4 to Fig 2.8. This supports heuristic knowledge as well as theoretical expectations. Force requirements are generally higher in the case of more complex die shapes.
    (a) A break from this general trend can be noted in Fig 2.4 (a), where pressure curve for the higher-complexity profile S3 is below that for the lower-complexity profile H2. The conclusion is that a solid die, even with the same or a somewhat higher C value (based on the complexity definitions used), can have a lower pressure curve than a hollow one. This is in general supported by experience. Hollow profiles have an additional member in the die set called the mandrel, and thus require more force than solid ones, unless the solid profiles are very complicated.

(a)

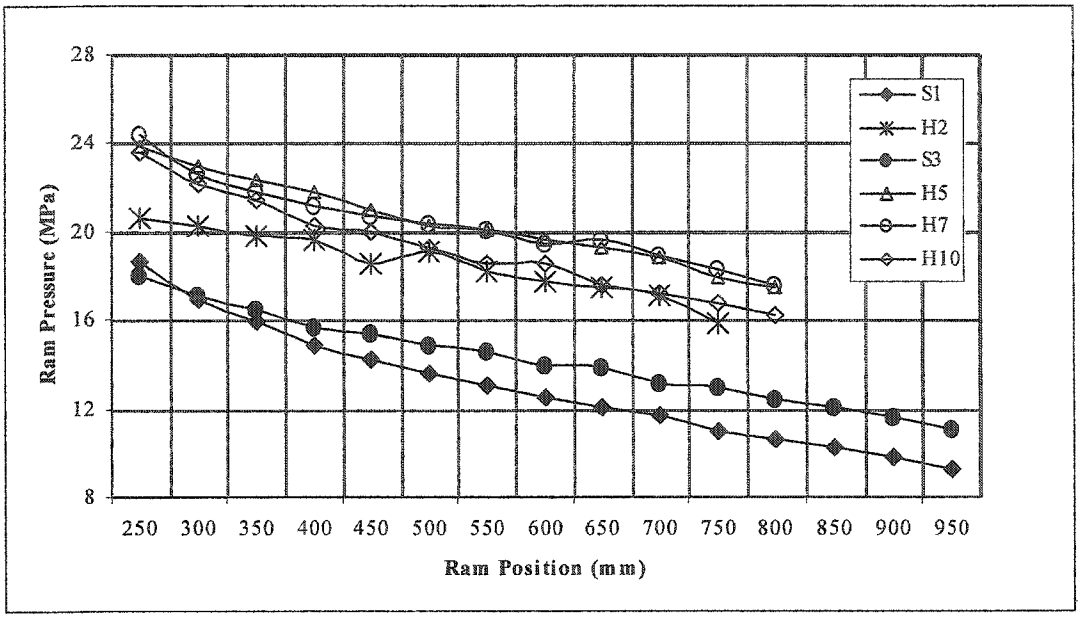

(b)

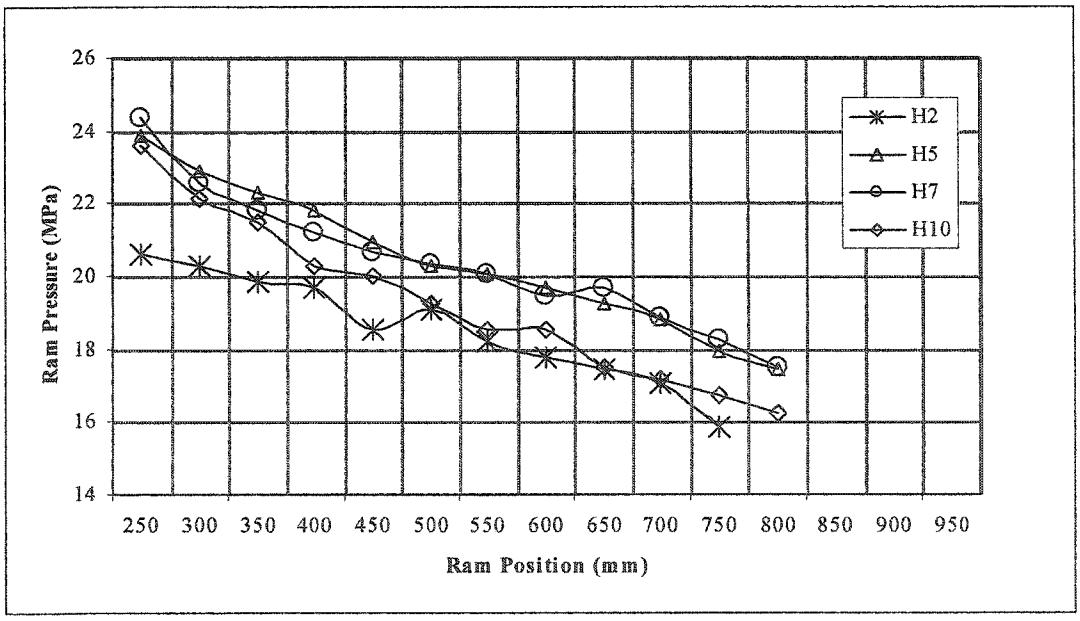

Figure 2.4 Variation of ram pressure against ram position for different complexities, at a constant ram speed of 20 m/min; solid and hollow profiles (a), hollow profiles only (b)

(a)

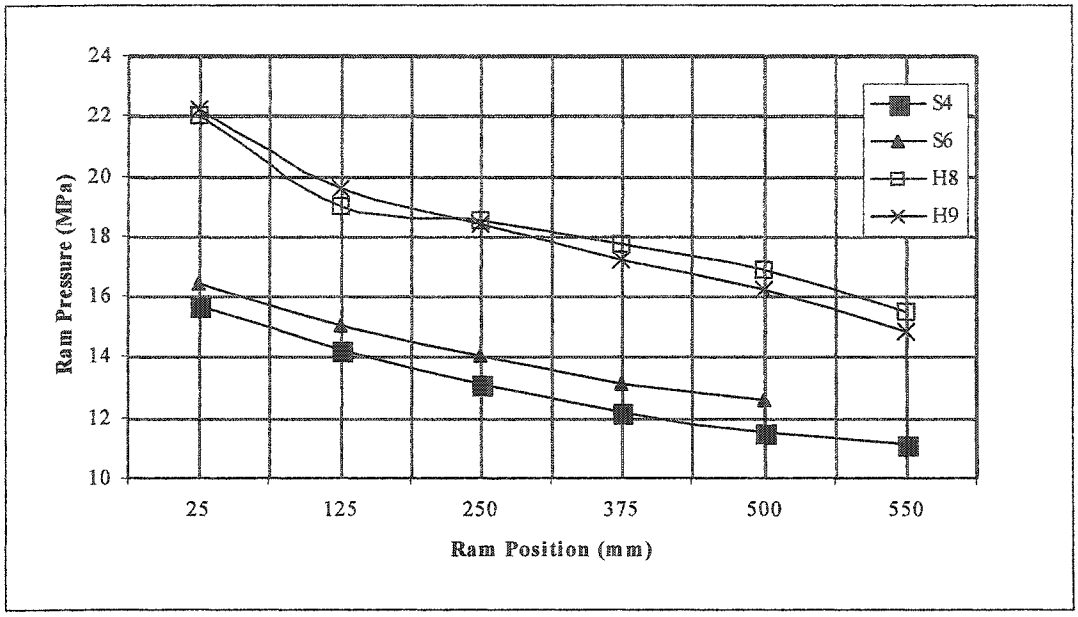

(b)

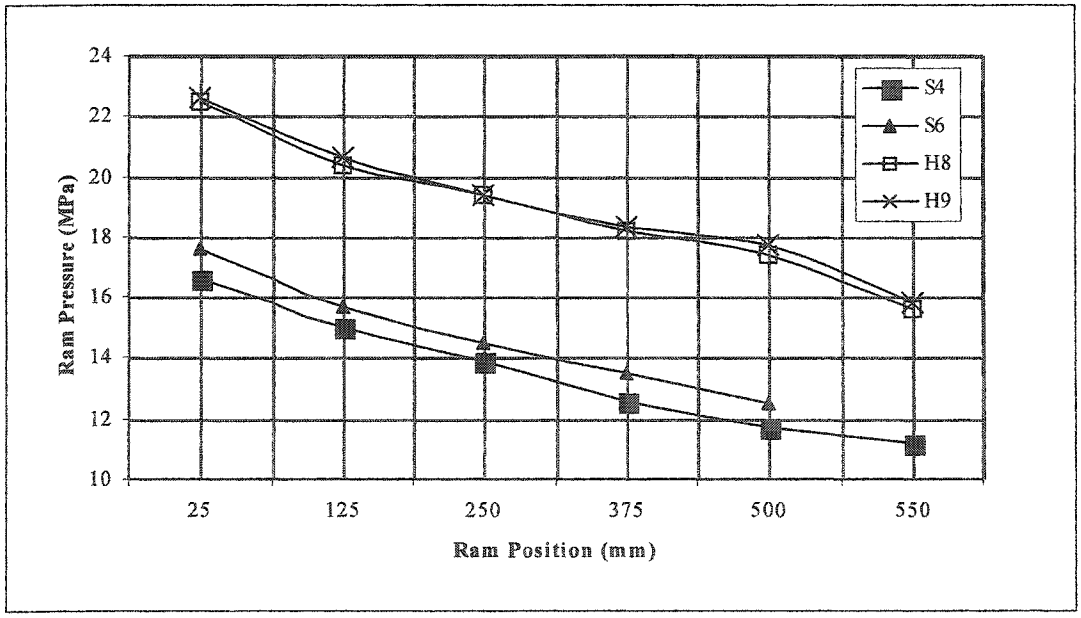

Figure 2.5 Variation of ram pressure against ram position for different complexities, at constant ram speeds of 15 m/min (a) and 20 m/min (b)

(a)

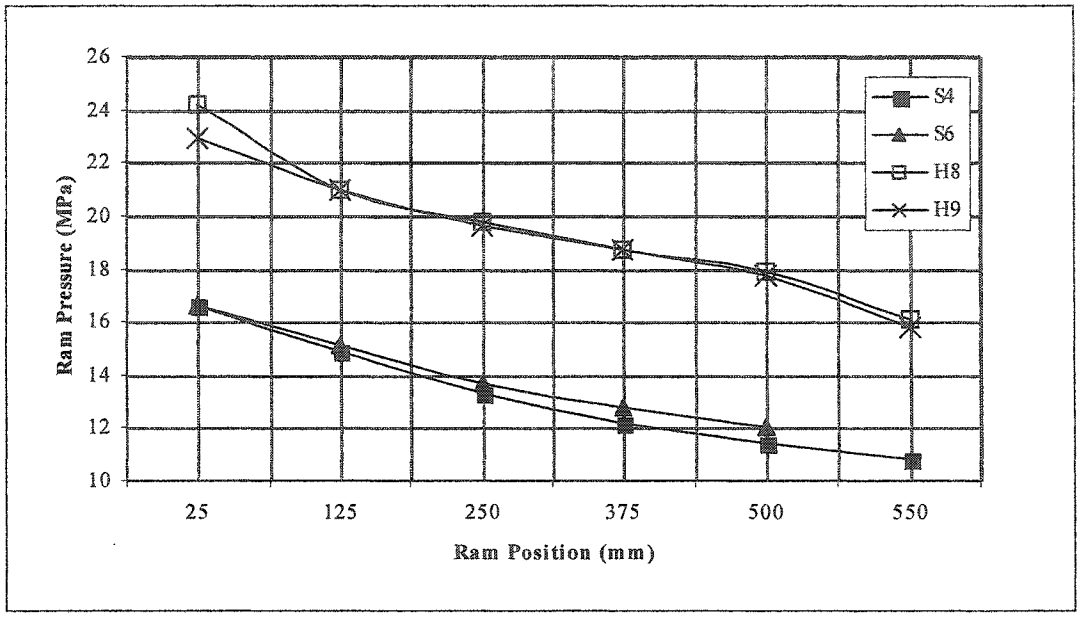

(b)

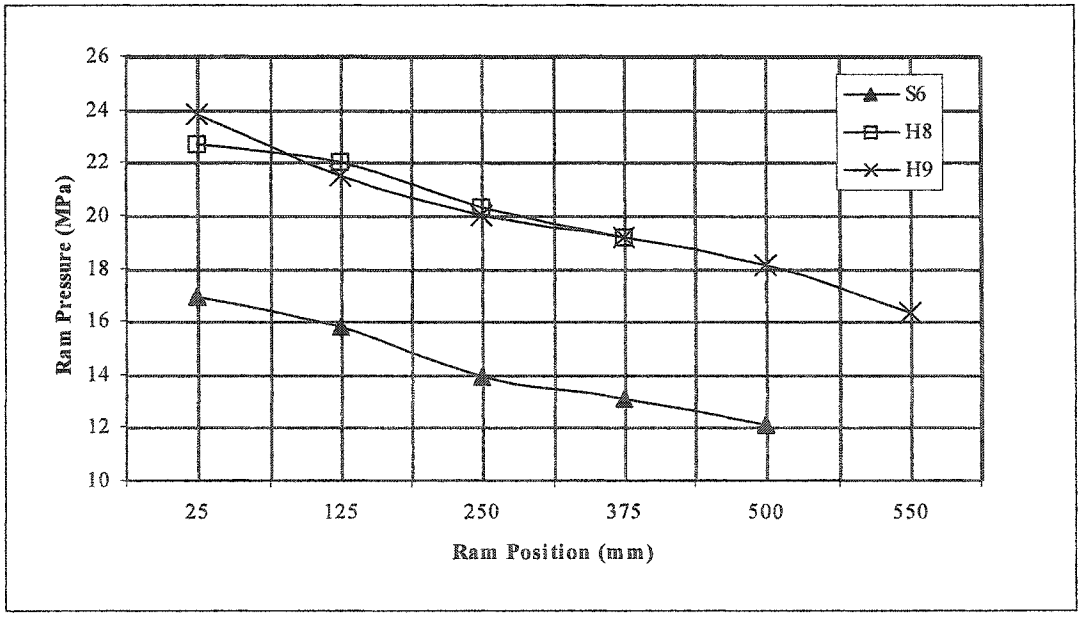

Figure 2.6 Variation of ram pressure against ram position for different complexities, at constant ram speeds of 25 m/min (a) and 30 m/min (b)

(a)

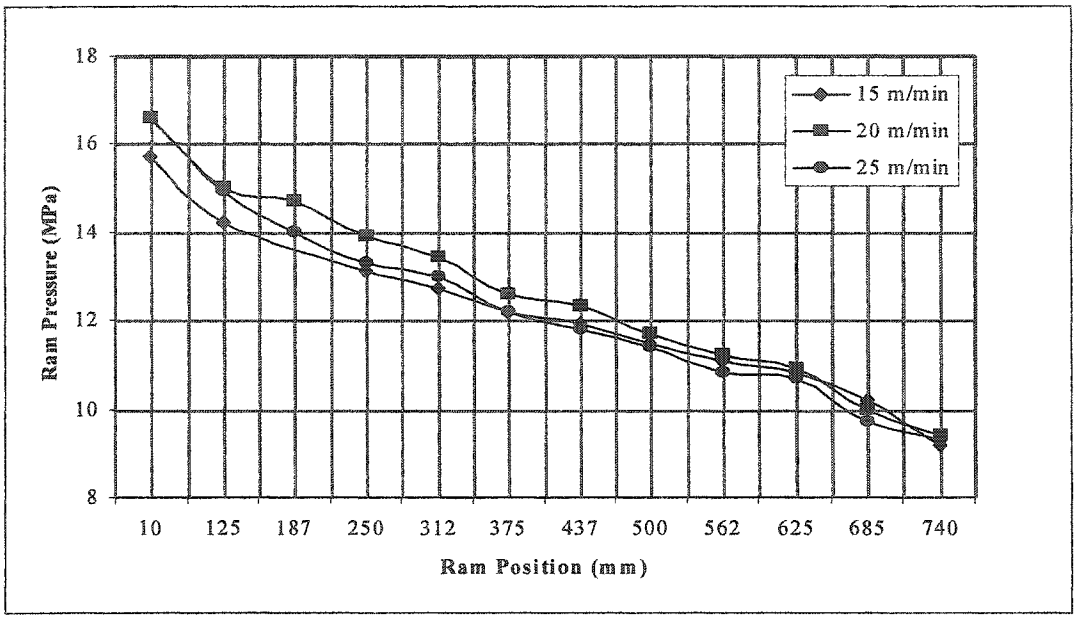

(b)

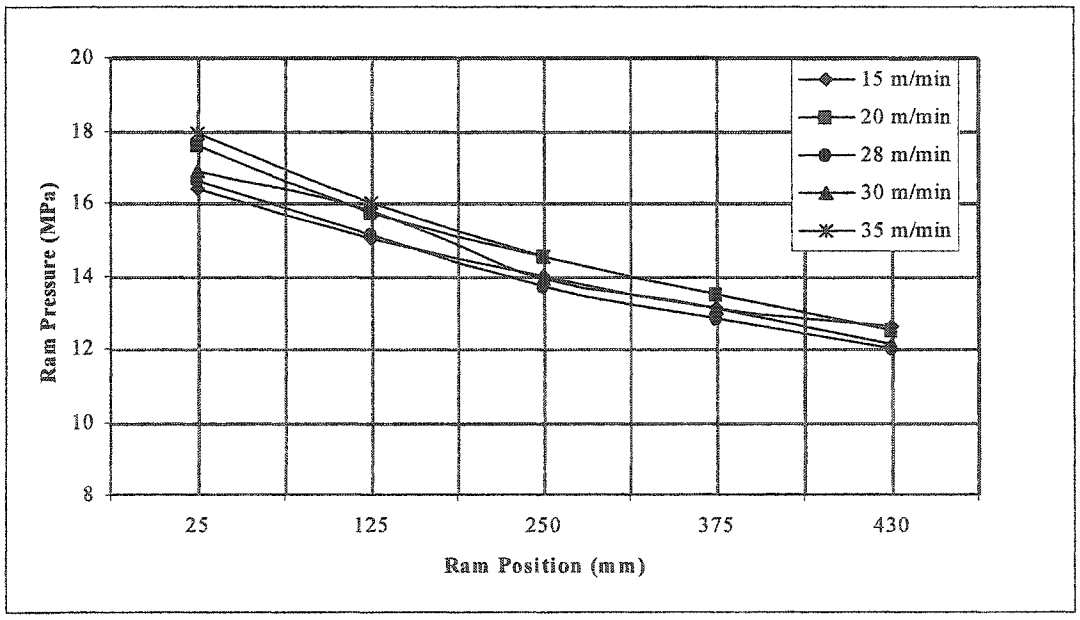

Figure 2.7 Variation of ram pressure against ram position for solid profiles S4 (a) and S6 (b) at different ram speeds

(a)

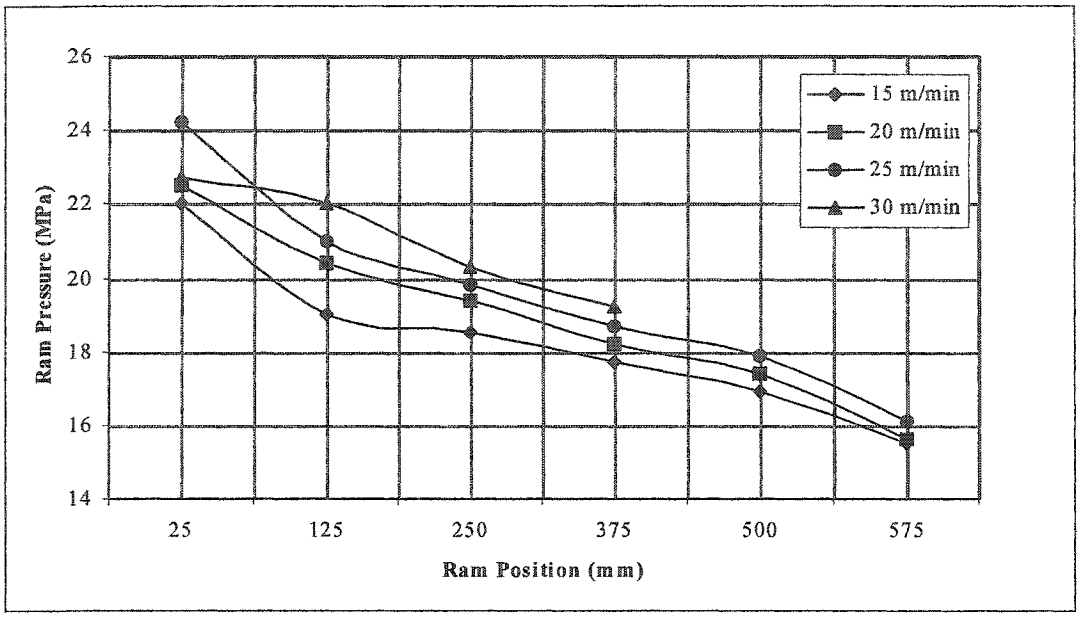

(b)

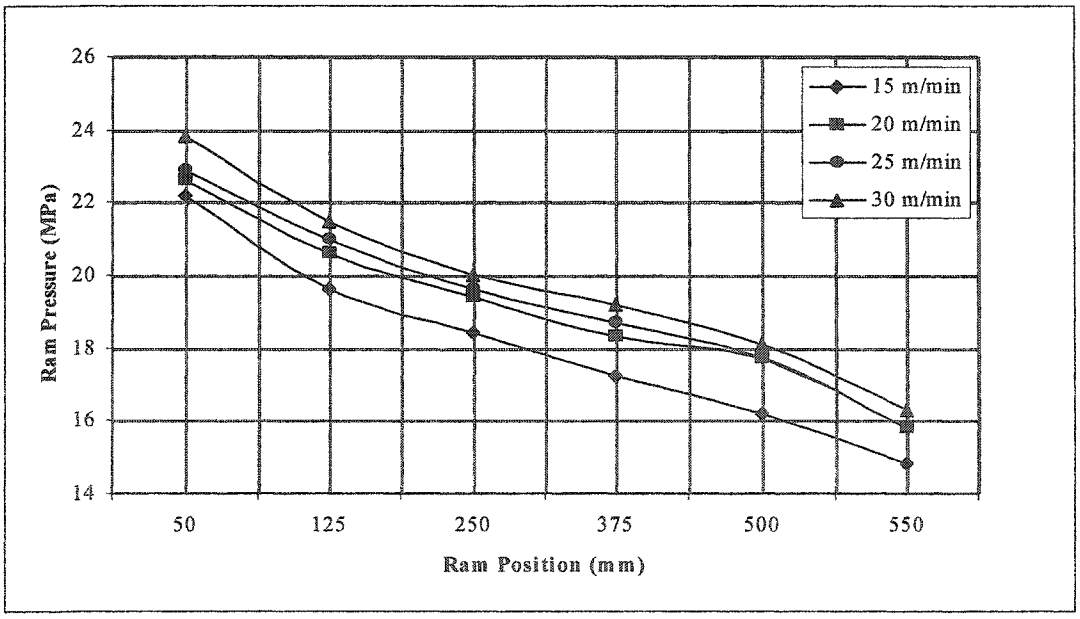

Figure 2.8 Variation of ram pressure against ram position for hollow profiles H8 (a) and H9 (b) at different ram speeds

A clear recommendation from this observation would be that solids, semihollows, and hollows should be treated separately, rather than ranking profiles on the basis of complexity index alone. The classification shown in Fig 2.9, proposed by Laue and Stenger [1981] on the basis of degree of difficulty in extrusion, follows this philosophy.

(b) This observation also points towards the need for an improved definition of complexity index *C*. The definition should include more geometric parameters of the profile than simply its perimeter, area, or weight per unit length.

2. Figures 2.5 and 2.6 reveal that pressure curves for solid shapes are bunched close together; similarly, all hollow curves lie near each other; and there is a notable spacing between the two groups of curves. This observation strengthens the conclusion drawn above about considering solids and hollows as two distinctly different groups with regards to complexity considerations. We can also notice that there is an increase in the pressure differential between solid and hollow curve sets with increasing ram speed. Increase in extrusion pressure with increasing ram speed is expected, as extrusion pressure is directly proportional to average strain rate, and strain rate directly depends on extrusion speed.

2.4.3 Pressure v/s Ram Speed for Fixed Shape Complexity

For this category of data, variation of ram pressure at different ram velocities was recorded against advancing ram position, one die at a time. The information is summarized in a graphical form in Figures 2.7 and 2.8. There is a general trend of higher-pressure curves for higher ram speeds (excepting a couple of deviations). This trend is expected, as explained above: higher ram speeds translate into higher extrusion pressures.

2.4.4 Shape Complexity

Two definitions (out of the four available in published literature) have been used here to calculate the complexity index *C*. Apart from possible experimental aberrations mentioned earlier, the major reason for deviations in pressure variation from general trends appears to be deficiencies in the complexity definitions used. This strongly points

Section category	Section type	Examples
A	Simple bar	
B	Shaped bar	
C	Standard sections	
D	Simple solid sections	
E	Semihollow sections	
F	Sections with abrupt section transitions and thin walls; wide sections	
G	Sections with difficult tongues and very narrow inlets	
H	Tubes	
J	Simple hollow sections	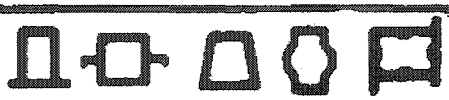
K	Difficult hollow sections; hollow sections with two or more cavities	
L	Tube sections with external projections	
M	Tube shapes with internal projections or K + L	
N	Large or wide hollow sections	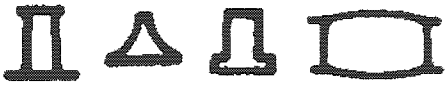

Figure 2.9 Profile classification based on degree of difficulty in extrusion, proposed by Laue and Stenger [1981]

towards the ***need for a new and improved definition of complexity index***, particularly one that incorporates more extrusion parameters such as number of cavities per die, extrusion ratio, number of sharp corners, etc. In a later chapter (chapter-3), a better definition of complexity will be proposed that would yield a more consistent and realistic prediction of extrusion pressure.

Despite some inexplicable fluctuations, all observations tend to suggest that pressure variation in extrusion is inherently linked with shape complexity. This provides strong grounds for the premise that a pressure-prediction module should be developed in terms of complexity indexes, and should be based on the reference pressure of a simple die profile. This issue will be explored in detail in chapter-3.

2.4.5 General Observations

Apart from the possibility of minor experimental errors, fluctuations from general trends can be attributed to one (or a combination) of the following factors. These general observations are applicable to all graphs in this chapter and to studies described in later chapters as well.

1. The entire process is computer-controlled, with the CADEX software automatically making corrections and allowances if any operating condition changes. A set of data usually becomes reliable only after 4-5 billets have gone through and the computer settings have stabilized. However, some orders are rather small, requiring only 2-3 billets. Also, the industry runs a particular profile at a predetermined optimum speed, and cannot afford to have experimental runs at different speeds (required for speed variation analysis) for more than a few billets. In such cases, the computer might still be correcting its pressure settings to get a constant ram speed; thus the fluctuations.
2. Sometimes the process has to be temporarily stopped, for instance when the billet loading mechanism is not working properly, or when the preheating ovens are behaving erratically. CADEX would try to readjust to these forced discontinuities, resulting in nonstandard data.

3. As mentioned earlier, billet lengths can sometimes be different for different profiles. As extrusion pressure directly depends on the billet length remaining to be extruded (equation 1.9), some fluctuations from general trends in pressure behavior can be expected.
4. All hot extrusion experiments have been conducted in the industry. The advantage is that all analyses are based on real world data generated through actual billet and die materials, process conditions, and profile complexities. On the other hand, the data sets have not been derived from predesigned statistical experiments, and care must be taken in generalizing the conclusions.
5. In a predesigned experiment, profiles could have been selected having different complexities but the same extrusion ratio (R). However, the study being based on real commercial profiles, R values for these sections range from 36 to 96; a rather large variation. As extrusion ratio is an important factor contributing to pressure variation (equation 1.9), deviations from general pressure trends can be expected. This further strengthens the conclusion drawn in section 2.4.4 above, that a new definition of complexity index (incorporating R as a parameter) is seriously needed.

CHAPTER 3
EXTRUSION PROCESS:
COMPLEXITY BASED PRESSURE PREDICTION

3.1 INTRODUCTION

The immense popularity and commercial viability of extrusion, especially for aluminum profiles, is based on two major factors:

1. Aluminum has a high degree of extrudability compared to other metals, and aluminum extrusions are light, strong, and almost maintenance-free.
2. Extrusion is a very versatile process, capable of producing very simple to highly complicated and intricate geometries with a high degree of accuracy.

Figure 3.1 illustrates the complexity of the profiles produced and the dies used.

3.1.1 Need for New Complexity Definition

As mentioned earlier in chapter-2, various researchers have coined different definitions for shape complexity of extrusion dies, based on geometrical parameters. The simplest definition depicts complexity index as the ratio of profile perimeter to profile cross-sectional area. Other definitions are in terms of ratios of perimeter to weight, circumscribing circle diameter to minimum wall thickness, profile perimeter and equivalent circular perimeter, etc. Unfortunately, these definitions suffer from various major drawbacks:

1. They do not yield a consistent ranking of die profiles in terms of shape complexity.
2. Predicted extrusion pressure often gives widely fluctuating values.

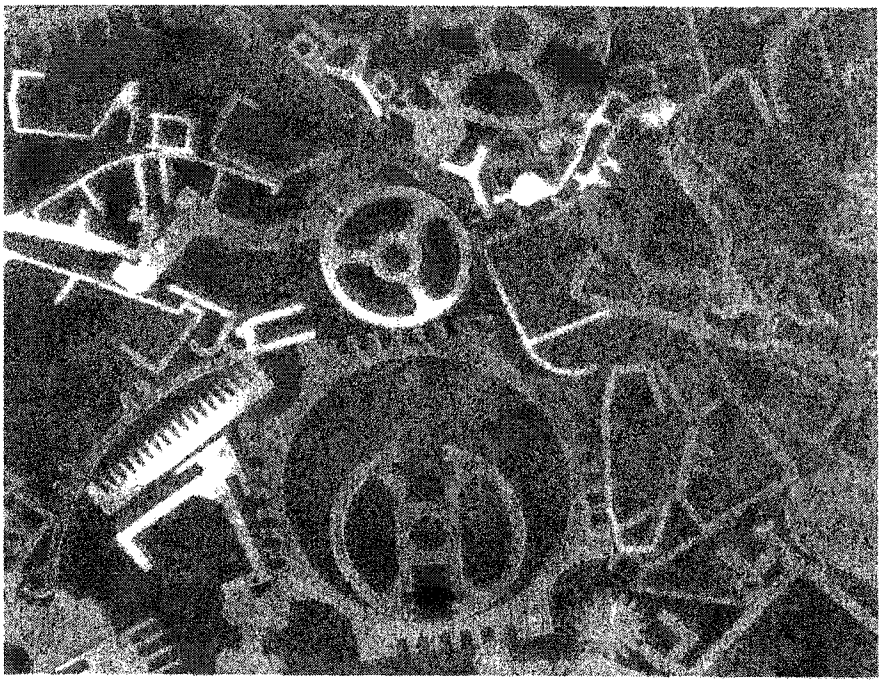

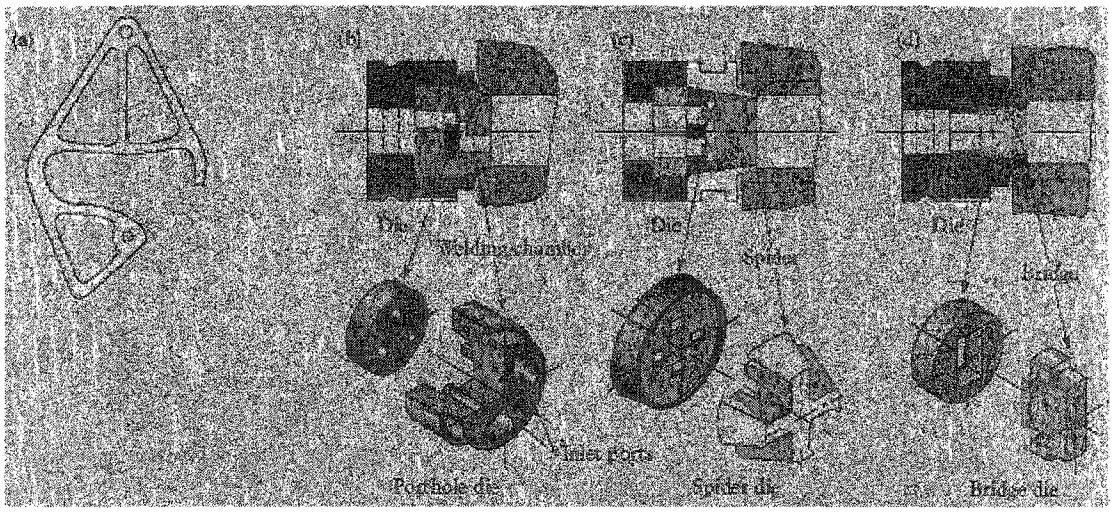

Figure 3.1 Versatility and complexity of extrusion profiles (above) and extrusion dies (below)

3. Pressure variation study reported in chapter-2 revealed some inconsistencies in pressure-complexity behavior during hot extrusion of solid, hollow, and semihollow profiles. Apart from experimental irregularities, the major reason for the observed deviations was found to be inadequate complexity definitions.

All of these observations suggest that a new definition of extrusion shape complexity is seriously needed.

3.1.2 CURRENT WORK

Semi-Analytical Model for Pressure Prediction: Results are reported in this chapter from a study targeted at the development of a semi-analytical model for prediction of the needed extrusion pressure, based on the mechanics of deformation during extrusion. In a conceptual form, the model is

$$p_c = \psi\,(C,\, p_s), \tag{3.1}$$

and

$$p_s = \varphi\,(X_1,\, X_2,\, \ldots,\, X_N), \tag{3.2}$$

where

$p_c \equiv$ extrusion pressure for die of a complex shape,

$p_s \equiv$ extrusion pressure for die of a simple (standard) shape,

$X_i \equiv i$th variable or parameter affecting the extrusion process, and

$C \equiv$ complexity index.

New Complexity Definition: The study also involves the development of a new and more consistent definition of complexity for extrusion profiles. This new definition is a natural progression of the conclusions drawn in the previous chapter, and is in line with the premise that extrusion pressure for a complex profile can be expressed in terms of pressure for a simple profile and complexity index of the complex profile. The definition is empirical in nature, based on data from a large number of extrusion runs involving a total of twenty seven (27) different dies, profile complexity ranging from simple solids and hollows to quite complex ones. A variety of regression schemes were explored, including exponential, logarithmic and power law formats.

3.2 Extrusion Pressure

Referring back to section 1.5 of chapter-1, we recall that Fig 1.8 (a) was a schematic illustration of the important process and geometric parameters involved in direct extrusion. The final expression for extrusion pressure was given by equation (1.9). Value of the average flow stress $\overline{Y}_f$ for the billet material (Al-6063 in our case) at the elevated temperatures involved (425-475°C) can be found from the chart based on temperature-compensated strain rates reported by Sheppard [1999].

3.3 Complexity Index

Equation (1.8) for extrusion pressure is valid for the simplest extrusion geometry, when both the billet and the die have a solid circular cross section, and when only billet-container friction has been considered, billet-die friction assumed to be insignificant. A complex cross section obviously requires a higher extrusion force. As described earlier, the most basic definition of **complexity index** for a given die profile is that it is *the ratio of the pressure required to extrude the profile relative to the extrusion pressure for a round cross section of the same area.*

To determine the shape complexity of any profile by this definition, we must first experimentally determine the actual extrusion force or pressure required to extrude that profile under the given conditions of ram speed, billet and container temperatures, lubrication agent and method used, etc. We then have to determine the pressure required to extrude a simple solid circular cross section of the same area as the profile under consideration, under the same extrusion environment. Complexity index would then be the *ratio of the two pressures.*

This method entails several problems. Complexity index, both intuitively and by definition, should be a *function of geometry (shape) only.* But the above definition would involve non-geometric factors such as ram speed, friction coefficients, temperatures, etc.

Complexity index for the same profile would then be different under different operating conditions; not an acceptable scenario.

The four complexity definitions found in published literature were reported in chapter-1 (equations 1.15 to 1.19). Unfortunately, these definitions do not yield a consistent ranking of die profiles in terms of shape complexity. When actual pressure curves for dies of a wide range of complexity are studied, none of these definitions gives the same order of increasing profile complexity as the ascending pressure curves obtained. Moreover, the extrusion pressure predicted by these definitions (based on the pressure mathematically obtained for a solid section of equal area) often gives widely fluctuating values. It thus appears necessary to coin a new and more consistent and robust definition of extrusion shape complexity.

3.4 Experimentation and Data Collection

All extrusion runs for this study were carried out in collaboration with ALUPCO, Dammam. The environment was commercial hot extrusion of structural aluminum sections. A total of twenty seven (27) different dies were used, profile complexity ranging from simple solids and hollows to quite complex ones. Die material (heat treated and surface hardened H-13 steel) and billet material (Al-6063) remained the same for all experiments. Various runs at a ram speed of 3.8 ± 0.1 mm/s were carried out for 15 different die profiles, while another set of 12 profiles were extruded at 3.2 ± 0.1 mm/s speed.

As before, a broad classification of solid (S), hollow (H) and semihollow (SH) is used for identification of profile type. Sketches of some of the profiles used in the study are shown in Fig 3.2. Geometrical and other relevant data of the die profiles included in the study are summarized in Table 3.1. Terminology used has been explained earlier in Table 1.2. Section perimeter (P_s), section area (A_s), and circumscribing circle diameter (CCD) of the profiles are calculated from manufacturer's profile drawings for each die.

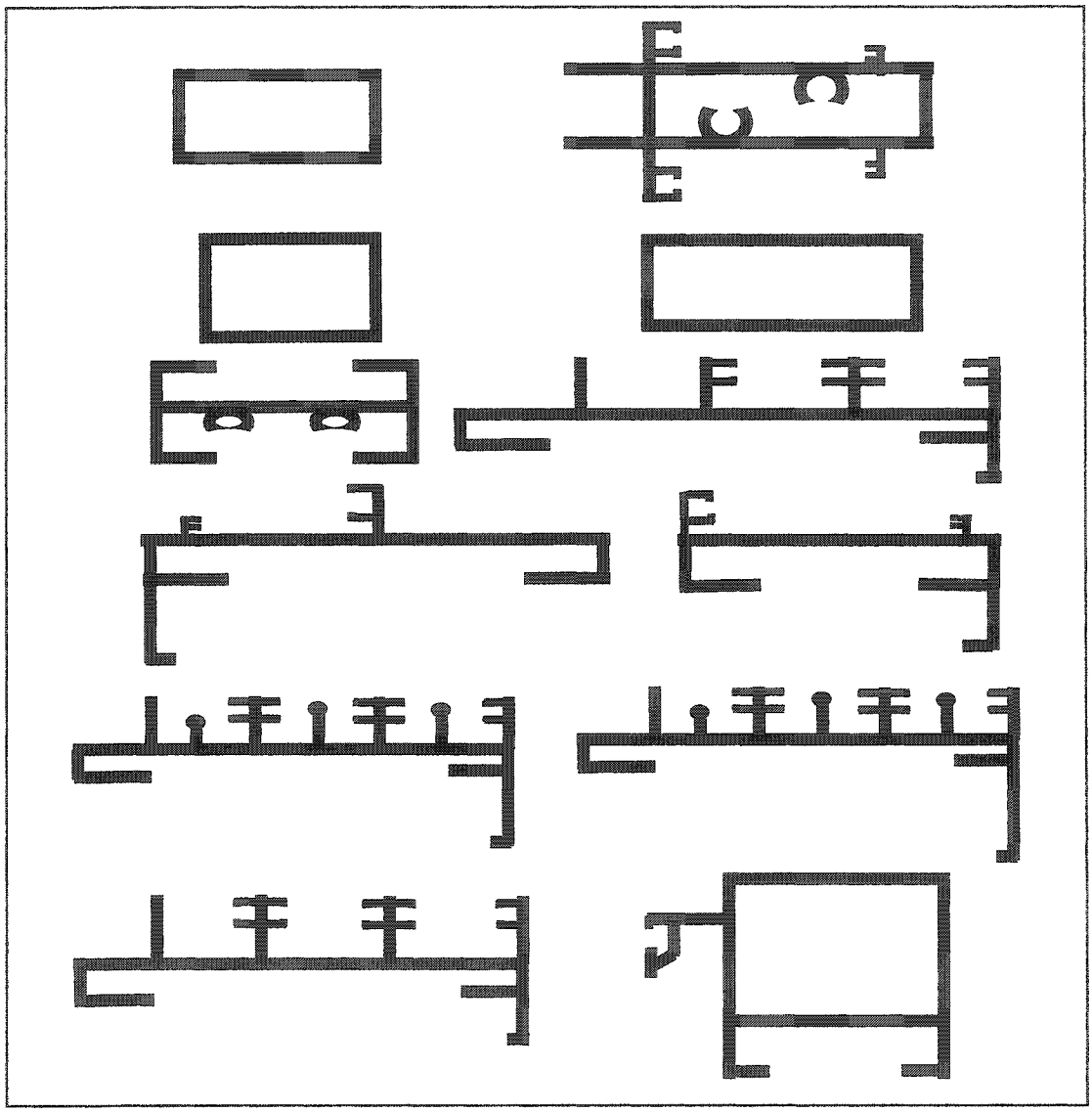

Figure 3.2 Sketches of some of the die profiles used in the study

Table 3.1 Geometrical data of profiles studied

S. No.	Die Type	Die No.	Ram Speed (mm/s)	P_s (mm)	P_0 (mm)	A_s (mm^2)	W_s (g/m)	T_m (mm)	*CCD* (mm)	Billet Length (mm)	*n*	*R*
Ram Speed: 3.8 ± 0.1 mm/s												
1	S	D1	3.7	545	67.63	364	983	1.35	116.62	715	2	74.62
2	H	D2	3.7	120	43.27	149	403	1.3	44.72	560	6	60.77
3	SH	D3	3.7	228	51.49	211	570	1.3	50.09	684	4	64.37
4	H	D4	3.8	160	50.26	201	543	1.3	56.57	500	4	67.57
5	H	D5	3.8	288	57.82	266	718	1.3	62.29	780	4	51.06
6	S	D6	3.8	395	57.82	266	718	1.3	97.62	510	2	102.12
7	S	D7	3.8	404	57.49	263	710	1.3	100.12	522	3	68.85
8	H	D8	3.8	135	40.88	133	359	1.1	41.8	798	6	68.08
9	H	D9	3.8	160	46.36	171	462	1.1	56.57	763	4	79.42
10	SH	D10	3.8	229	47.95	183	494	1.1	54.64	770	4	74.21
11	H	D11	3.8	362	103.41	851	2298	2.7	103.64	866	1	63.84
12	SH	D12	3.9	336	62.92	315	851	1.3	77.39	716	3	57.49
13	H	D13	3.9	240	61.91	305	824	1.3	89.44	741	2	89.06
14	H	D14	3.9	350	71.34	405	1093	1.8	83.63	852	2	67.07
15	S	D15	3.9	272	112.77	1012	2732	2	96.38	933	1	53.68
Ram Speed: 3.2 ± 0.1 mm/s												
16	H	D16	3.1	383	128.35	1311	3540	2.5	148.51	1122	1	41.44
17	H	D17	3.2	280	66.98	357	964	1.3	107.7	864	2	76.09
18	H	D18	3.2	247	57.92	267	721	1.3	61.56	655	4	50.87
19	H	D19	3.2	230	60.58	292	788	1.3	101.12	725	2	93.02
20	S	D20	3.2	544	64.79	334	902	1.2	116.62	704	2	81.33
21	SH	D21	3.2	220	46.63	173	467	1.1	51	728	4	78.50
22	SH	D22	3.2	220	51.61	212	572	1.2	63.4	612	4	64.06
23	H	D23	3.2	248	55.71	247	667	1.1	61.56	787	3	73.31
24	H	D24	3.3	120	46.76	174	470	1.3	44.72	714	4	78.05
25	H	D25	3.3	276	64.10	327	883	1.3	91.75	744	2	83.07
26	SH	D26	3.3	294	53.88	231	624	1.1	62.29	730	3	78.39
27	H	D27	3.3	384	118.10	1110	2997	3	119.62	1051	1	48.94

Equivalent circle perimeter (P_0) is obtained from

$$P_0 = 2\sqrt{\pi A_s}\ . \tag{3.3}$$

Extrusion ratio for a multi-cavity die is given by [Saha 2000]

$$R = \frac{Billet\ Area}{\text{Pr}ofile\ Area} = \frac{\pi D_b^{\,2}/4}{nA_s}, \tag{3.4}$$

where D_b is the billet or container diameter, and n is the number of cavities.

3.5 Proposed Complexity Index

The new definition of complexity index, proposed in this chapter, is founded on the premise that

1. complexity is a function of profile ratio (actual section perimeter to equivalent circle perimeter),
2. complexity of solid circular profile is 1.0, and
3. complexity is a function of the ratio of actual section pressure to pressure of equivalent circular profile (determined analytically).

The proposed complexity definition is based on the perimeter-ratio (P_s/P_0) based power law format, similar to the Altan formula (equation 1.19)

$$C = \alpha + \beta\left(\frac{P_s}{P_0}\right)^{\gamma}. \tag{3.5}$$

The constants α, β, and γ are determined statistically by regression of experimental hot extrusion data obtained for a variety of die complexities and somewhat different operating conditions, as reported above.

Ram speeds selected for this study were in the 3-4 mm/s range. Average extrusion temperature (accounting for billet and die preheat temperatures, container temperature, and temperature rise due to heats of friction and deformation) was worked out to be 460°C (733 K). Value of the average flow stress $\overline{Y}_f$ at this average working temperature

was found to be about 40 MPa, determined from temperature-flow stress charts shown in Fig 3.3 [Sheppard 1999].

After running a variety of regression runs, using various exponential, logarithmic and power law formats, the model proposed above for complexity index was determined to be the best suited. At the end of a large number of regression and curve-fitting runs, the final expression obtained (resulting in a consistently better value of the coefficient of determination, r^2) to characterize the *new complexity index* (C) is

$$C_5 = 0.95 + 0.05\left(\frac{P_s}{P_0}\right)^{1.5} . \qquad (3.6)$$

Table 3.2 lists the actual maximum pressure (p), and the maximum pressure for solid circular profile of an equivalent-area (p_0) for the 27 dies selected for the study. The flow stress value reported above is used to find extrusion pressure for the equivalent-area round profile through equation (1.9). Reference complexity index gives the pressure ratio p_s/p_0. Values of the four complexity indices reported in the literature (C_1 to C_4) are listed for each profile, together with the new C_5 value.

3.6 Results and Discussion

Values of complexity index for each die profile studied, according to the four definitions reported in literature as well as the new definition, are plotted in an *ascending order* in Fig 3.4. The third definition ($C_3 = CCD/T_m$) has not been included in the comparison, as its values are too far from those of all other definitions. Following observations can be made:

1. The curve that follows the reference curve, ratio of actual to circular-area pressure (p_s/p_0), most closely is that for the newly proposed definition (C_5).
2. The next best approximation is for C_4, the definition suggested by Altan et al, though it exhibits large discrepancies for a few profiles. For lower complexities, both the power-law definitions (Altan formula C_4 and new definition C_5) yield

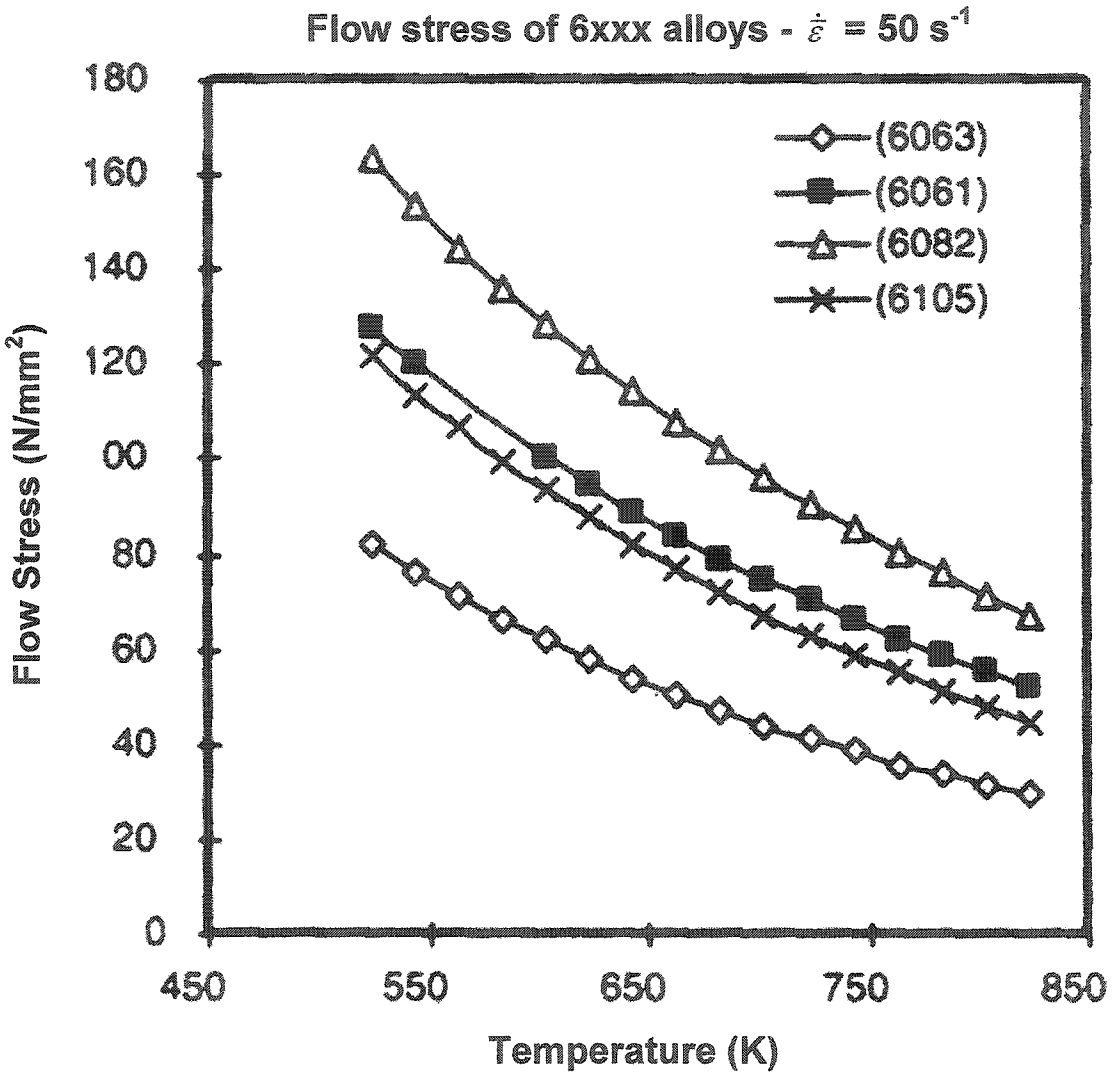

Figure 3.3 Flow stress at elevated temperatures for 6xxx aluminum alloys, including strain rate effect [Sheppard 1999]

Table 3.2 Proposed complexity index (C_5) compared with existing ones

S. No.	Die Type	Die #	Ram Speed (mm/s)	p_s (MPa)	p_0 (MPa)	Reference C (p_s/p_0)	C_1	C_2	C_3	C_4	C_5
1	S	D1	3.7	596.41	389.99	1.53	1.50	0.55	86.39	3.17	2.09
2	H	D2	3.7	478.60	334.62	1.43	0.81	0.30	34.40	1.18	1.18
3	SH	D3	3.7	535.66	374.64	1.43	1.08	0.40	38.53	1.55	1.42
4	H	D4	3.8	498.85	320.62	1.56	0.80	0.29	43.52	1.25	1.23
5	H	D5	3.8	441.78	394.58	1.12	1.08	0.40	47.92	1.72	1.51
6	S	D6	3.8	460.19	340.18	1.35	1.48	0.55	75.09	2.49	1.84
7	S	D7	3.8	425.22	328.06	1.30	1.54	0.57	77.02	2.59	1.88
8	H	D8	3.8	640.59	411.56	1.56	1.02	0.38	38.00	1.27	1.25
9	H	D9	3.8	511.73	407.08	1.26	0.94	0.35	51.43	1.30	1.27
10	SH	D10	3.8	592.73	406.50	1.46	1.25	0.46	49.67	1.65	1.47
11	H	D11	3.8	497.01	429.68	1.16	0.43	0.16	38.39	1.32	1.28
12	SH	D12	3.9	572.48	379.86	1.51	1.07	0.39	59.53	1.85	1.57
13	H	D13	3.9	522.78	404.97	1.29	0.79	0.29	68.80	1.40	1.33
14	H	D14	3.9	554.07	427.39	1.30	0.86	0.32	46.46	1.70	1.49
15	S	D15	3.9	509.89	443.12	1.15	0.27	0.10	48.19	1.13	1.14
16	H	D16	3.1	585.36	490.26	1.19	0.29	0.11	59.40	1.21	1.21
17	H	D17	3.2	565.12	436.09	1.30	0.78	0.29	82.85	1.48	1.38
18	H	D18	3.2	491.48	356.41	1.38	0.93	0.34	47.35	1.50	1.39
19	H	D19	3.2	484.12	401.85	1.20	0.79	0.29	77.78	1.38	1.32
20	S	D20	3.2	502.53	390.08	1.29	1.63	0.60	97.18	3.38	2.17
21	SH	D21	3.2	566.96	395.97	1.43	1.27	0.47	46.36	1.64	1.46
22	SH	D22	3.2	539.34	352.55	1.53	1.04	0.38	52.83	1.50	1.39
23	H	D23	3.2	566.96	411.18	1.38	1.00	0.37	55.96	1.56	1.42
24	H	D24	3.3	570.64	391.48	1.46	0.69	0.26	34.40	1.15	1.16
25	H	D25	3.3	511.73	403.10	1.27	0.84	0.31	70.58	1.51	1.40
26	SH	D26	3.3	524.62	396.52	1.32	1.27	0.47	56.63	1.89	1.59
27	H	D27	3.3	522.78	475.32	1.10	0.35	0.13	39.87	1.26	1.24

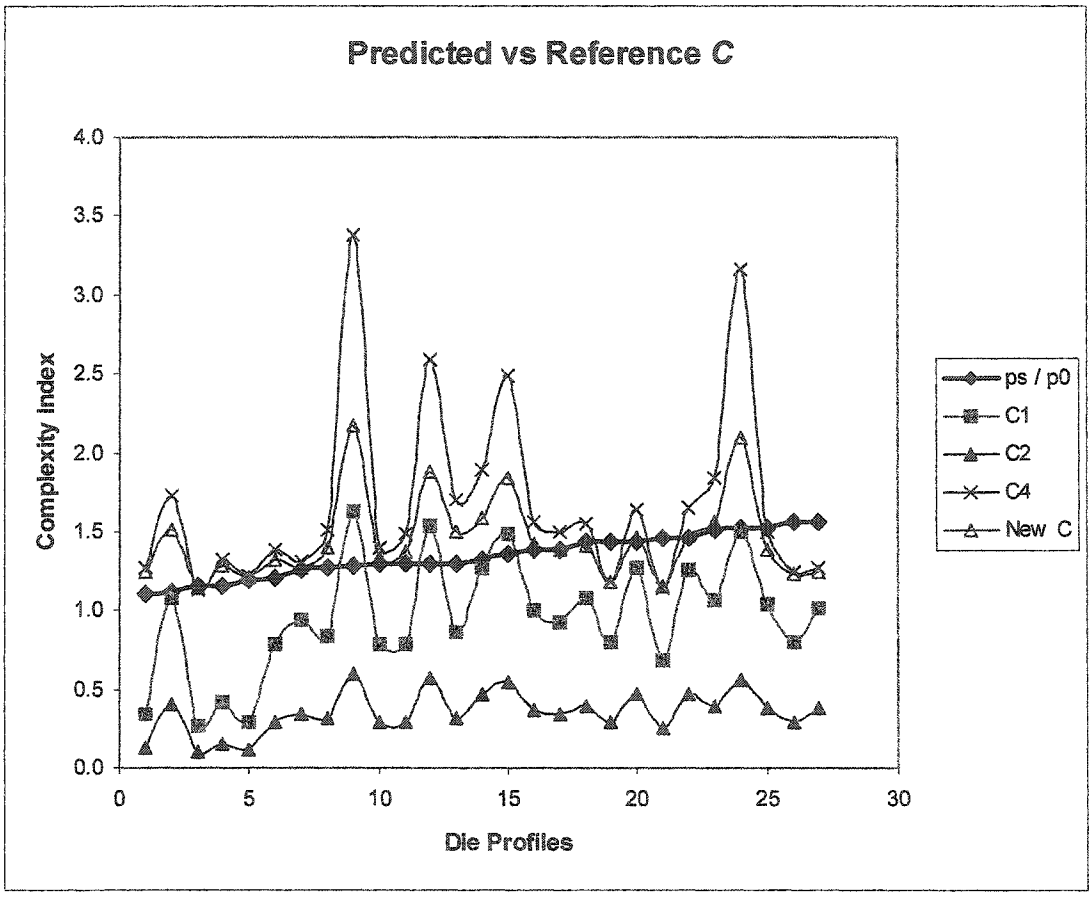

Figure 3.4 Comparison of complexity indices (C) with reference C (p_s / p_0); proposed definition yields closest values.

quite similar values. However, as complexity increases, the two definitions give significantly different values.

3. C_1 and C_2 display the largest deviations from reference behavior, C_2 being the worst case.
4. An interesting conclusion is that though all definitions predict different values of complexity, the *trend* in all the curves is similar.

Table 3.3 lists the actual maximum ram pressure (p) encountered in each extrusion run, the predicted maximum extrusion pressure according to the five complexity definitions, and the percentage error in prediction. Average error for each definition is shown in bold in the last row of the table. Referring to equation (3.1) given above, the predicted pressure for a complex profile, in terms of the calculated pressure for a simple solid circular profile of equivalent area (using equation 1.9), would be

$$\text{Predicted } p_s = C * p_0. \tag{3.7}$$

As the actual section pressure recorded experimentally is p_s, the error in prediction (predicted versus actual section pressure) comes out to be

$$\begin{aligned} \%\ Error &= 100 * (\text{Predicted } p_s - \text{Actual } p_s) / (\text{Actual } p_s) \\ &= 100 * (C * p_0 - p_s) / p_s \end{aligned} \tag{3.8}$$

Following observations can be made from the table:

1. Smallest average error (8.59 %) is observed for the newly proposed complexity model.
2. Next best approximation (24.86% average error) is exhibited by C_4, the Altan formula, which is similar to the newly proposed model but its parameters provide lesser accuracy in prediction.
3. Definition $C_3 = CCD / T_m$ yields extremely large errors, and should thus be excluded from the comparison.

Table 3.3 Actual and predicted maximum pressure (p) values and error comparison

				Predicted p (MPa)					Percent Error				
S. No.	Die Type	Die No.	p_s (MPa)	C_1	C_2	C_3	C_4	C_5	C_1	C_2	C_3	C_4	C_5
1	S	C1	596.4	583.9	216.2	33689.2	1235.5	816.5	-2.1	-63.7	8538.5	107.2	36.9
2	H	C2	478.6	269.5	99.6	11511.1	394.4	395.2	-43.7	-79.2	3340.0	-17.6	-17.4
3	SH	C3	535.7	404.8	149.9	14435.3	580.2	530.4	-24.4	-72.0	3753.1	8.3	-1.0
4	H	C4	498.8	255.2	94.5	13951.8	401.0	395.6	-48.8	-81.1	4251.5	-19.6	-20.7
5	H	C5	441.8	427.2	158.3	18906.5	679.2	594.2	-3.3	-64.2	4691.5	53.7	34.5
6	S	C6	460.2	505.2	187.1	25544.7	846.8	626.9	9.8	-59.3	7409.2	84.0	36.2
7	S	C7	425.2	503.9	186.7	25265.8	849.1	617.2	18.5	-56.1	7601.5	99.7	45.2
8	H	C8	640.6	417.8	154.8	15639.4	524.3	514.5	-34.8	-75.8	3700.0	-18.1	-19.7
9	H	C9	511.7	380.9	141.0	20935.2	531.1	517.2	-25.6	-72.5	5042.7	3.8	1.1
10	SH	C10	592.7	508.7	188.4	20191.9	672.4	598.3	-14.2	-68.2	4867.3	13.4	0.9
11	H	C11	497.0	182.8	67.7	16493.2	565.1	548.9	-63.2	-86.4	3738.5	13.7	10.4
12	SH	C12	572.5	405.2	150.0	22613.2	701.6	595.3	-29.2	-73.8	5853.1	22.6	4.0
13	H	C13	522.8	318.7	118.0	27862.0	567.7	539.3	-39.0	-77.4	6780.0	8.6	3.2
14	H	C14	554.1	369.4	136.9	19857.1	725.0	638.2	-33.3	-75.3	4546.1	30.9	15.2
15	S	C15	509.9	119.1	44.1	21354.2	498.5	504.0	-76.6	-91.3	4719.0	-2.2	-1.2
16	H	C16	585.4	143.2	53.0	29123.4	595.2	592.1	-75.5	-90.9	5840.4	1.7	1.2
17	H	C17	565.1	342.0	126.7	36128.2	645.3	600.7	-39.5	-77.6	8184.6	14.2	6.3
18	H	C18	491.5	329.7	122.1	16877.3	535.5	495.5	-32.9	-75.2	4635.4	9.0	0.8
19	H	C19	484.1	316.5	117.3	31257.4	555.5	530.4	-34.6	-75.8	7678.5	14.8	9.6
20	S	C20	502.5	635.3	235.3	37909.5	1318.7	845.2	26.4	-53.2	9618.3	162.4	68.2
21	SH	C21	567.0	503.5	186.5	18358.7	647.9	579.1	-11.2	-67.1	4536.4	14.3	2.1
22	SH	C22	539.3	365.9	135.6	18626.6	529.6	490.0	-32.2	-74.9	5183.3	-1.8	-9.1
23	H	C23	567.0	412.8	152.9	23011.2	639.7	583.7	-27.2	-73.0	5496.4	12.8	3.0
24	H	C24	570.6	270.0	100.0	13467.0	448.9	452.4	-52.7	-82.5	3340.0	-21.3	-20.7
25	H	C25	511.7	340.2	126.0	28449.4	610.3	563.0	-33.5	-75.4	6957.7	19.3	10.0
26	SH	C26	524.6	504.7	186.8	22453.9	749.5	629.4	-3.8	-64.4	5562.7	42.9	20.0
27	H	C27	522.8	164.4	60.9	18952.6	600.8	590.9	-68.5	-88.4	3887.3	14.9	13.0
						Average Error (%)			**-29.5**	**-73.9**	**5546.4**	**24.9**	**8.6**

4. The first two definitions, C_1 and C_2, give negative errors indicating non-conservative pressure prediction, which should be avoided for realistic calculations of power requirement and press capacity, etc.

Maximum extrusion pressure (p) values are plotted for each die profile (in an ascending order) in Fig 3.5. Some noticeable conclusions are:

1. The actual p curve is most closely approximated by the curve for the proposed definition (C_5).
2. The next best prediction is for C_4 (Altan model). However, there are large deviations for some profiles. Discrepancy between C_4 and C_5 becomes noticeable at higher complexities.
3. C_1 and C_2 both yield p-values significantly lower than the actual ones, C_2 giving the largest overall error. Altan and the proposed complexity models thus yield *conservative* estimates of maximum extrusion pressure.
4. Once again, the variation *trend* in all the curves (including the actual p plot) is almost the same, though all definitions predict different values.

The Altan formula (definition C_4) yields much closer pressure predictions compared to the other complexity definitions, but still results in relatively large errors (average error of around 25%) when actual profiles of varying complexity are studied; thus the need for a new complexity index. As stated earlier, the new definition (C_5) follows the same power-law model as C_4, and is also based on the perimeter ratio (P_s/P_0) described by equation (3.4). Values of the parameters α, β, and γ are obviously different. Figure 3.6 gives a comparison of the complexity values obtained by the two definitions, profiles being arranged in increasing order of complexity. For profiles of lower complexity, both definitions yield similar values. For more complex profiles, the difference between C_4 and C_5 becomes significant, C5 values being much closer to the reference complexity index (p_s/p_0).

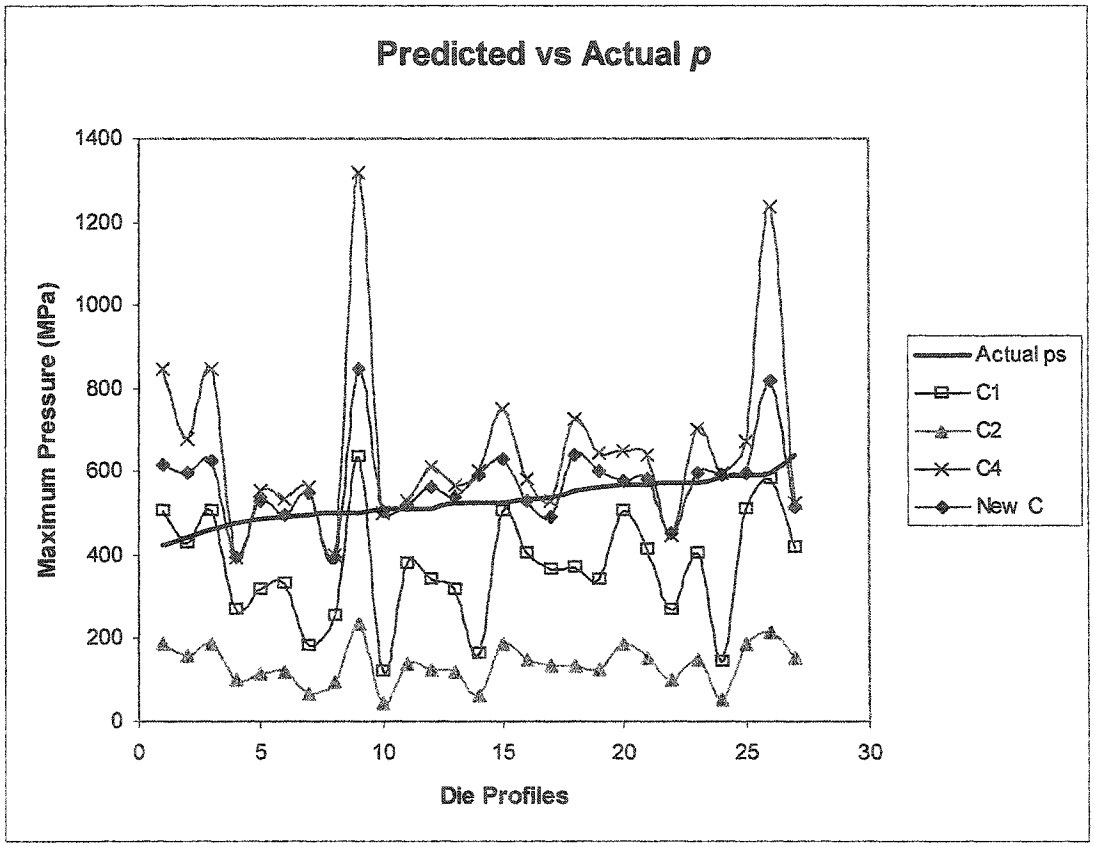

Figure 3.5 Comparison of predicted and actual maximum pressure values; proposed complexity index results in lowest error.

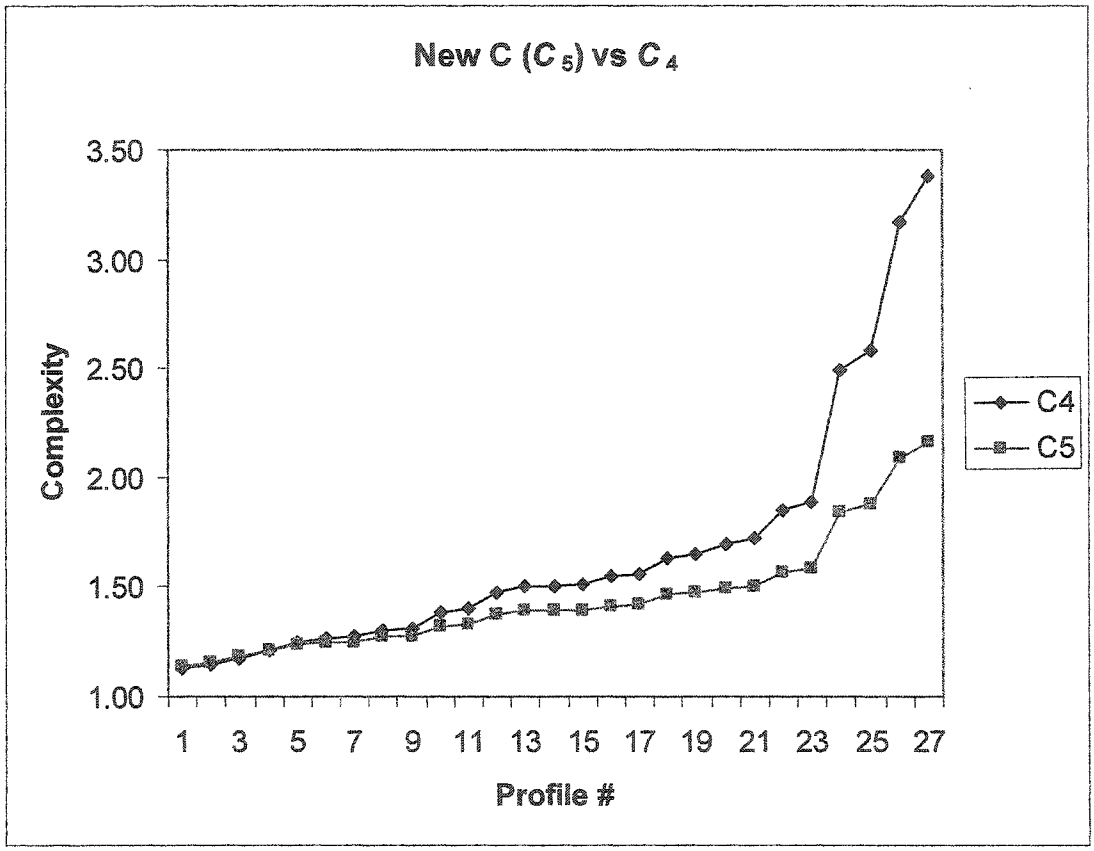

Figure 3.6 Comparison of the new complexity index (C_5) and the Altan formula (C_4); differences become significant at higher complexities.

CHAPTER 4
EXTRUSION PROCESS: DEFORMATION BEHAVIOR

4.1 INTRODUCTION

In extrusion, the desired shape is obtained by plastic deformation of the billet material achieved by forcing it through a die. In any simple homogeneous and uniaxial compression (or tension), the metal flows plastically when the stress (σ) reaches the value of the flow stress ($\bar{\sigma}$). Once the applied force exceeds the shear strength of the material, sticking friction at the container surface becomes the dominant friction mode, and deformation takes place through shear in the bulk of the material.

4.1.1 Investigation of Cold Extrusion

Experiments and analysis presented in the preceding chapters were in the domain of hot aluminum extrusion, with emphasis on pressure variation and pressure prediction. Study of cold extrusion is equally important, especially because of two major factors.

1. Friction effects (which play a significant role in the variation of pressure, temperature, metal flow, and product quality) become negligible in hot extrusion in comparison with cold extrusion.
2. Strain hardening behavior of billet material, which can critically affect metal flow and other process parameters, is again insignificant in hot extrusion as compared to cold working.

4.1.2 Current Work

Among other important issues in metal extrusion, *optimization of metal flow* ranks at the very top. It is of crucial importance as it directly affects extrusion speed (essential for higher productivity), extrusion pressure and internal friction (resistance offered by the

dead metal zone adds to the other factors that contribute to pressure behavior), mechanical properties and surface finish of the extruded product, etc. It is reasonable to assume that material flow properties, die-workpiece and container-workpiece heat transfer and friction conditions, die profile, and die design all affect metal flow. However, the mechanism of dead zone formation is not understood well enough to forecast with an acceptable degree of accuracy what is happening. Predictive numerical models are limited because of this lack of perception of the physics of the process [Stambler 1997].

Experimental and Numerical Study: Results are presented in this chapter from an experimental and numerical investigation of cold extrusion. Experiments have been performed on flat-face dies, fabricated from H13 tool steel and heat treated and surface hardened to approximately the same specifications as commercial extrusion dies. Three workpiece materials have been experimented with: Al-6063 as it is the most common aluminum alloy in the construction sector, and pure aluminum and lead for their better extrudability. Extrusions have been carried out at four different speeds. Numerical modeling has been done using commercial finite element packages, for a range of variation of different extrusion parameters.

Study of Deformation Behavior: It has been established by various studies that the size and shape of the dead metal zone, and the pattern and homogeneity of flow lines in extrusion are directly related to the die cone angle α, to friction at the billet-container interface, and to a lesser extent at the billet-die interface friction. However, there are several other factors that can significantly affect extrusion metal flow. Unfortunately, these aspects have not been examined in detail in most of the published literature. Many studies use model materials (such as plasticine) for metal flow study, lack of real material properties contributing to inconsistencies with actual metal behavior. Numerical investigations are generally limited to the discussion of only one or two factors at a time. Also, enough experimental data is usually not available for satisfactory validation of numerical models, especially for metal flow pattern and dead metal zone analysis. The current study focuses on a comprehensive investigation, covering both *experimental and numerical* aspects, of *metal flow pattern and dead metal zone formation* in cold extrusion.

A number of actual billet materials have been studied, and the die material is the same as the one most commonly used in commercial hot and cold extrusion. Contribution and interrelationship of five important factors are investigated:

(i) Ram speed

(ii) Billet material

(iii) Extrusion pressure

(iv) Extrusion ratio

(v) Shape complexity.

All the complexity definitions discussed so far (including the new definition proposed in chapter-2) are considered here for analysis. Definition C_2 has been dropped from the analysis because of its similarity to definition C_1. As explained earlier, $C_1 = P_s/A_s$ and $C_2 = P_s/W_s$ differ by only a constant multiple (material density), and are thus essentially the same.

4.2 EXPERIMENTATION

An extrusion chamber assembly (consisting of container, bolster and ram) and three different compatible dies were designed and manufactured in collaboration with a commercial extrusion setup. Geometric details of the three dies are given in Table 4.1 and shown through sketches in Fig 4.1. Figure 4.2 (a) illustrates the actual dies, while Fig 4.3 shows all the components of the extrusion chamber assembly. To emulate real world extrusion environment, these flat-face dies (90° die angle) were fabricated from H13 die steel (in collaboration with a commercial extrusion die manufacturing plant). Advanced machining techniques such as EDM were employed, and dies were later subjected to standard heat treatment and surface hardening routines. Split billets of aluminum, lead, and Al-6063 were prepared to study metal flow patterns and dead metal zones; Fig 4.2 (b). A 250-kN Instron universal testing machine, fitted with an extensometer (LVDT) and hooked up to a computer through a data logger, was used in the compression mode to perform and record the cold extrusion experiments; Fig 4.4.

Table 4.1 Geometrical details, and complexity indices, of the die profiles studied

Die #	D_b	P_s	A_s	P_0	T_m	CCD	R	C_1	C_3	C_4	C_5
D1	19	43.98	153.9	43.98	14	14	1.84	0.29	1.00	1.00	1.00
D2	19	56	148.8	43.23	2.5	18.45	1.91	0.38	7.38	1.02	1.02
D3	19	60.8	138.9	41.78	5.6	21.5	2.04	0.44	3.84	1.03	1.04

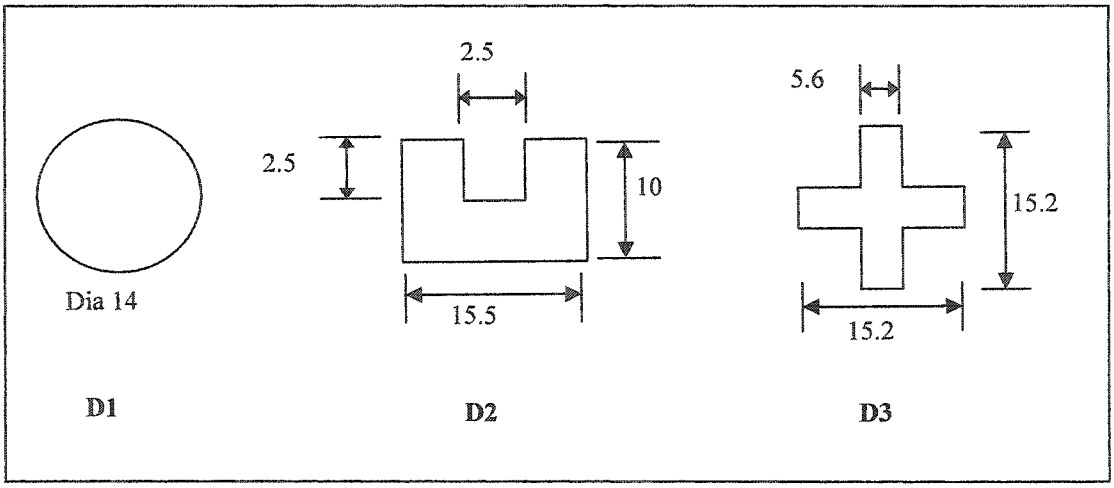

Figure 4.1 Profiles and dimensions of the dies used in the study, diameter of the cylindrical billet being 19 mm for all cases

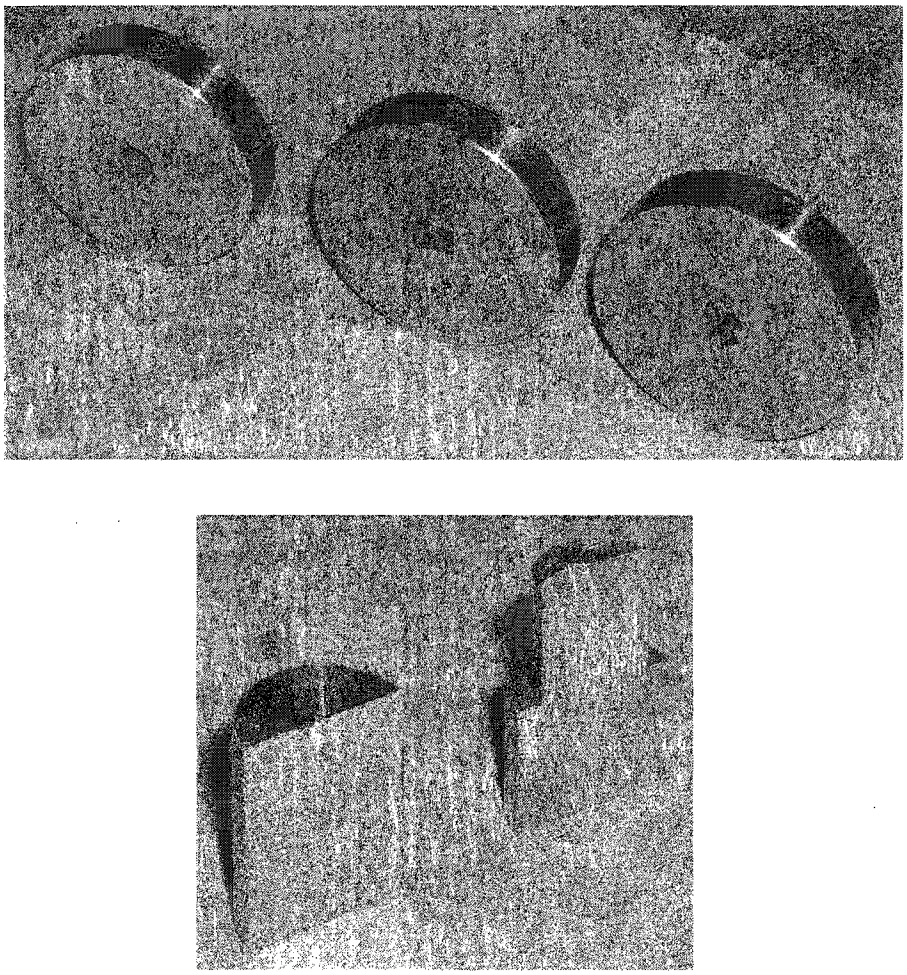

Figure 4.2 Photographic exhibits of the three dies (above) and the split cylindrical billet before and after extrusion (below)

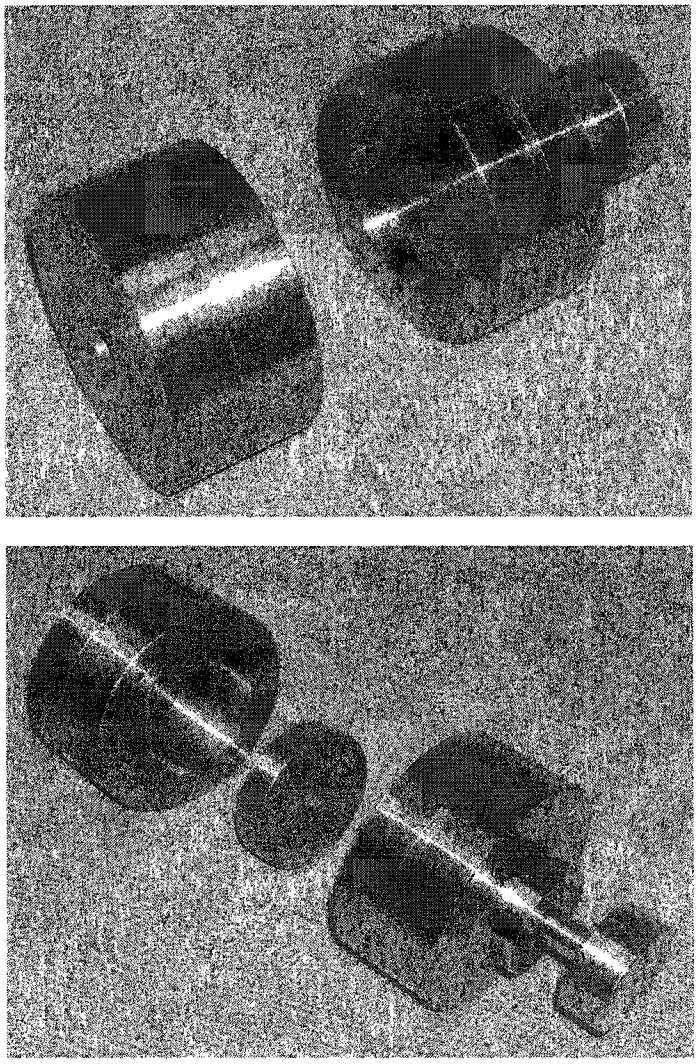

Figure 4.3 Components of the extrusion chamber assembly: two-piece container, die backer, die, and ram (plunger)

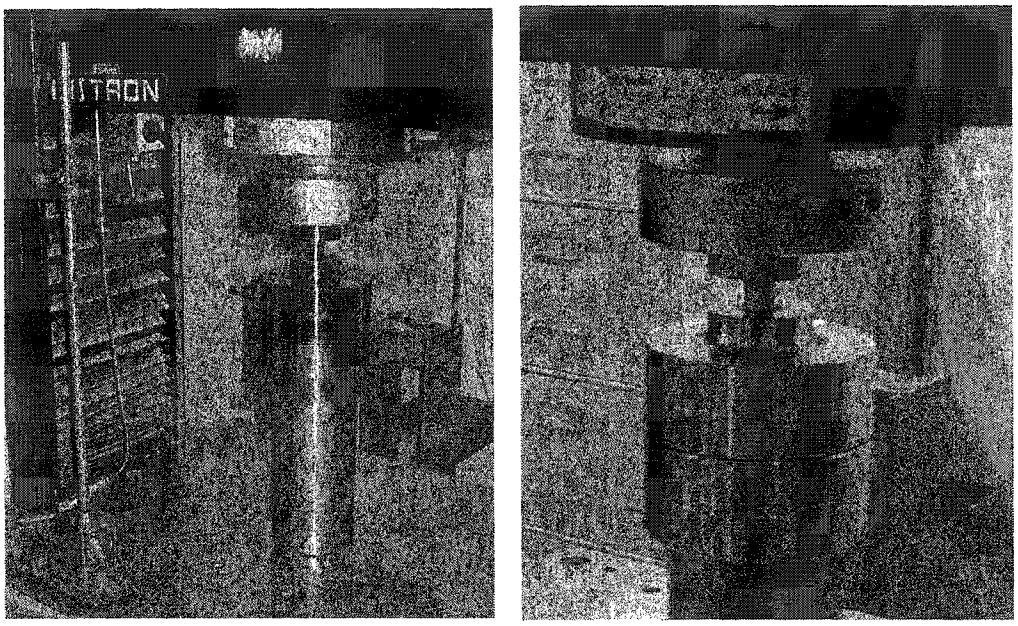

Figure 4.4 Experimental setup: extrusion chamber assembly fixed in a universal testing machine (used in compression mode), serving as an extrusion press

Each split billet was partially extruded, so that metal flow pattern and dead metal zone at the leading end of the unextruded billet could be studied. Various extrusion runs were carried out through each die, using the three billet materials in turn, and employing four different ram speeds (1 mm/min, 2 mm/min, 5 mm/min and 10 mm/min). All the experiments were carried out under cold conditions (room temperature). To avoid possible deterioration of the split surface due to excessive sticking friction, aluminum and Al-6063 billets were annealed to improve their ductility and flow characteristics, and a clear lubricant (petroleum jelly) was used during extrusion. Metal flow pattern and dead metal zone from each extruded sample were studied under a microscope, and recorded. Standard etching techniques were sometimes utilized for better visualization. Values of ram force exerted at different locations (as the ram advanced along the container) were recorded in the computer through the data logger.

4.3 Numerical Modeling and Computer Simulation

Extrusion runs on the three dies were simulated using the commercial finite element package ANSYS 7.0. To study the dynamic effects of changing ram speed, the software utilized was ANSYS-LSDYNA. Lead and aluminum being soft metals, further softened by annealing, billet material was modeled as elastic-perfectly plastic. As the container, die and billet surfaces were highly polished, and as a lubricant was also used, coefficient of friction was assumed to be negligible. Properties of the different billet materials used in the actual experiments and the finite element simulations are listed in Table 4.2.

Due to the symmetrical nature of the solid circular die (die #1), a 2D model was deemed to be sufficient, with an axis of symmetry along the line representing the split billet surface; Fig 4.5. The 2D 6-node triangular structural solid element PLANE2 (possessing plasticity, large deformation and large strain capabilities) was used in the axisymmetric mode to model the material geometry in ANSYS. As ANSYS-LSDYNA has a different set of element types, the explicit 2D structural solid element PLANE162 (capable of representing translations, velocities and accelerations) was used for explicit dynamic analysis. Meshing was done using 1210 elements, grid refinement being used

Table 4.2 Mechanical properties of materials used in the study [Callister 2000, Shigley et al. 2004]

Material	Elastic Modulus (GPa)	Yield Strength (MPa)	Poisson's Ratio	Density / Unit Weight (kN/m^3)
Lead	36.5	10.34	0.425	111.5
Annealed Aluminum	71	27.56	0.334	26.6
Annealed Al-6063	71	48.23	0.334	26.6
Al-6063 T6	71	172.25	0.334	26.6
Carbon Steel C1010	207	192.92	0.292	76.5
Stainless Steel 304	190	378.95	0.305	76

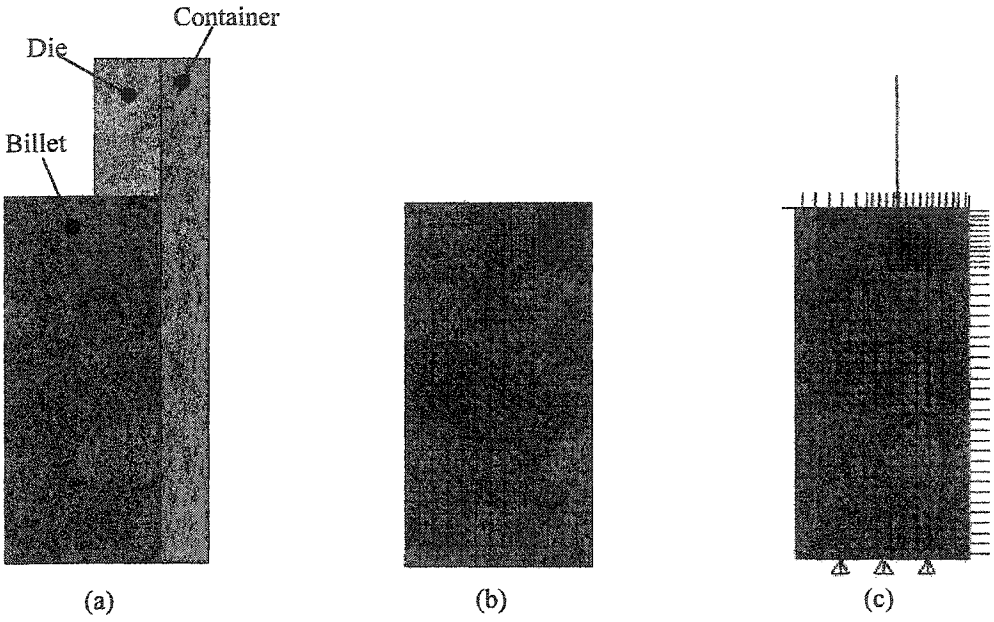

Figure 4.5 2D axisymmetric representation of the extrusion layout (a), finite element meshing of the billet (b), billet-container and billet-die contact pairs and applied load (c)

near the die entrance area of the billet to assist smooth flow of elements in the dead metal zone and surrounding regions. Contacts were defined at the billet-container and billet-die interfaces, container and die being modeled as rigid materials. Load was applied (in the form of displacement in ANSYS, and as velocity in ANSYS-LSDYNA) at the free end of the billet to replicate the ram pressure.

To represent the shape and geometry of the other two dies, 3D modeling had to be used. The 8-node 3D structural solid element SOLID164 was used for explicit dynamic analysis in ANSYS-LSDYNA. Die #2, having only one axis of symmetry, had to be modeled as shown in Fig 4.6 Model for die #3, possessing biaxial symmetry, is depicted in Fig 4.7. With grid refinement near the front end of the billet, 6737 elements were required by the solid model for die #2, and 21730 elements for die #3.

4.4 Results and Discussion

Photographs of metal flow patterns and dead metal zones, viewed through a microscope, and graphical outputs from numerical simulation are appended below. Photographs are generally identified by a tag number: digits for the die # and ram speed are separated by a dash in each case: tag number 1-10 represents extrusion through die #1 at a ram speed of 10 mm/min.

4.4.1 Deformation Zones

Consistent with the findings of published works, there were various regions of interest in cold metal extrusion in terms of metal flow. Four distinct regions could be identified from photographic records of metal flow, as illustrated by Fig 4.8. In the *dead metal zone* (*DMZ*), the metal does not flow as it does in the rest of the billet. The *shear zone* (*SZ*) is the region where material shearing begins to take place and which defines the shear direction. In the *general deformation zone* (*GDZ*), material flow takes on the shape and direction defined by the *SZ*, and it forms the larger region where material deformation takes place. The middle portion of the billet forms the *un-deformed zone* (*UDZ*), where

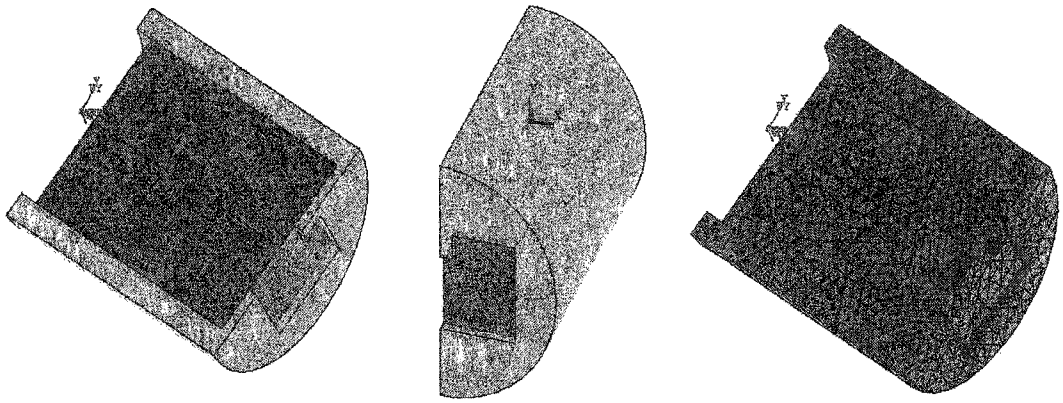

Figure 4.6 Two views of the 3D geometry and finite element mesh for the billet and die model of die #2

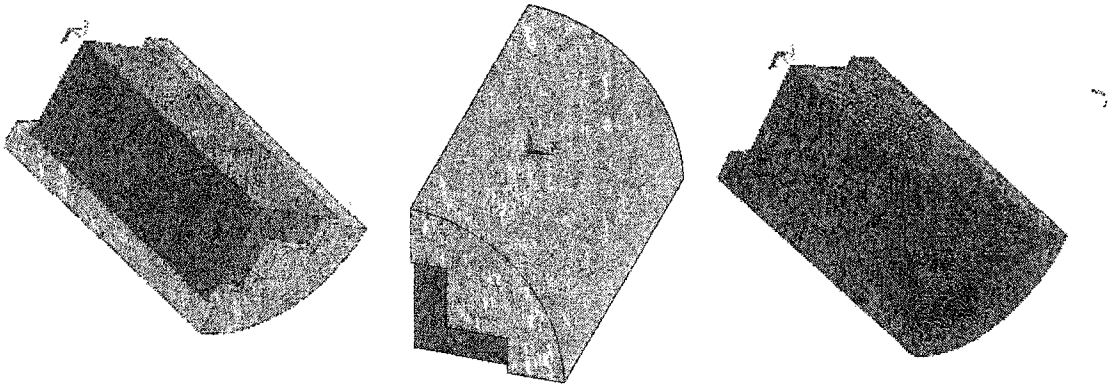

Figure 4.7 Solid modeling and finite element meshing for the billet and die arrangement of die #3

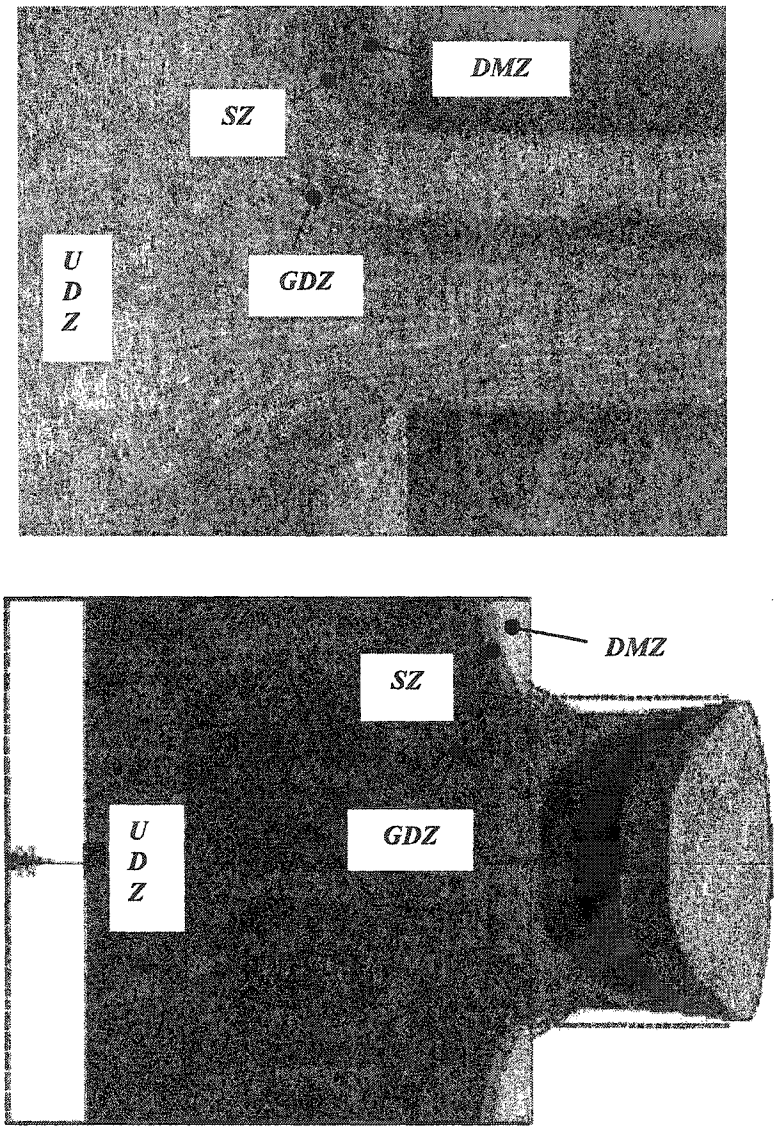

Figure 4.8 Actual photograph (above) and ANSYS simulation (below) showing various regions of metal flow in cold metal extrusion

metal flow takes place with no appreciable deformation. Numerical simulation gives an identical picture.

4.4.2 Evolution of Dead Metal Zone

Contrary to the notion that extrusion is a steady-state process, recent studies strongly suggest that the process is an evolving one. From a short-duration initial transient state it moves to a steady state for most of the extrusion run, and finally becomes non-steady again towards the end of the ram stroke. The process may have non-steady characteristics even during the so-called steady state [Lee et al. 2002, Zhou and Duszczyk 2003]. Figure 4.9 shows ANSYS simulation of the gradual changes occurring in the dead metal and other deformation zones as extrusion moves from the transient state into the steady region. In accordance with the findings of current research, it can be clearly seen that geometry of the dead-metal-zone (regions of light and dark shade near the upper right corner) changes during extrusion. During the initial non-steady state, the deformation zone is built up with increasing strain rates toward the die entrance. As extrusion continues, the deformation zone expands towards the rear end and the periphery of the billet, while the dead metal zone undergoes some shrinkage. It should be pointed out here that actual experimental visualization of the evolving metal flow pattern and dead metal zone geometry (showing the situation at each incremental ram advance location) would be extremely difficult to obtain, while numerical simulation gives a revealing insight into the phenomenon.

4.4.3 Effect of Billet Material

We can see the consequence of changing the billet material while keeping die shape complexity and ram speed constant in Fig 4.10. As the material changes from the relatively hard and strong alloy (Al-6063) to the softer aluminum and lead, flow lines become sharper and more deeply gouged, dead metal zone becomes smaller and narrower, and flow lines get steeper. Differences in material properties affecting the deformation behavior of the metal can be the contributing factor. As expected, higher-

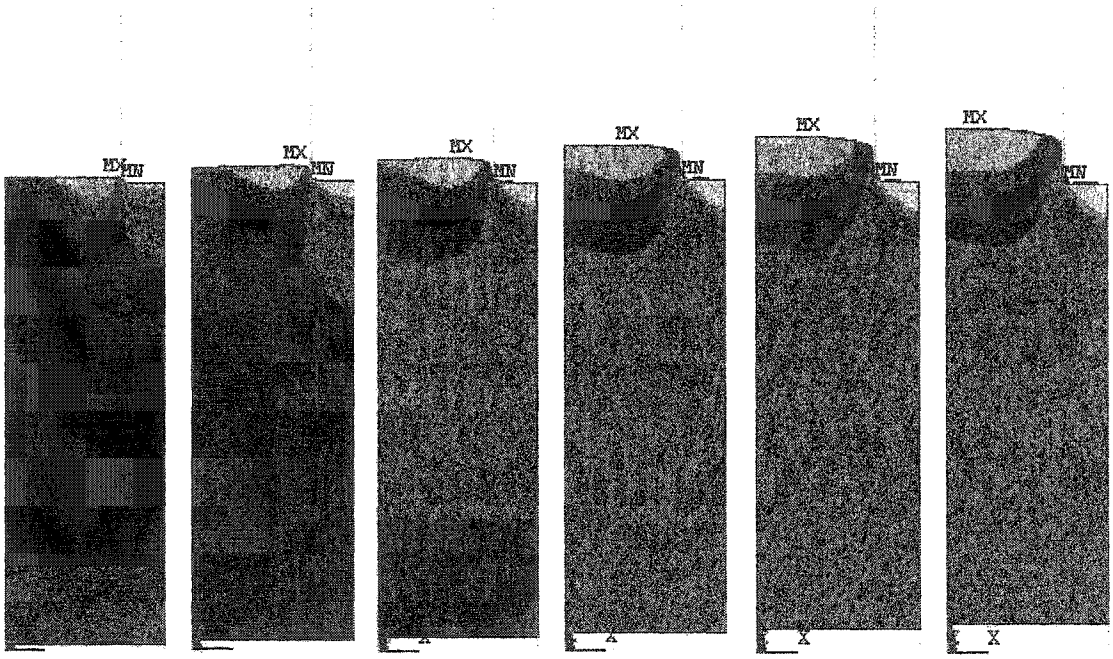

Figure 4.9 Evolution of DMZ after ram advance of 0.25, 0.5, 0.75, 1.0, 1.25 and 1.5 mm. During the initial extrusion stage, the DMZ increases in size, and then stabilizes.

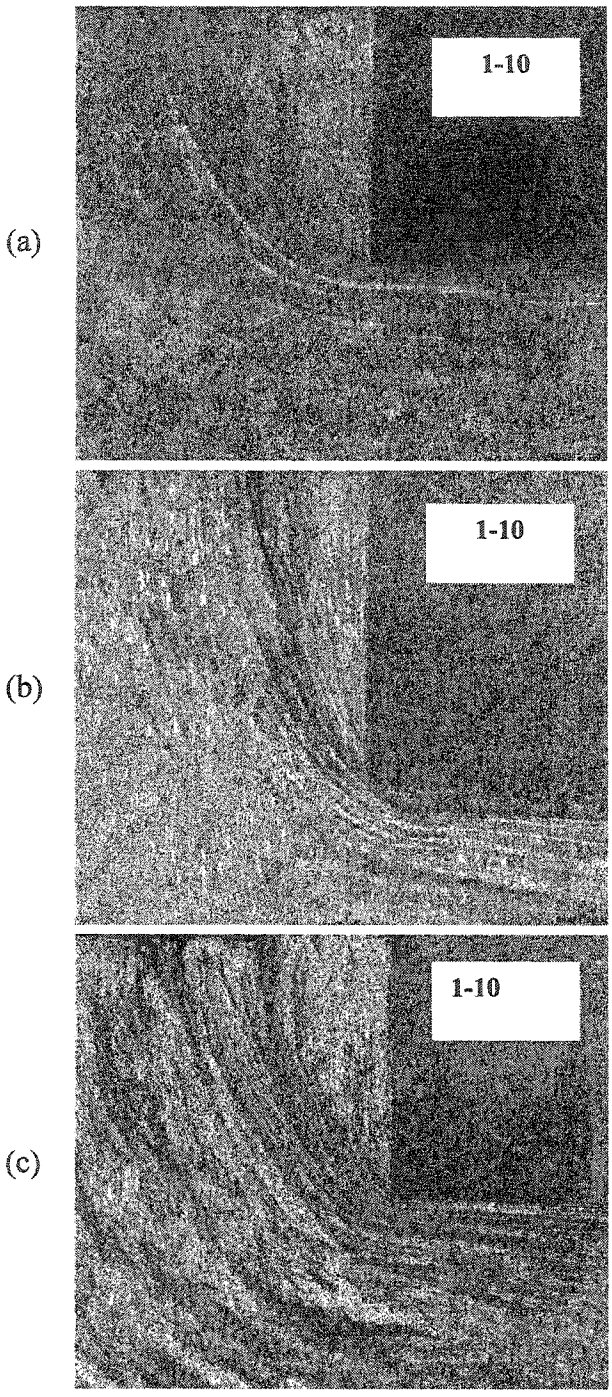

Figure 4.10 Metal flow pattern through the same die and at the same ram speed for three different materials: Al-6063 (a), aluminum (b), and lead (c)

strength billet materials produce larger and wider deformation zones as compared to the weaker metals.

Finite element simulation for the same materials strengthened these findings. To have a wider coverage of material types, simulations were carried out for all materials listed in Table 4.2. Figure 4.11 (a, b, c) shows the simulated flow pattern for the three metals used in the experiments, and for three metals of higher toughness: stainless steel 304, carbon steel C1010, and Al-6063 T6 (Fig 4.11 (d, e, f)). The trend of somewhat larger DMZ for higher-toughness material is reconfirmed. However, the variation in DMZ due to material change is not as significant as that observed due to other factors such as extrusion speed and extrusion ratio (described in the following pages).

4.4.4 Effect of Ram Speed

Figure 4.12 shows the effect of increasing ram speed on metal flow pattern when die profile remains the same (die # 1). Ram speed is increased from 1 mm/min to 10 m/min for Al and Pb. The observed trend appears to be independent of the billet material extruded. As the ram speed is increased, the general pattern is:

1. Flow lines become sharper and more well-defined.
2. Flow lines get steeper.
3. Dead metal zone becomes narrower and somewhat smaller in size.
4. Flow lines get more closely packed together.
5. Metal flow becomes more distorted.

ANSYS-LSDYNA simulations of extrusion runs at the same two speeds, carried out for Al-6061 T6 and pure aluminum, are shown in Fig 4.13. Behavior established from experimental photographs is again replicated in the simulation runs. Reduction in DMZ size may be due to the improved plasticity and reduced friction caused by the relatively higher temperatures at higher ram speeds. However, DMZ size is not the only decisive factor. Shape and orientation of the DMZ also play important roles. If the DMZ is oriented in such a way that metal flow is along an almost 45° plane, there is minimal

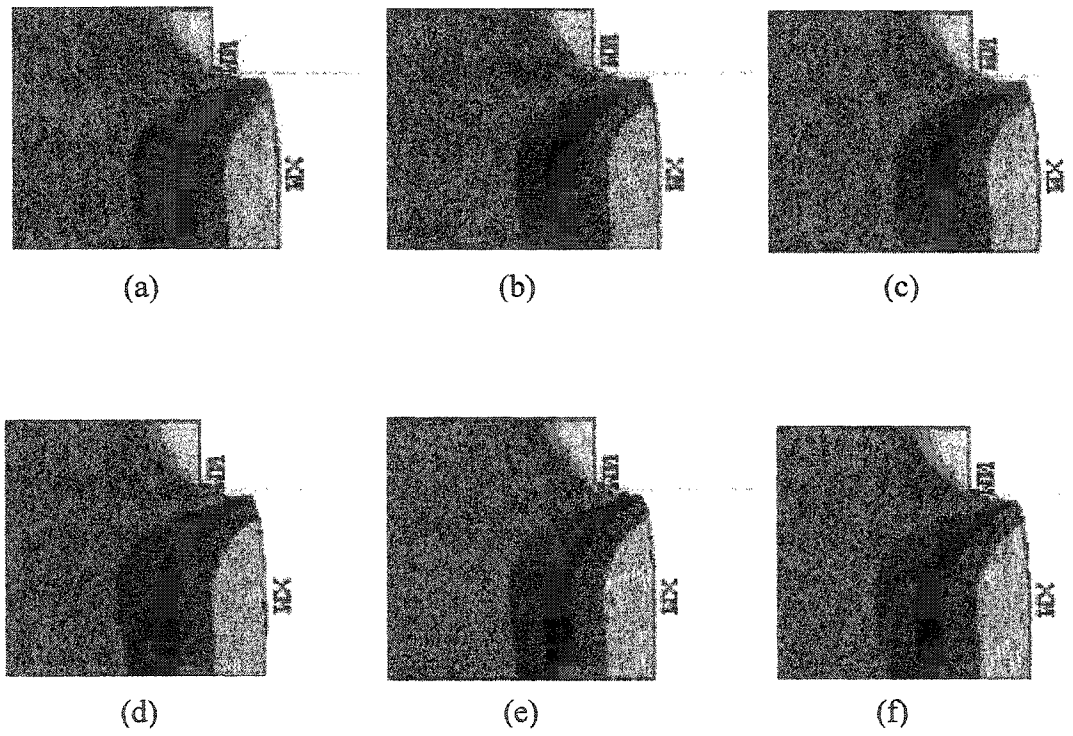

Figure 4.11 Simulated DMZ and metal flow pattern through the same die for annealed Al-6063 (a), Al (b), Pb (c), stainless steel 304 (d), carbon steel C1010 (e), and Al6063-T6 (f)

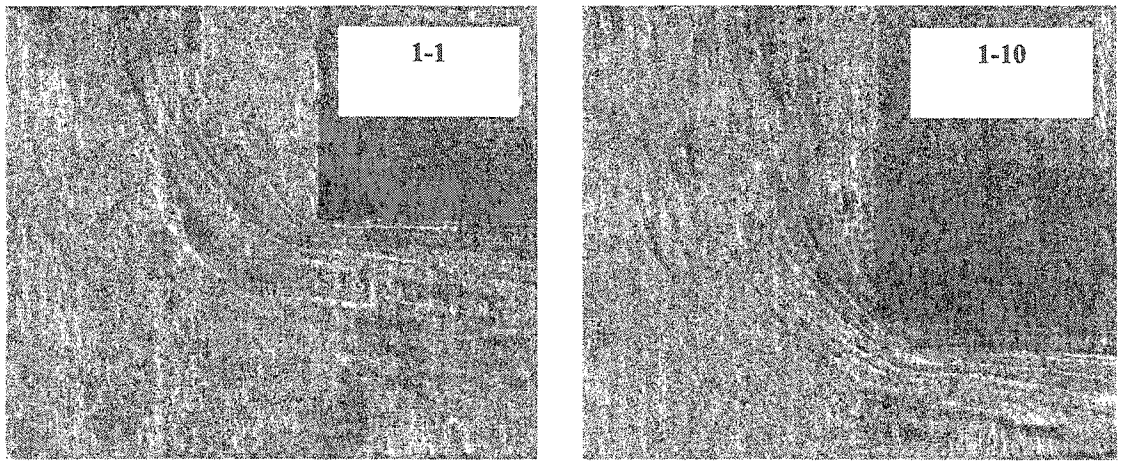

(a)

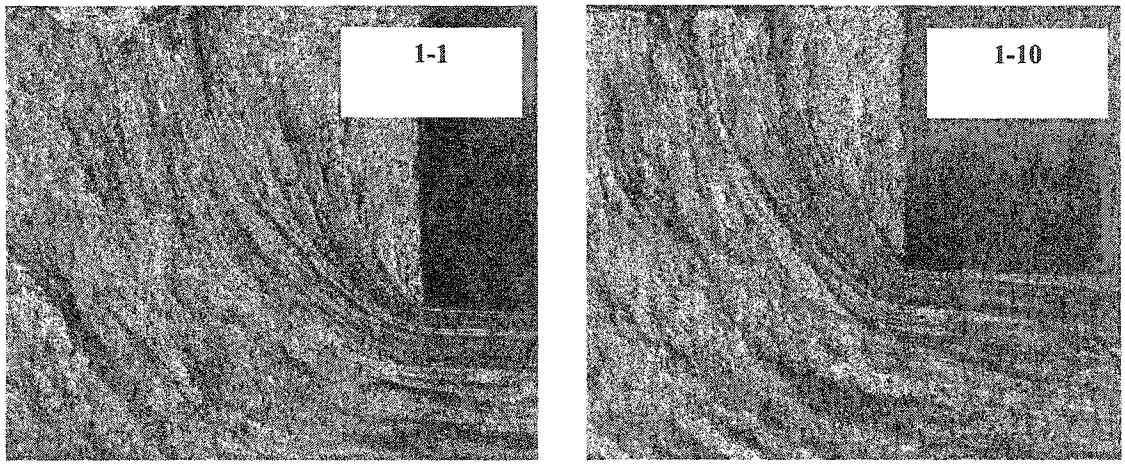

(b)

Figure 4.12 Metal flow pattern at ram speeds of 1mm/min and 10 mm/min through die # 1, during extrusion of aluminum (a) and lead (b)

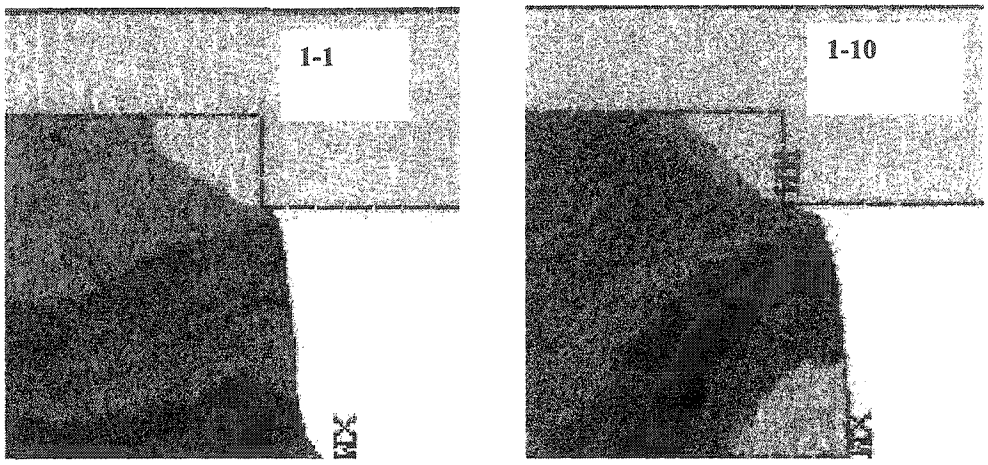

(a)

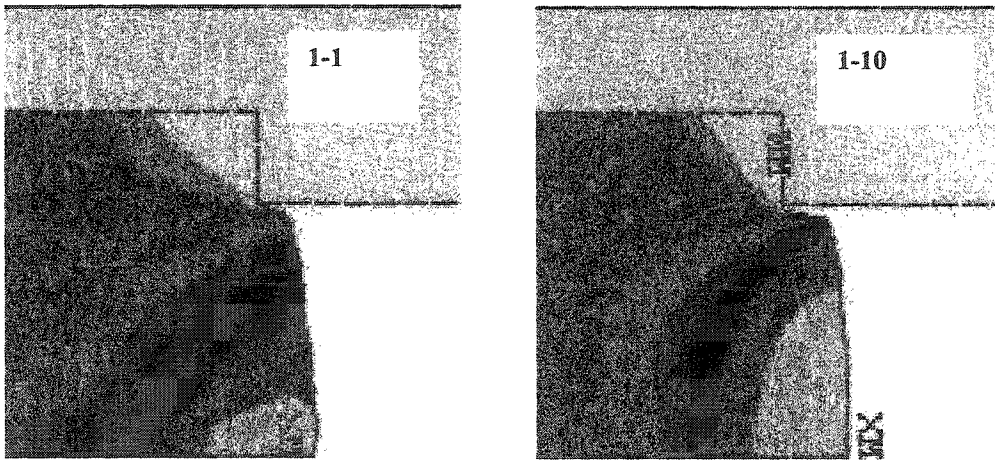

(b)

Figure 4.13 Size and shape of DMZ at ram speeds of 1 mm/min and 10 mm/min during simulated extrusion of alloy Al6061-T6 (a) and aluminum (b)

distortion. However, a DMZ of the same size but with different shape and orientation can cause a much more distorted flow. The issue needs to be investigated further.

These observations play a critical role in determining optimum productivity in a commercial extrusion plant. Higher extrusion speeds, resulting in smaller DMZ, reduce obstruction to metal flow and can thus yield higher productivity. However, the associated increased distortion in metal flow leads to several speed-related product defects. A judicious balance should thus be maintained between high ram speeds and good product quality.

4.4.5 Effect of Extrusion Ratio

Figure 4.14 illustrates the variation in the size and shape of the dead metal zone due to a change in the extrusion ratio (R). All extrusion simulations are through the same profile section (solid circular), but three different R values of 2.1, 1.8, and 1.6. The smallest dead metal and shear zones are for the smallest R, and the *DMZ* consistently increases in size and spread for increasing values of R. As the extrusion ratio increases, the die opening reduces while the confinement zone (where movement of the billet material is blocked by the corner formed by the die and container) increases. Material flow is restricted by this obstruction until the applied pressure overcomes the material shear strength, forcing the material to start flowing along the direction of internal shear. The *DMZ* is thus larger for a larger extrusion ratio. To corroborate these simulation findings, experimental runs should be carried out for dies having the same profile but varying extrusion ratio. More observations regarding this issue are presented in a later section.

4.4.6 Effect of Shape Complexity

Figure 4.15 depicts metal behavior with changing complexity of the die profile. For the alloy metal Al-6063, at the ram speed of 5 mm/min, the *DMZ* appears to get smaller and narrower with increasing die complexity. However, for the medium complexity die #2, there is a larger *DMZ* compared to that for the simplest die #1. At the higher extrusion speed of 10 mm/min, the *DMZ* first narrows down a little, and then broadens as complexity increases. Flow lines generally become steeper with increasing shape

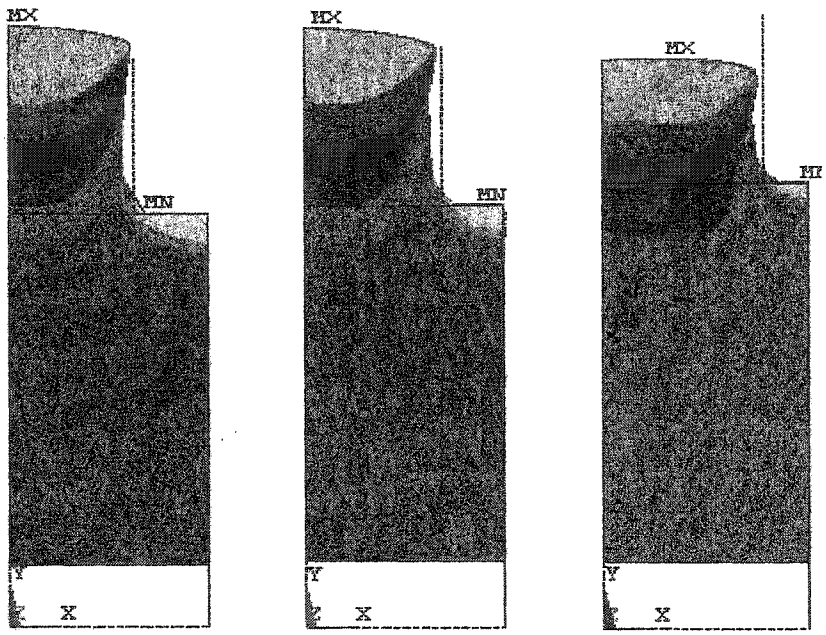

(a) (b) (c)

Figure 4.14 Simulation of material deformation for the same die (die #1) with varying extrusion ratio of 2.1 (a), 1.8 (b) and 1.6 (c)

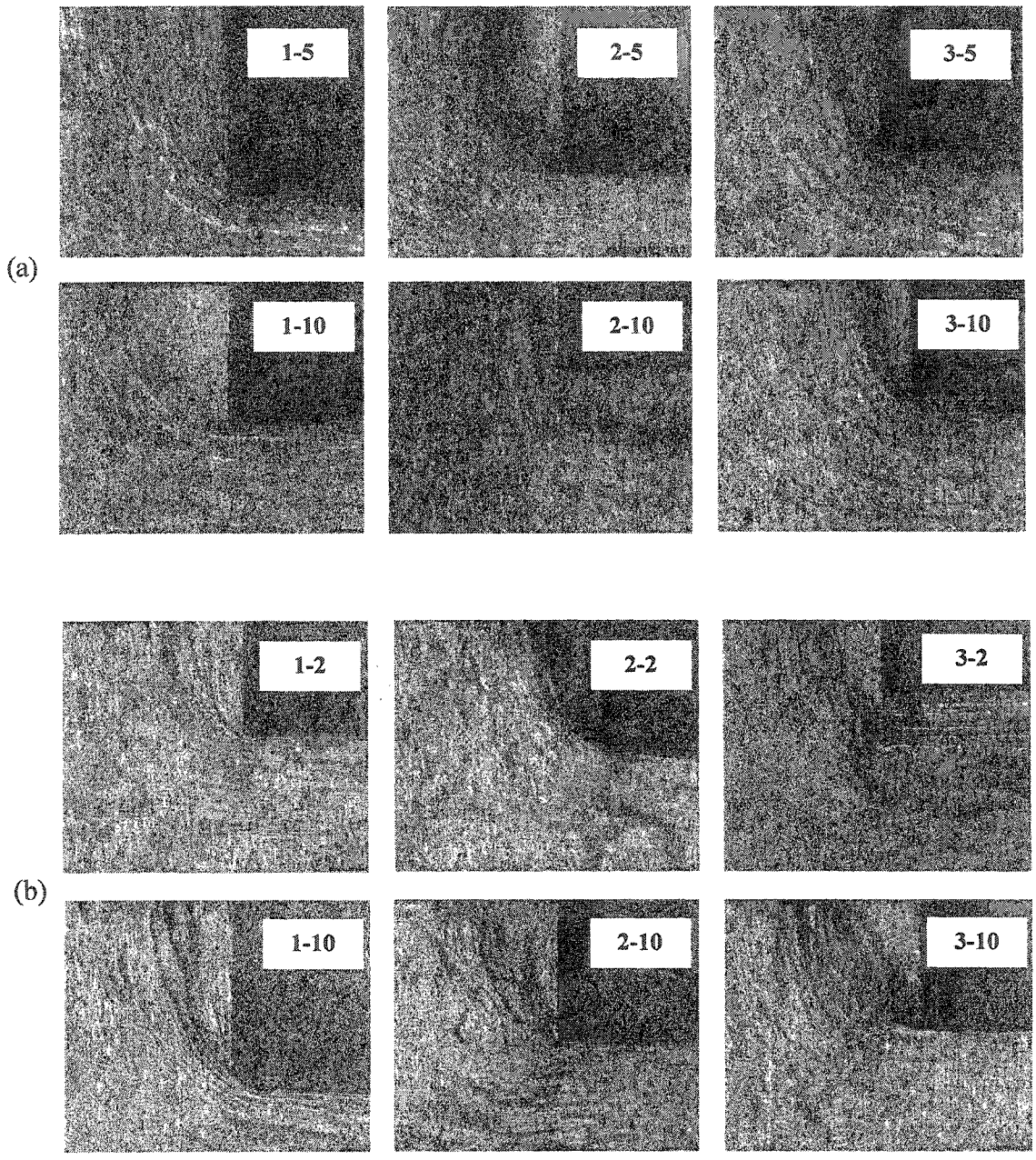

Figure 4.15 Metal flow pattern and dead metal zone with increasing shape complexity (profile # 1, 2, 3) at constant ram speeds of 2, 5, 10 mm/min: (a) Al-6063, (b) Aluminum

complexity, showing similar discrepancies as the *DMZ*. For pure Al, at both the speeds of 2 mm/min and 10 mm/min, the *DMZ* shows a trend of becoming larger and broader as the profile complexity increases. Flow lines generally become less steep and more rounded off.

Figure 4.16 shows outputs from simulated extrusion runs for the three dies at ram speeds of 5 mm/min and 10 mm/min. The same erratic behavior of DMZ size and metal flow pattern against changing die complexity can be observed as seen in actual experimental photographs above. To get a clearer picture of this behavior, variation of DMZ size is plotted against profile complexity and against ram speed in Fig 4.17 and Fig 4.18. All the complexity definitions discussed in earlier chapters have been covered, including the new definition proposed in chapter-2. Definition C_2 has been omitted due to its similarity with definition C_1.

For the same die, DMZ size decreases with increasing ram speed (Fig 4.17), confirming earlier observations. However, as can be seen from this graph and from the simulation outputs, there is only a small reduction in DMZ size with changing ram speed. Also, characterizing DMZ size by the diagonal length of the DMZ area is only one possible interpretation. Depending on whether we are performing a 2D or a 3D analysis, DMZ size can also be represented by its area or volume, or the aspect ratio. Further work needs to be done on these lines for a clearer picture of the issue.

Variation pattern in terms of changing complexity is again inconsistent; Fig 4.18. For definitions C_1, C_4, and the newly proposed C_5, DMZ size first increases and then decreases with increasing complexity. It should be noted that according to all of these three definitions, complexity increases from die #1 to die#2 to die#3. For definition C_3, which ranks die #2 as the most complex, DMZ size increases with an increase in complexity.

These inconsistencies are rather perplexing. Had it been merely an experimental observation, the natural tendency would be to attribute these discrepancies to experimental errors or material inhomogeneities (which cannot be discounted altogether). However, numerical results amply corroborate the experimental findings. Other factors,

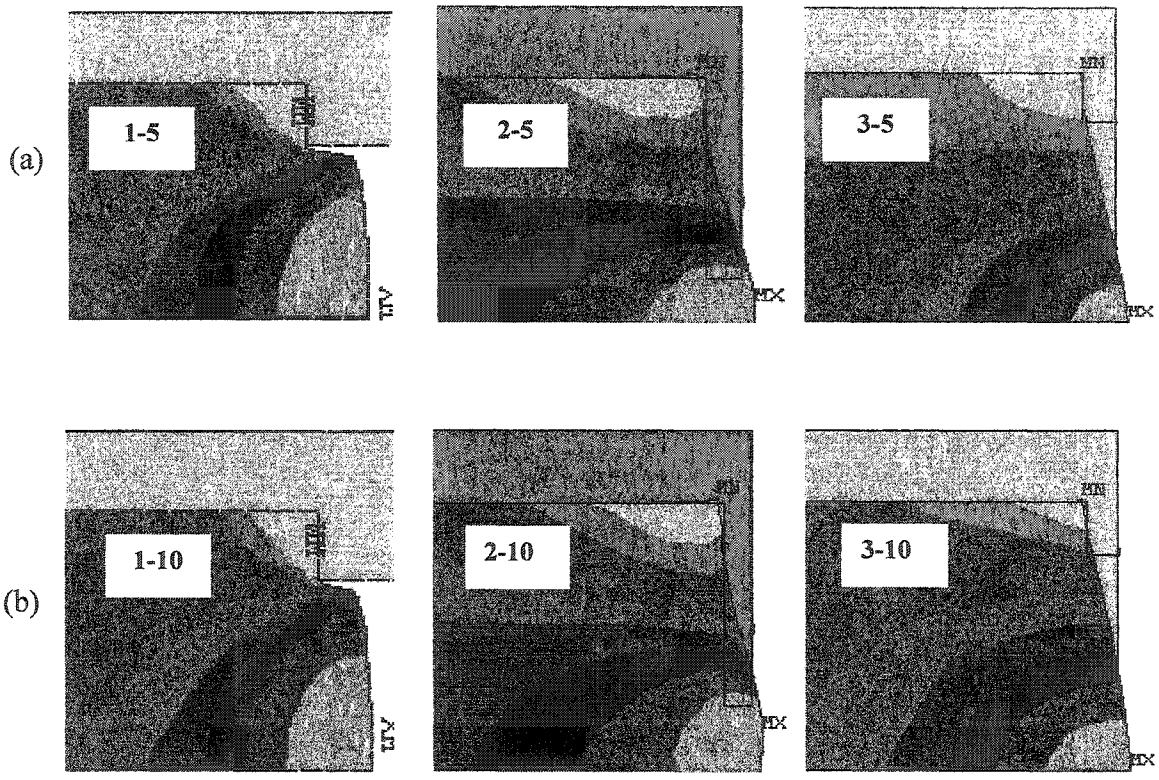

Figure 4.16 DMZ size and metal flow in simulated extrusion of annealed aluminum through dies 1, 2, and 3 at ram speeds of 5 mm/min (a) and 10 mm/min

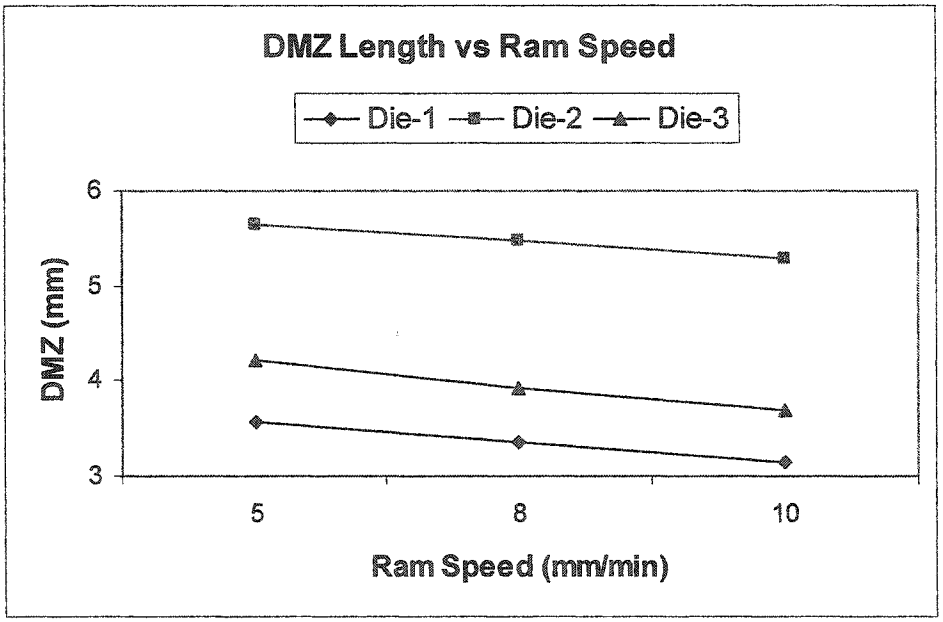

Figure 4.17 Variation of DMZ size with increasing ram speed

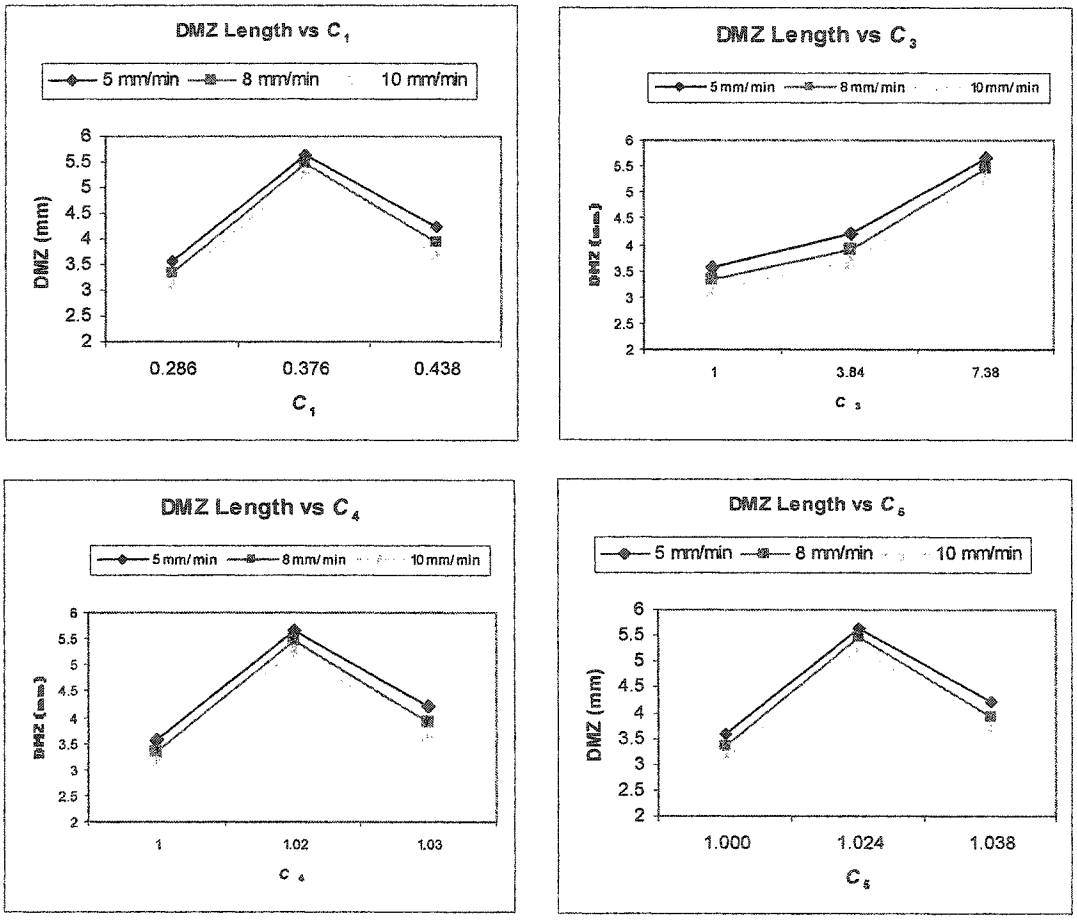

Figure 4.18 Variation of DMZ size with increasing complexity, according to the definitions C_1, C_3 , C_4, and C_5; C_2 is neglected due to its similarity with C_1.

not generally considered in complexity discussions, may be responsible for the irregular behavior. First of all, researchers agree that there are limitations to our understanding of the actual physics of material deformation in the extrusion process [Stambler 1997]. Secondly, though metal deformation is definitely affected by profile complexity, several contending issues are also involved:

1. Symmetry of the die profile may play a significant role in metal flow. Though both are somewhat more complicated than the simplest solid circular shape (die #1), die #2 has only a single axis of symmetry, while die #3 possesses biaxial symmetry. Many prevalent definitions on the other hand attach a higher complexity rating to die #3 because of its considerably larger perimeter. Effect of symmetry (or lack of it) on metal flow pattern needs to be investigated in more detail.
2. As pointed out above, extrusion ratio (R) has long been recognized as a very important profile parameter. As the listed complexity definitions do not include extrusion ratio as a defining parameter, it should be expected that a complexity-based rationalization of the metal flow pattern would not be satisfactory, based on these definitions.
3. Definition $C_3 = CCD/T_m$ is the only one that yields the consistent behavior of increasing DMZ size with increasing complexity. However, this definition was earlier (chapter-2) found to be the weakest in terms of pressure prediction, so we cannot regard it as a robust indicator of complexity.
4. It was established in chapter-2 that the newly proposed complexity definition (C_5) gives the best prediction for extrusion pressure in comparison with the four definitions found in published literature. However, even this definition proves to be inconsistent in explaining metal deformation behavior. This observation indicates that we need a still newer definition of extrusion shape complexity, incorporating all significant geometric parameters of a die profile (including extrusion ratio), and yielding better correspondence with experimental

observations of DMZ size, pressure, etc. Attempts at more realistic and robust complexity definitions are reported in a later chapter.

A look at the velocity profiles (Fig 4.19) and metal flow behavior (Fig 4.20) obtained from extrusion simulations for the three dies lends further insight into the relationship between die complexity and metal flow. Pattern for the two biaxially symmetric dies (die #1 and die #3) is more homogeneous than that for the die with only one axis of symmetry. This would indicate that asymmetric dies having no symmetry (quite common in commercial extrusion practice) would have even more inhomogeneous metal flow. Also, because of the asymmetrical geometry about the longitudinal axis, more metal flow is concentrated in the upper half of die #2 ((Fig 4.19 (b) and Fig 4.20 (b)). This leads to higher pressures from one side of the exiting product, resulting in the extrusion defect known as *twists* or *bends*, requiring subsequent corrective action. Die designers have to carefully look into these issues to guarantee optimum die life and minimum product defects.

4.4.7 Various Effects

The foregoing sections clearly establish that numerically simulated outcomes are reasonably accurate representations of actual extrusion experiments. A comprehensive data base was thus generated using ANSYS and ANSYS-LSDYNA simulation outputs to explore areas that are difficult to handle experimentally. Some of the advantages and added insight that FEM simulations provided over and above the experimental runs are:

1. Compared to only three billet materials used in the experiments (lead, annealed aluminum, and annealed alloy Al-6063), simulations were carried out for six different materials (Al6063-T6, carbon steel C1010, and stainless steel 304, in addition to the above three).
2. As against only three extrusion ratios of the die profiles used, numerical runs covered six different extrusion ratios for each die complexity.
3. Simulations were carried out at five different ram speeds for the various material-extrusion ratio combinations.

(a)

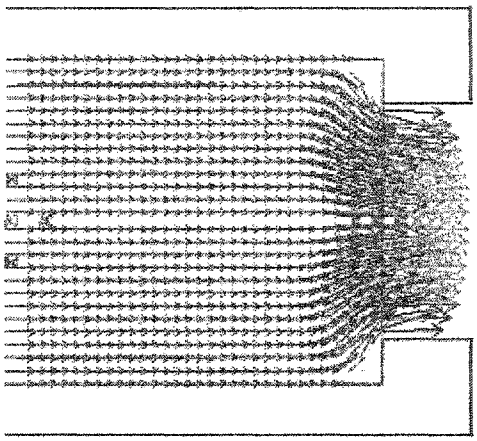

(b)

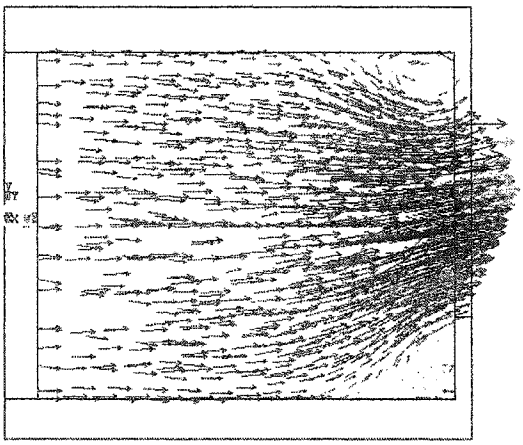

(c)

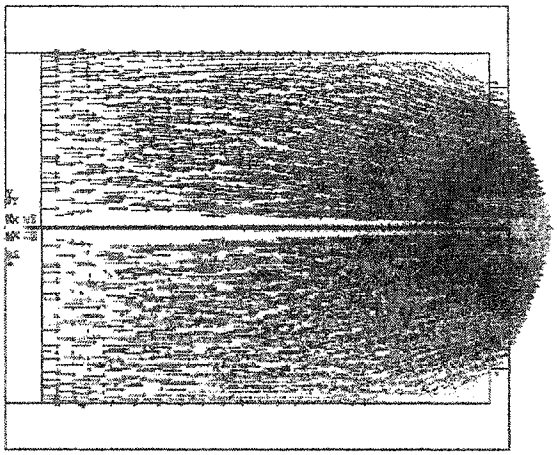

Figure 4.19 Simulated velocity profiles for the three dies: die #1 (a), die #2 (b), and die #3 (c)

(a)

(b)

(c)

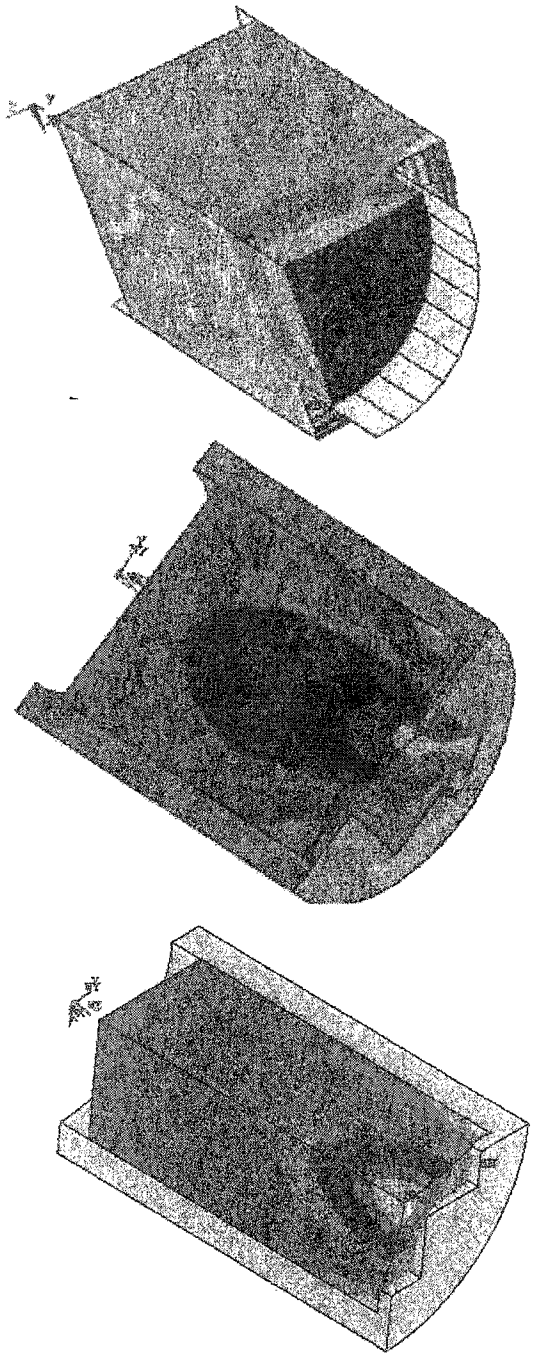

Figure 4.20 Dead metal zone behavior and pattern of metal flow seen during 3D simulation of extrusion of annealed aluminum through the three dies: die #1 (a), die #2 (b), and die #3 (c)

4. Numerical runs provided metal flow pattern, DMZ size, extrusion pressure, and other data at various stages of the process (after ram advance of 0.25, 0.5, 0.75, 1.0 mm, etc). This is something which is very difficult and time consuming to perform experimentally. The simulation results thus provided us with revealing insight into the evolution of the process as the ram advances along the container and the billet undergoes varying stages of deformation.

The term *DMZ size* refers to the diagonal length of the dead metal zone, along the direction of internal shearing of the metal. The actual shear surface that follows a somewhat convex curve has been approximated with a straight line in this work. All the readings are at a stage when the ram has advanced about 1.25 mm along the container, steady state process conditions having been attained.

Figure 4.21 is a graphical representation of the variation of DMZ size and extrusion pressure against extrusion ratio at three different ram speeds (5mm/min, 8 mm/min, and 10 mm/min). Billet material (Al6063-T6) and profile complexity (die #1) were the same for all the cases. As expected, both DMZ size and extrusion pressure increase with increasing extrusion ratio, the pattern of variation being linear, barring some slight deviations. It is interesting to note that the highest curve is for the lowest ram speed, indicating that the dead metal zone size gets smaller as the extrusion speed increases. The same trend was earlier observed in the metal flow photographs of the split billets, and is now corroborated through these numerical results. Variation of extrusion pressure against extrusion ratio also shows an increasing linear trend. However, the highest curve is now for the highest ram speed. This result matches well with the mechanics of metal deformation in extrusion, as higher extrusion pressures are generally associated with higher extrusion speeds: extrusion pressure varies in direct proportion with the applied strain rate, and strain rate is directly proportional to extrusion velocity or ram speed.

Figure 4.22 shows the variation of DMZ size and extrusion pressure against extrusion ratio for the six different materials. As the extrusion ratio is increased, the DMZ size also generally increases, following almost a linear pattern. As expected, the lowest DMZ values are for the relatively soft and weak annealed aluminum and Al-6063 billets, while

(a)

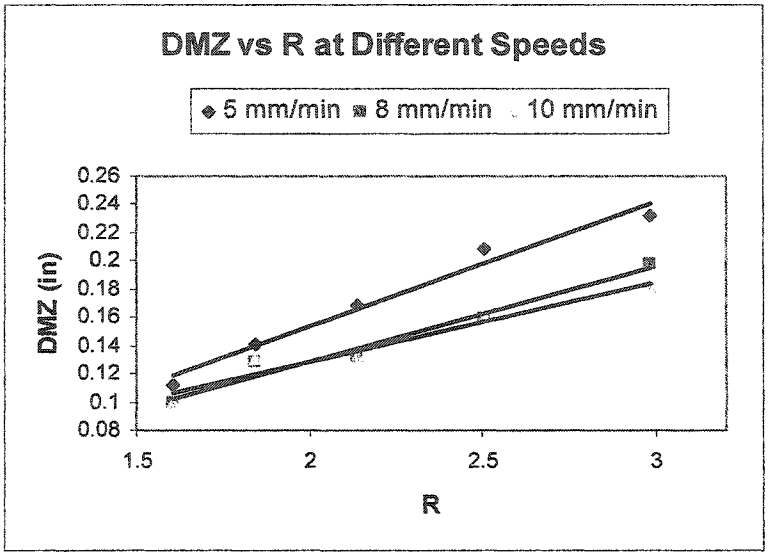

(b)

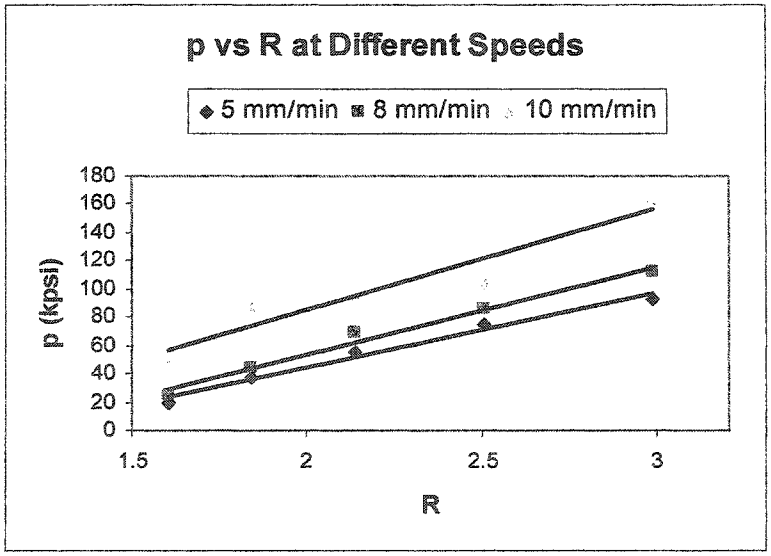

Figure 4.21 Variation of DMZ size (a) and extrusion pressure (b) with increasing extrusion ratio at ram speeds of 5, 8, and 10 mm/min for Al6063-T6

(a)

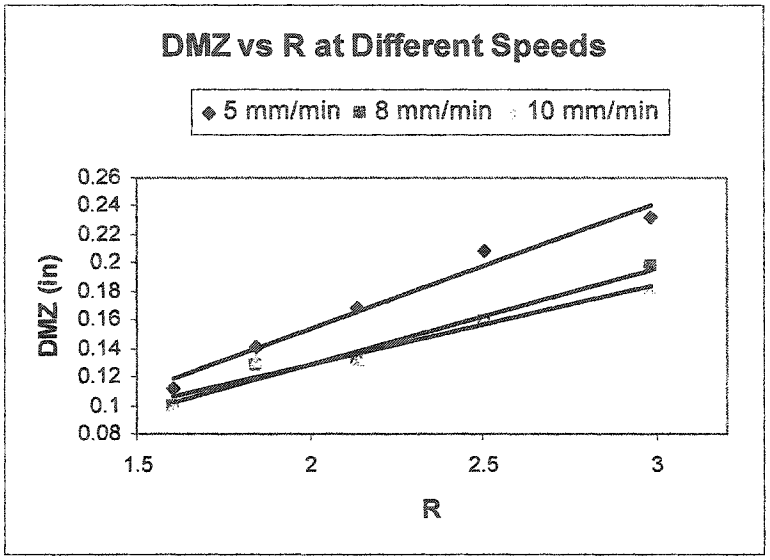

(b)

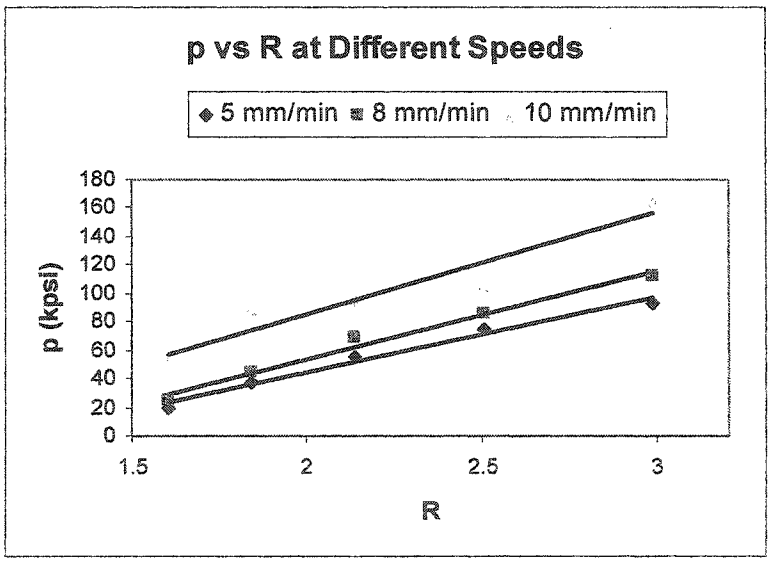

Figure 4.21 Variation of DMZ size (a) and extrusion pressure (b) with increasing extrusion ratio at ram speeds of 5, 8, and 10 mm/min for Al6063-T6

curves for the harder and tougher metals (Al6063-T6, carbon steel C1010, and stainless steel 304)) are progressively higher. Lead (Pb), the softest metal in the group studied, shows a non-conforming behavior by having DMZ values a little higher than annealed aluminum and annealed Al-6063. We should keep in mind however, that this outlier behavior may be due to the fact that lead is far heavier than all of the other metals studied (density of 0.411 lbf/in^3 compared to the value of 0/098 lbf/in^3 for aluminum and its alloys). The same linear trend can be observed for pressure variation. Again, as expected, tougher alloy metals require higher extrusion pressures as compared to pure aluminum, and higher pressure curves are in the order of increasing material toughness. Also, once again, lead shows higher pressures than annealed aluminum.

CHAPTER 5
EXTRUSION TOOLING:
FAILURE MODES AND MECHANISMS

5.1 INTRODUCTION

The last three chapters, covering various aspects of extrusion process, constitute ***Study-A***. Te second phase of the current work, designated as ***Study-B***, is about the role played by extrusion dies and tooling. A very important factor contributing to the performance and economics (efficiency and quality) of any hot metal-forming process is the service life of tooling. Product rework and rejects can be traced back to various defects spread over the die life-cycle: die design, die manufacture and heat treatment, and die service. Initiation and propagation of die damage can be caused by a number of mechanisms. Analysis of tool and die failure thus plays an important role in the prediction and prevention of die failure, and subsequently in improving process economics. This depends to a large extent on the knowledge of the manufacturing and service history of the failed tool and die. Such information is generally not very easily available, and especially not for a large number of die failures or a large spectrum of die profiles. Very few articles are available in literature that present failure analysis based on a substantial sample-size of real die breakdowns.

5.1.1 Current Work

Results are reported in this chapter from a study about the relationship between die profile and modes of die failure. In collaboration with a local industrial setup, a total of 616 die failures involving 17 different die profiles were studied. All dies were made of H-13 steel, while the billet material was Al-6063 in all the cases. The reported work covers the following important issues:

1. Classification of die failure modes and mechanisms,
2. Analysis of overall and class-wise break-up of failure modes,
3. Failure analysis for dies of different complexities, and
4. Shape-wise breakdown of each failure mode.

5.2 Extrusion Die Failure

Productivity, cost, and quality of the extruded profiles are directly related to the performance of the die set, apart from other factors such as billet material, extrusion press and ancillary equipment capability, and downstream operations such as age hardening, anodizing and painting. Due to its high cost, based on special material and processing, very fine tolerances, and high demands on repeated thermo-mechanical performance, the most critical extrusion component is the die. How often a die has to be scrapped and replaced with a new one directly contributes to the commercial viability of producing a certain profile.

Any failure analysis of extrusion dies must include their manufacturing and service history. Improper die material composition, presence of quench cracks, scales or inclusions, can all lead to premature die failure. A large percentage of die failures can be traced back to heat treatment problems. Other sources can be distortion during heat treatment, machining or service, erosion and/or pitting, corrosion, etc [Laue and Stenger 1981, ASM 1990]. Once a die is passed after some trial runs, the most common modes of in-service failure are *fatigue* (brittle failure through crack propagation), *wear* (gradual wearing out of the bearing surface), and *deflection* (plastic deformation).

5.3. Extrusion Die and Tooling

The die and tooling arrangement employed in direct extrusion of soft and medium grade aluminum alloys (1100, 3000 and 6000 series, including Al-6063) was shown in Fig 1.3 and the functions of the various components were listed in Table 1.1. Commercial aluminum extrusion overwhelmingly uses flat-face or square dies (die cone semi-angle of

90°). Configuration of a solid flat-face die was shown in Fig 1.7. It should be reiterated here that the most crucial part of any die is the *bearing* or *die land*, which is used to control the dimensions, profile, surface finish and speed of extrusion. Problems at the die bearing can seriously curtail die life.

As the generation of a hollow shape requires a solid obstruction to metal flow in the middle, which cannot be supported in a die alone, a flow obstruction-cum-distribution plate called a *mandrel* is placed in front of the die. Working principle of solid, semihollow and hollow dies was shown schematically in Fig 1.4. The three common die types used to produce hollow profiles are bridge, spider and porthole dies, as shown in Fig 3.1. An extrusion die is not a stand-alone component but an assembly consisting of various parts. Figure 5.1 shows front and rear views of actual production dies and the way they are assembled in the die ring, together with die and die-backer assembly for a solid profile and die-and-mandrel assembly for a hollow profile. Front and rear views of a typical die stack, consisting of the die ring assembly (die and die-backer fitted inside the die ring), bolster, and sub-bolster are shown in Fig 5.2.

5.4 Profile Terminology

Just as some terms are typically related to elements of an extrusion die, there is almost a standard terminology used to describe various features of the extrusion profiles commonly used in the construction sector. Some of the more common ones are shown in Fig 5.3. A partially open rectangular extension, usually attached to a hollow profile, is called a *tongue*. The slotted groove, on which a rubber lining is later fitted, typically for door and window brackets, is known as a *path* or *brush path*. Any sharp corner or sudden cross-section change is referred to as a *corner*. The flow distribution/control passages provided in the feeder plate (solid die) or mandrel (hollow die) are called *cavities*. Small appendages to the main profile, in effect minor sub-profiles, are termed *details*. A *screw hole* or *screw boss*, as the name implies, is used later for fastening the extruded section to a structure. A very small protrusion, either sharp or rounded, is designated as a *tip*.

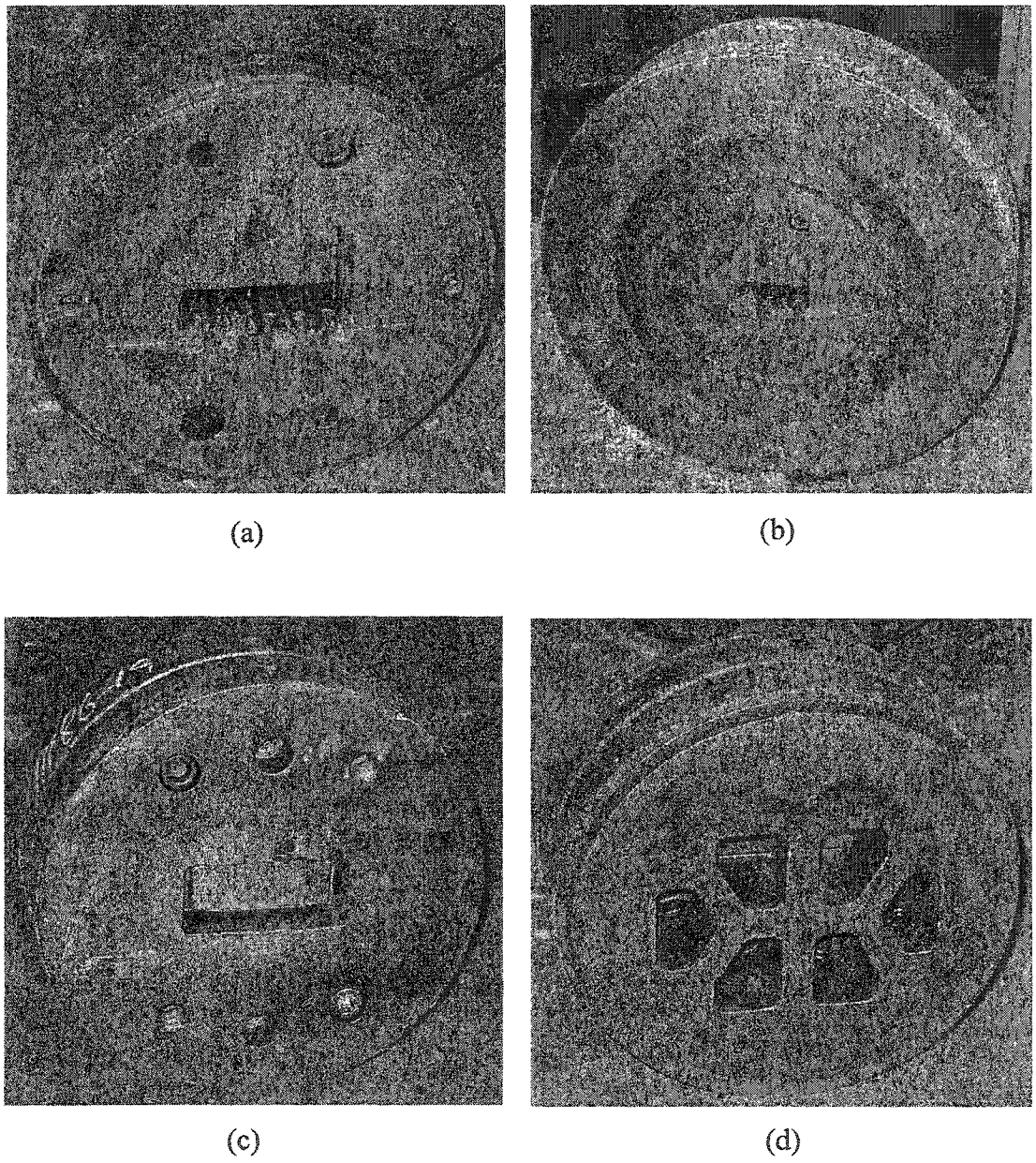

Figure 5.1 Production dies for aluminum extrusion: die and die backer for a solid profile fitted together (a), die and backer assembly fitted inside the die ring (b), front view (c) and rear view (d) of a die-and-mandrel assembly for a hollow profile [ALUPCO]

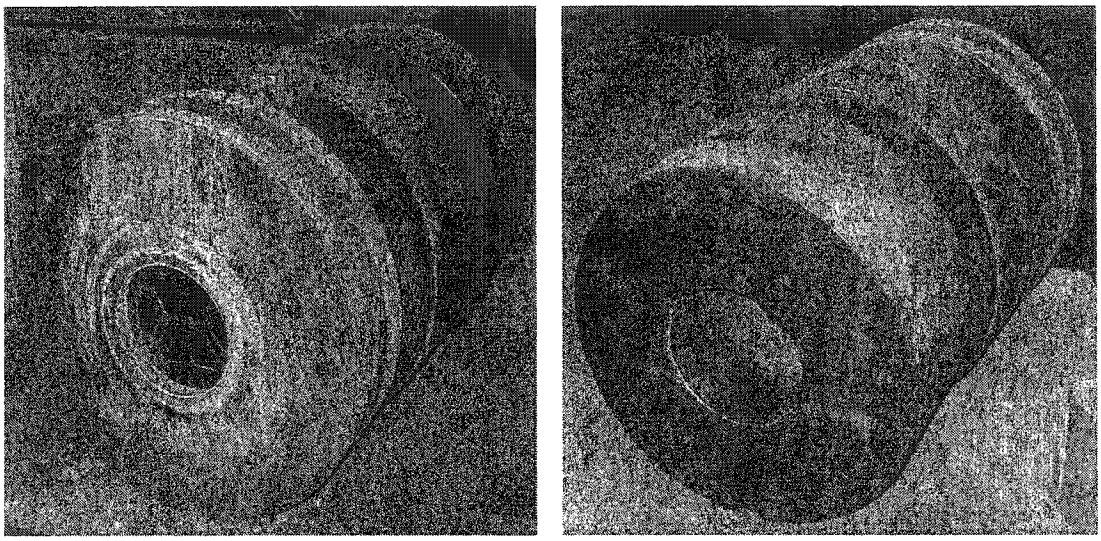

(a) (b)

Figure 5.2 Typical die stack: front view (a) and rear view (b) of die ring (die and die backer fitted inside), bolster and sub-bolster [ALUPCO]

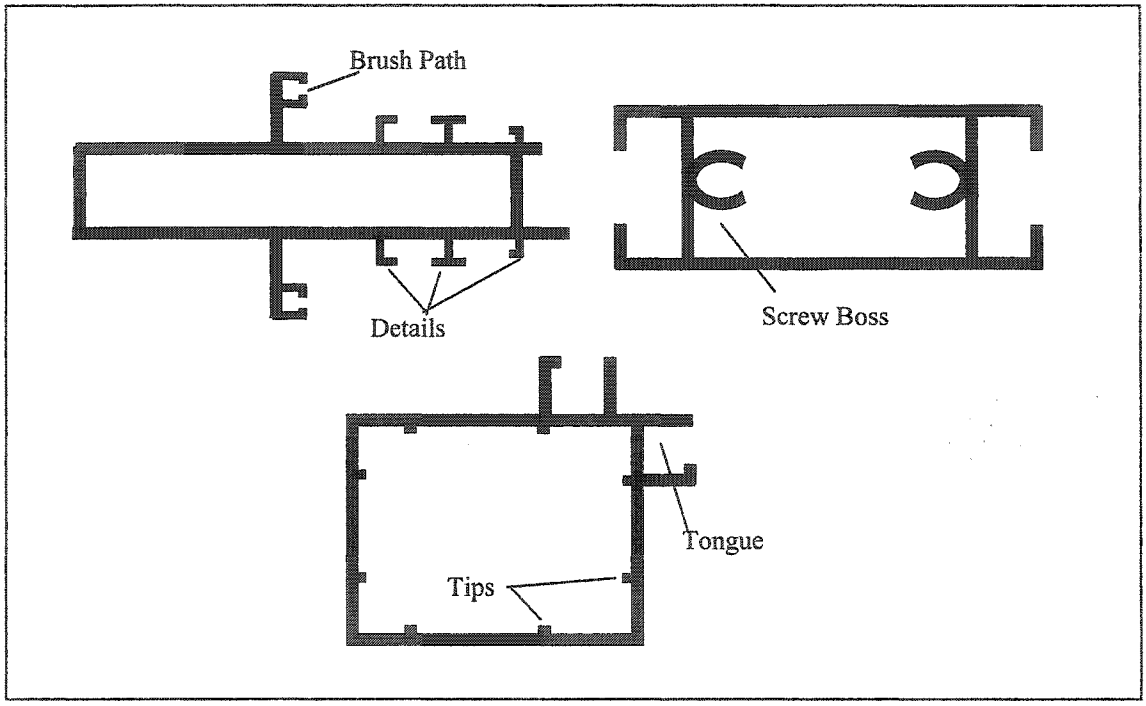

Figure 5.3 Some features of extrusion profiles common in the construction industry

5.5 Die Profile

Various definitions of complexity index for an extrusion profile have been described and analyzed in the preceding chapters. Broadly speaking, extrusion shapes can be classified into three groups according to their complexity: solid, semi-hollow, and hollow. Complexity increases from solid to semi-hollow to hollow shapes. Traditionally defined semi-hollow products appear to be almost like solid sections, but their form makes the use of a single-piece die impracticable. As the focus of the current study is on die failure mechanisms, details of profile complexity (as expressed by complexity index) have been avoided here, restricting the discussion to the broader grouping of solid, hollow, and semi-hollow shapes.

5.6 Major Modes of Die Failure

Tool failure in bulk metal forming (especially hot extrusion) is caused by a complex interaction of several influencing factors like *fracture*, *wear*, *plastic deformation*, and *thermal loads*. Fatigue fracture is the predominant failure mode for all but very simple profile geometries [Saha 2000].

5.6.1 Fatigue Fracture

During service an extrusion die experiences both mechanical and thermal stresses. As temperature changes are rather gradual, thermal stresses due to temperature differences are generally not very critical. Mechanical stresses are cyclic in nature, going from zero to maximum and back during extrusion of each billet. The maximum stress in aluminum extrusion can be around 186 MPa (27,000 psi), especially in cold extrusion of large profiles [Laue and Stenger 1981]. These cyclic stresses, joining forces with preexisting flaws (such as micro quench cracks produced during heat treatment), can lead to crack growth and ultimate fatigue failure. The failure mechanism is influenced by

(a) material properties, geometric tolerances, and surface finish of the *billet*,

(b) material properties, heat treatment and surface hardening, and geometrical details of the *die and tooling*,

(c) stress distribution and variation with time and temperature during the *extrusion process*, and

(d) stiffness and kinematics of the *press and affiliated tooling*.

Fatigue failures are mostly located at positions of high stress concentration such as sharp corners, section changes, stamp marks, etc.

Figure 5.4 [Pöhlandth 1989] shows schematically the significant failure mechanisms for an extrusion die. The occurrence of fatigue fracture is especially high for high extrusion ratios, and small fillet radii, resulting in high stress concentration. Crack initiation may be further promoted by machining marks. Failure by forced rupture (due to overload) rarely occurs in practical application, and can often be traced to human errors.

Further details of fatigue and fracture failure in extrusion dies and tooling can be found in Choi et al. [1998], Hambli and Badie-Levet [2000], Sudhakar [2002], and Cosenza et al. [2004].

5.6.2 Wear

Die wear is a tribological effect and can be defined as the progressive loss or removal of material from the operating surface of components (die surfaces in our case). By changing the topography of the die land, wear can cause severe surface damage leading to product defects and finally die failure. During preheating of the aluminum billet, a very hard layer of aluminum oxide (Al_2O_3) is formed on the surface. Also, preheating of the die set leads to the formation of an iron oxide layer on the die land. Repeated interaction of these two layers leads to wear at the die bearing surface.

Wear is generally classified as adhesive, abrasive, corrosion, fatigue, erosion, fretting, or impact wear [Saha 2000]. The three more common wear types are described by Schey [2000].

(a) *Adhesive wear* occurs when a pressure welded joint is stronger than one of the contacting bodies, and rips out a particle from that body (Fig 5.5 (a)).

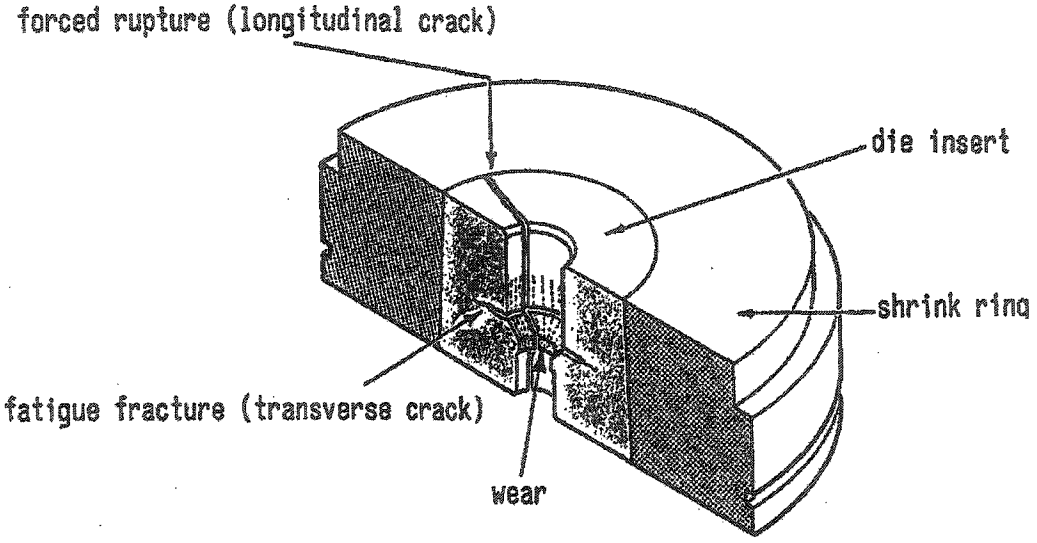

Figure 5.4 Schematic illustration of fracture of dies in direct extrusion of a rod [Pöhlandth 1989]

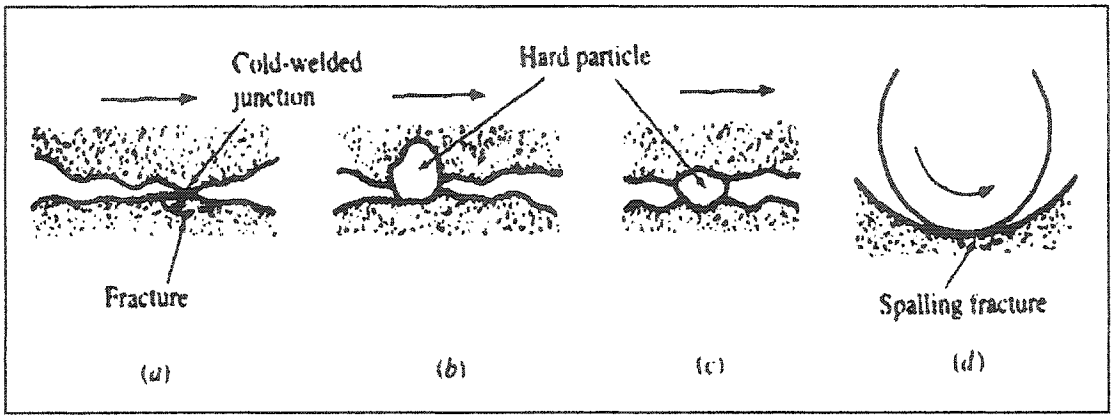

Figure 5.5 Progressive loss of material through wear may be caused by (a) formation of adhesive junctions, (b) rubbing (abrasion) by a hard particle embedded in one of the mating surfaces, (c) abrasion by a hard particle trapped between surfaces, or (d) fatigue resulting from repeated frictional loading [Schey 2000].

(b) *Abrasive wear* is caused by hard particles, whether they are within one of the contacting bodies (*two-body wear*, Fig 5.5 (b)) or are interposed between the two components (*three-body wear*, Fig 5.5 (c)).

(c) *Fatigue wear* occurs when the repeated passage of a component over the surface of the other component leads to the separation of small particles from the surface (Fig 5.5 (d)).

In direct extrusion, the process becomes complicated due to high pressure and relative velocity at the billet-container and billet-die interfaces. Adhesive and abrasive actions work together with sudden temperature fluctuations and prolonged exposures to elevated temperatures. Abrasive wear is more gradual, but is quite accelerated at high temperatures. Resulting die wash (wear) is at times aggravated by adhesive wear.

Aluminum has a strong tendency to adhere on to steel surfaces. An adhesive layer thus forms on the die bearing. Formation of this adhesive layer depends on various factors.

(a) Temperature developed in the die bearing,

(b) Extrusion speed,

(c) Shape and geometry of the die profile

(d) Die bearing length,

(e) Surface roughness parameters of die bearing,

(f) Hardness of the bearing surface.

Temperature and speed are the most critical of these factors. For billets preheated to the same temperature, die bearing temperature rises more at higher ram speeds. This is due to a higher strain rate and increased shear deformation (through sticking friction) at the die land. An adhesive layer begins to develop due to the increase in temperature, and slowly builds up with repeated extrusion cycles. This repetitive buildup of adhesive layers may ultimately lead to surface detachment and die failure by wear. It was reported by Thedja et al. [1992] that die wear begins on the output side of the die bearing and progresses in a direction opposite to that of extrusion. According to other studies, the deepest wear traces can be found also at the leading edge [Saha 1998] or in the middle [Björk et al. 1999,

Sundqvist et al. 1994]. The disagreement in these findings is most likely caused by differences in extrusion conditions, bearing parameters, extrudate geometries, etc. Saha [1998] observed significant bearing washout (die wear) on a hollow die studied, and the wear increased at higher extrusion speeds. More wear spots were found on the mandrel bearing surface than on the cap bearing. Wear patterns observed by Gutovskaya et al. [2004] in a hollow die are shown in Fig 5.6.

More detailed description of wear in extrusion and other metal forming dies can be found in Björk et al. [1999, 2001], Lee and Im [1999], Müller [2002] and Gotovskaya et al. [2004].

5.6.3 Plastic Deformation

Also known as **deflection** or **bending**, plastic deformation of dies is also a significant failure category in extrusion, especially for very complicated profiles extruded through dies with high tongue ratios. Large localized stresses on the tongue, combined with local high temperatures, can cause bending. Some dies fail due to mandrel deflection caused by unbalanced stresses acting on the die face. Higher pressures on one side of the die or mandrel compared to the other can be due to misalignment or improper die design, or arise during extrusion of unsymmetric profiles.

Deflection of the die faces caused by the combination of high pressures and elevated temperatures tends to close the opening. This can cause undersizing of the extruded profile. Deflection has been generally observed to be greatest at the center of the die and gradually reduces towards the periphery [Saha 2000]. Amount of die deflection is a function of temperature rise in the die, die design, and support tooling. Saha [1996, 1997] established that maximum temperature in the billet occurs during extrusion at the corner very close to the die exit. The higher the temperature rise in the die, the lower the hardness of the die. More die deflection is expected because of this decreased hardness.

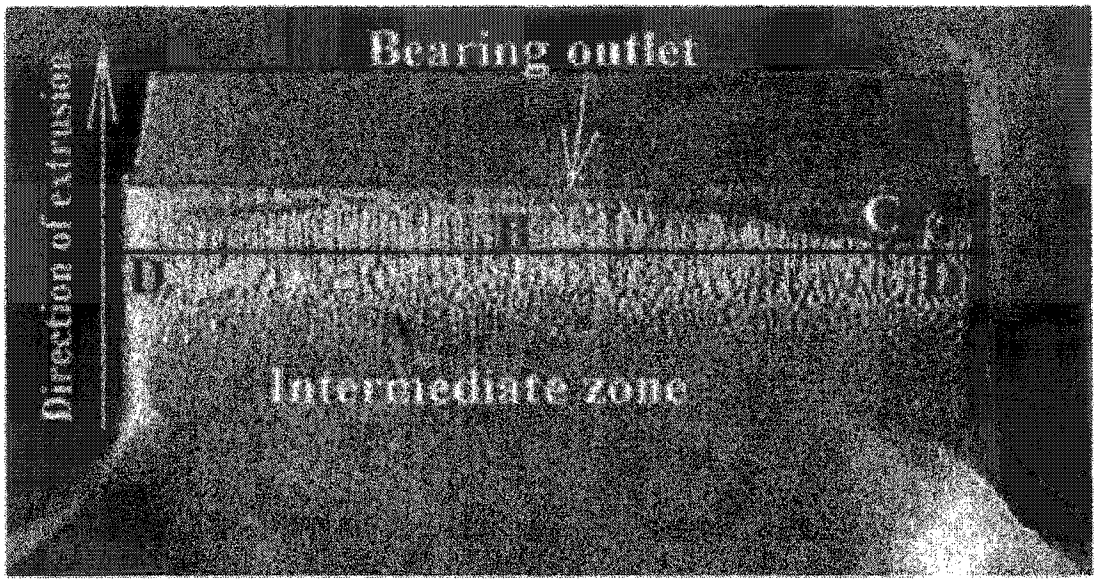

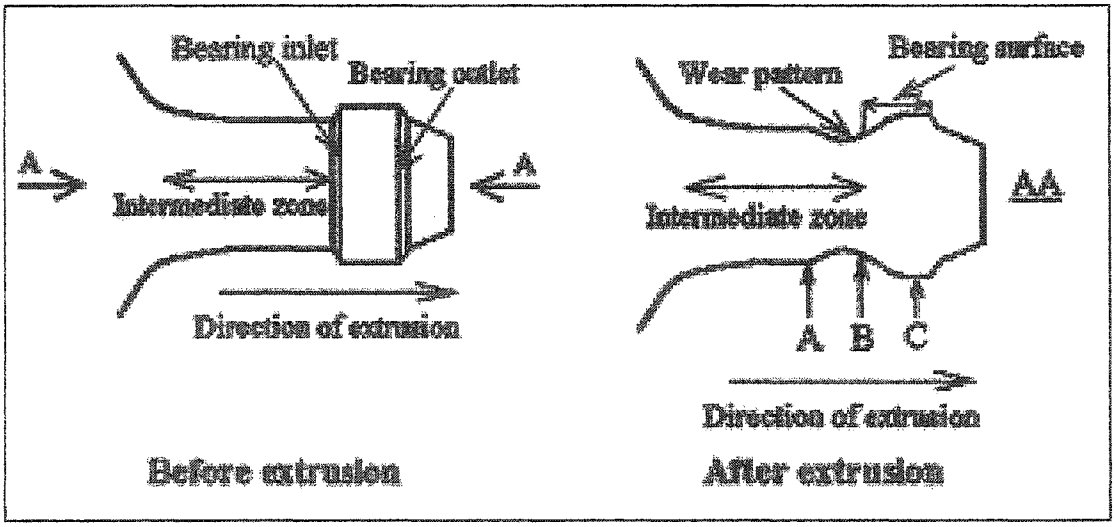

Figure 5.6 Wear pattern in the mandrel of a hollow die (above); sketch showing mandrel before and after extrusion (below); longitudinal sectional view of the mandrel shows excessive wear. [Gutovskaya et al. 2004]

5.7 Die Failure Data

All the data for this work were collected in collaboration with ALUPCO, Dammam. The statistics and analysis cover 17 different die profiles (actually 28 profiles, if we consider number of cavities per die), and a total of 616 die failures occurring over a period of about 10 years. The environment was hot extrusion (425-475°C temperature range), performed with H-13 steel as the die material and Al-6063 as the billet material. Figure5.7 shows simplified sketches of all the die profiles included in the study.

5.8 Die Failure Mechanisms

The bulk of aluminum extrusion finds application in the construction industry. Most of the extruded shapes in hot extrusion of Al-6063 are thus native to the construction milieu. Consequently, some of the terminology related to die failures is also area-specific, though many terms are of a more general nature. A ***crack*** refers to a visible, generally uneven fissure on the surface as opposed to a ***break***, which results in the component being actually broken into two or more pieces. A ***chip-off*** indicates a small piece chipping off from a surface, not a large enough chunk to categorize it as a break. ***Wash-out*** of a surface implies tiny but significant individual or aggregate craters and depressions caused by erosion or pitting. Plastic deformation due to thermal and/or mechanical stresses may result in a component or part of it being ***deflected*** or ***bent***. Severe wear and tear caused by factors such as impact, hard metal impurities in the billet, or any other mechanism not classified above, is termed as ***damage***.

The more prevalent terms used by the industry to identify failure mechanisms related to various die and tooling features commonly encountered in construction aluminum extrusion are listed in Table 5.1. For purposes of analysis, they have been divided into five major classes. All fatigue related failures, surface fatigue, and microchipping/cracking due to mechanical and/or thermal stresses are categorized as ***fracture***. Gradual surface deterioration due to various factors is classified as ***wear***. Going out of shape (bending or deflection) of a part or sub-component owing to excessive plastic deformation is labeled as ***deflection***. When failure is due to a combination of any

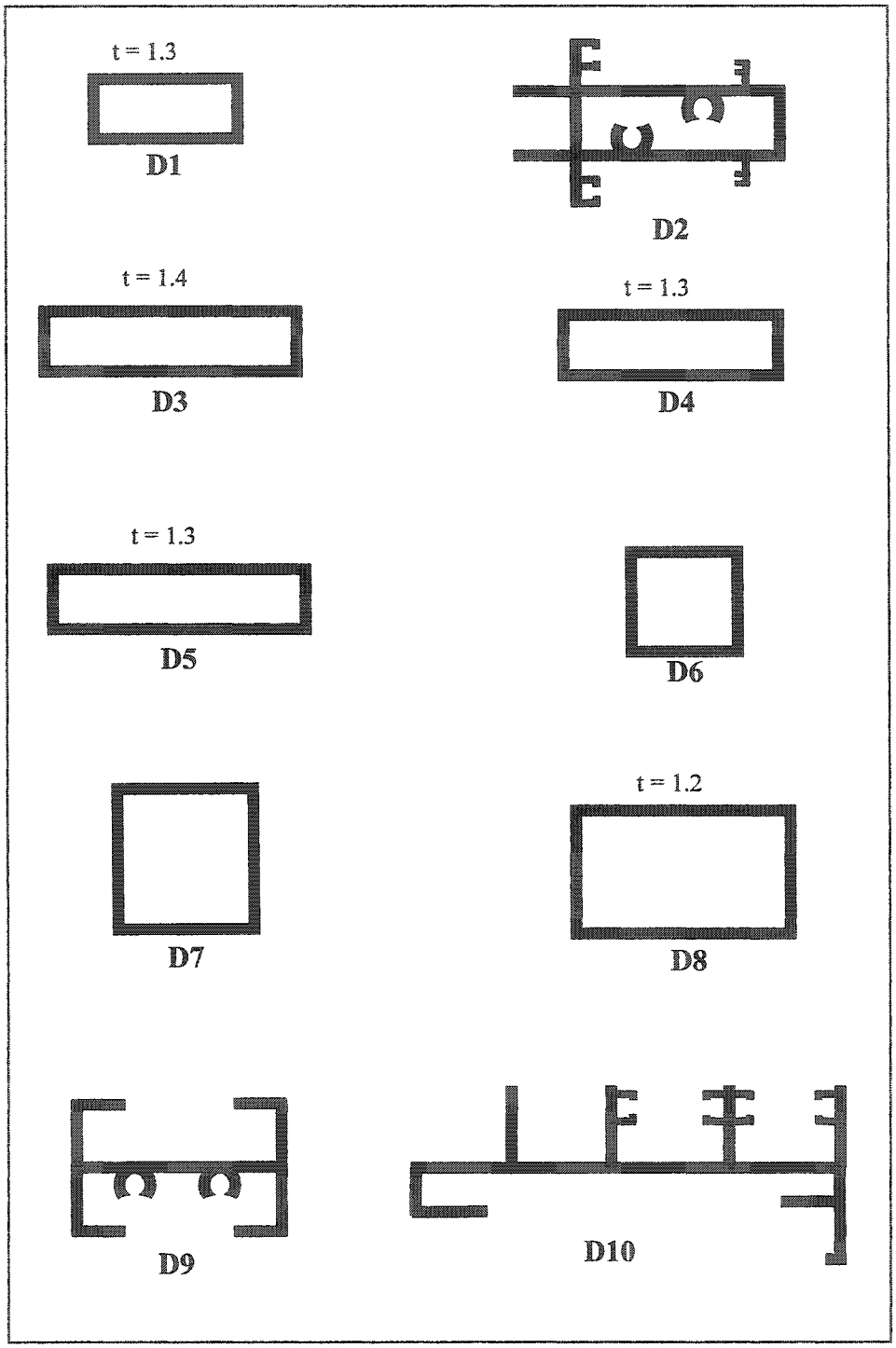

Figure 5.7 (a) Sketches of the die profiles used in the study

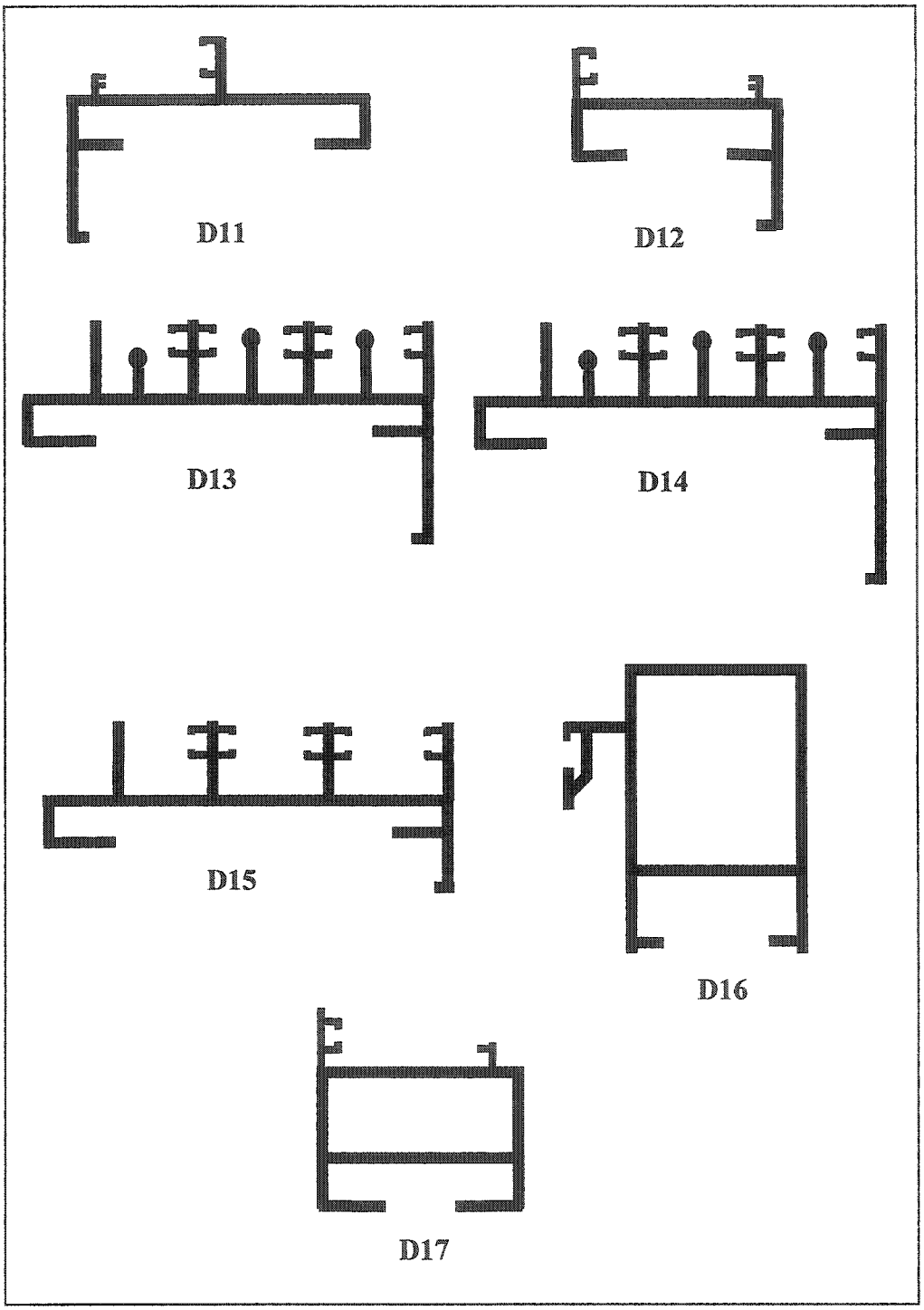

Figure 5.7 (b) Sketches of the die profiles used in the study

Table 5.1 Categorization of die failure mechanisms

Failure Mode	Failure Mechanisms
Fracture (F)	Path/brush-path broken (PB/BPB), Bearing chip-off (BCO), Corner crack (CC), Die broken/cracked (DB/DC), Bearing broken/cracked (BB/BC), Cavity broken (CvB), Detail broken (DtB), Screw/screw-hole broken (ScB/SHB), Surface cracked (SfC), Tongue broken/cracked (TB/TC), Tip broken (TpB)
Wear (W)	Bearing wash-out (BWO), Dimension change/ oversize/overweight (DimC/OS/OW)
Deflection (D)	Cavity/die deflected (CvD/Df), Tongue bent/deflected (TBt/TDf)
Mixed mode (Mx)	Mixed mode (Mx)
Miscellaneous (Msc)	Bearing/cavity damage (BDm/CvDm), Die/bearing soft (DS/BS), nitriding oven failure (NOF)
Mandrel failure (M)	Mandrel broken/cracked/ deflected (MB/MC/MDf)

of the above-mentioned factors, it is termed ***mixed-mode***. Failures that cannot be precisely categorized into one of the above (such as overall softening of the die or bearing area due to a fault in the nitriding oven) fall under the ***miscellaneous*** category. When the die set has to be scrapped due to any failure occurring in the mandrel (only for hollow and semi-hollow dies), the classification is ***mandrel failure***.

It must be kept in mind that in actual tooling failures, various failure mechanisms are simultaneously active.

(i) Microscopic cracks are always present in plates received from steel suppliers. Some of these cracks are enlarged during die manufacturing (for example during the EDM method of spark erosion [Pöhlandt 1989]) and subsequent heat treatment and surface hardening. Such a preexisting flaw would obviously undergo crack propagation during the cyclic thermal and mechanical loading of the die.

(ii) During extrusion, each billet is forcibly pushed past the die bearing to obtain the desired section shape. Due to the high pressures involved, the die land is slowly and gradually worn out. If there are intermittent inclusions of hard particles in the billet material, the wear may be more pronounced in certain locations than in others.

(iii)Due to the repeated application of such high pressures together with elevated temperatures, critical locations (such as details and thin sections) undergo gradual plastic deformation.

All of the three major failures modes (*fracture*, *wear*, and *deflection*) are thus competing against each other. Due to any particular combination of process parameters in a certain situation, one of these modes may become dominant, and the die ultimately fails due to that failure mode. The reported failure mode is the one which was finally responsible for scrapping the die, but in reality all the three mechanisms were coexisting and competing against each other.

5.9 Results and Discussion

Table 5.2 lists all the failure mechanisms, categorized into the five failure modes discussed above. *Die type* tells us whether the die is of the solid (S), hollow (H) or semi-hollow (SH) profile category. *Number of cavities* refers to the number of profile cavities arranged in a prescribed layout in a multiple-cavity die. This is an important parameter as it would change the extrusion ratio of the die, even when the die profile is exactly the same. Normalized failure probabilities (based on the total number of failures of all types) were worked out for each failure mechanism, and for each major failure mode.

5.9.1 Overall Analysis

Figure 5.8 shows an overall breakup of die failure modes. It is quite evident that the dominant failure mode (for all die shapes taken on the whole) is fatigue fracture (46%), followed by wear (26%) and then deflection (19%). Mixed failure modes (4%) and the various failure mechanisms categorized as miscellaneous (2%) comprise the remaining die failure patterns. Failures caused at the mandrel (including all the three modes: fracture, wear and deflection) constitute 3% of the total failures. The observations support intuitive reasoning:

1. Most of the solid profiles have a large number of sharp corners, projections and protrusions, slots and grooves, combination of thin and thick sections, and generally possess lack of symmetry. Even simple hollows have higher complexities due to the inclusion of a mandrel and welding chambers. Fatigue-based failure is therefore the principal failure mode.
2. With the continually repeated friction between the extremely hard aluminum-oxide layer on the billet and the iron-oxide layer at the bearing surface, excessive wear at the die land is the second major failure mode.
3. Due to the elevated temperatures and pressures involved, and the necessity of relatively high extrusion speeds aimed at higher productivity, plastic deformation and deflection of critical sections is the third significant mode of failure.
4. Rest of the failure classes are obviously not major players in the die failure arena.

Table 5.2 Failures of dies of different types by various failures modes

DIE DETAILS				FAILURES						
S.No.	Die #	Die Type	No. of Cavities	Fracture	Wear	Deflection	Mixed-Mode	Misc	Mandrel	Die-Type Total
1	D1	H	3		3	1				4
2			4	2	21	16	3	1	2	45
3	D2	H	2	13	7	1	1		3	25
4			3	21	2	1		1	1	26
5	D3	H	1		8	2	2		5	17
6			2	1	3	1				5
7	D4	H	2	2	16	15	3		2	38
8	D5	H	1		1		1			2
9			2	1	7	9	2			19
10	D6	H	2			1				1
11			3		4	5				9
12			4		2	1	1			4
13	D7	H	4	1	8	12	2			23
14	D8	H	1		6	14	2		1	23
15	D9	S	2	10	5	1	2			18
16	D10	S	1	47	2		1	1		51
17			2	13						13
18	D11	S	1	25	7	5	3			40
19			2	17	2	1		2		22
20	D12	S	2	20	1					21
21			4	43	5					48
22	D13	S	1	14	2			2		18
23	D14	S	1	6	5					11
24	D15	S	1	16	11			2		29
25	D16	SH	2		5	3	2			10
26			3	4	8	17		2		31
27	D17	SH	2	20	15	5		1	3	44
28			3	12	2	5				19
		Failure-Mode Totals		**288**	**158**	**116**	**25**	**12**	**17**	**616**

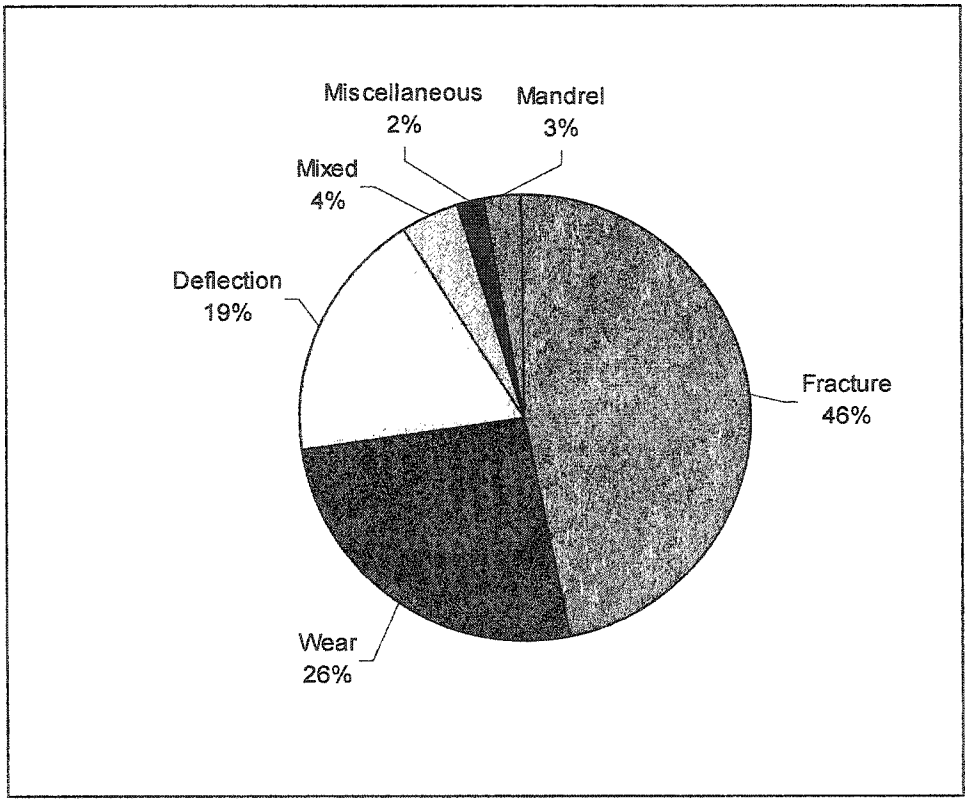

Figure 5.8 Overall breakup of die failure modes

Fracture type failures: It is interesting to note from Fig 5.9 that the leading fracture-type failure is that related to path/brush-path breakdown. In the aluminum construction industry, a very large number of dies is for varieties of door and window sections. Brush paths are the most frequently repeated critical elements in such sections, and thus play a predominant role in fatigue failures.

Wear type failures: Figure 5.10 indicates that wear failures are almost exclusively of the dimension-change type (oversize and overweight are also categories of the same). In this case, even though only part of the bearing surface has been worn out, the extrusions are out-of-dimensions with reference to the tolerances prescribed by the client. Thus most of the dies have to be scrapped much before complete wash-out of the die land. It should be pointed out here that this die rejection takes place after several correction-cleaning-renitriding cycles have already taken place, and repair of the bearing surface is no more feasible.

Deflection type failures: As expected, deflection-type failures (Fig 5.11) are almost exclusively found at the bearing. With uneven and unsymmetrical sections, and maximum pressures and friction forces working here, the bearing is the most likely location to undergo excessive plastic deformation. As tongues are minor bearing surfaces in themselves, they are the next obvious deflection concentration locations; but as tongues are not present in most of the dies, their contribution is only a small fraction of the total deflection failures.

Other failure modes: Miscellaneous die failures (Fig 5.12) also follow the anticipated. Bearing damage is the major contributor, with die/bearing softening and failure of the nitriding oven are next in line. Nitriding oven failures indicate suboptimal hardening and/or heat treatment of the die, making the die and its bearing surface softer than required, thus leading to incorrect extrusion shapes and other flaws.

5.9.2 Profile-Based Failure Analysis

Solid profiles: As described earlier, solid dies are generally the lowest on the complexity scale. However, a look at the profiles included in this study would indicate that on an average the hollow profiles (D1, D2, D3, D4, D5, D6, D7, D8, D16 and D17) are far less

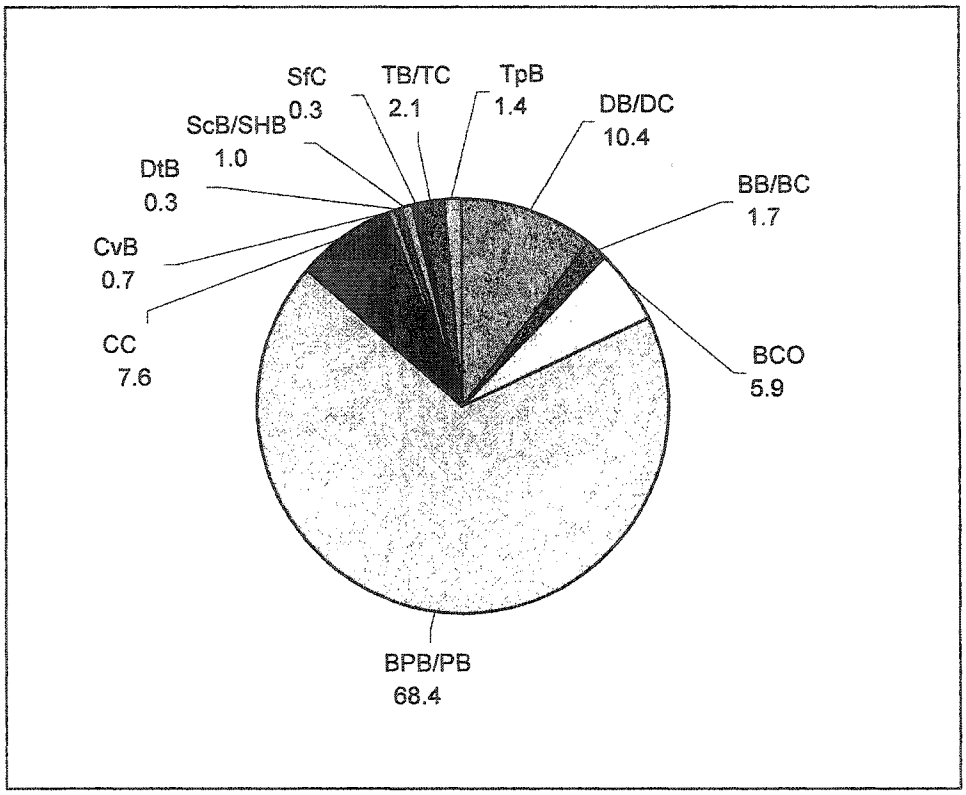

Figure 5.9 Breakup of fracture type failures (288 fracture failures out of 616 total failures)

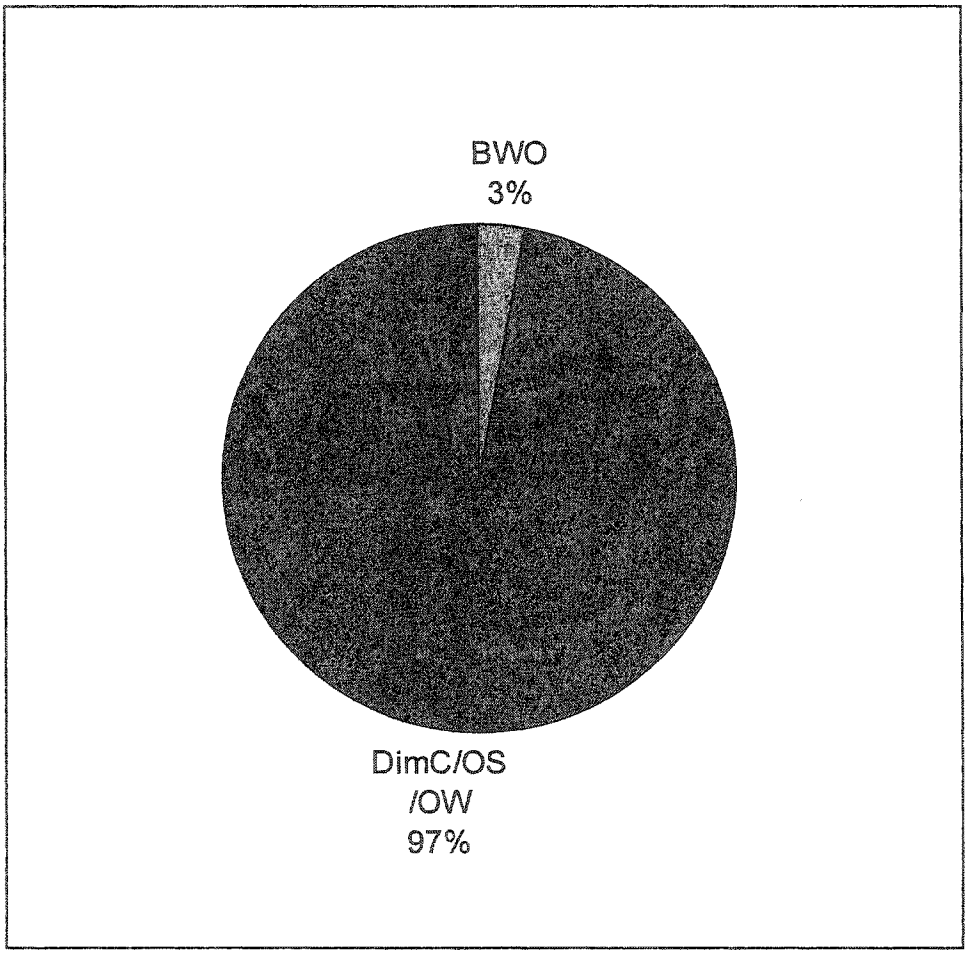

Figure 5.10 Breakup of wear type failures (158 wear failures out of 616 total failures)

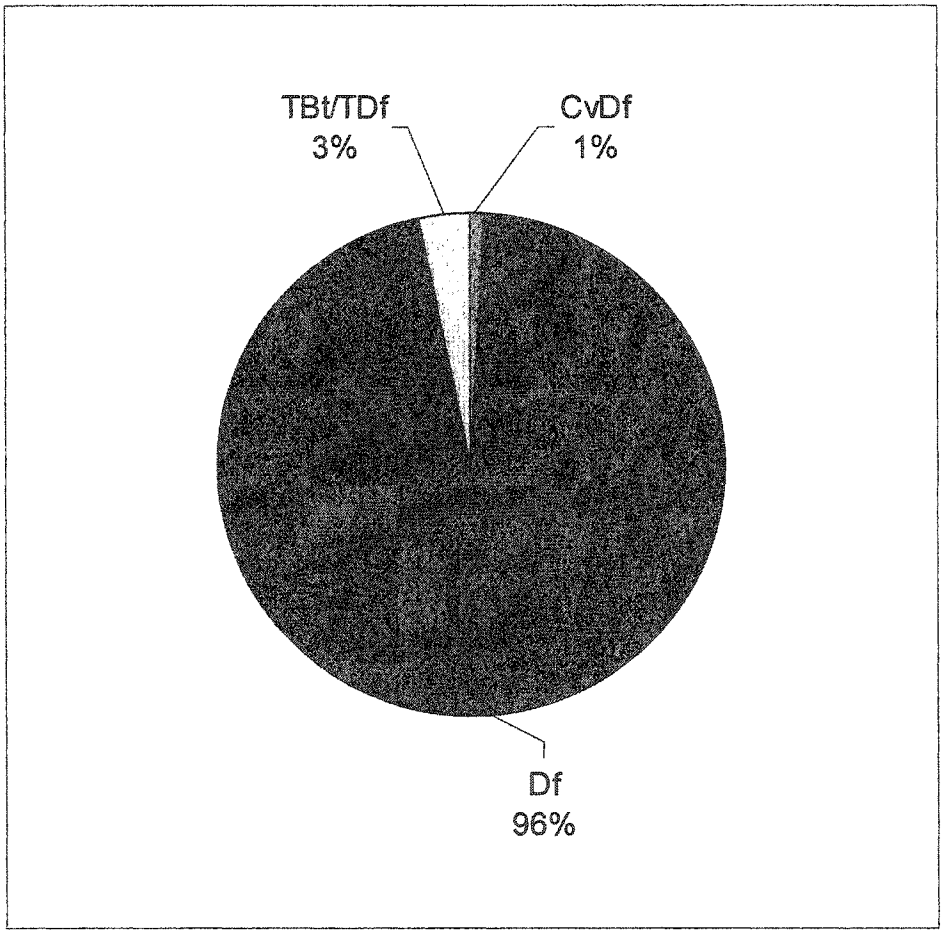

Figure 5.11 Breakup of deflection type failures (116 deflection failures out of 616 total failures)

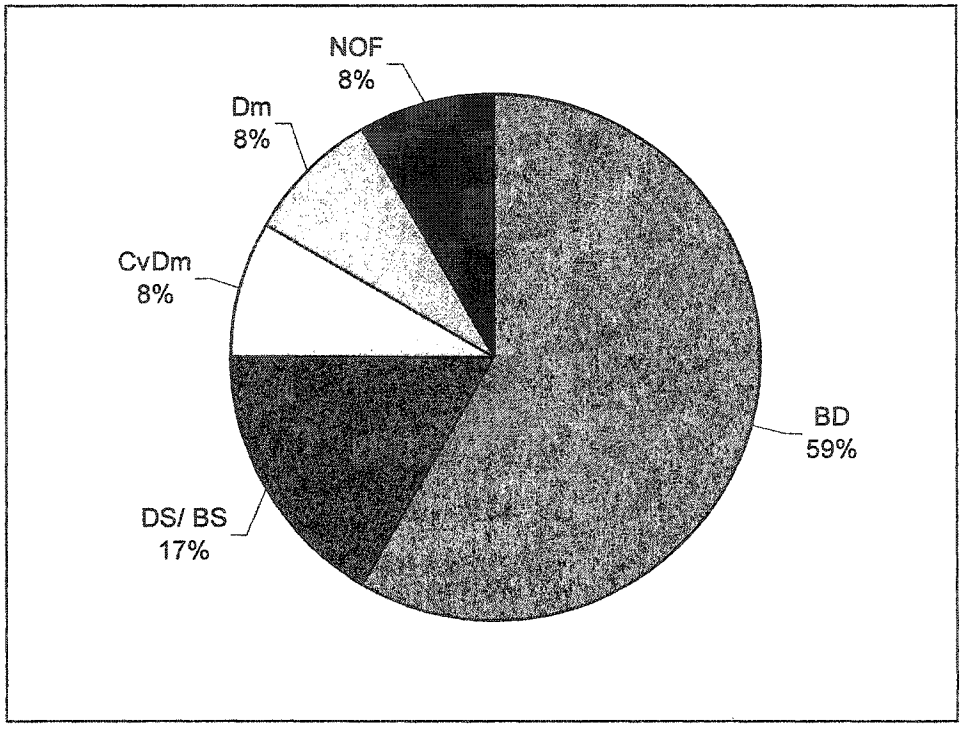

Figure 5.12 Breakup of miscellaneous die failures (12 miscellaneous failures out of 616 total failures)

complex than the solid ones (D9, D10, D11, D12. D13, D14 and D15). Solids have a profusion of stress raisers such as screw bosses, brush paths, tips, and details. This trend is not only true of this selection, but is generally representative of the entire construction aluminum industry. That is why Figure 5.13 shows (as already hinted at in the overall analysis) that fatigue/fracture (77%) is the principal failure category among solid dies. Wear contributes a meager 15%, while deflection failure is an almost insignificant 3%. Obviously, there is no mandrel failure. In the absence of a mandrel and consequent flow disruptions and rewelding of the metal before entry into the bearing cavity (as in hollow dies), forces at the die land in a solid die are far less wear-critical. A similar reasoning would indicate lower heat of friction and deformation which, together with lower extrusion forces, would minimally contribute to plastic deformation and deflection.

Hollow profiles: For hollow dies (Fig 5.14), fracture is relegated to a mere 17% while wear (36%) and deflection (33%) are almost equally dominant failure modes. Mandrel failures constitute 6% of hollow die rejections. The predominance of wear and deflection failures in hollow dies has just been rationalized above, additional flow distribution cavities of the mandrel and the subsequent weld chambers not only adding to the complexity of the die set, but also creating increased forces and friction and higher temperatures at bearing entry. This increased proportion of wear and deflection breakdowns is understandable, but what is the reason behind the significantly lower contribution of fracture failures? Of the various dies selected for this study, hollow dies are usually pure hollows, with few, if any, projections like tongues, brush paths, etc. Minor grooves, slots, projections, and other *details* involving sharp corners and abrupt section changes are generally far more prevalent in solid dies than in hollow ones. This implies a significantly lower contribution of fracture failures in the hollow dies studied.

Semihollow profiles: Semihollow dies show a very peculiar trend. All the three major failure types play almost equal roles, with 34% fracture breakdowns, and 29% each of wear and deflection failures; Fig 5.15. This should be expected. Semi-hollow dies are a cross between hollow and solid ones; the presence of a mandrel creates its innate

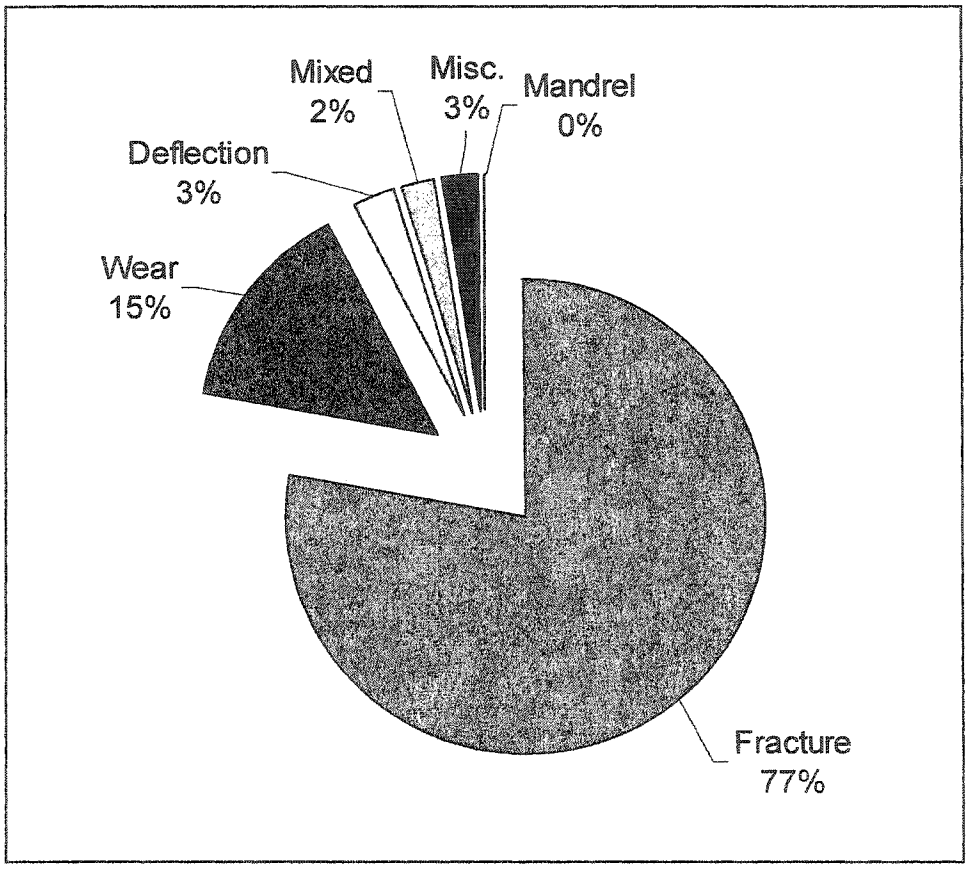

Figure 5.13 Failure mode probabilities for solid dies (271 solid die failures out of 616 total failures)

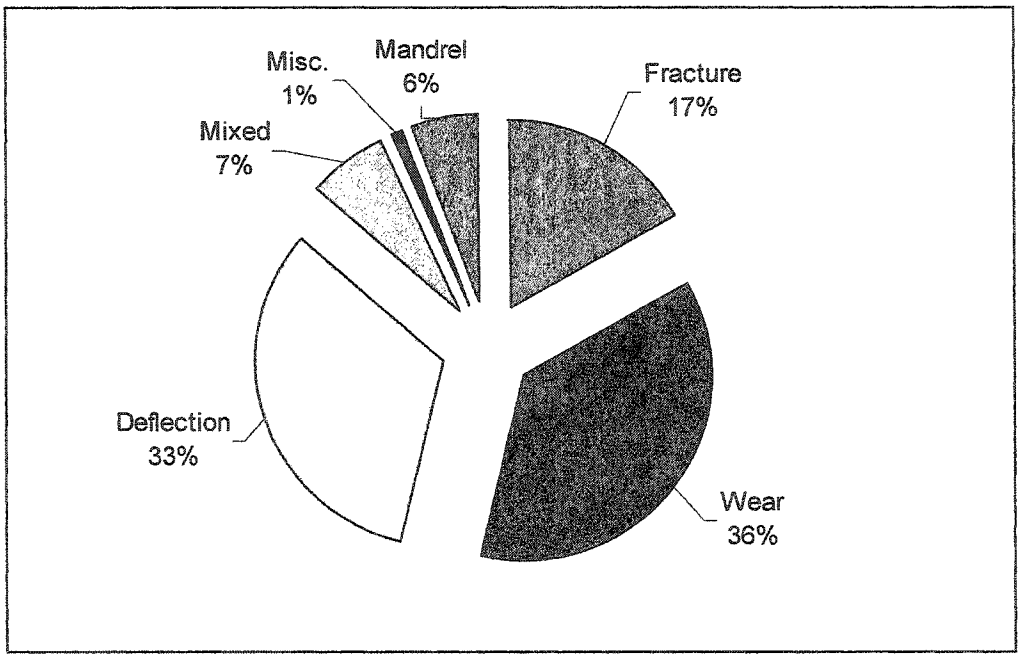

Figure 5.14 Failure mode probabilities for hollow dies (241 hollow die failures out of 616 total failures)

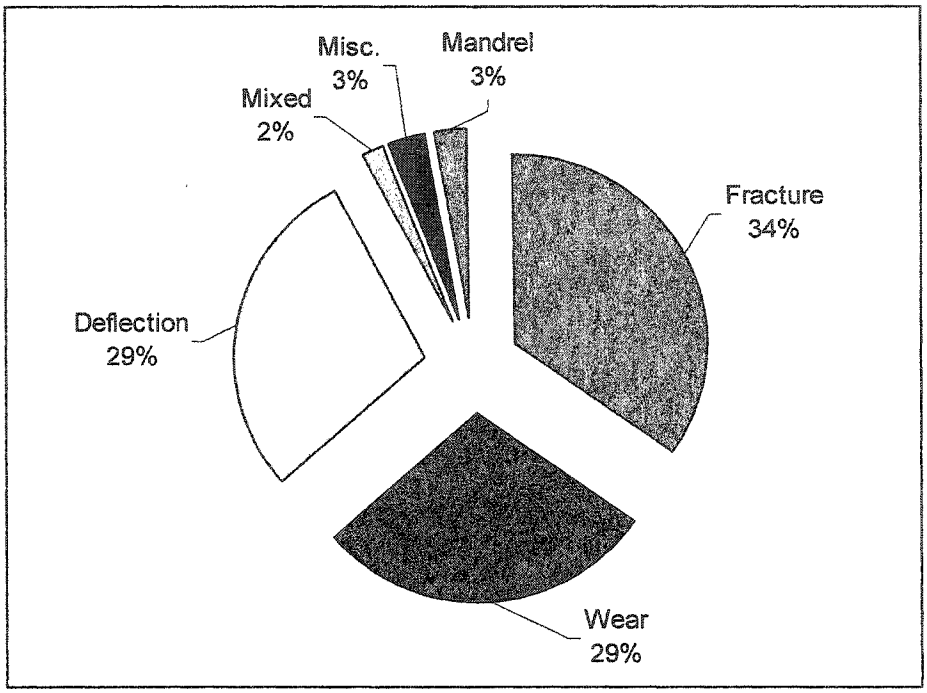

Figure 5.15 Failure mode probabilities for semihollow dies (104 semihollow die failures out of 616 total failures)

complications, while the semi-solid extension accounts for the added details contributing to fracture.

It should be reiterated here that all probabilities reported in the tables and graphs have been normalized, considering the total number of failures (616) for all the dies, as against only solid or only hollow dies. For instance, the probability of fracture failures in solid dies reported here is 34.25% (based on 211 solid fracture failures out of a total 616 die failures studied) instead of 79.62% (211 fracture failures out of 265 total failures in solid dies).

5.9.3 Shape-Wise Breakdown of Failure Classes

We have just seen the distribution of major failure modes for each shape category separately. Figure 5.16 to 5.21 offer a look at things from the opposite viewpoint, taking each failure class and studying the failure spread for the different die shapes (solid, hollow and semi-hollow). If we take only fracture failures (288 out of a total 616 breakdowns), 74% of these failures were in solid dies, 14% in hollow dies and 12% in semihollow ones; Fig 5.16. The interesting point to note is that this indicates almost equal probabilities of failure by fracture for both hollow and semihollow dies, but to a far lesser extent than that for solid ones. This supports our earlier inference that the predominant failure mechanism for solid dies is fatigue fracture.

Figure 5.17 reveals that out of the 158 dies failing through wear-related problems, 56% were hollow, 25% were solid, and 19% were semihollow. The large proportion of hollow dies failing by this mode is expected, confirming the previous conclusion that hollow dies fail primarily through wear. But it is worth noticing that the failure response of solid and semihollow dies to wear is not far different from each other, even though one class employs mandrels while the other does not.

Out of 116 dies scrapped due to plastic deformation (Fig 5.18), 68% were hollow, 26% semihollow, and only 6% were solid. Additional friction, temperatures and forces at the bearing inlet due to the presence of the mandrel and reweld chambers in hollow dies, as explained earlier, are responsible for the large proportion of deflection failures going to

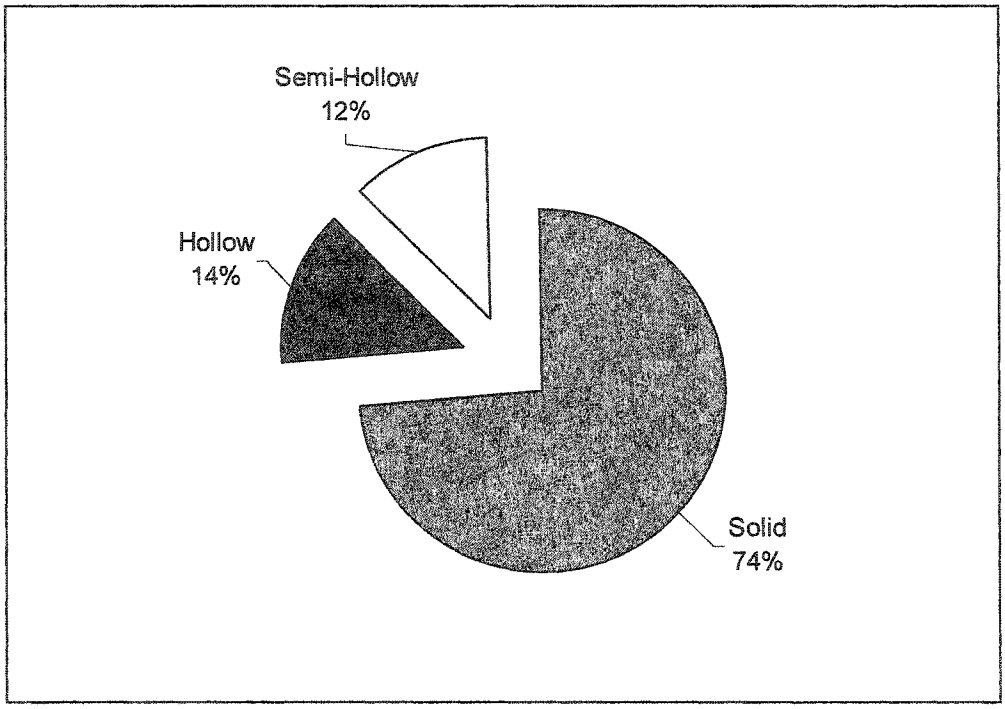

Figure 5.16 Shape-wise distribution of fracture-related failures (288 fracture failures out of 616 total failures)

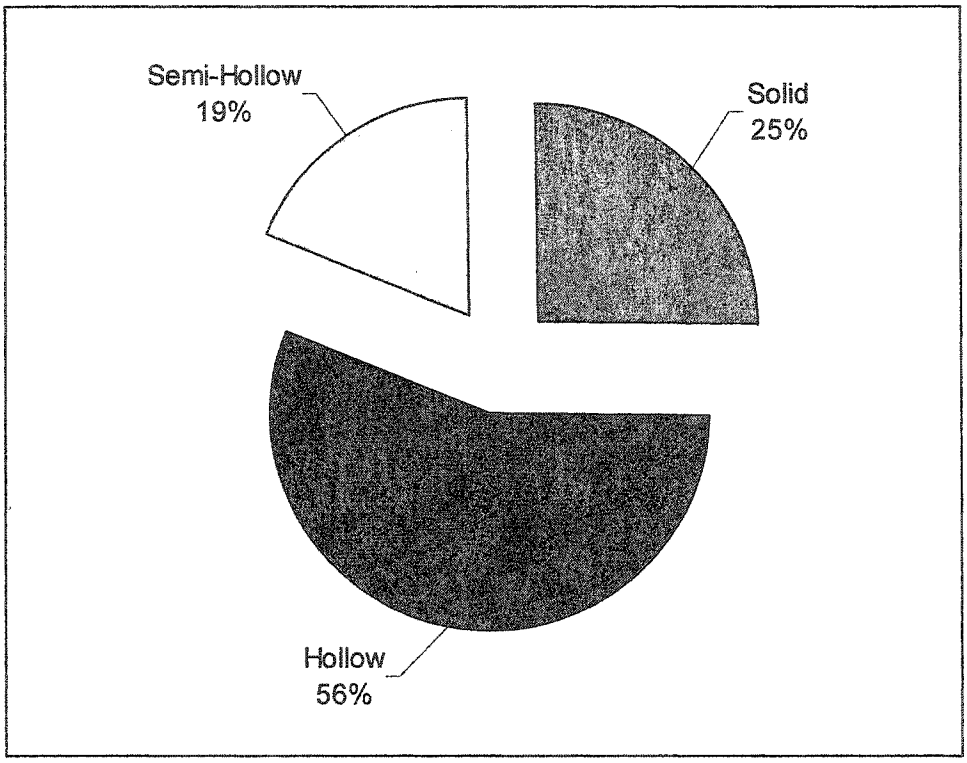

Figure 5.17 Shape-wise distribution of wear-related failures (158 wear failures out of 616 total failures)

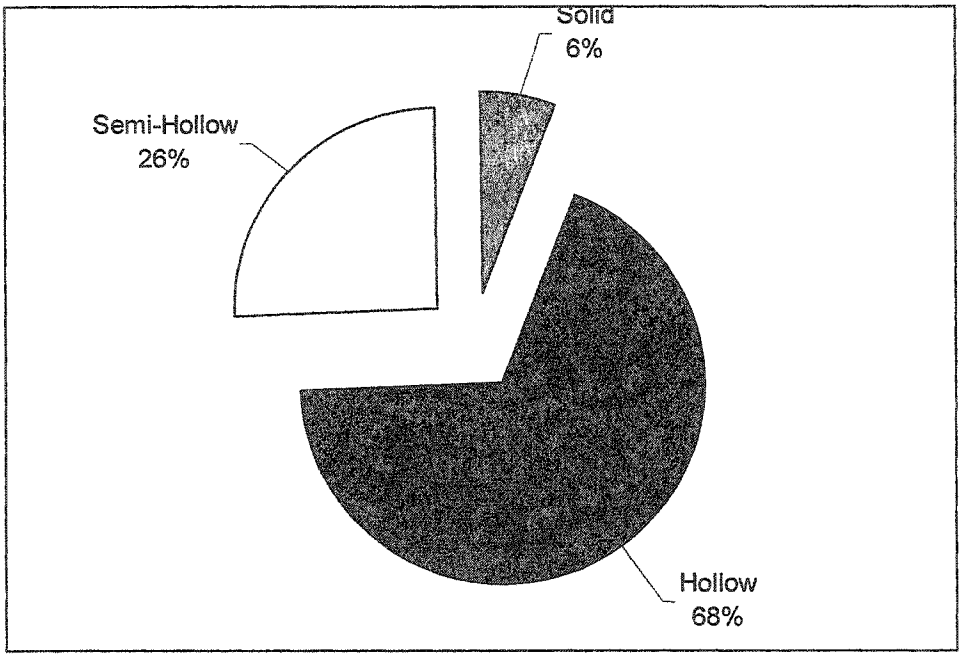

Figure 5.18 Shape-wise distribution of deflection-related failures
(116 deflection failures out of 616 total failures)

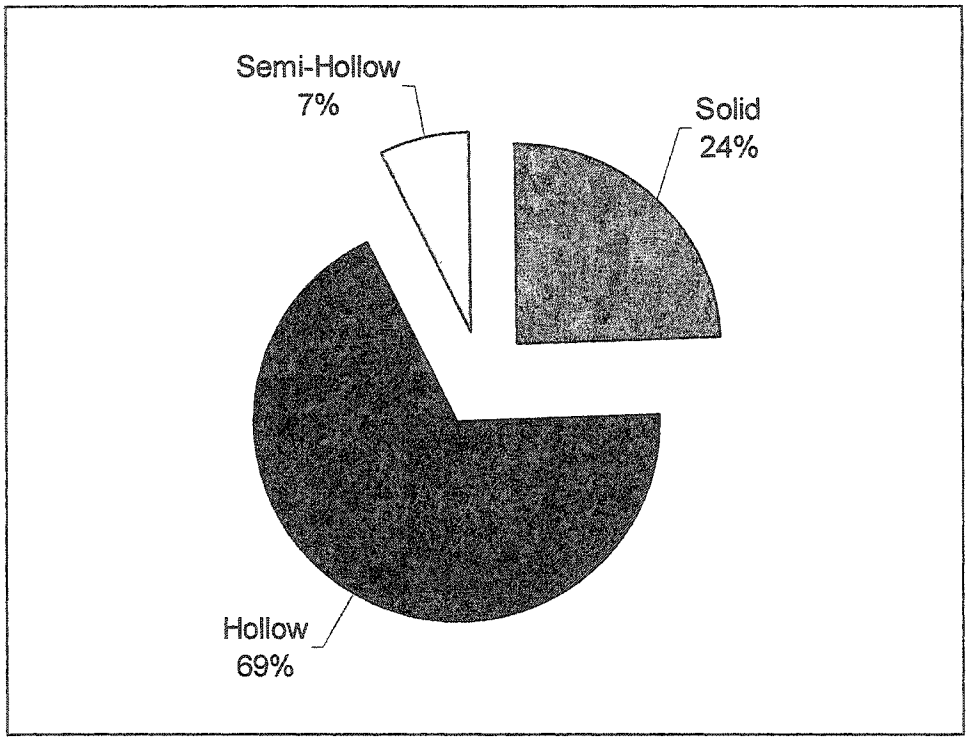

Figure 5.19 Shape-wise distribution of mixed-mode failures (25 mixed-mode failures out of 616 total failures)

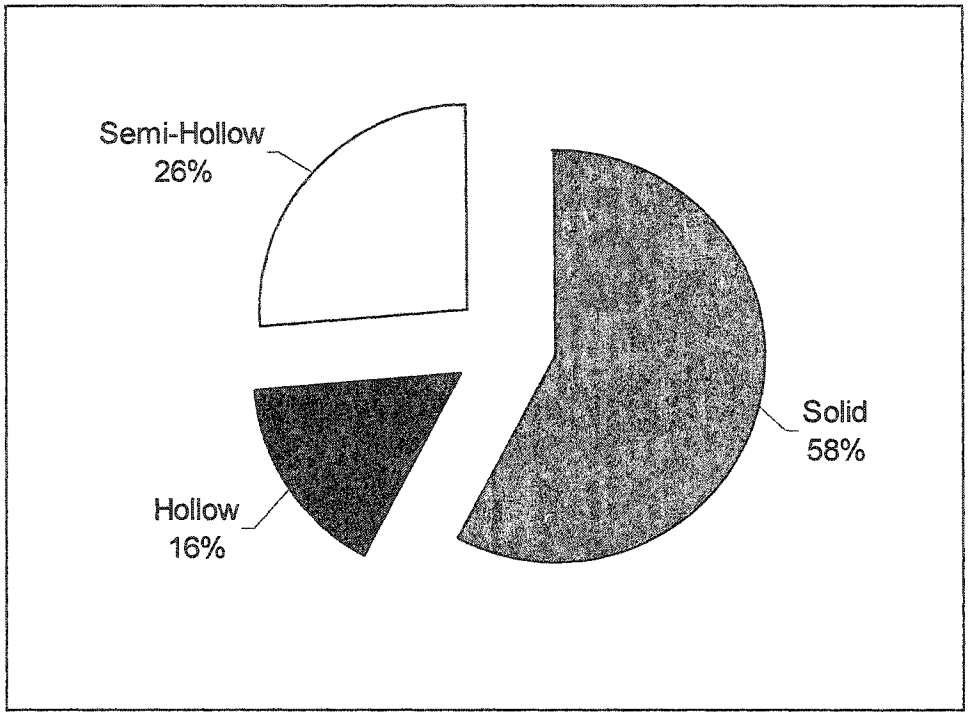

Figure 5.20 Shape-wise distribution of miscellaneous failures (12 miscellaneous failures out of 6161 total failures)

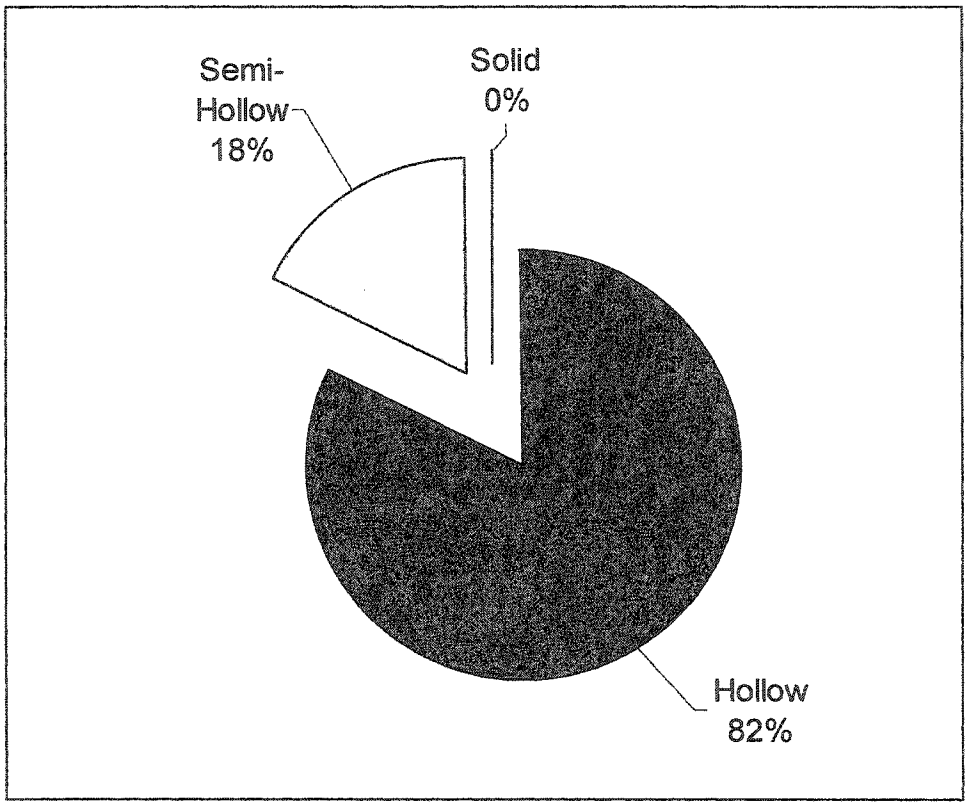

Figure 5.21 Shape-wise distribution of mandrel-related failures (17 mandrel failures out of 6161 total failures)

hollow dies. It is interesting to note, however, that the share of solid dies in this failure type is almost insignificant.

Figures 5.19 to 5.21 reveal that out of he remaining failure categories, mixed-mode failures (more than one failure mode found to be the cause of die rejection) are predominant in hollow dies (69%), miscellaneous breakdowns in solid dies (58%), and mandrel failures in hollow ones (82%). Obviously, solid dies have no mandrel failures.

CHAPTER 6
EXTRUSION TOOLING:
PROBABILISTIC STUDY OF DIE LIFE

6.1 INTRODUCTION

As mentioned in the previous chapter, of all the equipment and tooling involved in a hot forming process, the most critical component is usually considered to be the die due to its superior precision and reliability requirement. Dies and ancillary tooling are exposed to high pressures, elevated temperatures, mechanical and thermal fatigue. Cost and engineering difficulty are obviously high because of factors such as special material and processing, very fine tolerances, and high demands on repeated thermo-mechanical performance. Critical to any study involving efficiency, productivity, or overall economy of any hot forming operation is thus an analysis of tooling performance in terms of *die life* and *die reliability* assessment and prediction.

As concluded in chapter-2, a complex extrusion profile generally requires a higher pressure and a greater force than a simple shape. Varying section thickness, sharp corners and bends, grooves and passageways, etc increase the stresses considerably. Hot working environment further aggravates the situation through repeated thermo-mechanical stresses and fatigue effects. Higher forces and pressures should in general lead to a reduction in die life. It thus appears to be a reasonable conclusion that the working life of an extrusion die is definitely linked to profile complexity.

6.1.1 Current Work

Results are presented in this chapter from a study about the probabilistic behavior of service life of tooling in commercial aluminum extrusion, and the exploration of the

relationship between die reliability and profile complexity. Mostly the same set of experimental data that was used for the assessment of die failure modes and mechanisms in the last chapter is now analyzed from a die reliability viewpoint, some cases representing outlier behavior being dropped. A total of 595 die failures involving 17 different die profiles (23 profiles, considering different extrusion ratios) were studied. All dies were made of H-13 steel, while the billet material was Al-6063 in all the cases. Considering die life to be a random variable, an attempt was made to fit a reasonable probability distribution to the 23 different data sets. Rather than adopting a non-parametric approach, a number of probability distributions most popularly employed in reliability analyses were explored. The second part of the study is concerned with evaluation of shape complexity of the die profiles studied according to the definitions used so far, and exploration of any possible patterns between die complexity and die reliability. The complexity definitions investigated here are the four published ones (C_1, C_2, C_3, and C_4) and the newly proposed definition C_5.

6.2 Die Failure Probability and Reliability

Expressed in terms of the random variable t (time to failure for a die), the *probability density function* (PDF) has the physical meaning of "probability that failure takes place at a time between t and $(t + \Delta t)$."

$$f(t)\,\Delta t = P\{t \le t \le \Delta t\}, \qquad t > 0. \tag{6.1}$$

The associated *cumulative distribution function* (CDF) is the "probability that failure takes place at a time less than or equal to t."

$$F(t) = P\{t \le t\} \tag{6.2}$$

Reliability is the term used to express the "probability that a component or system will perform satisfactorily for a specified period of time (t) under a given set of working conditions" [Lewis 1996].

$$R(t) = P\{t > t\} \tag{6.3}$$

Obviously,

$$R(t) = 1 - F(t), \tag{6.4}$$

and

$$R(t) = \int_0^t f(t')dt'. \tag{6.5}$$

Also, from the properties of a PDF, it is clear that

$R(0) = 1$,

and

$R(\infty) = 0$.

6.2.1 Some Related Probability Distributions

On the basis of any given small or large data set, a non-parametric analysis can be performed to get a statistical relationship between t and $F(t)$. On the other hand, there are quite a few standard probability distributions that can describe the behaviour of a random data sample. With reference to reliability studies, and specifically in the context of failure of hot working dies, the following distributions are more relevant.

Normal distribution: In this distribution, life of a component or system is determined from the time-to-failure PDF

$$f(t) = \frac{1}{\sqrt{2\pi}\sigma} \exp\left[-\frac{1}{2}\left(\frac{t-\mu}{\sigma}\right)^2\right]. \tag{6.6}$$

Parameters of the distribution are the mean (μ) and the variance (σ^2) or the standard deviation (σ). If we use the transformation $z = (t - \mu)/\sigma$, we get

$$f_z(z) = \frac{1}{\sqrt{2\pi}} \exp\left(-\frac{1}{2}z^2\right). \tag{6.7}$$

The standardized normal CDF is then defined as

$$F(t) = \Phi\,[(t-\mu)/\sigma], \tag{6.8}$$

having a distribution with $\mu_z = 0$ and $\sigma_z = 1$. Values of $\Phi(z)$ can be found from standard tables.

Lognormal distribution: If x is a normally distributed random variable, and we have $x = \ln(t)$, then t is said to be lognarmally distributed. It is described by the PDF

$$f(t)=\frac{1}{\sqrt{2\pi}\omega t}\exp\left\{-\frac{1}{2\omega^2}\left[\ln\left(\frac{t}{t_0}\right)\right]^2\right\}, \tag{6.9}$$

where the two parameters t_0 and ω are given by $\mu_X = \ln(t_0)$, and $\sigma_X = \omega$. Using the transformation $z = (1/\omega)\ln(t/t_0)$, we can express the CDF in terms of the standardized normal integral as

$$F(t)=\Phi\left[\frac{1}{\omega}\ln\left(\frac{t}{t_0}\right)\right]. \tag{6.10}$$

Weibull distribution: Particularly justified for situations where the *worst link* or the largest of many competing flaws is responsible for failure, the Weibull distribution is described by the PDF

$$f(t)=\frac{m}{\theta}\left(\frac{t}{\theta}\right)^{m-1}\exp\left[-\left(\frac{t}{\theta}\right)^m\right]. \tag{6.11}$$

The CDF is given by

$$F(t)=1-\exp\left[-\left(\frac{t}{\theta}\right)^m\right]. \tag{6.12}$$

Here, θ is called the *scale parameter*, while m is known as the *shape parameter*.

Extreme value distributions: Asymptotic extreme value distributions are generally used in reliability engineering when the number of variables from which the data is collected is very large. The *minimum extreme-value distribution* is frequently used as an alternative to Weibull in describing strength or capacity of the system or component. Obviously, the minimum strength component will decide whether the system fails under a given loading situation. It is described by

$$f(t)=\frac{1}{\Theta}e^{(t-u)/\Theta}\exp\left[-e^{(t-u)/\Theta}\right], \tag{6.13}$$

and

$$F(t)=\exp\left[-e^{(t-u)/\Theta}\right]. \tag{6.14}$$

6.3 Regression in the Reliability Domain

If a sufficiently representative sample of time-to-failure data is available, and we want to see whether a standard distribution fits the data reasonably well or not, we adopt the following regression strategy. Suppose we want to examine the Weibull distribution. We know that

$$R(t) = 1 - F(t) = e^{-(t/\theta)^m}. \tag{6.15}$$

Taking natural log twice, we get

$$\ln[-\ln\{1 - F(t)\}] = m\ln(t) - m\ln(\theta). \tag{6.16}$$

Comparing this with the standard equation of a straight line ($y = ax + b$), we can see that

$$y = \ln[\ln\{1 - F(t)\}], \tag{6.17}$$

together with $m = a$, and $b = -m\ ln(\theta)$. We can follow the same procedure for regressing the data to other distributions described above. This regression technique has been summarized in Table 6.1 for all the distributions mentioned. To assess how well a standard distribution fits a given data set, a measure of the *goodness of fit* known as the *coefficient of correlation* (r^2) is generally used.

6.4 Experimental Data and Calculations

The die life (time to failure) data collected for this study were all from ALUPCO, Dammam. Seventeen (17) different die profiles, ranging in complexity from the simplest hollow (box or rectangular) to quite complex solid and hollow shapes, were included in the study. If we consider dies with different extrusion ratios as different from each other, there were 23 profiles in all. A total of 595 die failures involving the various dies are reported here. Time-to-failure is expressed in terms of the total weight extruded before failure (one metric ton = 1000 kg). Die geometrical data are taken directly from actual profile drawings. Values of circumscribing circle diameter (*CCD*), extrusion ratio (R), and the complexity indices (C_1, C_2, C_3, C_4, C_5) are calculated for each die profile and for

Table 6.1 Regression scheme for reliability distributions

Distribution	***F(t)***	**Transformation** $y = ax + b$	y	x	**Parameters**	
Weibull	$1-\exp[-t/\theta)^m]$	$\ln\ln\left[\frac{1}{1-F(t)}\right] = m\ln(t) - m\ln(\theta)$	$\ln\ln\left[\frac{1}{1-F(t)}\right]$	$\ln(t)$	$\hat{m} = a$	$\hat{\theta} = \exp(-b/a)$
Extreme Value	$1-\exp[-e^{(t-u/\Theta)}]$	$\ln\ln\left[\frac{1}{1-F(t)}\right] = \frac{1}{\Theta}t - \frac{u}{\Theta}$	$\ln\ln\left[\frac{1}{1-F(t)}\right]$	t	$\hat{\Theta} = 1/a$	$\hat{u} = -b/a$
Normal	$\Phi\left(\frac{t-\mu}{\sigma}\right)$	$\Phi^{-1}[F(t)] = \frac{t}{\sigma} - \frac{\mu}{\sigma}$	$\Phi^{-1}[F(t)]$	t	$\hat{\sigma} = 1/a$	$\mu = -b/a$
Lognormal	$\Phi\left(\frac{1}{\omega}\ln\left(\frac{t}{t_0}\right)\right)$	$\Phi^{-1}[F(t)] = \frac{1}{\omega}\ln(t) - \frac{1}{\omega}\ln(t_0)$	$\Phi^{-1}[F(t)]$	$ln(t)$	$\hat{\omega} = 1/a$	$\hat{t}_0 = \exp(-b/a)$

each *number of cavities* in a die. The statistics are summed up in Table 6.2, together with average die life (*mean time to failure, MTTF*) figures.

CDF of die life for each case is calculated using the *mean rank formula*

$$\hat{F}(t) = \frac{1}{N+1}, \quad i = 1, 2, 3, \ldots, \mathrm{N} \tag{6.18}$$

where N is the total number of observations, and t is the time-to-failure (weight extruded). Regression calculations for Weibull, extreme-value (minimums), normal, and lognormal distributions are carried out according to the scheme outlined in Table 6.1.

6.5 Results and Discussion

After plotting the regressed die failure data, straight lines are fitted to the graphs and the goodness-of-fit values (coefficient of correlation, r^2) are obtained. As a sample, Fig 6.1 shows the regression plots for one of the dies studied (die # D6). Defining parameters for each distribution type (m and θ for Weibull, Θ and u for extreme-value, μ and σ for normal, ω and t_0 for lognormal) are also calculated. Dies having different number of cavities (resulting in different extrusion ratios) for the same extrusion profiles are treated as different data sets.

6.5.1 Goodness of Fit

Table 6.3 outlines the goodness of fit in terms of the coefficient of correlation (r^2) for the probability distributions considered for each die failure data set. Weibull (average $r^2 \geq 0.95$), normal ($r^2 \geq 0.94$), and lognormal ($r^2 \geq 0.92$) distributions yield the best overall fit for reliability data, Weibull being the leader. Figure 6.2 strengthens the conclusion. Minimum extreme value and exponential distributions generate the weakest fit.

Weibull distribution is widely used in reliability analyses for describing the distribution of times to failure and of strengths. As mentioned earlier, it is particularly suited for situations where a *weakest-link* or the largest of many competing flaws is responsible for failure. Minimum extreme value (EV) distribution is closely related to the Weibull distribution and is thus often used for similar purposes, such as representation of

Table 6.2 Geometrical and complexity data, and *MTTF* for profiles studied

S. No.	Die Type	Die No.	P_s (mm)	A_s (mm^2)	W_s (g/m)	n	T_m (mm)	CCD (mm)	D_0 (mm)	R	P_0	C_1	C_2	C_3	C_4	C_5	MTTF (kg)
1	H	D1	120	149	403	4	1.3	44.7	224	66.12	43.27	0.81	0.30	34.40	1.18	1.18	30827
2	H	D2	228	211	570	2	1.3	50.1	186	64.39	51.49	1.08	0.40	38.53	1.55	1.42	14870
3	H		228	211	570	3	1.3	50.1	224	62.26	51.49	1.08	0.40	38.53	1.55	1.42	27533
4	H	D4	288	266	718	2	1.3	62.3	186	51.07	57.82	1.08	0.40	47.92	1.72	1.51	24072
5	H		288	266	718	3	1.3	62.3	224	49.38	57.82	1.08	0.40	47.92	1.72	1.51	32233
6	H	D5	247	267	721	3	1.3	61.6	224	49.20	57.92	0.93	0.34	47.35	1.50	1.39	20561
7	H	D6	240	328	902	1	1.4	102	180	77.58	64.20	0.73	0.27	72.84	1.37	1.31	15061
8	H	D7	200	253	684	2	1.3	82.5	180	50.29	56.39	0.79	0.29	63.43	1.33	1.28	9866
9	H	D8	240	305	825	2	1.3	102	224	64.60	61.91	0.79	0.29	78.45	1.40	1.33	12078
10	H	D9	140	176	475	3	1.3	49.5	186	51.46	47.03	0.80	0.29	38.07	1.21	1.21	14890
11	H		140	176	475	4	1.3	49.5	224	55.98	47.03	0.80	0.29	38.07	1.21	1.21	12518
13	H	D10	240	282	761	1	1.2	89.4	186	96.35	59.53	0.85	0.32	74.53	1.44	1.35	29694
14	S	D11	545	364	983	1	1.35	117	186	74.65	67.63	1.50	0.55	86.39	3.17	2.09	43726
16	S	D12	447	294	794	1	1.3	100	186	92.42	60.78	1.52	0.56	76.92	2.76	1.95	26292
17	S		447	294	794	2	1.3	100	224	67.02	60.78	1.52	0.56	76.92	2.76	1.95	37980
18	S	D13	345	236	637	2	1.3	51.6	186	57.57	54.46	1.46	0.54	39.70	2.25	1.75	26750
19	S	D14	290	192	518	2	1.3	65.3	186	70.76	49.12	1.51	0.56	50.23	2.07	1.67	23513
20	S		290	192	518	4	1.3	65.3	224	51.31	49.12	1.51	0.56	50.23	2.07	1.67	25459
21	S	D15	608	403	1088	1	1.3	127	186	67.42	71.16	1.51	0.56	97.32	3.48	2.20	34817
22	S	D16	694	483	1304	1	1.3	127	186	56.26	77.91	1.44	0.53	97.32	3.72	2.28	29977
23	S	D17	723	516	1393	1	1.35	133	186	52.66	80.52	1.40	0.52	98.43	3.77	2.30	35304

Table 6.3 Goodness of fit (r^2) values for die-life probability distributions

S.No.	Die #	Cavities	Correlation Coefficient (r^2)				
			Weibull	Exponential	Extreme-Value	Normal	Lognormal
1	D1	4	0.979	0.611	0.962	0.983	0.910
2	D2	2	0.907	0.573	0.853	0.899	0.908
		3	0.936	0.696	0.834	0.942	0.986
3	D3	2	0.984	0.831	0.812	0.923	0.973
		3	0.970	0.720	0.954	0.975	0.934
4	D4	2	0.962	0.914	0.815	0.918	0.966
		3	0.923	0.833	0.926	0.979	0.860
5	D5	1	0.971	0.924	0.844	0.940	0.969
6	D6	2	0.988	0.949	0.781	0.909	0.980
7	D7	2	0.952	0.913	0.789	0.893	0.954
8	D8	3	0.908	0.695	0.886	0.918	0.879
		4	0.901	0.726	0.780	0.868	0.954
9	D9	4	0.945	0.764	0.904	0.956	0.871
10	D10	1	0.957	0.765	0.913	0.969	0.894
11	D11	1	0.957	0.600	0.967	0.972	0.848
		2	0.947	0.919	0.833	0.919	0.959
12	D12	1	0.962	0.800	0.903	0.972	0.876
		2	0.940	0.878	0.844	0.921	0.914
13	D13	2	0.946	0.934	0.885	0.961	0.879
14	D14	2	0.965	0.921	0.858	0.948	0.908
		4	0.966	0.815	0.906	0.980	0.886
15	D15	1	0.909	0.804	0.777	0.881	0.960
16	D16	1	0.976	0.730	0.952	0.983	0.942
17	D17	1	0.968	0.863	0.869	0.960	0.953
	AVERAGE		0.951	0.799	0.869	0.940	0.923

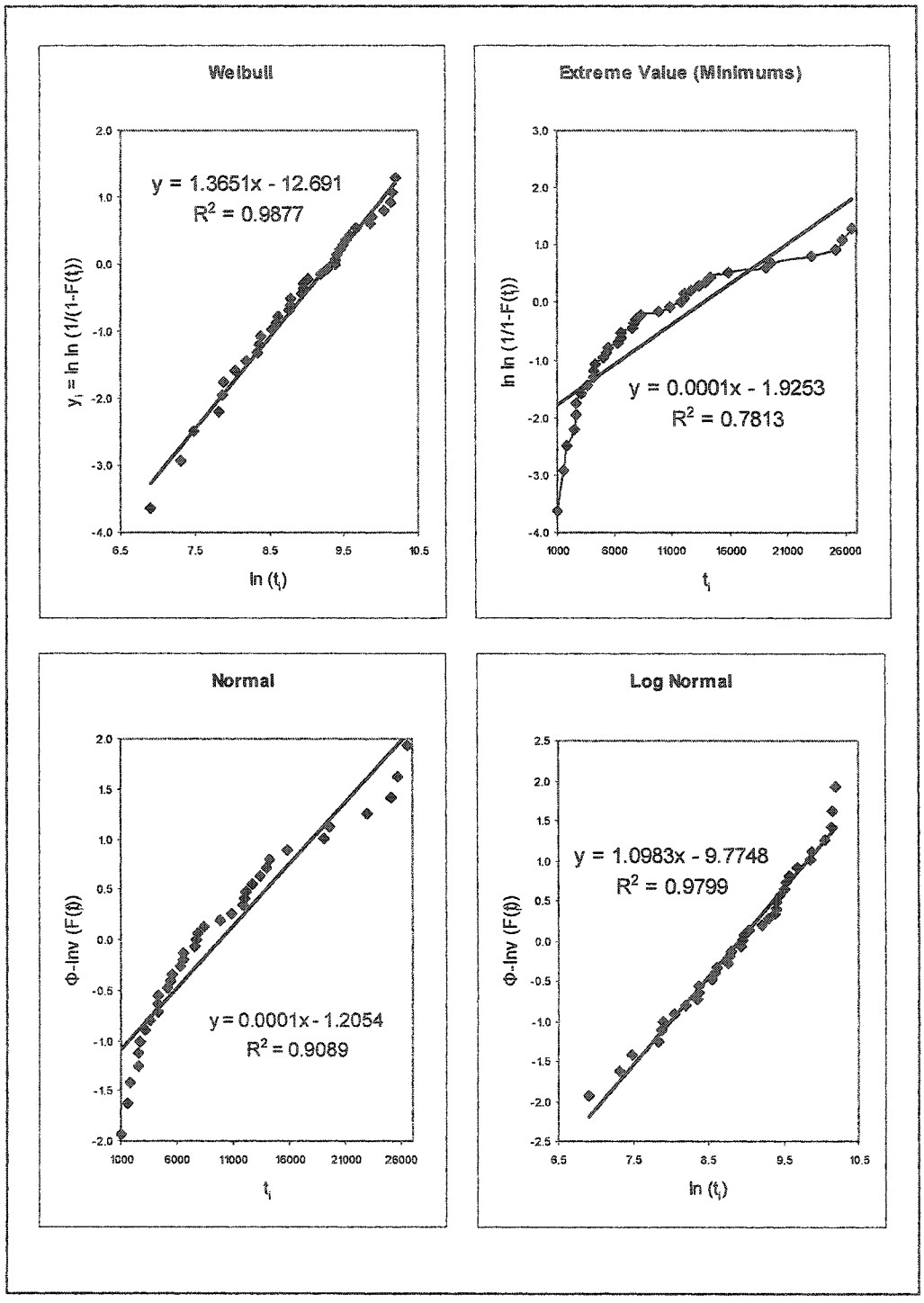

Figure 6.1 Regression plots of various probability distributions for die life data of die # D6

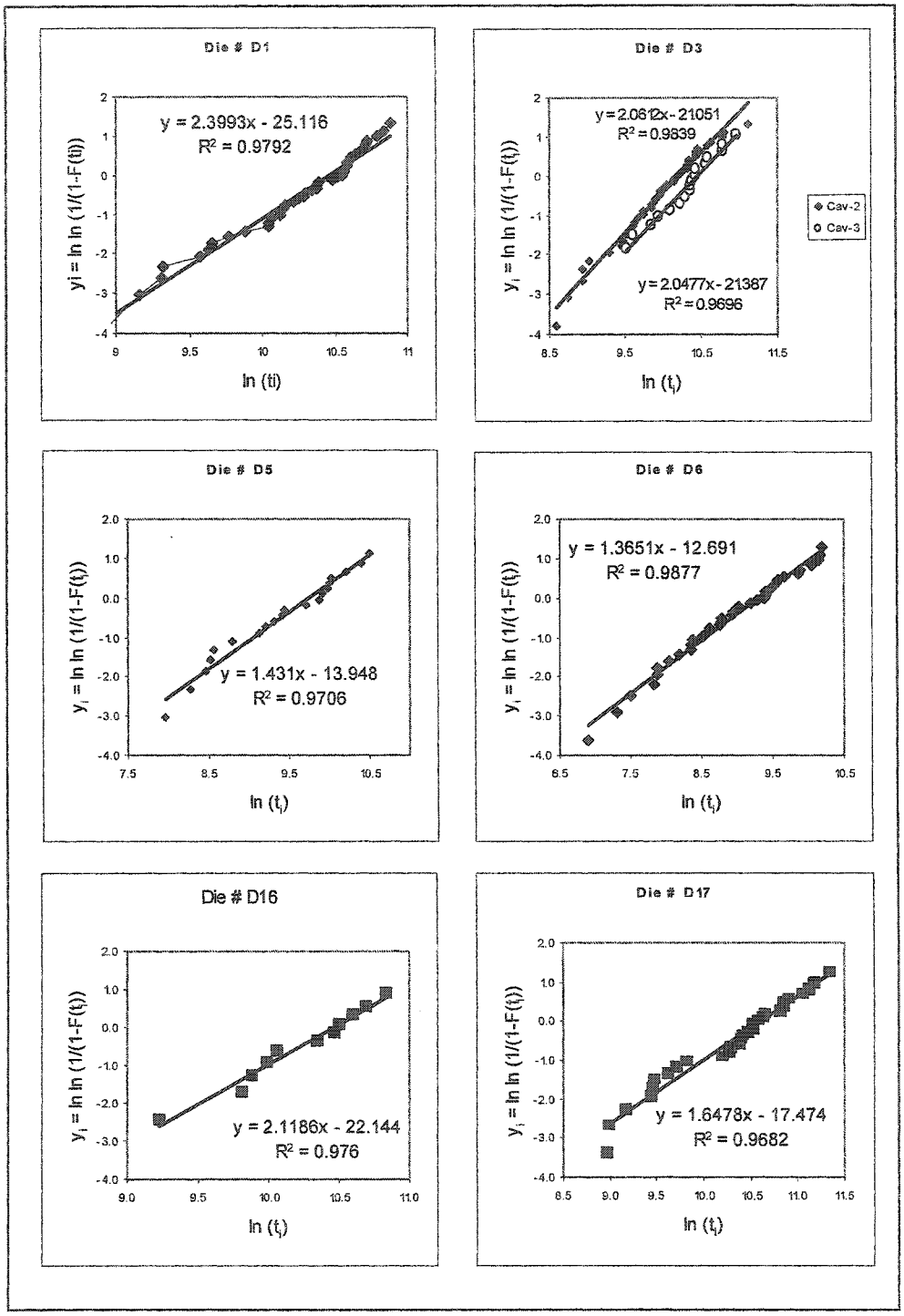

Figure 6.2 Weibull distribution shows a very good fit ($r^2 \geq 0.97$) for die life data for various die profiles.

failure times. By using the transformation $x = \ln(y)$, the equations in x for minimum EV distribution will reduce to a Weibull distribution in y. If not Weibull, then minimum EV distribution would be expected to closely fit failure data. For the failure data of extrusion dies studied, however, Weibull distribution provides a far closer fit than the extreme value one.

As described earlier, lognormal and normal distributions are closely related, exactly the same way as Weibull and minimum EV distributions are. Together, the two normal-type plots yield about a 93% fit to the failure data. These PDF's are generally the most popular as they are uniformly spread out on both sides of the mean and are not skewed to the left or right like other distributions. So the fact that a significant number of failure data sets studied are agreeably represented by normal-like distributions may be well received.

Weibull, normal, and lognormal PDF's are generally the most popular distributions to represent wear-out type failures. Such failures correspond to increasing failure rates. Each distribution reflects a slightly different failure rate model. In this study, Weibull type failure rate comes out to be relatively the best, although normal or lognormal models cannot be ignored completely. The mathematical ease to work with a Weibull model when deciding optimal die replacement strategies or determining number of dies needed for a given production run makes it more attractive.

6.5.2 Weibull Parameters

As mentioned above, distribution parameters were calculated for all curve fittings carried out. Being the overall best fit, we here mention only the Weibull distribution described by $F(t) = 1 - exp[-(t/\theta)^m]$. The shape parameter (m) ranges from 0.85 to 3.19, while the scale parameter (θ) varies between 10902.58 kg and 50666.25 kg for various dies. The die life t is expressed in kg extruded.

5.3 Profile Geometry and Reliability

Plots of m and θ against C_1, C_2, C_3, and C_5 are shown in Figures 6.3 to 6.7. As expected, the shape parameter (m) exhibits almost the same behavior for all complexity indices. The

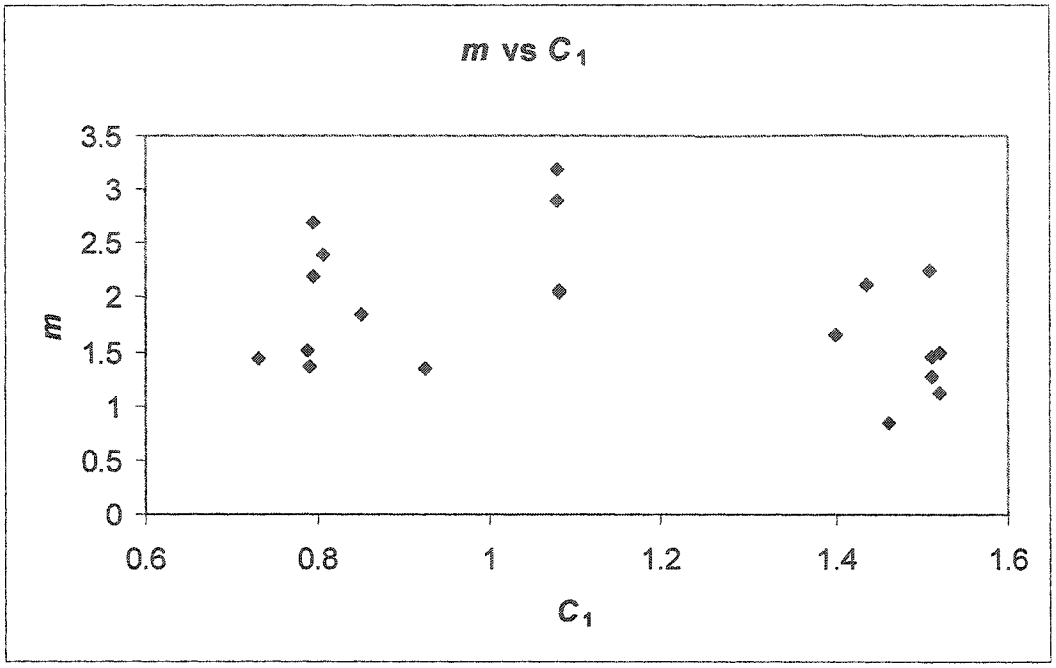

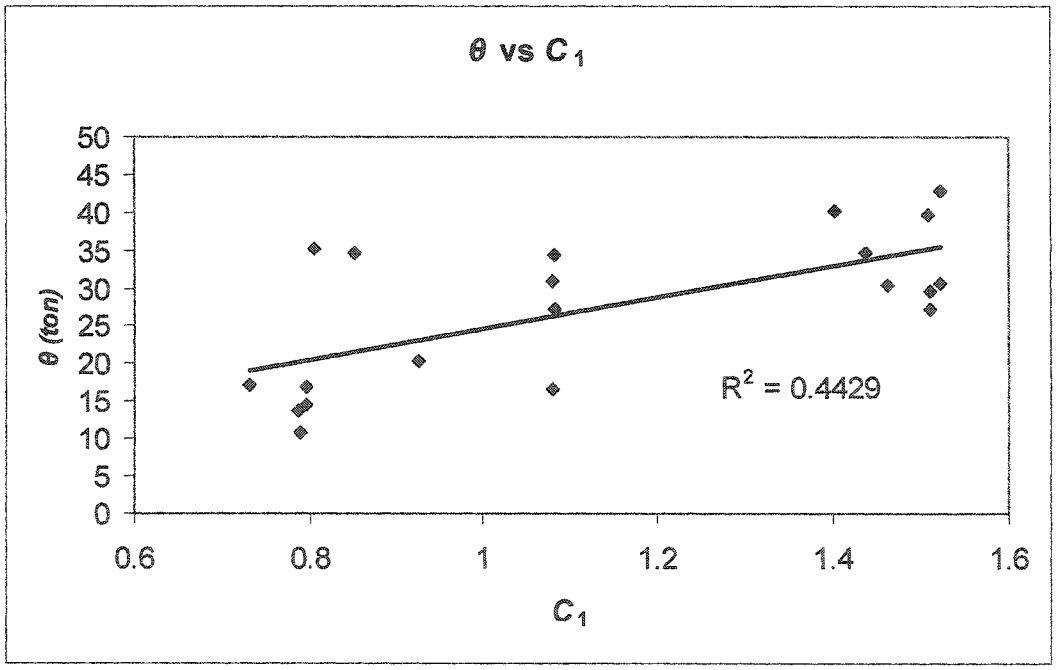

Figure 6.3 Variation of Weibull shape parameter (m) and scale parameter (θ) against complexity index C_1, for the die life data studied

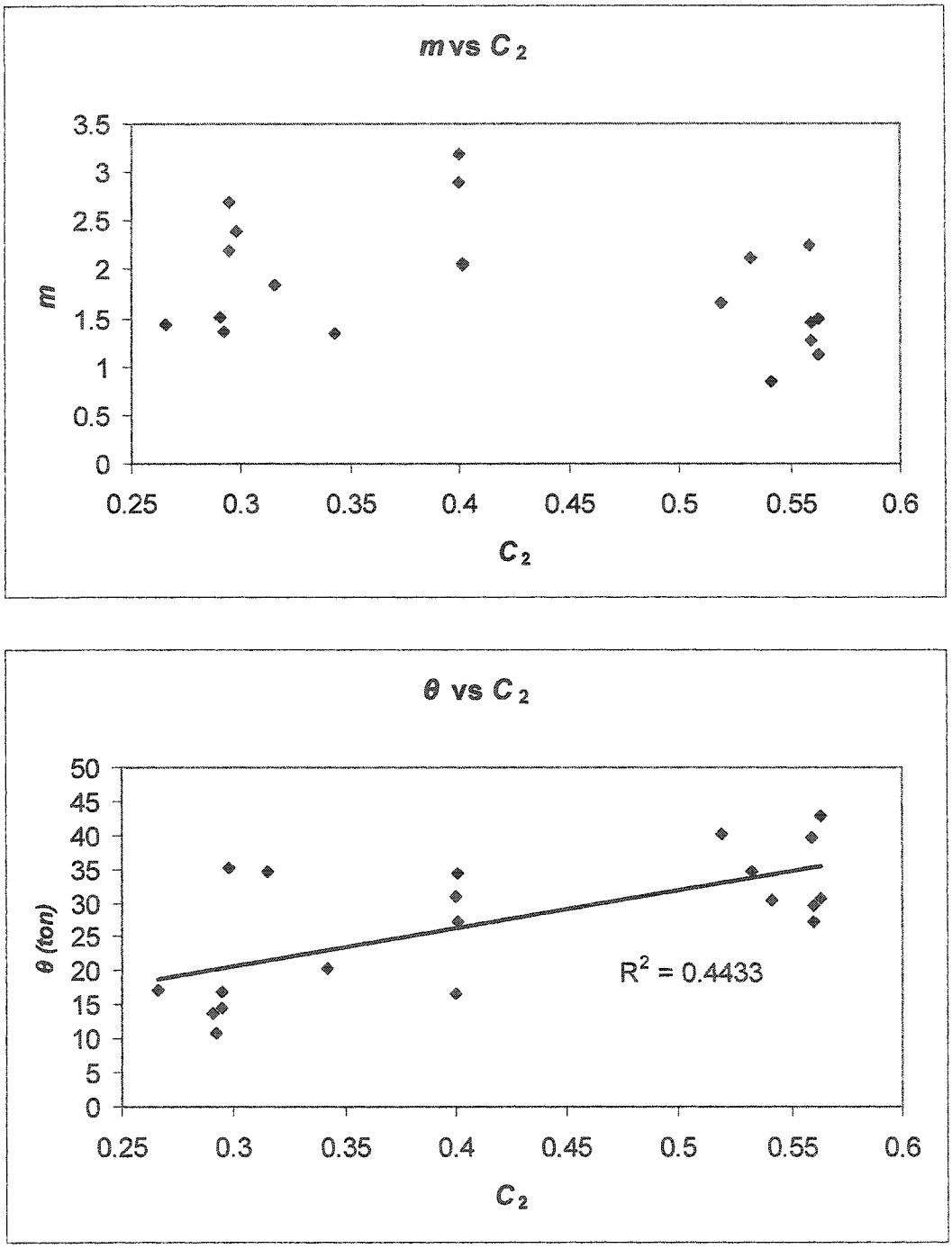

Figure 6.4 Variation of Weibull shape parameter (m) and scale parameter (θ) against complexity index C_2, for the die life data studied

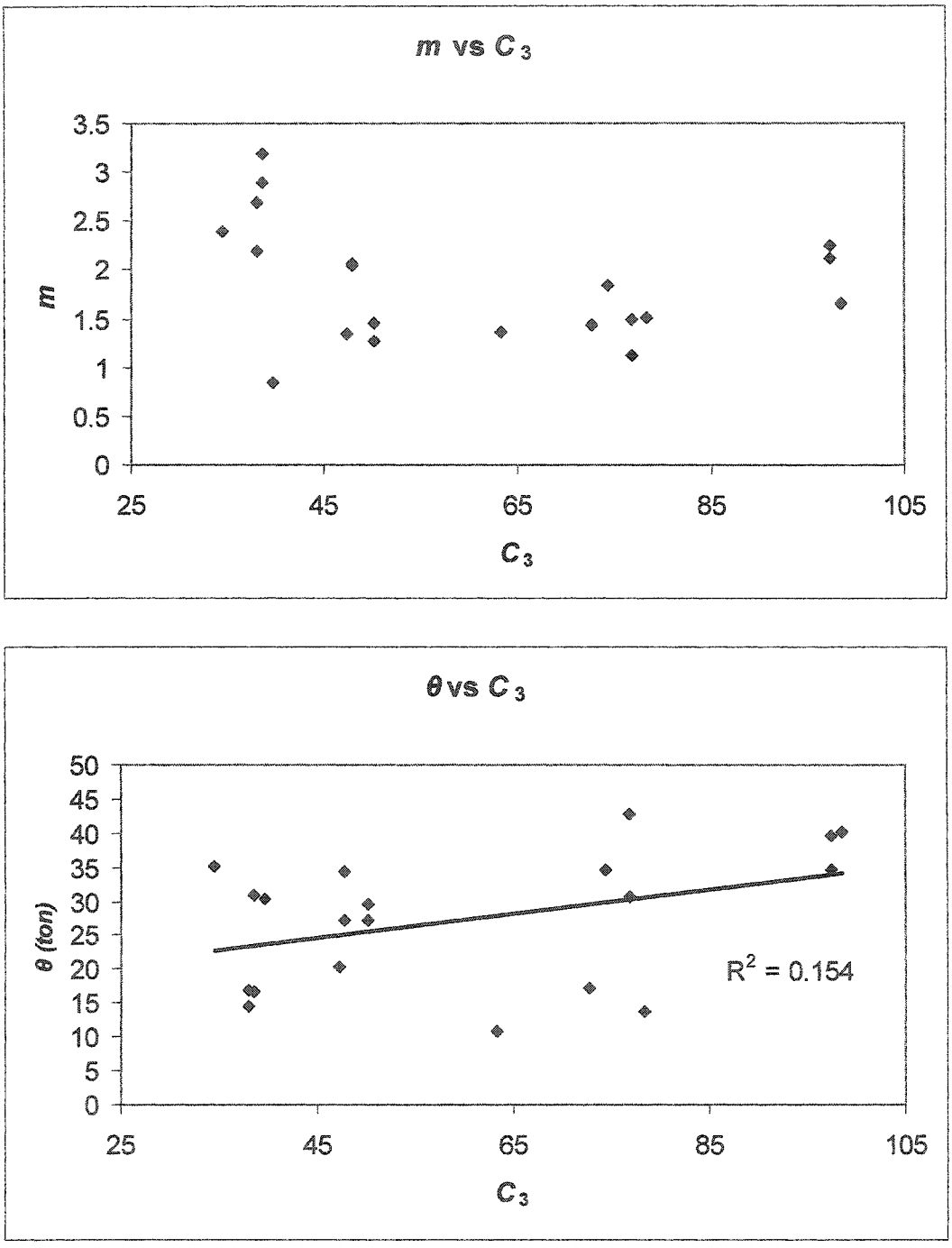

Figure 6.5 Variation of Weibull shape parameter (m) and scale parameter (θ) against complexity index C_3, for the die life data studied

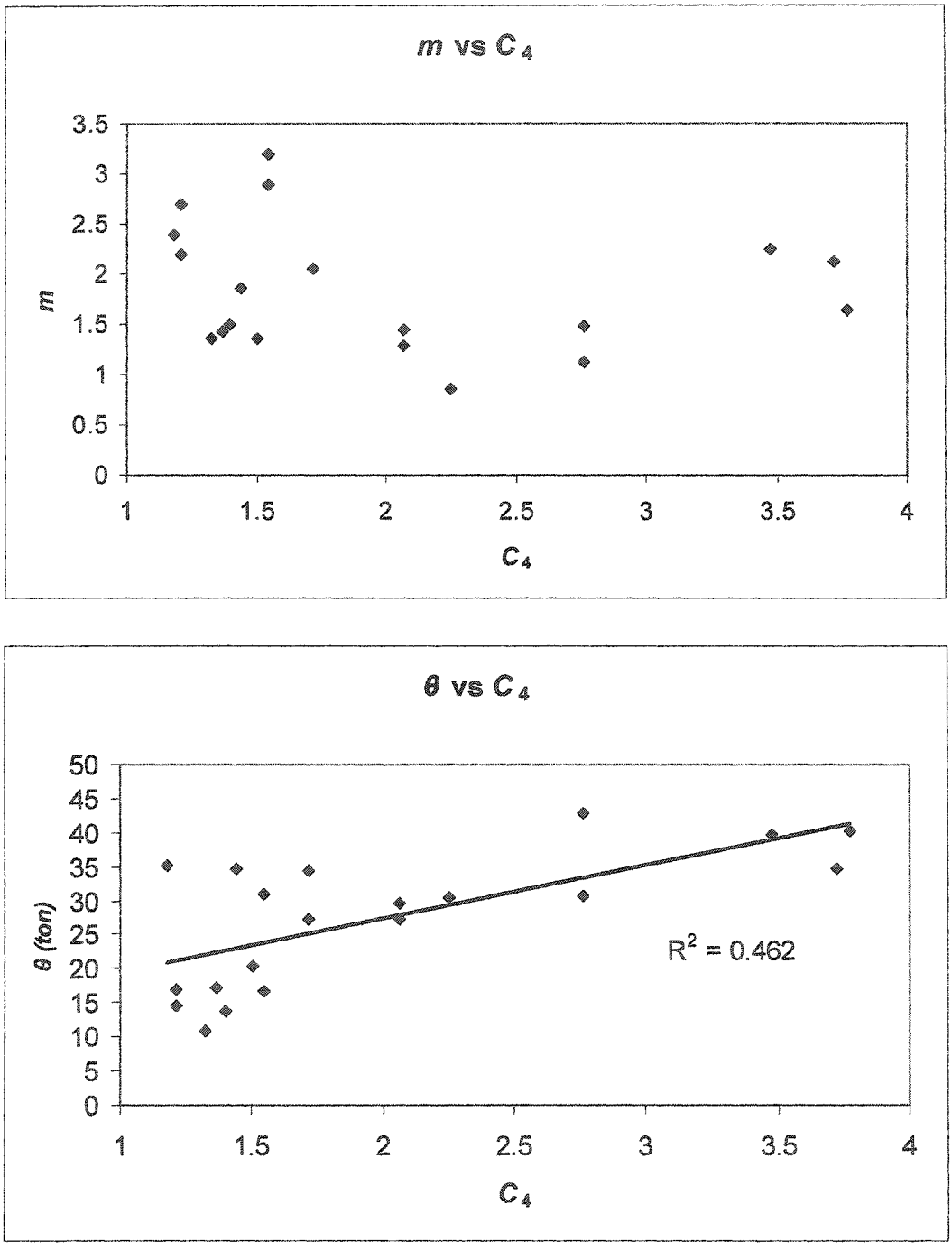

Figure 6.6 Variation of Weibull shape parameter (m) and scale parameter (θ) against complexity index C_4, for the die life data studied

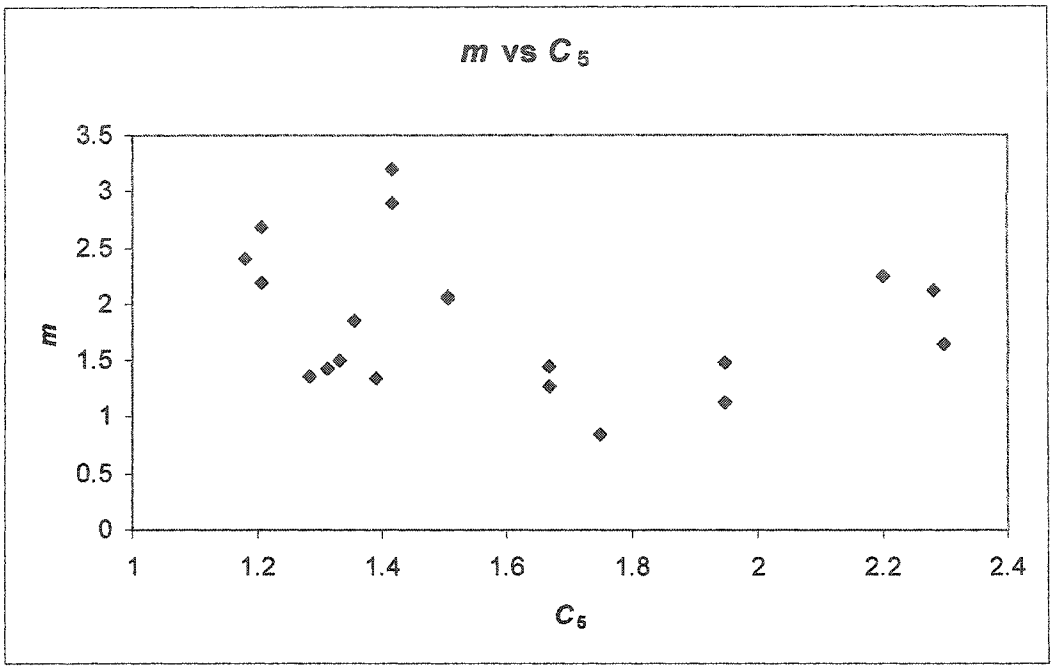

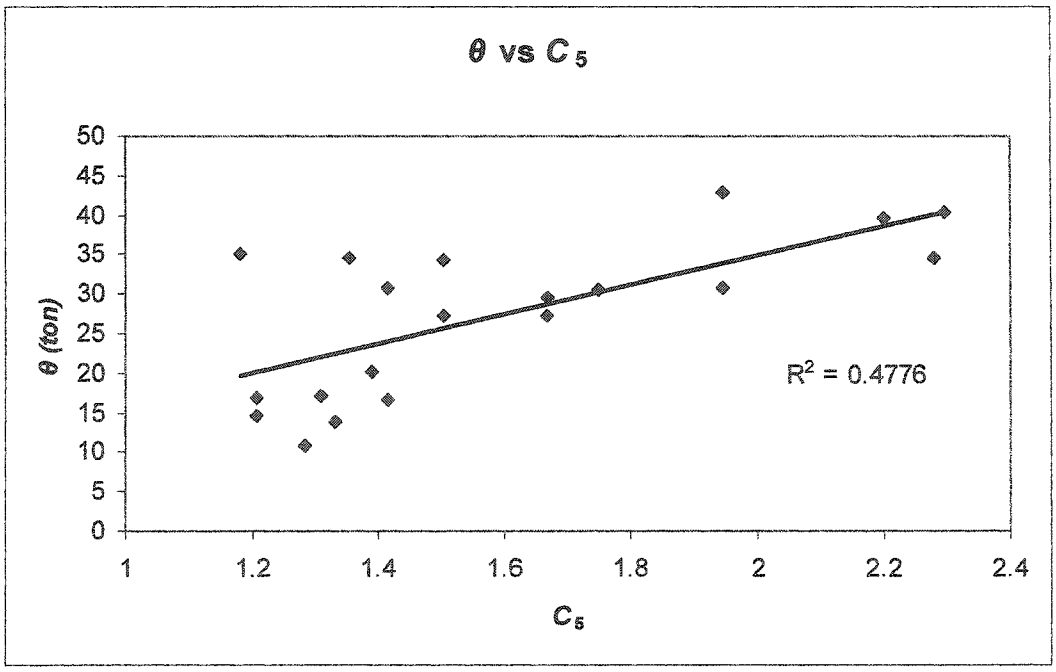

Figure 6.7 Variation of Weibull shape parameter (m) and scale parameter (θ) against complexity index C_5, for the die life data studied

large scatter indicates the absence of any significant correlation, and thus a constant value of m for all complexity definitions. The scale parameter (θ), however, shows a definite link with profile complexity. This is also as expected, because θ is an indicator of the average die life, and is therefore affected by how complicated a die profile is.

1. Complexity definitions C_1, C_2, and C_4 show a significant correlation with θ, C_4 being the most strongly correlated.
2. Definition $C_3 = CCD/T_m$ exhibits the weakest correlation, in effect almost a negligible one. This corroborates the findings of chapter-3, where pressure predictions were also far from realistic for C_3.
3. Definitions C_1 and C_2 show exactly the same variation against θ.
4. The strongest correlation is observed for the newly proposed definition C_5 developed in chapter-3, closely followed by the Altan definition C_4.
5. The variation trend in all of the cases is *contrary to intuitive reasoning* that average die life should decrease with increasing complexity.

As mentioned above, it is intuitively and heuristically known, and established in the preceding chapter that die failure and profile complexity are definitely linked together. It is therefore gratifying to note that there is a notable correlation (though not a very strong one) between scale parameter and different die complexity indices reported in literature. It is almost a unanimous consent that shape complexity is some sort of a function of profile perimeter. That is why C_1 is one of the most common definitions used and it is good to observe that C_1 shows a relatively high correlation with θ. Assuming density of the billet material to be constant (which is practically true in our case), definitions C_1 and C_2 differ only by a constant value. Their variation against θ should hence be essentially the same, which it is. It was determined in chapter-3 that the Altan definition C_4 yields the best pressure prediction among the four published complexity definitions. It is good to observe that C_4 also results in the highest complexity-θ correlation value. It is also really satisfying to note that the new definition (C_5) proposed in chapter-3 is better than all published definitions in the die life domain, as it was for extrusion pressure prediction, though C_4 also exhibits only a slightly lower correlation coefficient.

The one totally *unexpected observation*, as pointed out above, is that *average die life does not decrease with increasing shape complexity*. Increasing complexity obviously indicates higher localized stress concentrations and hence earlier failures. Also, the rather weak correlation (maximum of about 48%) between complexity and θ is not as anticipated. These two observations greatly reinforce an earlier conclusion that conventional definitions of shape complexity do not represent many form features and geometrical details of the die profile. An improved complexity definition might streamline the results and demonstrate trends that follow engineering intuition more closely. The next chapter will be reporting a new study on die life and die failures, involving critical geometrical features of a die profile not generally addressed in reported shape complexity definitions (for instance extrusion ratio, stress raisers such as number of sharp corners, etc).

Focus in this discussion was on the complexity index of the section profile. However, when there is a *multi-hole* die (more than one cavities in the same die set), there can be significant other factors such as *layout symmetry* (how the cavities are located about the horizontal and vertical die axes), *layout regularity* (whether cavities are situated on a pitch-circle or on the perimeter of a rectangle, triangle, etc), and *layout density* (number of cavities per unit length of pitch circle or rectangle perimeter). Any or all of these factors may be responsible for the less than strong complexity-θ correlation.

CHAPTER 7
EXTRUSION TOOLING:
COMPLEXITY BASED DIE LIFE PREDICTION

7.1 INTRODUCTION

Complexity is a measure of how complicated the geometry or shape of a metal forming die is. There is universal agreement on the fact that the simplest shape is a solid circular section, especially in the domain of extrusion. Hollows in general are more complex than solids, especially because hollows cannot be extruded without the inclusion of an additional component in the die set called the mandrel. Engineering common sense dictates that a more complex die will require a larger amount of extrusion force or pressure. This has been experimentally substantiated in a previous chapter. According to a basic definition, therefore, extrusion shape complexity is the ratio of the pressure required to extrude a complex profile to the pressure required for a solid circular profile of the same area. All of the complexity definitions reported in published literature (C_1 to C_4) are based on this interrelationship between extrusion pressure and profile complexity.

If a complex profile is more difficult to extrude than a simple one, and generates more stresses in the die, it should lead to an earlier die failure. In chapter-5, it has been confirmed that the working life of hot extrusion dies is definitely affected by profile complexity. Reported complexity definitions provide some sort of index to measure extrudability, and can thus be used for pressure prediction to a certain degree. Unfortunately, these definitions do not address the very important issue of die reliability, and generally yield a counter-intuitive trend of increasing die life with increasing complexity, as concluded in the last chapter. This is due to the reason that none of these definitions include all the significant geometrical features of a die profile. Even the new

definition proposed in chapter-3 (C_5), which gives a definitely better prediction of extrusion pressure than all other definitions found in published literature, yields the contradicting trend of increasing die life with increasing complexity.

7.1.1 Current Work

Attempt has been made in this chapter to develop a new definition of extrusion shape complexity that incorporates all the pertinent form features of a die, and provides a more reliable die life prediction tool. In contrast to existing definitions, which include only a few geometrical parameters, all pertinent form features of an extrusion die profile have been addressed. These include perimeter, area, minimum wall thickness, circumscribing circle diameter, billet diameter, number of cavities, extrusion ratio, and number of corners or sharp bends. Extrusion die failure data reported earlier have been reanalyzed from a die reliability viewpoint. Various regression strategies have been employed in developing a new and robust complexity definition. Both linear and power law formats of the definition result in the expected and natural trend of earlier die failures with increasing complexity, and yield a much better correlation with average die life than existing definitions.

7.2 Complexity and Form Features

As the word *shape complexity* implies, complexity is a measure of how complicated the *geometry* or *shape* or *form* of a metal forming die is. The simplest shape is a solid circular section. Even a solid square or rectangular profile is more complicated because it has four corners or sharp bends that act as stress raisers. In general, a hollow shape has a higher complexity than a solid one. This is especially true in extrusion, where hollows cannot be extruded without the inclusion of an additional component in the die set called the *mandrel*. Semi-hollows are shapes that are not completely hollow, but still require a mandrel for extrusion.

The basic form features of an extrusion die are D, A, P_s, P_o, A_s, W_s, N_1, N_2, R, T_m, and CCD, as described in Table 7.1 Some of these parameters are inter-related. For instance, equivalent circle perimeter can be derived from actual section perimeter:

Table 7.1 Form features describing the geometry of a typical extrusion die profile

Symbol	Name	Description	Units
D	Billet/container diameter	Diameter of billet or container	mm
A	Billet/container area	Area of billet or container	mm^2
P_s	Section perimeter	Perimeter of actual profile section	mm
P_o	Equivalent circle perimeter	Perimeter of solid circular section having same area	mm
A_s	Section area	Area of actual profile section	mm^2
W_s	Section weight	Weight per unit length of actual profile	g/mm
N_1	Number of cavities	Number of cavities of same profile in one die	
R	Extrusion ratio	Ratio of billet area to section area	
T_m	Minimum section thickness	Minimum wall thickness of actual profile section	mm
CCD	Circumscribing circle diameter	Diameter of circle containing the profile	mm
N_2	Number of corners	Number of corners or sharp bends (stress raisers) in actual profile section	

$$P_0 = 2\sqrt{\pi A_s}\,. \tag{7.1}$$

Similarly, section weight per unit length is a constant multiple (involving billet material density ρ) of section area:

$$W_s = \rho A_s\,. \tag{7.2}$$

Also, extrusion ratio R is a function of billet area and section area and, in turn, of billet or container diameter D_b:

$$R = \frac{A_b}{A_s} = \frac{\pi D_b^{\,2}/4}{A_s}\,. \tag{7.3}$$

The six remaining distinct and significant form features of an extrusion die are therefore P_s, A_s, N_2, T_m, CCD and R. Table 7.2 lists the values of these parameters for each of the dies studied, together with the average die life $MTTF$. The new definition includes all of these six profile features.

7.3 Profile Complexity and Die Life

The three principal modes of extrusion die failure are fatigue fracture, surface wear, and excessive plastic deformation. It is reasonable to expect that dies for complex profiles would lead to earlier failures through fracture. Similarly, thin and intricate sections in the die would wear out more quickly. Also, complicated die shapes under high extrusion pressures and temperatures would bend or deform much faster. It was established in chapter-5 that the working life of a hot extrusion die (terminated by fracture, wear, or plastic deformation) is definitely linked to the complexity of the profile being extruded through the die. In chapter-6 (Figures 6.3 to 6.7) a notable correlation was found to exist (though not a very strong one) between Weibull scale parameter (θ), which is an indicator of the average die life (expressed by the number of kilograms extruded before failure), and different die complexity indices.

Values of the four complexity indices found in published literature (C_1, C_2, C_3, C_4), and the complexity value based on the new definition (C_5), are summed up in Table 7.3 for each die profile. Values of the average die life ($MTTF$) are plotted against each of

Table 7.2 Significant geometric parameters (form features) and average die life (*MTTF*) of the dies studied

S.No.	Die Type	Die #	*Ps* (mm)	*As* (mm^2)	N_2	T_m (mm)	*CCD* (mm)	*R*	*MTTF* (kg)
1	H	D1	120	149	4	1.30	44.72	66.12	30,827
2	H	D2	228	211	12	1.30	50.09	62.26	27,533
3	H	D3	288	266	14	1.30	62.29	51.07	24,072
4	H	D4	288	266	14	1.30	62.29	49.38	32,233
5	H	D5	247	267	18	1.30	61.56	49.20	20,561
6	H	D6	240	328	4	1.40	101.98	77.58	15,061
7	H	D7	200	253	4	1.30	82.46	50.29	9,867
8	H	D8	240	305	4	1.30	101.98	64.60	12,078
9	H	D9	140	176	4	1.30	49.497	51.46	14,890
10	H	D10	140	176	4	1.30	49.497	55.98	12,518
11	H	D11	240	282	4	1.20	89.44	96.35	29,694
12	S	D12	545	364	19	1.35	116.62	74.65	43,726
13	S	D13	447	294	12	1.30	100	92.42	26,292
14	S	D14	447	294	12	1.30	100	67.02	37,980
15	S	D15	345	236	10	1.30	51.61	57.57	26,750
16	S	D16	290	192	11	1.30	65.3	70.76	23,513
17	S	D17	290	192	11	1.30	65.3	51.31	25,459
18	S	D18	608	403	20	1.30	126.52	67.42	34,817
19	S	D19	694	483	28	1.30	126.52	56.26	29,977
20	S	D20	723	516	28	1.35	132.88	52.65	35,304

Table 7.3 Complexity indices, average die life (*MTTF*) and extrusion ratio (R) of the dies studied

S. No.	Die Type	Die #	C_1	C_2	C_3	C_4	C_5	R	*MTTF* (kg)
1	H	D1	0.81	0.30	34.40	1.18	1.18	66.12	30,827
2	H	D2	1.08	0.40	38.53	1.55	1.42	64.39	14,870
3	H	D3	1.08	0.40	47.92	1.72	1.51	51.07	24,072
4	H	D4	1.08	0.40	47.92	1.72	1.51	49.38	32,233
5	H	D5	0.93	0.34	47.35	1.50	1.39	49.2	20,561
6	H	D6	0.73	0.27	72.84	1.37	1.31	77.58	15,061
7	H	D7	0.79	0.29	63.43	1.33	1.28	50.29	9,867
8	H	D8	0.79	0.29	78.45	1.40	1.33	64.6	12,078
9	H	D9	0.80	0.29	38.07	1.21	1.21	51.46	14,890
10	H	D10	0.80	0.29	38.07	1.21	1.21	55.98	12,518
11	H	D11	0.85	0.32	74.53	1.44	1.35	96.35	29,694
12	S	D12	1.50	0.55	86.39	3.17	2.09	74.65	43,726
13	S	D13	1.52	0.56	76.92	2.76	1.95	92.42	26,292
14	S	D14	1.52	0.56	76.92	2.76	1.95	67.02	37,980
15	S	D15	1.46	0.54	39.70	2.25	1.75	57.57	26,750
16	S	D16	1.51	0.56	50.23	2.07	1.67	70.76	23,513
17	S	D17	1.51	0.56	50.23	2.07	1.67	51.31	25,459
18	S	D18	1.51	0.56	97.32	3.48	2.20	67.42	34,817
19	S	D19	1.44	0.53	97.32	3.72	2.279	56.26	29,977
20	S	D20	1.40	0.52	98.43	3.77	2.295	52.66	35,304

these complexity indices and the extrusion ratio in Fig 7.1. It is easy to infer from the table and the graph that

1. The definitions are not consistent with each other in ranking the dies in terms of increasing profile complexity.
2. None of the definitions yields the same ordering of profile complexity as the average die life *MTTF*.
3. All the definitions are rather weakly correlated with *MTTF*. The new definition C_5 yields the relatively strongest correlation of $r^2 = 50.01$ %. Definition C_4 is the next best, with correlation of 48.4%. The weakest correlation of $r^2 = 18.8\%$ is demonstrated by definition C_3.
4. Though extrusion ratio (R) is considered to be a very important extrusion parameter, its correlation with average die life is negligibly small (4.76%).
5. There is a *trend of increasing die life with increasing shape complexity*, which is *against intuitive judgment that a die should fail earlier as its complexity increases*.

It is obvious from these observations that there is an acute need for a new complexity index definition for extrusion die profiles. This definition should include all of the important geometrical or form features of an extrusion die, should be aimed at a significantly higher correlation with average die life compared to the existing definitions, and should redress the anomalous trend between die life and complexity.

7.4 Results and Discussion

Details of this work can also be found in Sheikh et al. [June 2004] and Qamar et al. [May 2004]. As mentioned above, it is natural to expect that complexity of a die profile should contribute towards die failure. This has been confirmed by the die failure study reported in chapter-5. Presented below are two models (linear and power-law) to study the relationship between die complexity and die life.

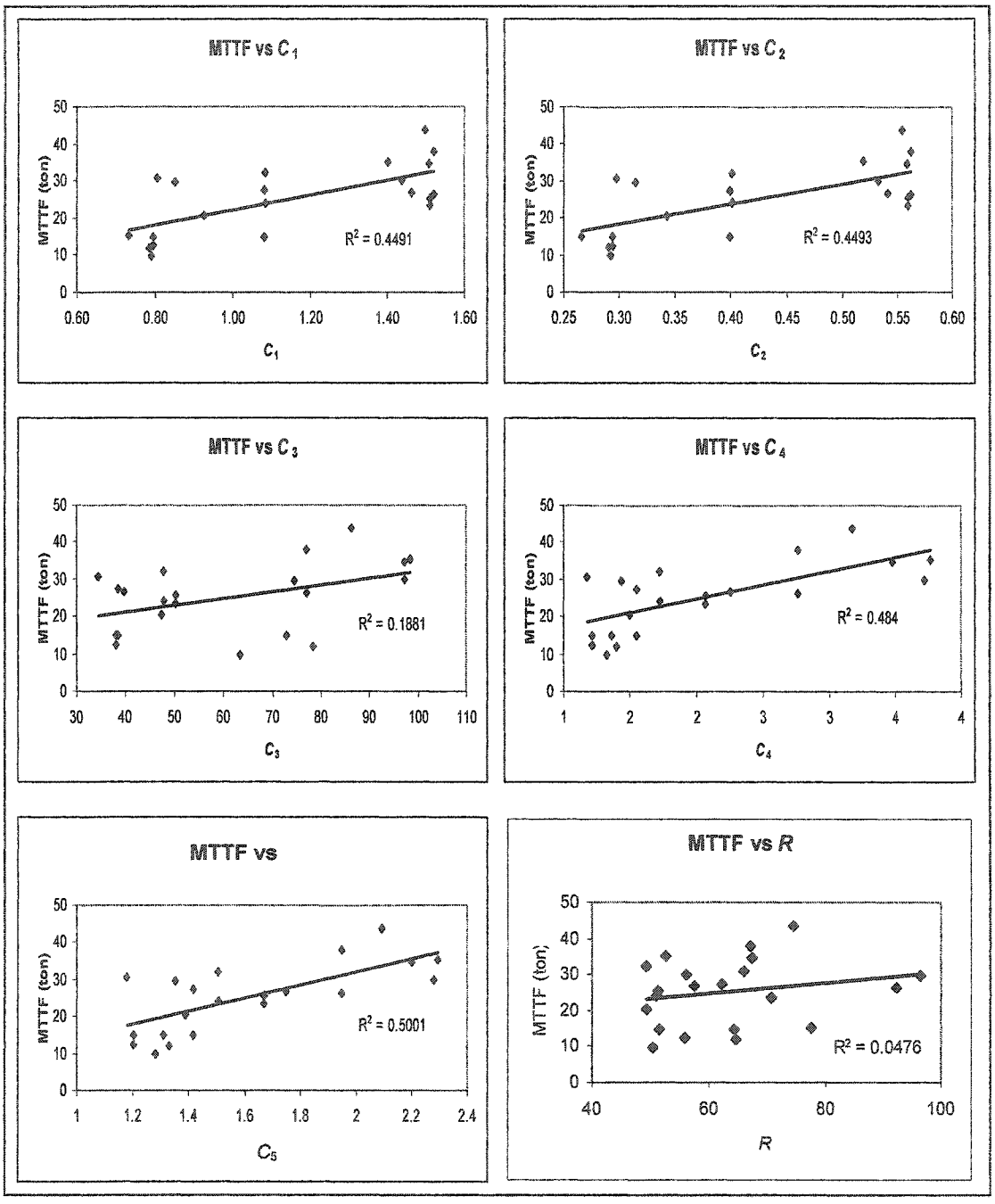

Figure 7.1 Existing complexity indices (C_1, C_2, C_3, C_4 and C_5) and extrusion ratio (R) show a rather weak correlation with MTTF

7.4.1 Linear Complexity-MTTF Relationship

Assuming a linear relationship between average die life and the six critical form features of a die profile mentioned above, we can define:

$$MTTF = K_1 + a_1 P_s + b_1 A_s + c_1 N_2 + d_1 T_m + e_1 CCD + f_1 R + Interaction\ Terms. \quad (7.4)$$

The intercept K_1 and the coefficients a_1, b_1, c_1, d_1, e_1, and f_1 have been determined through multiple linear regression performed using the package *StatGraphics*. All multi-factor interactions between the profile parameters (starting from 2-factor and going up to 6-factor) were investigated, but they turn out to be insignificant. After exploring the various possibilities, the final regressed equation came out to be

$$MTTF = 16520 + 46.28\ P_s - 46.33\ A_s + 560.18\ N_2 - 7073.44\ T_m - 90.86\ CCD + 263.14\ R \quad (7.5)$$

Values of *MTTF* predicted by equation (7.5) are tabulated and compared with the actual average die life values in Table 7.4, and plotted in Fig 7.2. Compared to the best correlation coefficients of $r^2 = 50.01\%$ (for C_5) and 48.4% (for C_4) for earlier definitions, equation (7.5) yielded a much higher value of **64.5%**. Predicted *MTTF* is generally quite close to the actual *MTTF* value, resulting in an average error (all dies taken together) of only 5.1%.

7.4.2 New Linear-Model Complexity Index

We now come to the formulation of the new complexity index definition for extrusion dies, based on multiple linear regression. From equation (7.5) we have

$$MTTF = 16520\ (1 + 0.0028\ P_s - 0.0028\ A_s + 0.0339\ N_2 - 0.4282\ T_m - 0.0055\ CCD + 0.0159\ R) \quad (7.6)$$

As pointed out earlier, it is both an intuitive and a logical assumption that average die life decreases with increasing complexity of the die profile. Thus

$$MTTF \propto \frac{1}{Complexity}.$$

Based on this premise, the new complexity index, derived from equation (7.6), is

Table 7.4 Prediction of average die life *MTTF* in terms of the two new form feature based complexity indexes

S.No.	Die Type	Die #	MTTF (ton)	C_6	C_7	Predicted MTTF (ton)	
						Linear (C_6)	Logarithmic (C_7)
1	H	D1	30.827	0.77	0.58	21.552	18.225
2	H	D2	27.533	0.62	0.54	26.654	29.883
3	H	D3	24.072	0.69	0.55	23.952	25.036
4	H	D4	32.233	0.70	0.56	23.507	24.240
5	H	D5	20.561	0.69	0.55	23.822	25.870
6	H	D6	15.061	1.04	0.60	15.918	15.165
7	H	D7	9.8665	1.29	0.62	12.841	11.799
8	H	D8	12.078	1.16	0.60	14.276	14.151
9	H	D9	14.89	0.98	0.61	16.935	14.077
10	H	D10	12.518	0.91	0.60	18.123	15.260
11	H	D11	29.694	0.65	0.55	25.543	24.625
12	S	D12	43.726	0.47	0.53	35.019	34.459
13	S	D13	26.292	0.45	0.52	36.346	37.894
14	S	D14	37.98	0.56	0.54	29.663	27.835
15	S	D15	26.75	0.58	0.54	28.418	28.039
16	S	D16	23.513	0.54	0.53	30.699	31.395
17	S	D17	25.459	0.65	0.56	25.582	23.061
18	S	D18	34.817	0.48	0.53	34.242	33.093
19	S	D19	29.977	0.46	0.53	36.058	32.603
20	S	D20	35.304	0.49	0.54	33.993	28.624
				Percent Error		**5.110**	**0.977**

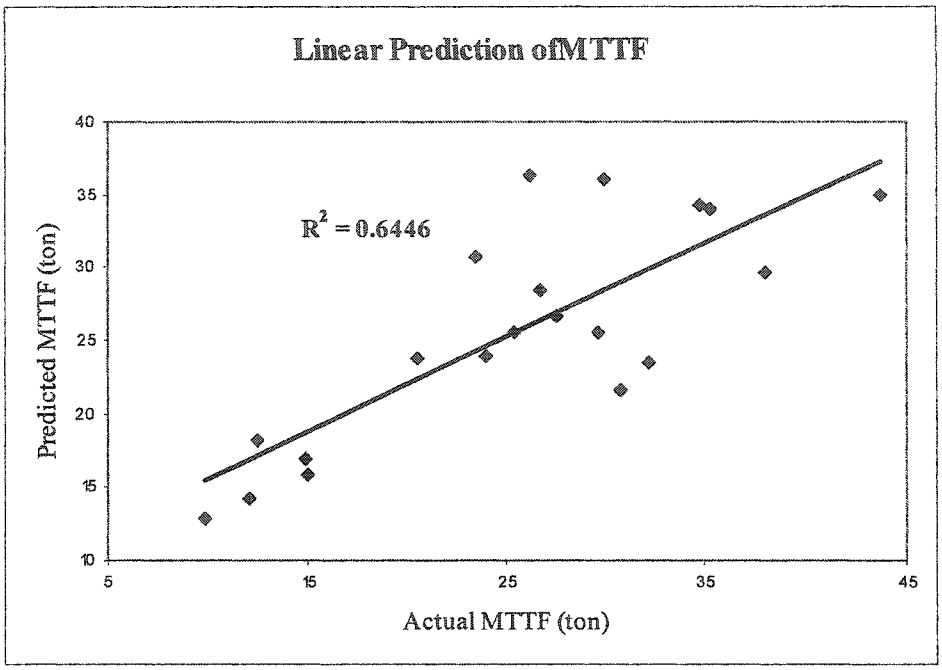

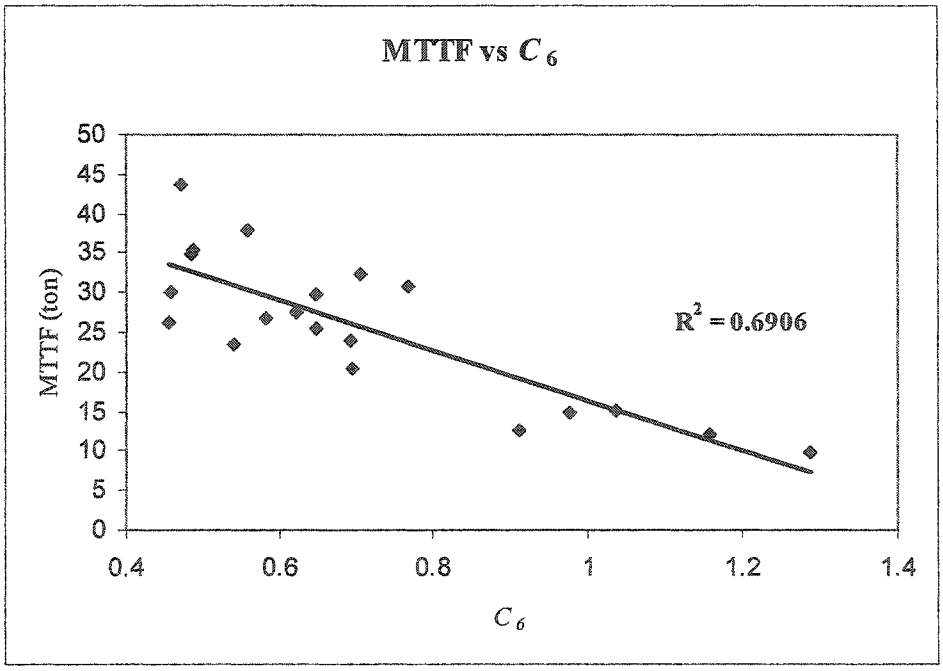

Figure 7.2 Prediction of MTTF using the new complexity definition based on multiple linear regression, and its correlation with average die life

$$C_6 = \frac{1}{1 + 0.0028P_s - 0.0028A_s + 0.0339N_2 - 0.4282T_m - 0.0055CCD + 0.0159R}. \quad (7.7)$$

This new definition incorporates all the critical form features that characterize the geometry of a die profile, and can thus be described as a more faithful representation of *shape complexity*. As can be seen from Fig 7.2, this complexity index not only satisfies the natural expectation of reduction in average die life with increasing die complexity, but also exhibits a far higher life-complexity correlation than all of the previous definitions.

7.4.3 Logarithmic Complexity-MTTF Relationship

In an attempt to improve the new complexity definition (C6) developed above, let us now assume a power-law relationship between average die life and form features:

$$MTTF = K_2 P_s^{a_2} A_s^{b_2} N_2^{c_2} T_m^{d_2} CCD^{e_2} R^{f_2}. \quad (7.8)$$

Taking natural log on both the sides, we get

$$\ln MTTF = \ln K_2 + a_2 \ln P_s + b_2 \ln A_s + c_2 \ln N_2 + d_2 \ln T_m + e_2 \ln CCD + f_2 \ln R. \quad (7.9)$$

Multiple linear regression can now be used for these logarithmic variables to find out the values of the coefficients. The intercept ($\ln K_2$) and the coefficients ($\ln a_2$, $\ln b_2$, $\ln c_2$, $\ln d_2$, $\ln e_2$, and $\ln f_2$) have been again been determined using the package *StatGraphics*:

$$\ln MTTF = 6.363 + 0.274 \ln P_s - 0.101 \ln A_s + 0.42 \ln N_2 - 1.336 \ln T_m - 0.418 \ln CCD + 0.956 \ln R. \quad (7.10)$$

The final equation, going back from this linear logarithmic form to the original power-law format, came out to be

$$MTTF = 580 P_s^{0.27} A_s^{-0.1} N_2^{0.42} T_m^{-1.34} CCD^{-0.42} R^{0.96}. \quad (7.11)$$

Predicted values of *MTTF*, based on this equation, are listed in Table 7.4 and plotted in Fig 7.3. Compared to the correlation coefficient of r^2 = 64.5% for the new linear-model complexity index C_6 (which was itself far higher than all the earlier complexity definitions), equation (7.11) yields an even higher value of 70.14%. *MTTF* predictions

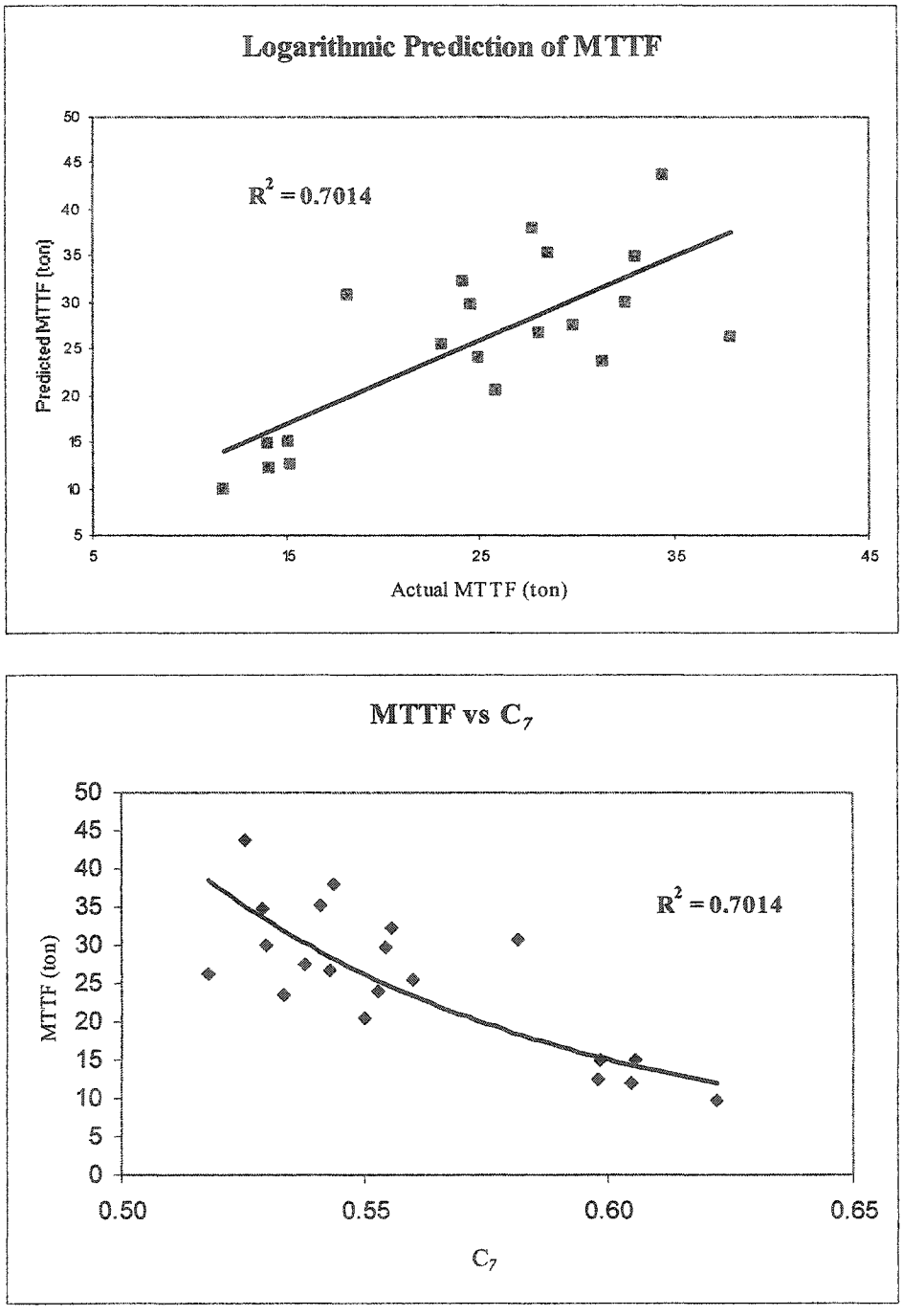

Figure 7.3 Prediction of MTTF using the new complexity definition based on multiple power law regression, and its correlation with average die life

from this model are very close to the actual die life values, resulting in a negligibly small average error of less than one percent.

7.4.4 New Logarithmic-Model Complexity Index

From equation (7.10) we can get

$$\ln MTTF = 6.363\,(1 + 0.043\ln P_s - 0.016\ln A_s + 0.066\ln N_2 - 0.21\ln T_m - 0.066\ln CCD + 0.15\ln R) \tag{7.12}$$

Keeping in mind that average die life and profile complexity are inversely proportional ($MTTF \propto 1/Complexity$), the new complexity index derived from equation (7.12) is

$$C_7 = \frac{1}{P_s^{0.043} A_s^{-0.016} N_2^{0.066} T_m^{-0.21} CCD^{-0.066} R^{0.15}}. \tag{7.13}$$

Behavior of this *shape complexity index* against average die life can be seen in Fig 7.3. It includes all the significant form features characterizing a die profile, satisfies the natural expectation of earlier die failures for more complex die profiles, and demonstrates the highest *MTTF-C* correlation compared to all the previous complexity definitions.

It should be pointed out here that equations (6, 7) and (11, 13) represent the *combined* or *aggregate* effect of the six significant form features of a die profile on die life and shape complexity. It is necessary to apply caution in trying to establish cause-and-effect relationships between *MTTF* and *individual* parameters (*Ps*, *As*, N_2, *Tm*, *CCD*, *R*) through these equations. They do not represent controlled experimentation (in accordance with statistical design of experiments). It will be wrong to interpret these equations by *isolating* each parameter. All the data has been collected from the industry, and has not been studied from a factorial design approach (in which each factor can be isolated and the interaction effects are obtained by varying the other parameters). The data is representative of actual industrial process, and the models provide a good predictive tool.

CHAPTER 8
EXTRUSION TOOLING: FRACTURE TOUGHNESS OF HOT WORKING TOOL STEELS

8.1 INTRODUCTION

Hot working tool steels such as AISI H11, H12 and H13 are some of the most common tool materials for a number of hot metal working processes (rolling, forging, extrusion, drawing, etc). Commercial aluminum extrusion almost universally uses H13 steel dies. As pointed out before, quality and economy in metal forming are primarily influenced by the performance and reliability of the die and die set. The main objectives are longest die life and minimum performance degradation during operation. As established earlier, the most common causes of die failure are fracture, wear, and deflection. These three major die failure modes were described in detail in chapter-5. It was concluded therein that because of intricate die geometries (stress raisers) and high thermal and mechanical stresses of a cyclic nature, fatigue fracture is the most dominant die failure mode. Plane-strain fracture toughness (K_{IC}) is an important material property in the prediction and prevention of fracture, and in damage tolerance assessment of ductile materials. Failure prediction and life estimation of dies require a reasonably accurate determination of K_{IC} of the die material. Hot metal forming is carried out at elevated temperatures, making the use of room temperature material properties invalid. High-hardness and high-toughness requirements for hot work die steels are met through a judicious combination of heat treatment (tempering) and surface hardening. Standard K_{IC} testing is difficult, time-consuming and costly even at room temperatures. K_{IC} determination at elevated operating temperatures for tempered and hardened tool steels becomes even more difficult. That is

why very little information on K_{IC} values of tool steels is available in published literature and even from tool steel manufacturers.

8.1.1 Current Work

Charpy impact energy (*CVN*) is often used as an indirect measure of fracture toughness of a given material. Attempts made in literature at *CVN*-K_{IC} correlations do not generally apply to tool steels, and are not suitable for high temperature predictions. This chapter presents results from a study aimed at the development of a reasonable *CVN*-K_{IC} correlation for the hot work tool steel H13, subjected to various tempering cycles and tested at different elevated temperatures. Greatly scattered information about mechanical properties of H13 steels has been collected and consolidated from published literature and from tool steel manufacturers. Published data has been augmented through in-house experiments on heat treatment of H13 steel (annealing, hardening, tempering, and quenching) and determination of room temperature and elevated temperature mechanical properties. Judicious interpolation and extrapolation of experimental data has also been carried out to generate a wholesome data matrix. Models have been developed for prediction of room temperature and elevated temperature K_{IC} values based on hardness (*HRC*) and impact energy (*CVN*) data.

8.2 Fracture Toughness of Tool Steels

8.2.1 Indirect K_{IC} Determination

Charpy impact energy (*CVN*) has often been used as an alternate, though indirect, measure of the fracture toughness of a given material. The test is easier, faster, and less costly than K_{IC} testing, and can be adapted to high-temperature testing as well. If a correlation between *CVN* and K_{IC} is available having some degree of accuracy, failure analysis and life prediction of metal forming dies would be greatly facilitated. Though some *CVN*-K_{IC} correlations have been attempted in literature, they suffer from the following drawbacks.

1 They mostly deal with low and medium-strength steels while tool steels belong to the very-high and ultra-high strength category.
2 They usually apply to the lower-shelf (negative to just above room temperatures) *CVN* values.
3 They do not generally address the issues of various tempering and operating temperatures.

8.2.2 H13 Tool Steel

AISI H13 is a versatile chromium-molybdenum hot work tool steel that is widely used in both hot and cold working applications. Its typical composition is (0.40% C, 0.40% Mn, 1.00% Si, 5.25% Cr, 1.35% Mo, 1.00% V). However, the composition range is

C (%)	Si (%)	Mn (%)	P (≤ %)	S (≤ %)	Cr (%)	Mo (%)	V (%)
0.37-0.42	0.90-1.20	0.30-0.50	0.03	0.03	5.00-5.50	1.20-1.50	0.90-1.10

The hot hardness (which is synonymous with hot strength) of H13 steel resists thermal fatigue cracking which occurs as a result of repeated heating and cooling cycles in hot working setups. Because of this highly desirable combination of high toughness and resistance to thermal fatigue cracking (also known as thermal checking), H13 is used for more hot work tooling applications than any other tool steel.

8.3 *CVN*-K_{IC} Correlations

Billets, dies and containers in commercial aluminum extrusion are preheated to temperatures in the range of 425°C-475°C. Actual temperatures can go beyond 500°C because of temperature rise due to heat generation by deformation and friction. Studies targeting the lower-shelf and transition-temperature properties of steels are therefore not pertinent in the context of hot metal forming. A few significant works related to prediction of K_{IC} values of steels in the upper shelf region are mentioned below.

For steels in the 760-1700 MPa yield strength range, Barsom and Rolfe [1970], and Rolfe and Novak [1970] came up with the correlation

$$\left(\frac{K_{IC}}{\sigma_Y}\right)^2 = 0.64\left(\frac{CVN}{\sigma_Y} - 0.01\right) \qquad (K_{IC}: \text{MPa}\sqrt{\text{m}},\ \sigma_Y: \text{MPa},\ CVN: \text{J}). \qquad (8.1)$$

For an ultrahigh-strength aircraft steel, Ault et al. [1971] suggested the empirical correlation

$$\left(\frac{K_{IC}}{\sigma_Y}\right)^2 = 1.37\left(\frac{CVN}{\sigma_Y}\right) - 0.045 \qquad (\text{MPa}\sqrt{\text{m}},\ \text{MPa},\ \text{J}). \qquad (8.2)$$

Correlations reported by Dougan [1982], Van der Sluys et al. [1983], Witt [1983] and Kussmaul and Roos [1984] for reactor pressure vessel steels are:

$$\left(\frac{K_{IC}}{\sigma_Y}\right)^2 = 0.893\left(\frac{CVN}{\sigma_Y} - 0.0291\right), \quad (\text{MPa}\sqrt{\text{m}},\ \text{MPa},\ \text{J}) \qquad (8.3)$$

and

$$\left(\frac{K_{IC}}{\sigma_Y}\right)^2 = 1.23\left(\frac{CVN}{\sigma_Y} - 0.0061\right) \qquad (\text{MPa}\sqrt{\text{m}},\ \text{MPa},\ \text{J}). \qquad (8.4)$$

Some of these results have been reviewed by Wallin [2000].

8.3.1 Proposed Correlation

AISI H13 (DIN 1.2344) is classified as *ultrahigh-strength low alloy steel* [METAOR 2003]. We can see from the preceding section that for both medium-strength and ultrahigh strength steels, the correlations found in published literature involve the ratios (K_{IC}/σ_Y) and (CVN/σ_Y). It may be pointed out here that determination of yield strength (σ_Y) at elevated test temperatures is demanding and costly as compared to room temperature testing, particularly when the samples are also subjected to different tempering cycles. Also, elevated-temperature yield strength is proportional to hot hardness, which is a direct measure of the material's ability to resist heat checking

(thermal fatigue cracking). Recognizing this, most of the hot work tool steel manufacturers provide a reasonable amount of data on hot hardness at different test temperatures, but usually list only room-temperature yield strength values.

That is why, rather than targeting a correlation for K_{IC} in terms of CVN and σ_Y, attempt has been made here to develop a strategy for determination of K_{IC} by employing (K_{IC}/HRC) and (CVN/HRC) ratios. A room-temperature correlation has been first worked out, depicting the behavior of H13 samples subjected to various tempering routines. Extension of the correlation to high-temperature properties is then discussed.

8.4 Experimentation and Data Collection

8.4.1 Published Sources

Experimental data for H13 and Premium H13 (slightly different composition compared to typical H13, but well within the specified composition range) hot work tool steels has been collected through an exhaustive search of published literature and from tool steel suppliers/manufacturers [ASM 1990, Bryson 1997, Thelning 1984, Roberts and Carey 1980, Unterweiser et al. 1982, Wilson 1975]. Collected data includes room temperature and elevated-temperature values of K_{IC}, CVN, HRC, and σ_Y of H13 samples that have been single-tempered and double-tempered at different tempering temperatures. Linear and higher-order curve fitting and extrapolation (as necessitated by the behavior of the existing curves) have been carefully used to generate additional data points required to give a more complete picture of the variation of material properties, and to evolve a comprehensive data matrix for H-13 properties available in literature.

8.4.2 In-House Experimentation

More data has been generated in-house through room-temperature hardness testing, and elevated temperature impact testing, on samples subjected to different tempering schedules. The experimental setup (digital furnaces and quenching oil bath used for heat treatment; Rockwell machine employed for hardness testing; impact testing machine and infra-red thermometer used to find CVN values) is shown in Fig 8.1 and Fig 8.2.

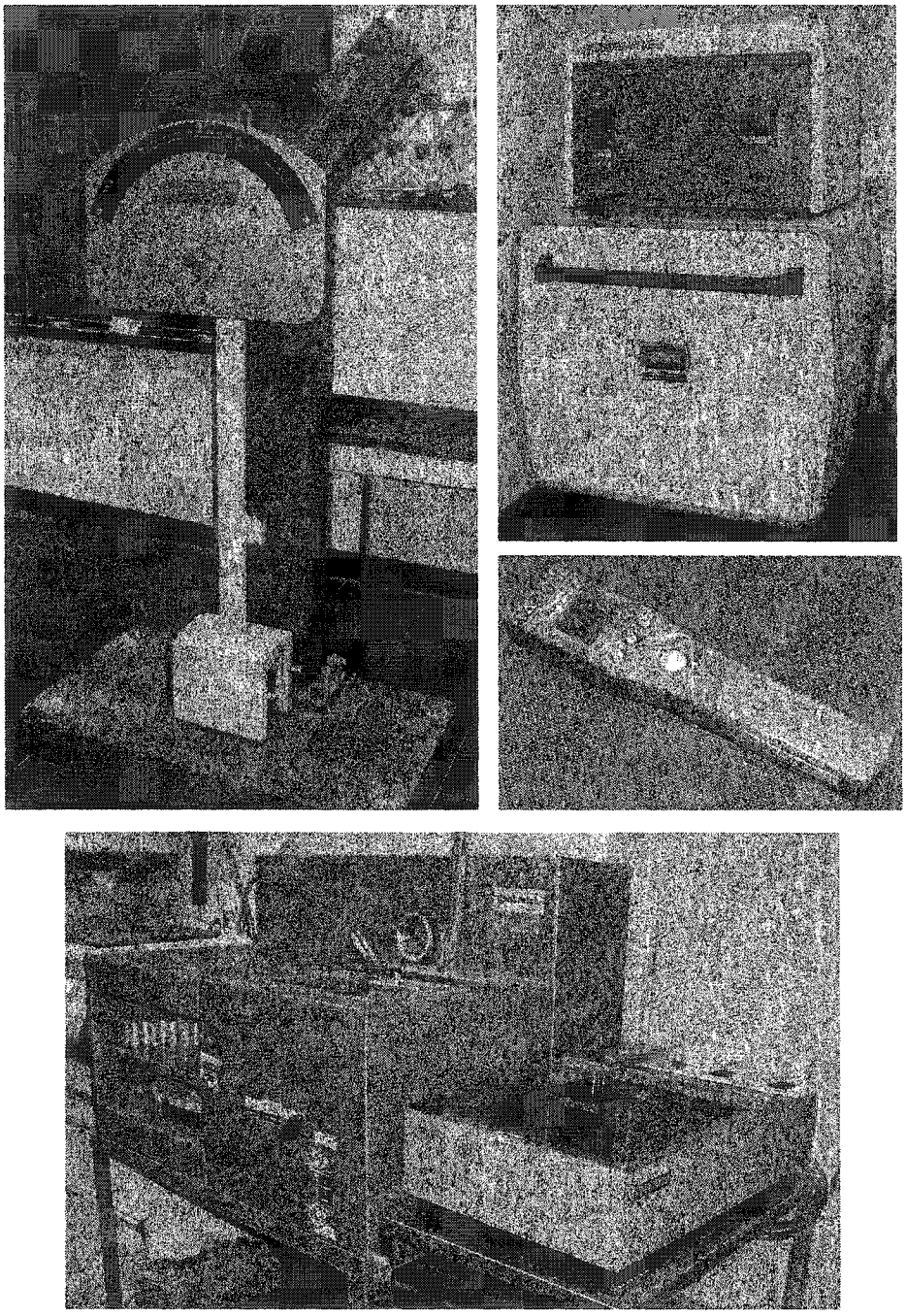

Figure 8.1 Experimental setup for in-house testing: Charpy impact tester (for *CVN* measurement), digital furnace (for heat treatment and hot testing), infrared thermometer (for non-contact instant temperature measurement), and oil bath (for oil quenching)

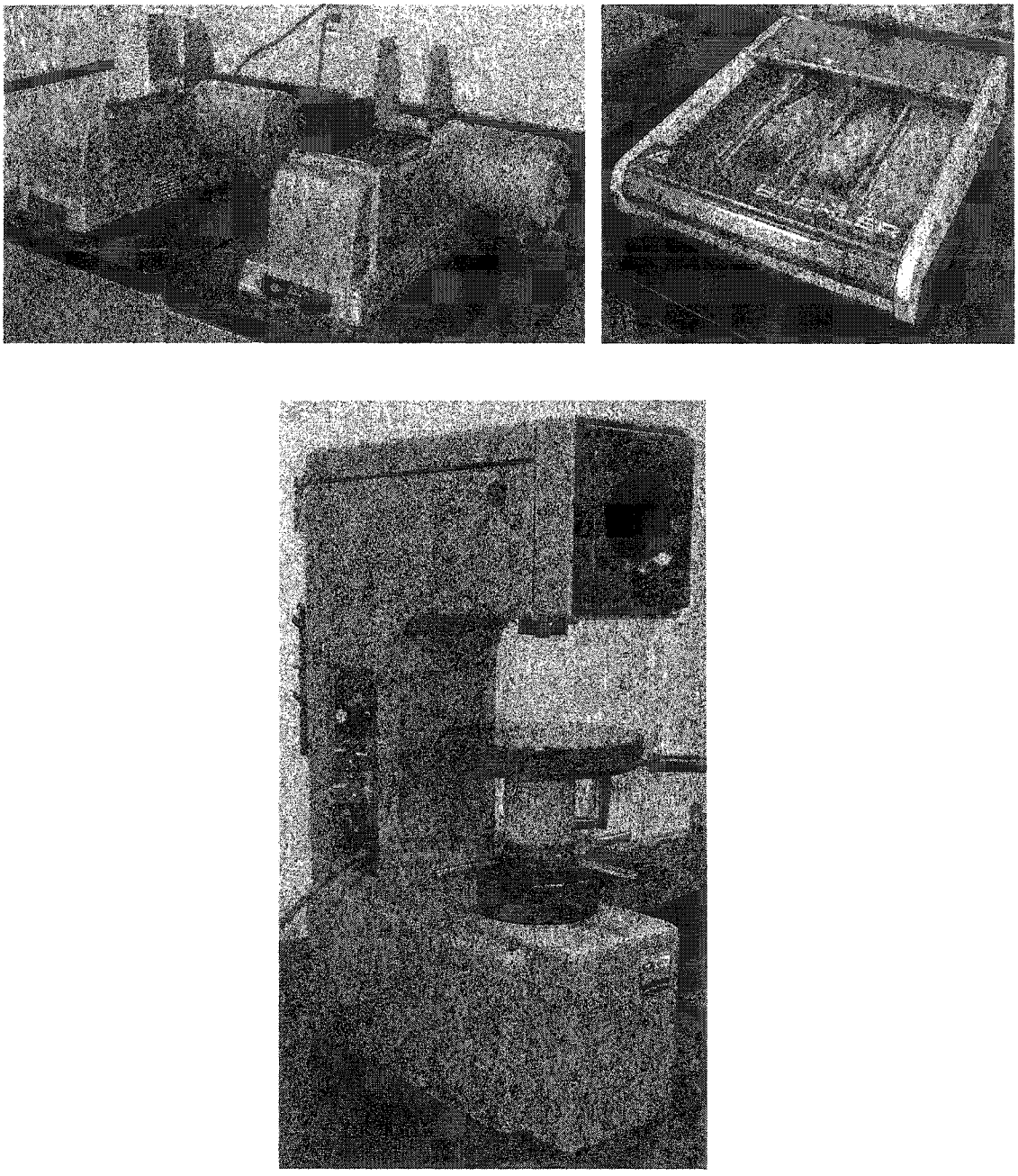

Figure 8.2 Experimental setup for in-house testing: Grinder and polisher (for sample preparation), and hardness machine (for *HRC* testing)

Standard Charpy impact specimens were made from H13 steel in collaboration with ALUPCO, at their die manufacturing plant in Jeddah. EDM wire cutting and high speed machining had to be used to achieve the required geometrical accuracy on the high-strength and high-hardness samples. Schematic diagram of the Charpy test setup and standard test specimen are shown in Fig 8.3. Experimental work consisted of the following stepwise procedures, as prescribed by standard texts and handbooks on heat treatment of hot work tool steels, especially H13 steel [ASM 1990, Bryson 1997, Thelning 1984, Roberts and Carey 1980, Unterweiser et al. 1982, Wilson 1975]:

Annealing: To remove any preexisting anomalies of material properties, all samples were first subjected to a careful annealing cycle:

1. Preheat to 200°C. Hold for 15 min.
2. Slowly heat to 850°C in a stepwise manner (200 → 400 → 600 → 850°C). Hold for 15 min at each step.
3. Hold for 2 hr at 850°C.
4. Slow cooling. Shutoff furnace and leave samples inside until cooled to 480°C.
5. Brisk cooling. Open furnace door, cool to room temperature.

Single Tempering: One set of samples followed the austenitizing-tempering-air cooling routine outlined below, to match single-tempered published data:

1. Slowly heat to austenitizing temperature (1050°C) stepwise: Room temp → 200 → 400 → 600 → 800 → 1050°C.
2. Hold at 1050°C for half hour (called soaking).
3. Remove from furnace. Air cool to 50-60°C.
4. As soon as temperature reaches 50-60°C, place in furnace already steadied at required tempering temperature. Hold for 2 hr.
5. Different sets of samples tempered at 425°C, 500°C, 550°C, and 600°C to match published data on single tempered samples.

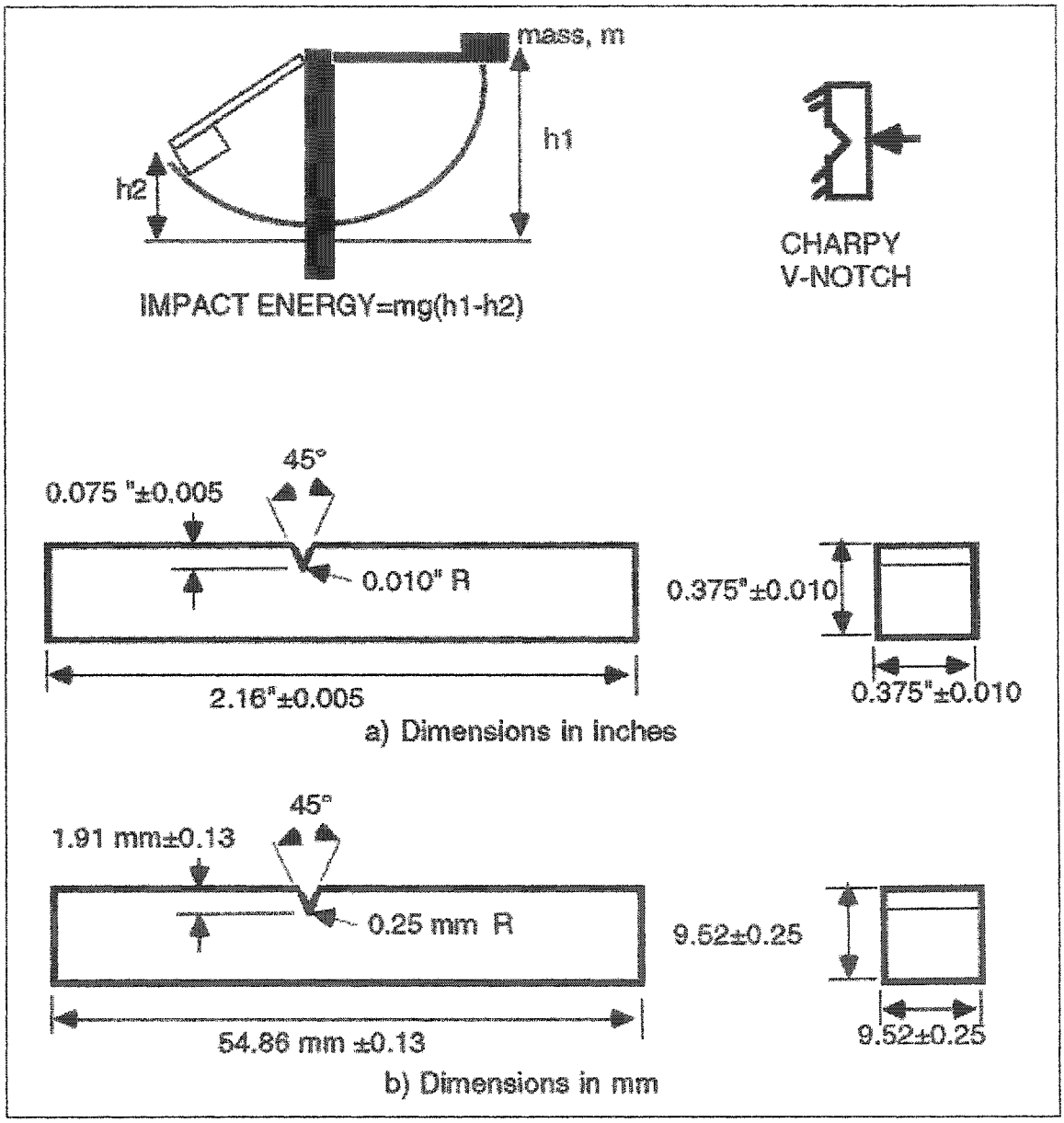

Figure 8.3 Schematic diagram showing Charpy impact test and its principle (a), and details of standard notched specimen for Charpy test

Double Tempering: Another set of samples underwent the following austenitizing-tempering-oil quenching routine, to be compared with similar double-tempered published data.

1. Slowly heat to 1010°C; Room temp → 200 → 400 → 600 → 800 → 1010°C.
2. Soak (hold) for half hour at 1010°C.
3. Remove from furnace. Oil quench to about 50-60°C.
4. Immediately place in furnace already steadied at required tempering temperature. Hold for 2 hr.
5. Remove from furnace. Air cool to room temperature, at least one hr.
6. Place in furnace steadied at the same tempering temperature as before. Hold for 2 hr.
7. Remove from furnace. Air cool to room temperature.
8. Different sets of samples tempered at 500°C, 550°C, 575°C, and 600°C to match published data on double tempered samples.

Hardness Testing: Stage-wise grinding was carried out on the samples, to remove oxide layers etc formed during heat treatment. A number of hardness readings were then taken at different positions on the sample, at room temperature, using the *HRC* hardness testing machine. Reported *HRC* values represent the average of the many readings recorded.

Hot CVN Testing: As can be seen from the photograph, the Charpy impact tester used does not have a built-in thermal chamber for testing at elevated temperatures. To overcome the problem, a digital furnace was placed right next to the impact testing machine. Furnace was heated to a temperature reasonable higher than that required for *CVN* testing. After holding the samples at this temperature for about 10 min, to allow uniform heating throughout, the sample was swiftly placed into the holder in the *CVN* machine, and the hammer was dropped. An infrared thermometer, with capability of instant temperature reading from a distance (laser beam centered on the sample in the holder), recorded the temperature at the time of impact. The impact energy reading from the dial was recorded for each case.

All the data (collected from published sources and generated inhouse) has been summarized in Tables 8.1 to 8.5, and forms the basis for the various graphs discussed below.

8.5 RESULTS AND DISCUSSION

8.5.1 Single Tempered Data

Single tempered data set (published and in-house) represents test samples that have been air cooled from the austenitizing temperature of 1050°C, and tempered for two hours at the listed tempering temperatures. Figure 8.4 shows the variation of room-temperature values of K_{IC}, *CVN*, and *HRC* against tempering temperature. As the curves clearly indicate, there is a definite correlation in the variation trend of the three quantities. K_{IC} and *CVN* first decrease and then increase with an increase in tempering temperature. *HRC* values exhibit a corresponding mirror behavior of an increase and then decrease with tempering temperature.

Figure 8.5 shows plots of (K_{IC}/HRC) and $(K_{IC}/HRC)^2$ versus (CVN/HRC), together with linear and quadratic polynomial regression results. The linear fit for (K_{IC}/HRC) gives slightly better results than those for $(K_{IC}/HRC)^2$: a correlation coefficient of r^2 = 58.2% as compared to r^2=53.8%. The resulting *CVN*-K_{IC} correlations are

$$\frac{K_{IC}}{HRC} = 2.4\left(\frac{CVN}{HRC}\right) + 0.17 \qquad \text{(MPa}\sqrt{\text{m}}\text{, J)}. \qquad (8.5)$$

$$\left(\frac{K_{IC}}{HRC}\right)^2 = 4.78\left(\frac{CVN}{HRC}\right) - 0.46 \qquad \text{(MPa}\sqrt{\text{m}}\text{, J)}. \qquad (8.6)$$

Various logarithmic, power law, and polynomial curve fitting techniques were also tried out. The best fit resulted for the quadratic polynomial case, yielding a considerably higher value of the coefficient of correlation (r^2 = 82.4% for K_{IC}/HRC and r^2 = 85.4% for $(K_{IC}/HRC)^2$).

Table 8.1 Room-temperature values of fracture toughness, hardness, and impact energy for H13 steel at different tempering (single) temperatures

Temper Temp (°C)	K_{IC}	*HRC*	*CVN*	*HRC*1	*CVN*1
400	47.7	54	14.82	47	9.8
425	43	55	12	48	8.1
450	38	55.5	9.65	49	5.8
468	34.5	55.8	7	49.4	3.8
475	33	55.9	6.14	49.5	3.1
482	31.5	56.1	6	49.6	2.5
500	27.4	56.3	5.68	49.8	2.7
518	25.2	55.8	7	49.3	4.5
530	24.3	54.8	9.2	49	6.1
550	23.1	54	11.65	47.9	8.4
566	25.1	52.8	13.1	47.4	9.7
593	32.5	50.7	15.4	45.7	11.6
600	33.2	50	16.38	45.1	13.1
625	52.4	47.66	18	43.5	14.5
650	77.7	45.8	20	41.5	16

K_{IC}, *HRC*, *CVN*: Air cooled from 1010°C, single tempered (2 h) at tempering temperature [ASM 1990, Thelnig 1984]
*HRC*1, *CVN*1: Air cooled from 1050°C, single tempered (2h) at tempering temperature [Inhouse-1]

Table 8.2 Room temperature data for variation of *HRC* against tempering (single and double) temperature; various sources

Temper Temp (°C)	*HRC*	Temper Temp (°C)	*HRC*	Temper Temp (°C)	*HRC*
Set-1		**Set-5**		**Inhouse-1**	
524	54	400	54	400	47
565	52	425	55	425	48
607	47	450	55.5	450	49
615	43	468	55.8	468	49.4
Set-2		475	55.9	475	49.5
527	52	482	56.1	482	49.6
555	50	500	56.3	500	49.8
575	48	518	55.8	518	49.3
593	46	530	54.8	530	49
605	44	550	54	550	47.9
Set-3		566	52.8	566	47.4
371	50.5	593	50.7	593	45.7
426	51.6	600	50	600	45.1
482	52.9	625	47.66	625	43.5
538	53.7	650	45.8	650	41.5
593	49.7	**Inhouse-2**			
Set-4					
371	50.5	500	50.5		
426	51.2	525	49		
482	51.9	550	46.8		
538	51.6	575	45.4		
593	46.0	600	43.2		

Set-1: Air cooled from 1010°C and double tempered (2 + 2 h) at tempering temperature [Kussmaul & Roos 1984]
Set-2: Oil quenched from 1010°C and double tempered (2 + 2 h) at tempering temperature [Kussmaul & Roos 1984]
Set-3: Air cooled from 1010°C and double tempered (2 + 2 h) at tempering temperature [ASM 1990]
Set-4: Air cooled from 980°C and double tempered (2 + 2 h) at tempering temperature [ASM 1990]
Set-5: Air cooled from 1010°C and single tempered (2 h) at tempering temperature [Thelnig 1984]
Set-6: Air cooled from 1010°C and double tempered (2 + 2 h) at tempering temperature [Van der Sluys et al. 1983]
Inhouse1: Air cooled from 1050°C and single tempered (2 h) at tempering temperature [Inhouse-1]
Inhouse2: Oil quenched from 1010°C and double tempered (2 + 2 h) at tempering temperature [Inhouse-2]

Table 8.3 Room temperature data for variation of *CVN* against tempering (single and double) temperature; various sources

Temper Temp (°C)	*CVN*	Temper Temp (°C)	*CVN*	Temper Temp (°C)	*CVN*
Set-1		**Set-5**		**Inhouse-1**	
524	10.0	518	7	400	9.8
565	10.0	530	9.2	425	8.1
607	18.0	550	11.65	450	5.8
615	18.0	566	13.1	468	3.8
Set-2		593	15.4	475	3.1
527	16.0	600	16.38	482	2.5
555	24.0	625	18	500	2.7
575	27.0	**Inhouse-2**		518	4.5
593	28.5			530	6.1
605	30.0			550	8.4
Set-6		500	13.2	566	9.7
510	10.0	525	14.5	593	11.6
538	8.5	550	21.8	600	13.1
566	8.5	575	25.1	625	14.5
593	10.9	600	27.4	650	16
621	15.9				

Table 8.4 (a) *CVN* values at elevated test temperatures for H13 steel heat treated to different tempering temperatures (various sources)

Test Temp (°C)	*CVN* (J) at different tempering temperatures (°C)						
	524	540	565	575	600	607	615
21	14	14	14	16.38	22.33	24	24
95	18.5	18.89	19.5	22	28.25	30	33.5
205	24.8	25.78	27.3	29.85	36.22	38	47.3
260	27	28.17	30	32.62	39.17	41	52
315	28.4	29.65	31.6	34.27	40.93	42.8	55
425	29.9	31.11	33	35.69	42.42	44.3	58.1
480	30.2	31.53	33.6	36.27	43.38	44.8	59
540	31	32.17	34	36.62	43.17	45	60
595	31.7	32.6	34	36.14	41.5	43	57
650	32.1	32.84	34	34.95	37.49	38	51.5

Table 8.4 (b) *CVN* values at elevated test temperatures for H13 steel heat treated to different tempering temperatures (Inhouse-2)

Test Temp (°C)	CVN (J) at different tempering temperatures (C)			
	500	550	575	600
350	28	29.5	31.5	37
400	28.5	30.2	33	38
450	29	30.5	34	39.5
500	29.5	31	34.5	40.5
550	30	31.5	35	40
600	30.5	32	34.5	38.5

Table 8.5 *HRC* values at elevated test temperatures for H13 steel heat treated to different tempering temperatures (various sources)

Test Temp (°C)	*HRC* at different tempering temperatures (°C)						
	524	**540**	**565**	**575**	**600**	**607**	**615**
21	42.42	44.2	46.99	48.1	51.5	55.85	56.94
95	42.31	44	46.64	47.7	51.5	56.36	57.58
205	41.80	43.4	45.90	46.9	50.5	55.11	56.26
260	41.25	42.9	45.47	46.5	50	54.48	55.6
315	40.36	42.1	44.81	45.9	49.2	53.42	54.48
425	37.78	39.7	42.70	43.9	46.9	50.74	51.7
480	36.33	38.2	41.13	42.3	45.3	49.14	50.1
540	33.80	35.9	39.19	40.5	42.9	45.97	46.74
595	29.75	32.4	36.54	38.2	39.4	40.94	41.32
650	21.30	21.8	22.59	22.9	26.5	31.11	32.26

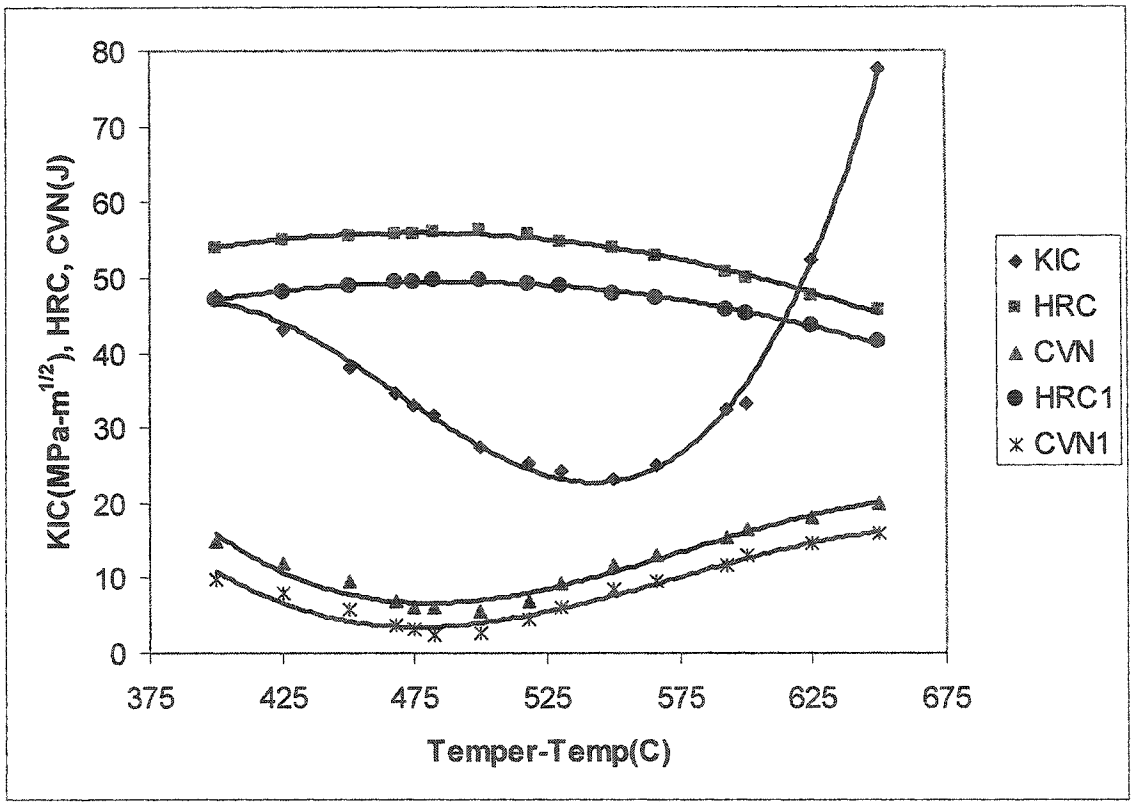

Figure 8.4 Room-temperature variation of K_{IC}, *CVN*, and *HRC* of H13 steel against tempering (single) temperature; various sources (Table 8.1)

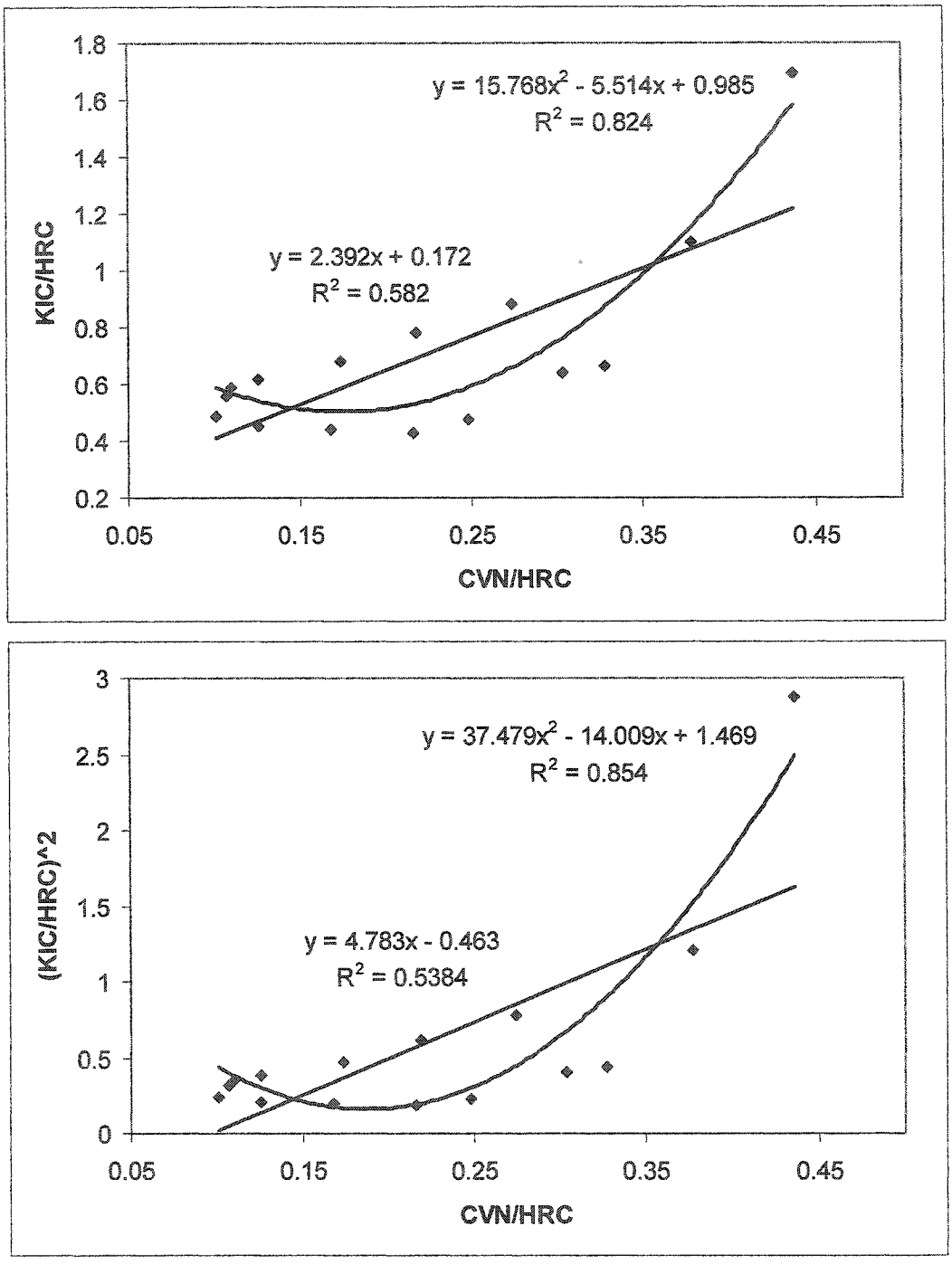

Figure 8.5 Plots and regression results of room-temperature variation of K_{IC}/HRC against CVN/HRC, and $(K_{IC}/HRC)^2$ against CVN/HRC for H13 steel

$$\frac{K_{IC}}{HRC} = 15.78\left(\frac{CVN}{HRC}\right)^2 - 5.51\left(\frac{CVN}{HRC}\right) + 0.985 \qquad \text{(MPa}\sqrt{\text{m}}\text{, J)}. \qquad (8.7)$$

$$\left(\frac{K_{IC}}{HRC}\right)^2 = 37.48\left(\frac{CVN}{HRC}\right)^2 - 14\left(\frac{CVN}{HRC}\right) + 1.469 \qquad \text{(MPa}\sqrt{\text{m}}\text{, J)}. \qquad (8.8)$$

The linear models, though exhibiting a seemingly weaker correlation, yield a wider prediction domain of reasonable K_{IC} values. They can be attractive if operating temperatures beyond 650°C are involved. However, we should keep in mind that optimum die performance (very high hardness to avoid wear, and high enough toughness to avoid fracture) is achieved in the 500-600°C operating temperature range (Fig 8.4). Equations (8.7) and (8.8) give reliable results with a high coefficient of correlation in the ($CVN/HRC \leq 0.45$) range, which is safely inside the optimum temperature limits mentioned above.

8.5.2 Double Tempered Data

Variation of room temperature *HRC* against tempering temperature is shown in Fig 8.6, for both single tempered and double tempered sample sets. Data are from several different sources, including inhouse experiments. It can be readily seen that the variation pattern for all types of samples is almost the same, the only difference being an offset from one curve to the other. Two pairs of curves are nearly identical.

Figure 8.6 also illustrates the behavior of *CVN* against tempering temperature. Again, the data sets are from different sources (including inhouse experimentation) and include cases of both single and double tempering. As in the case of *HRC*, *CVN* variation shows the same trend, different sample sets yielding curves that are slightly offset from each other.

The *CVN*-K_{IC} correlations derived in the preceding section were based on test specimens subjected to single tempering only. However, we can see from Fig 8.6 that the pattern of variation of room temperature values for both *CVN* and *HRC* against tempering temperature is almost the same for single tempered samples as for the double tempered

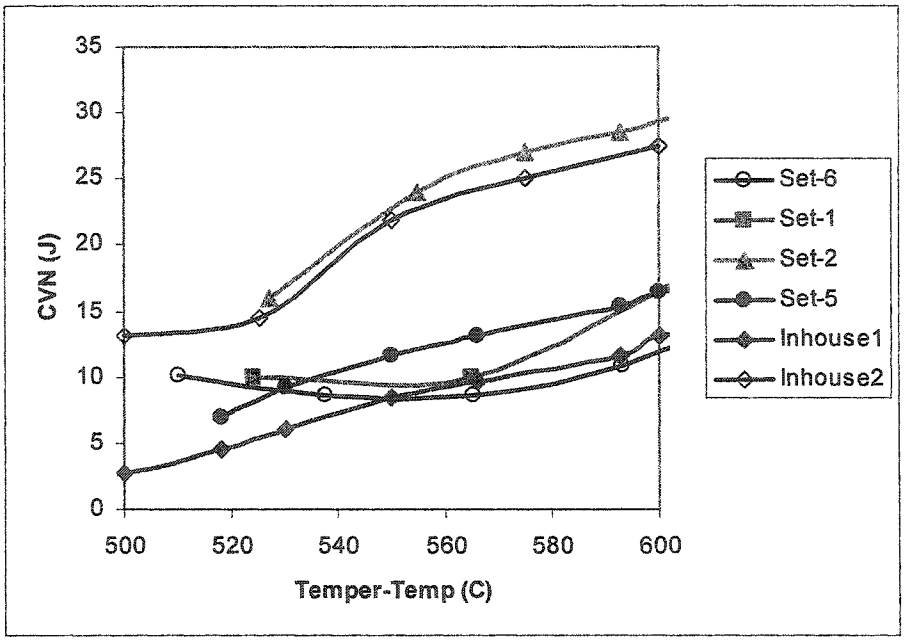

Figure 8.6 Variation of room temperature values of *HRC* and *CVN* of H13 steel against tempering temperature (single and double); different curves represent samples subjected to different tempering routines; various sources (Tables 8.2 and 8.3)

ones. It is therefore fairly reasonable to conclude that the correlations represented by equations (8.5) to (8.8) are also applicable in the case of double tempering.

8.5.3 Elevated Temperatures

Figure 8.7 shows us plots of *HRC* and *CVN* against increasing test temperature. Different plots are for samples tempered at different tempering temperatures (°C). All test specimens are double tempered, one set oil quenched and one air cooled from austenitizing temperature, before being tempered. As an example, the highest curve in the *CVN*-temperature graph represents samples tempered at 615°C, and gives the values of their Charpy impact energy (*CVN*) at different testing temperatures. Once again, the variation pattern is very similar, different curves being slightly offset from each other. As is expected, hardness values decrease with increasing test temperature, while impact strength increases.

Hot variation of *HRC* and *CVN* with tempering temperature is shown in Figure 8.8. Each curve represents experiments conducted at a certain test temperature. The lowest curve in the *HRC*-temper temperature graph, for instance, records the *HRC* values of samples that were heat treated to different tempering temperatures, but were all tested at a temperature of 595°C. Again, as would be expected of the general material behavior of steels, *HRC* decreases with increasing test temperature while *CVN* increases. As observed in all of the previous data sets, the variation trend for different sets of test specimens is almost identical.

It appears to be a viable conclusion that the tests conducted at elevated temperatures show a significant similarity in the pattern of variation of *CVN* and *HRC* as compared with room temperature tests. The proposed *CVN*-K_{IC} correlations based on hot hardness and hot impact strength are therefore of the same form as their room temperature counterparts.

$$\frac{K_{IC}(T)}{HRC(T)} = 2.4\left(\frac{CVN(T)}{HRC(T)}\right) + 0.17 \qquad \text{(MPa}\sqrt{\text{m}}\text{, J).} \qquad (8.9)$$

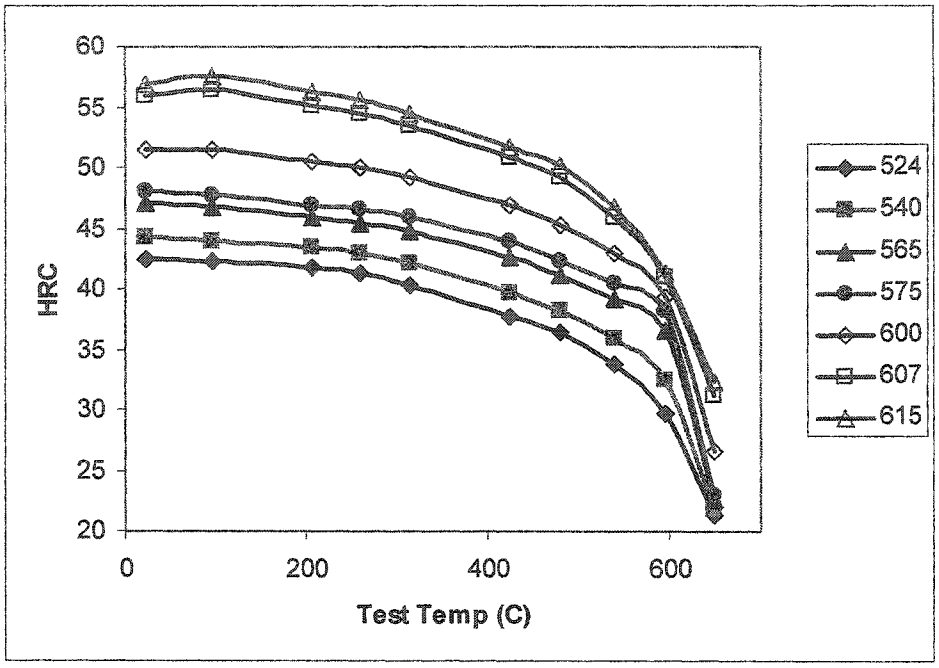

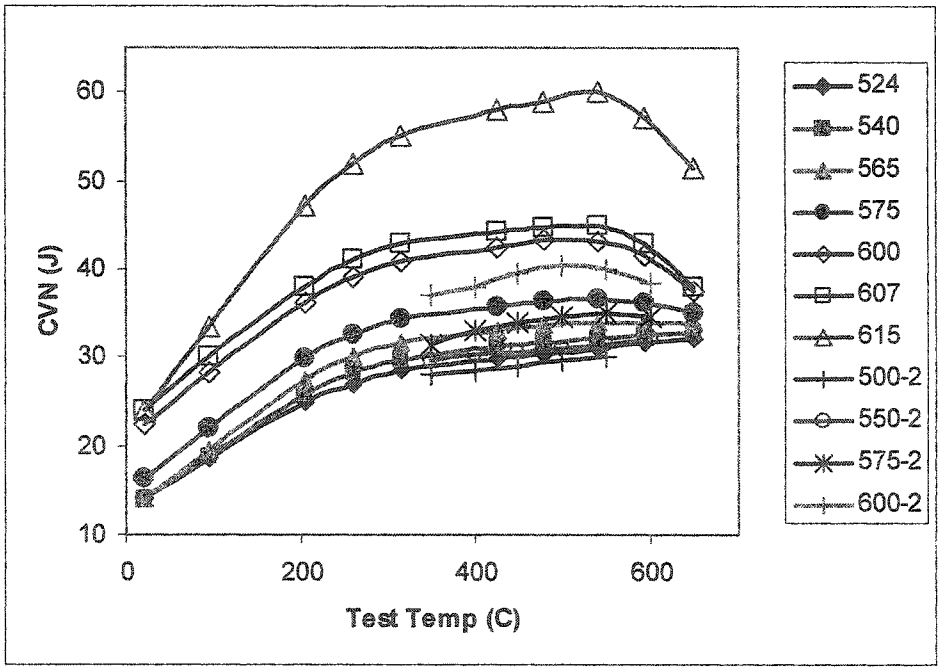

Figure 8.7 Variation of *HRC* and *CVN* for H13 steel against elevated test temperatures; different curves represent samples heat treated at different tempering (single and double) temperatures; various sources (Tables 8.4 and 8.5)

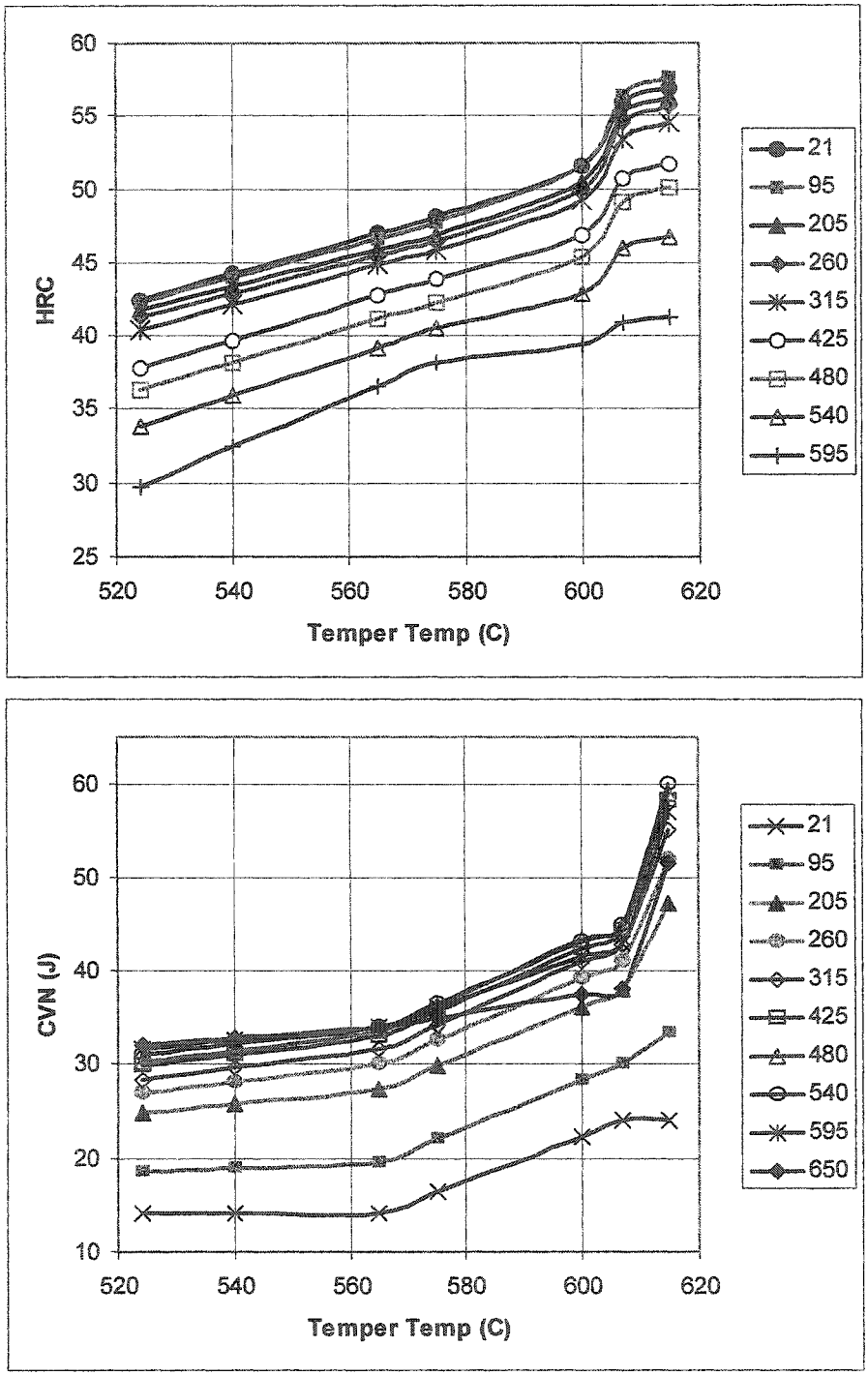

Figure 8.8 Variation of *HRC* and *CVN* of H13 steel against tempering (single and double) temperature; different curves represent samples tested at different elevated temperatures; various sources (Tables 8.4 and 8.5)

$$\left(\frac{K_{IC}(T)}{HRC(T)}\right)^2 = 4.78\left(\frac{CVN(T)}{HRC(T)}\right) - 0.46 \qquad \text{(MPa}\sqrt{\text{m}}\text{, J)}. \qquad (8.10)$$

$$\frac{K_{IC}(T)}{HRC(T)} = 15.78\left(\frac{CVN(T)}{HRC(T)}\right)^2 - 5.51\left(\frac{CVN(T)}{HRC(T)}\right) + 0.985 \qquad \text{(MPa}\sqrt{\text{m}}\text{, J)}. \qquad (8.11)$$

$$\left(\frac{K_{IC}(T)}{HRC(T)}\right)^2 = 37.48\left(\frac{CVN(T)}{HRC(T)}\right)^2 - 14\left(\frac{CVN(T)}{HRC(T)}\right) + 1.469 \qquad \text{(MPa}\sqrt{\text{m}}\text{, J)}. \qquad (8.12)$$

One point must be re-stressed here. H13 is a high-hardness, high-strength hot work tool steel. Plane strain fracture toughness (K_{IC}) testing (even at room temperatures) is a difficult and costly procedure, and quite sensitive to test parameters. The facilities to maintain test samples at precisely held elevated temperatures for long durations required by the test are often expensive. To perform these tests for a number of specimens that have been differently tempered, and to redo the experiments enough number of times to achieve a semblance of repeatability, magnifies the level of difficulty and cost. That is why, even a comprehensive search (both in the published literature and the suppliers/manufacturers domain) yielded only one set of room temperature K_{IC} values. Verification of the proposed correlations would require some K_{IC} experimentation for H13 steels at elevated temperatures. However, K_{IC} values calculated using the proposed correlations for different elevated temperatures in the commercial hot working range of 425°C-525°C were found to be quite realistic. These predicted numbers may be used as reasonable ballpark values in failure analysis and life prediction of hot work tool steels.

CHAPTER 9
EXTRUSION TOOLING: LIFE PREDICTION USING MONTE CARLO SIMULATION

9.1 INTRODUCTION

Due to the high cost of metal forming tools (especially in hot extrusion), one of the major goals is a longer tool life. Continued research in tool and process design is therefore targeted at minimization of tool failure. However, tool failure is a complex phenomenon, governed by an interaction of various mechanisms, and not easy to control or restrain. A more manageable approach is to make die failure *predictable*. Estimation and prediction of tool life thus becomes critically important.

9.1.1 Current Work

As established in chapter-5, the two most dominant failure mechanisms for extrusion dies (solid, hollow, and semihollow dies all taken together) are *fracture* and *wear*. In the first part of this chapter, a fracture mechanics based fatigue life prediction model is presented. A similar treatment is then presented for wear-related failures. Fracture and wear usually coexist as failure modes, and final die breakdown occurs due to the mechanism that becomes dominant. Therefore, a competing fracture-wear model has been later developed to represent the complete die failure situation. Attempt has been made to correlate the stochastic nature of various fatigue and wear related die parameters to die life. Monte Carlo simulation has been used to predict the life distribution of a die for a given set of manufacturing conditions and mechanical properties. Comparison of the simulated life with actual life data from the industry has also been presented. Some details of this work are available in Qamar et al. [June 2004].

9.2 FRACTURE FAILURE

Most of the information presented in this section is derived from Pöhlandt [1989], Roberts et al. [1998], ASM [1996], and Sanford [2003].

Repeated cycles of billet by billet loading-deformation-unloading in extrusion create a fatigue environment. Very few commercial extrusion profiles have simple geometries. Solids have predominantly high complexities, and hollows have mandrels and welding chambers in the die set. Fracture is thus the principal failure mode for extrusion dies and tooling. Schematic illustration of an edge crack in a simple hollow die is shown in Fig 9.1 (a).

Fracture mechanics is the mathematical analysis of the mechanical processes that lead to fracture failure. It includes the process of crack growth by such mechanisms as fatigue and stress corrosion as well as the final fracture event by cleavage or dimple rupture. Te analysis is based on established procedures used generally in solid mechanics, for example the theory of elasticity or continuum mechanics. The analysis concepts employ the stress and strain in a cracked body and the changes in strain energy that take place during cracking and fracture.

The *stress intensity factor* (K) is a scaling factor used in LEFM to describe the intensification of applied stress at the tip of a crack of known size and shape. At the onset of rapid (unstable) crack propagation in any structure containing a crack, the factor is called the *critical stress-intensity factor* or the *fracture toughness*. The *plane-stress fracture toughness* (K_C) is the value of stress intensity at which crack propagation becomes rapid in sections thinner than those in which plane-strain conditions prevail. K_I is the stress-intensity factor for a loading condition that displaces the crack faces in a direction normal to the crack plane; this loading configuration is also known as the opening mode of deformation.

$$K_I = \alpha\, f(a/W)\, \sigma \sqrt{\pi a}\,,$$

(a)

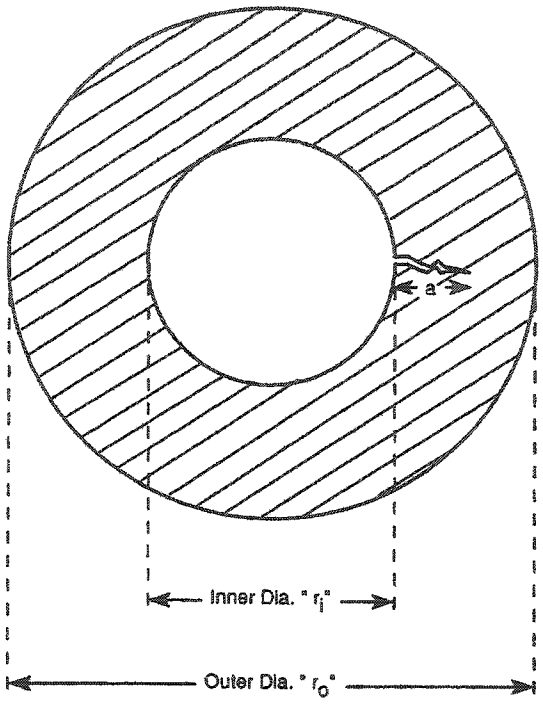

(b)

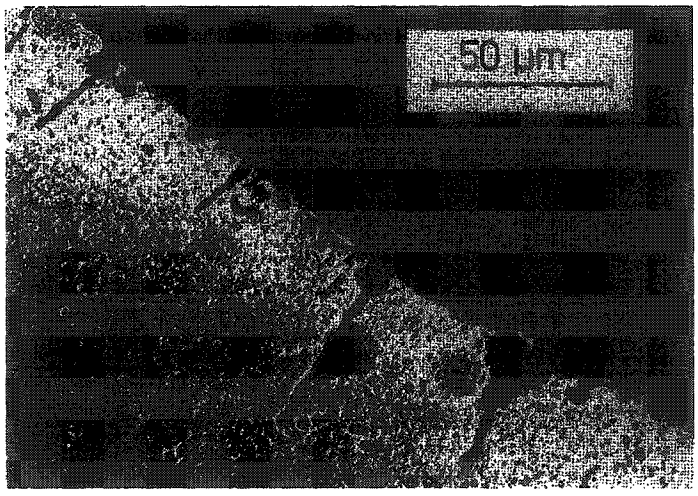

Figure 9.1 Schematic representation of edge crack in a hollow die (a), and formation of fatigue cracks at the surface defects of spark eroded Cr-Mo-V steel (b) [Pöhlandt 1989]

where a is the flaw-size, W is the specimen width, and σ is the applied remote stress. Crack geometry and loading configuration are represented by the factors α and $f(a/W)$. The minimum value of K_C for any given material and condition, which is attained when rapid (unstable) crack propagation in the opening mode is governed by plane-strain conditions, is referred to as the *plane-strain fracture toughness* (K_{IC}). This happens when either the applied remote stress or the flaw size reaches a critical value ($\sigma = \sigma_c$, or $a = a_c$).

9.2.1 Crack Initiation

In extrusion dies and tooling, cracks generally initiate at positions of high stress concentration such as section changes, sharp corners, stamp marks, etc. Crack initiation may be further promoted by machining marks. Due to manufacturing operations such as *spark erosion*, there may be preexisting cracks, such as those shown in Fig 9.1 (b). Crack depths of such cracks are typically about 0.01 mm. To improve wear resistance, die bearing surfaces are surface hardened, usually by nitriding. This nitriding process often results in the formation of small cracks (of the order of 0.05 mm for H13 tool steels). To achieve the desired hardness-toughness characteristics, dies are subjected to specific heat treatment routines (as outlined in chapter-8). Existing small flaws usually get enlarged during these operations. With such initial pre-operation cracks (crack depths of 0.05 to 0.1 mm), fracture mechanics type crack propagation takes over due to fatigue cycles during the actual extrusion process.

9.2.2 Crack Propagation

Die fracture can be caused by one of the following two mechanisms:

(a) *Hypercritical, instable crack growth*: In the presence of an existing defect, a crack takes only a few cycles to reach the critical size, resulting in forced rupture (Fig 5.4).

(b) *Subcritical, stable crack growth*: From an existing defect, crack growth is caused by fatigue or creep (or a combination of the two), resulting in ultimate fracture.

Both of these mechanisms are affected by different factors concerning the billet and die material, the process and the equipment. In hot extrusion, fatigue is the major contributor, effects of creep being negligible [Pöhlandt 1989].

For components having subcritical cracks, fracture is almost of no concern as long as the crack size is below the critical value under the given conditions. Under cyclic loading, crack propagation takes place until the stress intensity factor equals the fracture toughness of the die material. Large cyclic stresses, combined with regions of high stress concentration in cavities, lead to crack growth and ultimate failure. In general, cracks can grow only under tensile stresses, compressive stresses promoting crack closure and reduction of crack growth.

Figures 9.2 and 9.3 show idealized and experimental versions of the three stages of crack growth. The first part of the curve is the *crack initiation* or *Stage-I crack growth.* The second part is the *Stage-II crack growth* where a crack grows gradually and subcritically. Finally, when the fatigue crack grows to a length approaching the critical length for instability at the maximum applied stress level, the crack grows in an unstable fashion. This region is the *Stage-III growth.*

Fatigue crack growth data plot as a straight line on a log-log sale over some interval (*Stage-II*) for a wide variety of metallic materials. Crack growth velocity da/dN, as a function of the applied stress intensity range ΔK, can be approximated by the famous Paris law proposed by Paris and Erdogan:

$$\frac{da}{dN} = C(\Delta K)^m . \tag{9.1}$$

Values of the Paris constants C and m for a large number of metals has been reported by Sanford [2003] and Osgood [1982].

9.2.3 Fatigue Life or Cycles to Failure

We know that (neglecting the finite size factor $f(a/W)$ for simplicity),

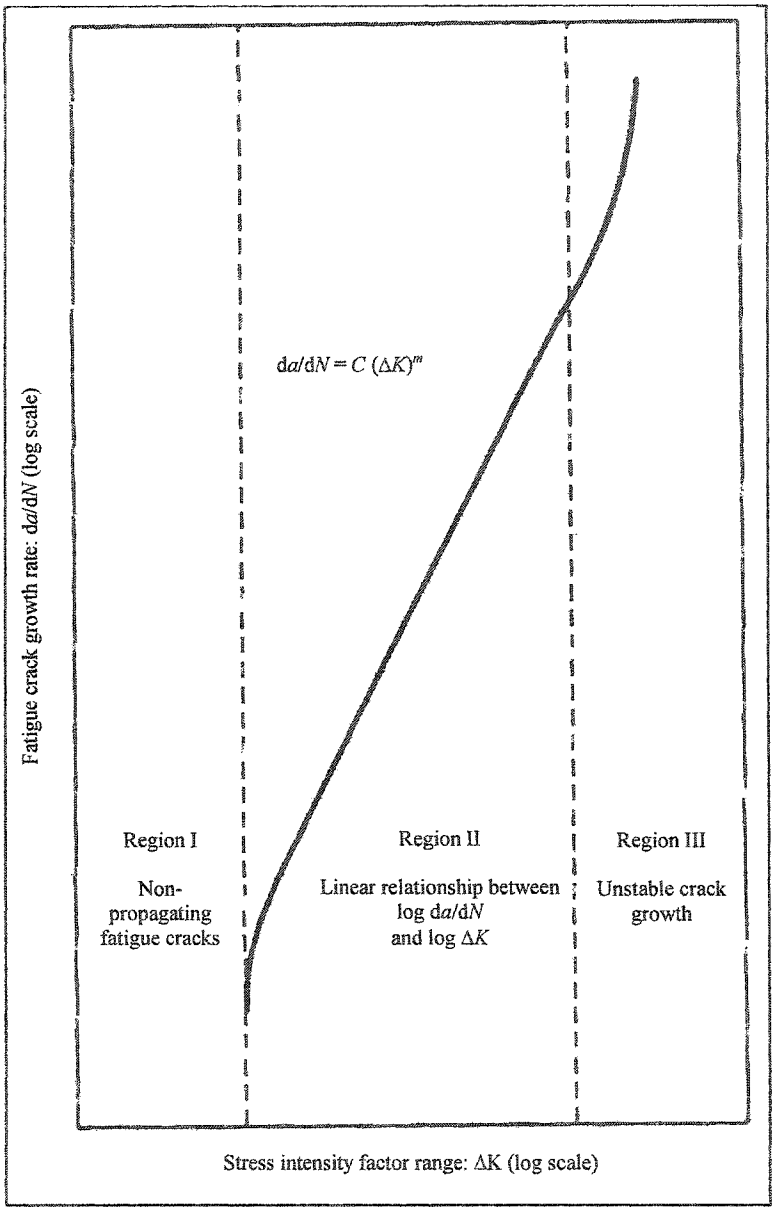

Figure 9.2 Idealized fatigue crack growth curve over the full range of applied ΔK on a log-log scale, identifying the three growth regions [Callister 2000]

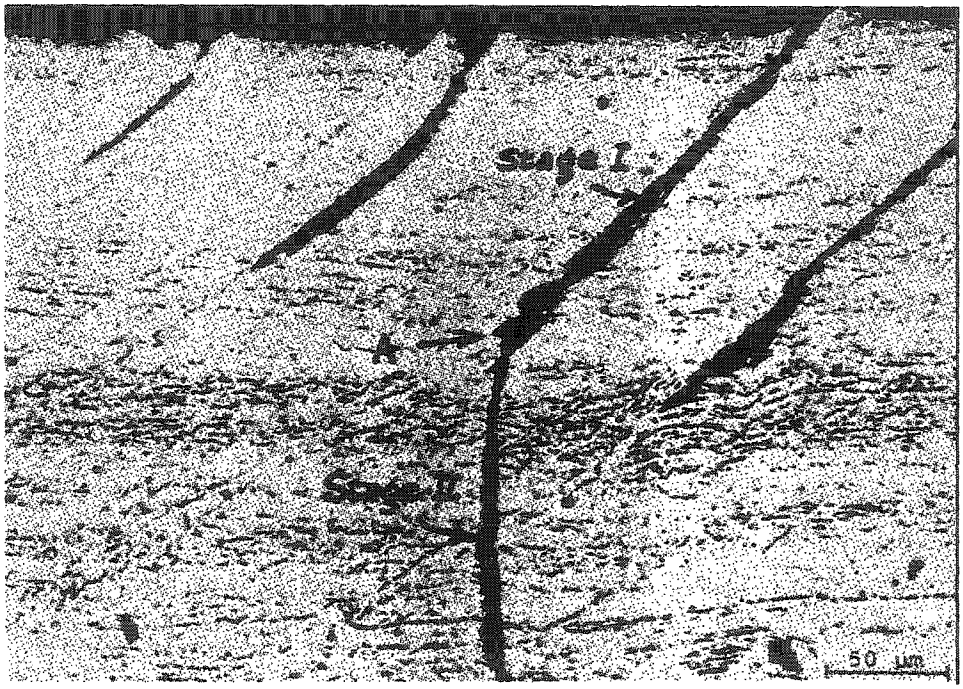

Figure 9.3 Microphotograph of gradual transition from *Stage I* to *Stage II* crack growth [Sanford 2003]

$$\Delta K = \alpha \Delta\sigma \sqrt{\pi a}\,, \tag{9.2}$$

where

$$\Delta\sigma = \sigma_{max} - \sigma_{\min}$$

Since each extrusion cycle starts from a minimum load of zero, $\sigma_{min} = 0$. Thus

$$\Delta\sigma = \sigma_{max}.$$

Substituting equation 9.2 into 9.1,

$$\frac{da}{dN} = C(\alpha\sigma_{\max}\sqrt{\pi a})^m\,. \tag{9.3}$$

This can be rearranged to give

$$dN = \frac{da}{C(\alpha\sigma_{\max}\sqrt{\pi a})^m}\,. \tag{9.4}$$

The fatigue life (or the number of cycles to failure) can now be obtained by integrating this equation:

$$N_f = \int_{N=0}^{N_f} dN = \frac{1}{C\alpha^m {\sigma_{\max}}^m \pi^{m/2}} \int_{a_0}^{a_c} \frac{da}{a^{m/2}}\,. \tag{9.5}$$

After simplification, this yields

$$N_f = \frac{(a_0)^{1-m/2} - (a_c)^{1-m/2}}{C(m/2-1)\alpha^m \pi^{m/2} {\sigma_{\max}}^m}\,. \tag{9.6}$$

Values of C and m can be found for ultrahigh strength steels (H13 tool steel falls under this category) from standard references. Size of preexisting cracks (a_0) in heat treated and surface hardened H13 steel (extrusion dies), as mentioned above, is generally in the 0.05-0.1 mm range. Value of the geometry factor (α) for an edge crack is 1.12. To find the crack size that would trigger an unstable crack growth, we start from

$$K_I = \alpha\sigma\sqrt{\pi a}\,. \tag{9.7}$$

Knowing that $a = a_c$ when $K_I = K_{IC}$, we get

$$a_c = \frac{1}{\pi}\left(\frac{K_{IC}}{\alpha\sigma_{\max}}\right)^2\,. \tag{9.8}$$

Treating the simple hollow (tube) die as a thick-walled cylinder with internal pressure, the maximum stress in equation (9.8) would be [Shigley et al. 2004]

$$\sigma_{\max} = p\left(\frac{r_o^{\,2} + r_i^{\,2}}{r_o^{\,2} - r_i^{\,2}}\right), \tag{9.9}$$

where r_o and r_i are the outer and inner radii of the tube.

Extrusion pressure p, as described earlier, is given by

$$p = \overline{Y}_f\left(\varepsilon + \frac{2L}{Db}\right), \tag{9.10}$$

where $\varepsilon = \ln R$ is the true strain and

$$R = \frac{A_b}{n_1 A_s} = \frac{D_b^{\,2}}{n_1(d_o^{\,2} - d_i^{\,2})} \tag{9.11}$$

is the extrusion ratio. Number of cavities in a die is n_1. Of course, at $L = L$, $p = p_{max}$ in equation (9.10). The inner diameter of the tube is obviously

$d_i = d_o - 2t$.

Flow stress of the material can be evaluated from [Saha 2000]

$$\overline{Y}_f = \overline{\sigma} = \overline{\sigma}_0\left(\frac{\dot{\bar{\varepsilon}}}{\dot{\bar{\varepsilon}}_0}\right)^{m^*}, \tag{9.12}$$

where $\overline{\sigma}_0$ is the known flow stress at a known average strain rate $\dot{\bar{\varepsilon}}_0$. A typical value of the exponent m^* at 500°C for Al-Mg-Si alloy (the category to which 6xxx alloys of aluminum belong) is 0.125 [Saha 2000]. At an average strain rate of 50 s^{-1}, the average flow stress for Al-6063 was found to be around 40 MPa [Sheppard 1999] using the graph shown in Fig 3.3.

The mean strain rate can be found from

$$\dot{\bar{\varepsilon}} = \frac{6V}{D_b}\ln R, \tag{9.13}$$

where V is the ram speed and R is the extrusion ratio [Kalpakjian 2003].

Assuming an edge-crack type flaw in our case, and disregarding the correction for finite width, introduces some inaccuracy. For a long part-through internal flaw ($a/t \leq$

0.75) in a cylinder subjected to internal pressure (as shown in Fig 9.4), stress intensity factor K_I can also be found using the set of equations listed below [Anderson 1991]:

$$K_I = \frac{2pR_o^2}{R_0^2 - R_i^2}\sqrt{\pi a}F\left(\frac{a}{t}, \frac{R_i}{t}\right) \tag{9.14}$$

$$F = 1.1 + A\left[4.951\left(\frac{a}{t}\right)^2 + 1.092\left(\frac{a}{t}\right)^4\right] \tag{9.15}$$

$$A = \left(0.125\frac{R_i}{t} - 0.25\right)^{0.25} \qquad \text{for } 5 \le R_i/t \le 10 \tag{9.16}$$

$$A = \left(0.2\frac{R_i}{t} - 1.0\right)^{0.25} \qquad \text{for } 10 \le R_i/t \le 20. \tag{9.17}$$

Knowing that $a = a_c = a_f$ when $K_I = K_{IC}$, we can find the final (critical) crack size by substituting the value of K_{IC} instead of K_I in equation (9.14). Rest of the procedure in determining fracture life (number of cycles to failure) would be the same as described above. Of course, solution for final crack length would involve an iterative procedure or numerical calculations. As this would have to be done for all 10,000 instances of the simulation, the procedure would require a lot of effort and computational time. That is why, the procedure outlined above has been adopted for this study.

9.2.4 Case Study

Actual die failure data (due to fatigue fracture and die land wear) have been collected from ALUPCO for the simple hollow dies shown in Fig 9.5 and 9.6. The tube die has been used to simulate both fracture and wear failure, while the box die is used only for parameter estimation of wear failures (described later in section 9.3.1). Die material was heat treated and surface hardened H13 steel, billet material being Al-6063. Average extrusion temperature was around 460°C, and ram speed was 5 mm/s. The average die life (*MTTF*) for the tube die was 722 extrusion cycles. Extrusion of each billet is considered to be one cycle, as the extrusion pressure goes from a minimum of zero to a maximum value, and then back to zero for each billet.

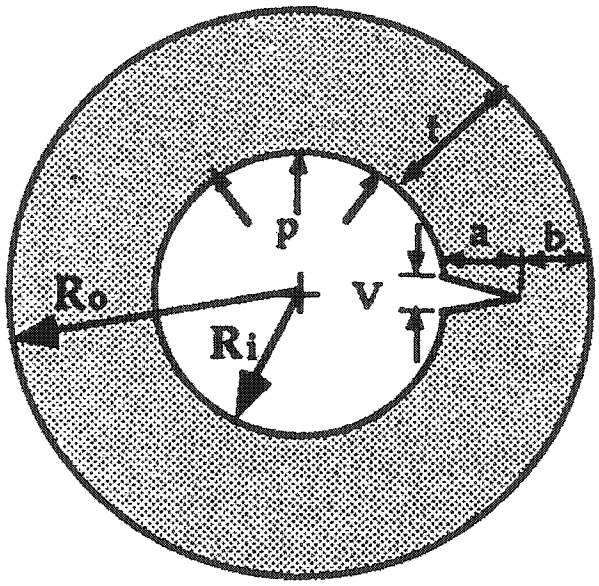

Figure 9.4 Long part-through internal flaw in a cylinder subjected to internal pressure [Anderson 1991]

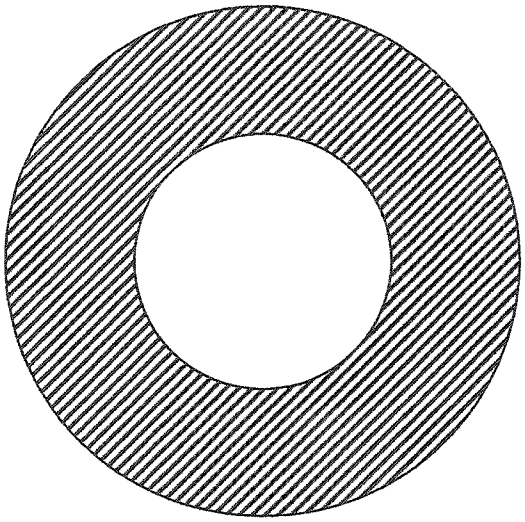

Figure 9.5 Profile section of the hollow die chosen for Monte Carlo simulation of die failure

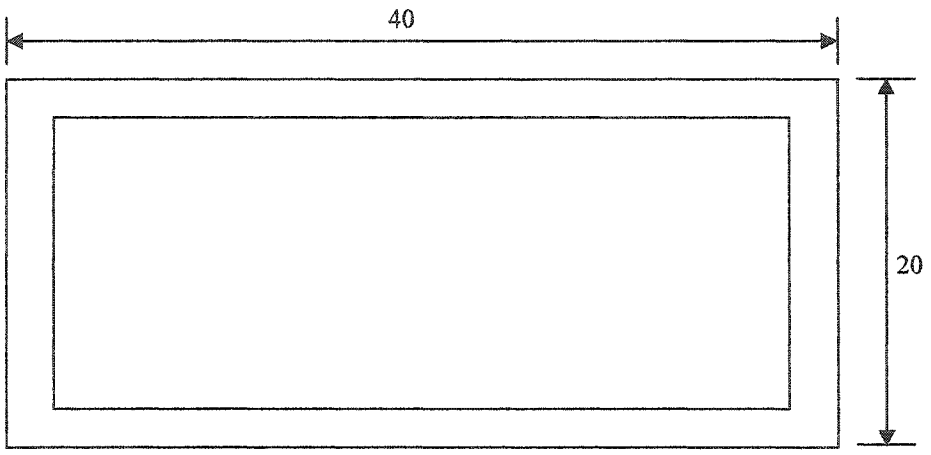

Figure 9.6 Geometrical details of the box profile die used for determination of mean and standard deviation of the wear parameter *m*

9.2.5 Probabilistic Nature of Die Life

Fatigue life and fracture mechanics based models for life prediction are generally deterministic in nature. On the other hand, geometric parameters of an extrusion die and experimentally determined material properties are random variables. Life of an extrusion die is thus largely probabilistic in character. It has been assumed here that geometric dimensions of the die profile and the billet (outer diameter d and thickness t of the tube, length L and diameter D_b of the billet) and initial crack size a_0 (preexisting flaws due to heat treatment and surface hardening) are normally distributed random variables. Mean (μ) and standard deviation (σ) values for profile dimensions are derived from tolerances specified on manufacturer's profile drawing, and those for initial crack size are based on studies about preexisting cracks due to spark erosion in tool steels [3]. The data is assumed to be spread within $\pm 3\sigma$ limits of the mean.

Plane strain fracture toughness K_{IC} of the die material is a strength property and is well represented by a Weibull distribution. Values of μ and σ and the Weibull parameters m and θ are based on variation in K_{IC} values of tool steels as reported in references such as ASM [1996] and tool steel manufacturers. Paris constant C of the die material, due to the nature of the Paris law equation, has a log-normal distribution. Mean, variance, and lognormal parameter values (y_0 and ω) are estimated from spread of crack growth data for tool steels, such as that shown in Fig 9.7 [Callister 2000]. Other quantities (Paris constant m, geometry factor α, flow stress exponent m^*, ram speed V, number of cavities n_1) have been treated as constants. Information about the distribution type, average values, standard deviations, etc of all the variables is listed in Table 9.1.

Usually only room temperature fracture toughness values of H13 tool steel are available for a few temper conditions [ASM 1996]. As discussed in the preceding chapter, recommended practice for optimum heat treatment of H13 steel being used for hot work dies is tempering to around 550°C (for a good combination of hardness and toughness). Average operating temperature in commercial aluminum extrusion is about 460°C. Using the linear prediction model (equation 8.9), based on hot hardness and hot *CVN* values, the value of K_{IC} for H13 steel for this temper condition and at this working temperature is

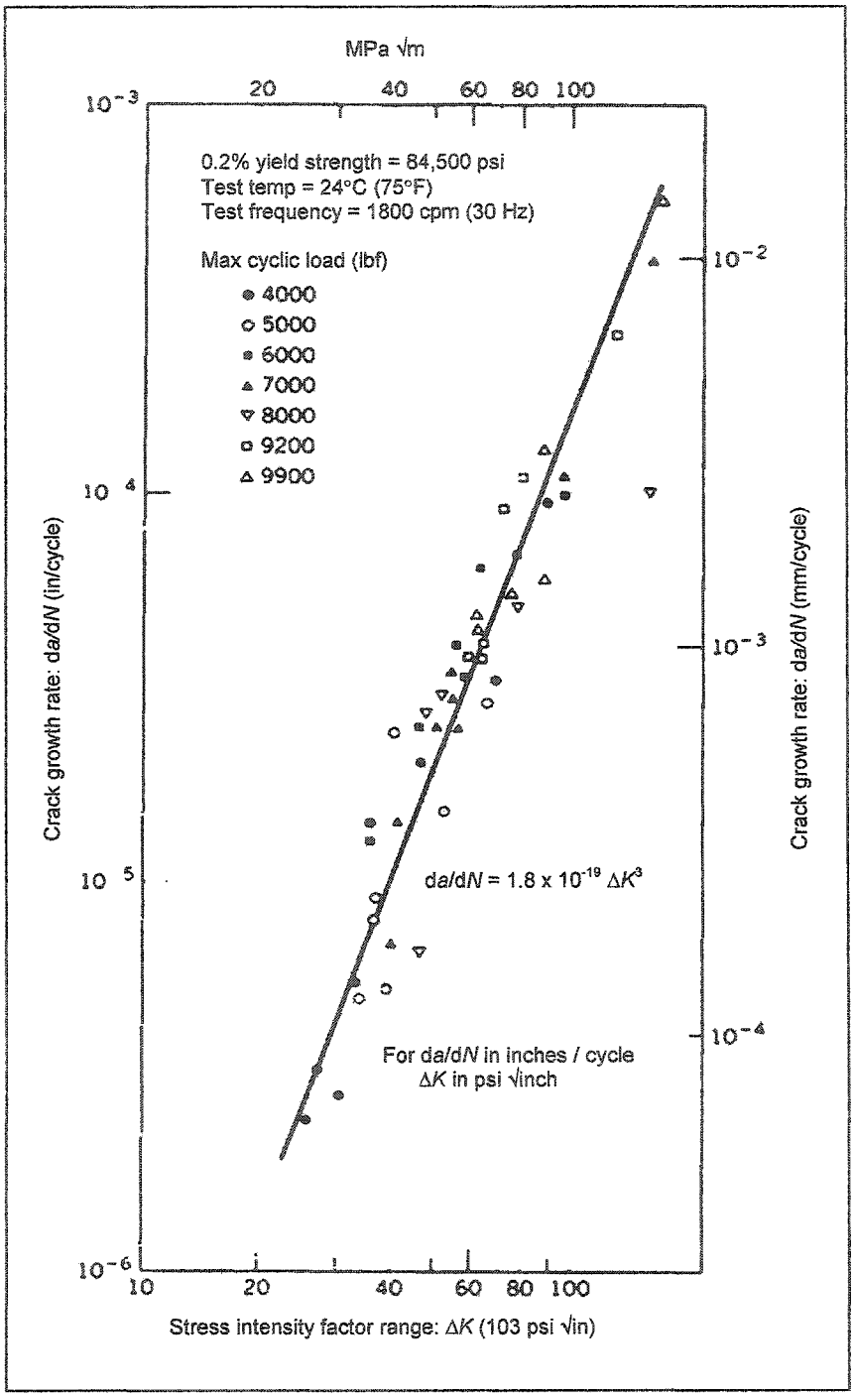

Figure 9.7 *da/dN* vs ΔK graph (log-log scale) for a Ni-Mo-V steel [Callister 2000]

Table 9.1 Variables involved, their distributions and values

Variable	Distribution	Mean Value	Std Deviation
Billet dia D_b	Normal	184 mm	0.5 mm
Billet length L	Normal	660 mm	4 mm
Die outer dia d_o	Normal	25.4 mm	0.1 mm
Die thickness t	Normal	1.6 mm	0.05 mm
Paris constant C	Lognormal	1.6×10^{-12}	5%
Paris exponent m	Constant	2.85	-
Fracture toughness K_{IC}	Normal	83.6 MP$\sqrt{}$m	5%
Ram speed V	Constant	5 mm/s	-
Initial crack size a_0	Normal	0.01 mm	10%
Geometry factor α	Constant	1.12	-
Number of cavities n_1	Constant	4	-

83.6 MPa$\sqrt{m}$. The quadratic models (equations 8.11 and 8.12) give a higher correlation coefficient, but the linear model gives more conservative predictions.

9.2.6 Monte Carlo Simulation — Fatigue

This simulation strategy is based on generating a large set (10,000 in our case) of independent random numbers Z_i, having a standard normal distribution (mean $\mu = 0$ and standard deviation $\sigma = 1.0$). These random numbers are then transformed into the required statistical distributions through appropriate transformations. For variables that are normally distributed (such as D_b, d_o, t, etc), we have

$$X_i = \mu_i + \sigma_i Z_i, \tag{9.18}$$

where μ is the mean and σ is the standard deviation of the variable based on actual data, as listed in Table 9.1. For variables having a log-normal distribution (such as the Paris constant C), the transformation is

$$X_i = \exp(\mu_l + \sigma_l Z_i), \tag{9.19}$$

where μ_l and σ_l are the mean and standard deviations of the log-normal data set. For a data set having a Weibull distribution (fracture toughness K_{IC}), random numbers U_i are generated using a uniform distribution (between the limits of zero and one) and the transformation used is

$$X_i = \theta [\ln (1/U_i)]^{1/m}, \tag{9.20}$$

m and θ being the shape and scale parameters of the Weibull data.

Once all the basic variables are randomly generated in this manner, the derived variables (such as a_c, σ_{max}, p, ε. etc) are calculated for all the 10,000 instances. Cycles (number of billets) to failure due to fatigue fracture are then calculated for each set of simulated variables using equation (9.6). Compared to an actual *MTTF* of 722 billets, the simulated average die life (due to fracture failure) comes out to be 759 cycles.

9.2.7 Die Life Distribution — Fatigue

After obtaining the simulated predictions for die failure by fracture, curve fitting is done (as described in chapter-6) to obtain standard probability distributions used in reliability studies (normal, lognormal, Weibull, and minimum extreme value). Weibull distribution,

shown in Fig 9.8, gives the best overall *goodness of fit* (correlation coefficient of r^2 = 97.8%), although lognormal or even normal model cannot be ignored completely. As evidenced by the graph, the Weibull line provides a good fit not only for the simulated data but also for the actual die life data. Shape parameter for the Weibull line, representing the scatter in die life, came out to be $m = 4.3$. Value of the scale parameter θ, an indicator of the average die life (*MTTF*), was 837 billets. Average die life (found to be 759 kg) is linked with the scale parameter and the scatter parameter by the equation

$$MTTF = \theta\, \Gamma\, (1 + 1/m), \tag{9.21}$$

where $\Gamma(\,)$ is the gamma function.

9.3 Wear Failure

The second most significant failure mode in extrusion dies, as established in chapter-5, is gradual *wear* of the die bearing surface. Mechanism for wear type failures was discussed in section 5.6.2, and shown in Figure 5.6. A combination of factors such intricate profile geometries, high pressures and temperatures, very hard die material, and extremely hard and abrasive surface layer of Al_2O_3 formed on the billet surface during preheating, lead to wear at the die land.

Saha [1998, 2000] studied the effect of extrusion speed and billet length on wear at the die (cap) and the mandrel shown in Fig 9.9. A thin walled square tube of Al-6063 was extruded through heat treated and nitrided H13 steel die. Average billet temperature was 460°C. Higher extrusion speeds are expected to increase wear due to abrasion. Longer billet lengths generate larger friction surfaces, the increased friction promoting wear. Effect of ram speed and billet length on wear at die land was therefore studied. Wear depth from these experiments [Saha 2000] have been replotted in Fig 9.10. The plots show that wear progresses almost linearly as more billets are extruded. A simple die wear model would thus be

$$W = mt + c, \tag{9.22}$$

where W is the wear depth in microns (μm), t is number of extrusion cycles (billets extruded), and m and c are the slope and intercept of the straight line representing the

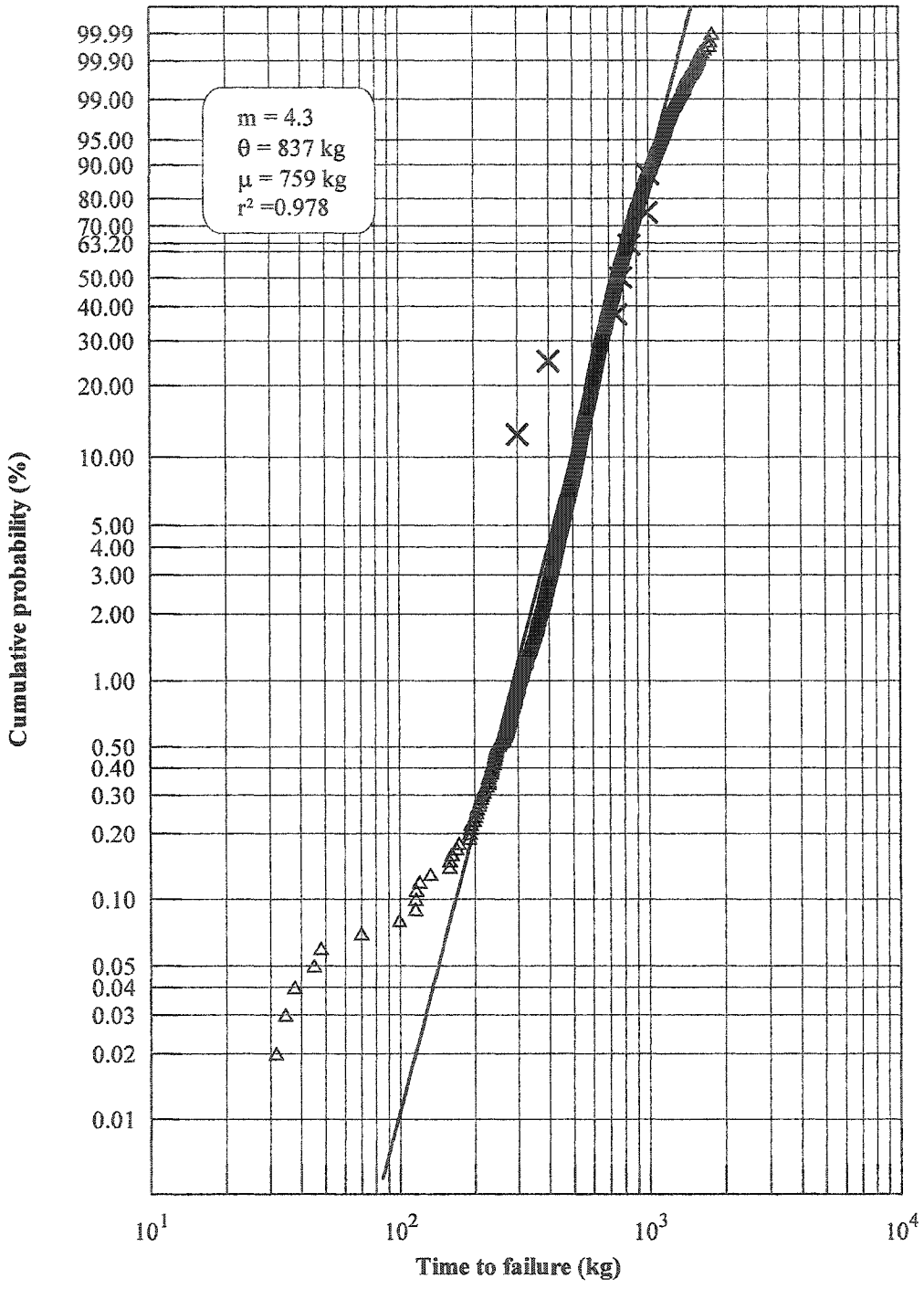

Figure 9.8 Plot showing simulated fracture life data and the fitted Weibull line

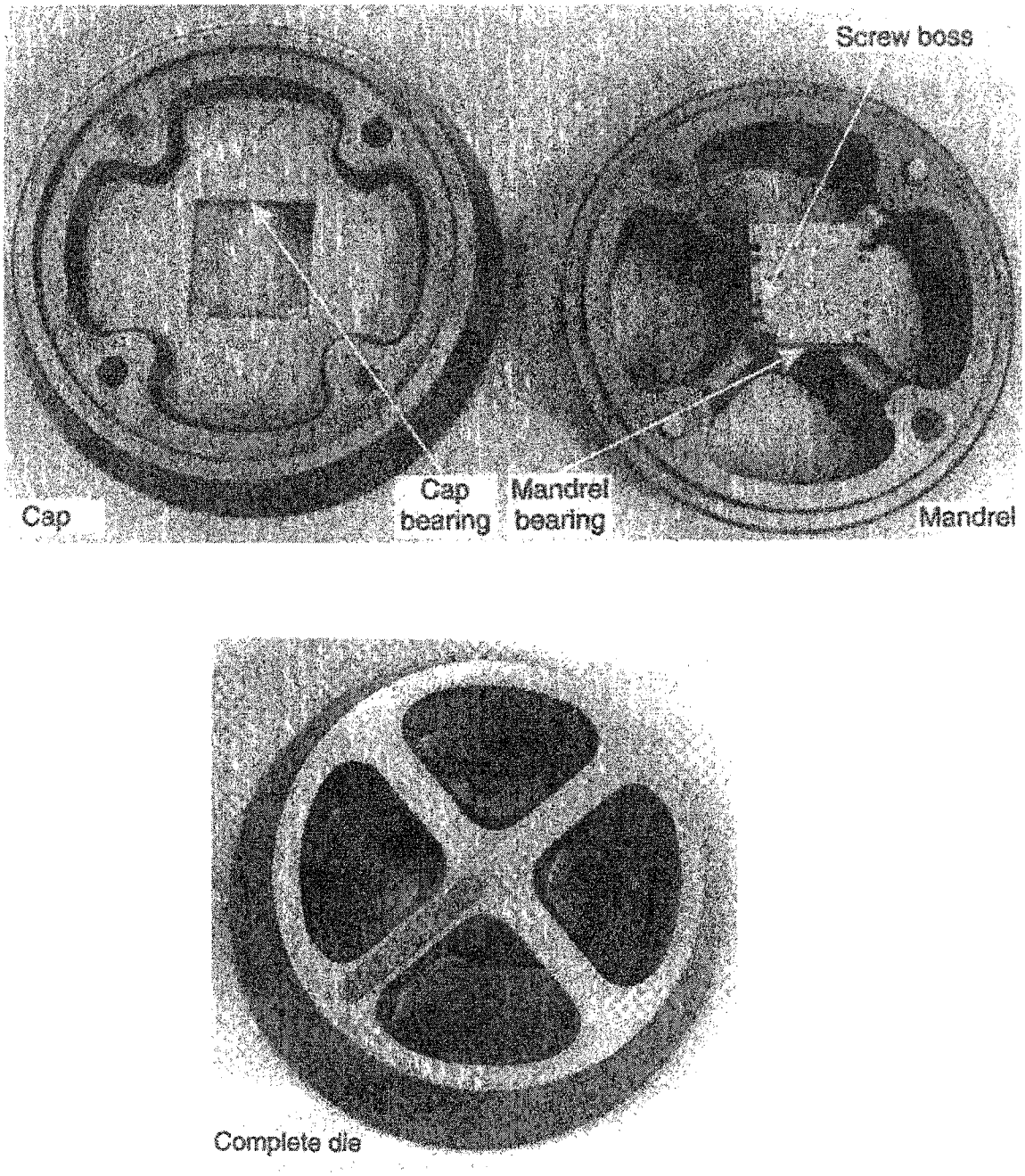

Figure 9.9 Bearing surface on the die (cap) and mandrel, and the assembled die set used for wear experiments in hot aluminum extrusion [Saha 2000]

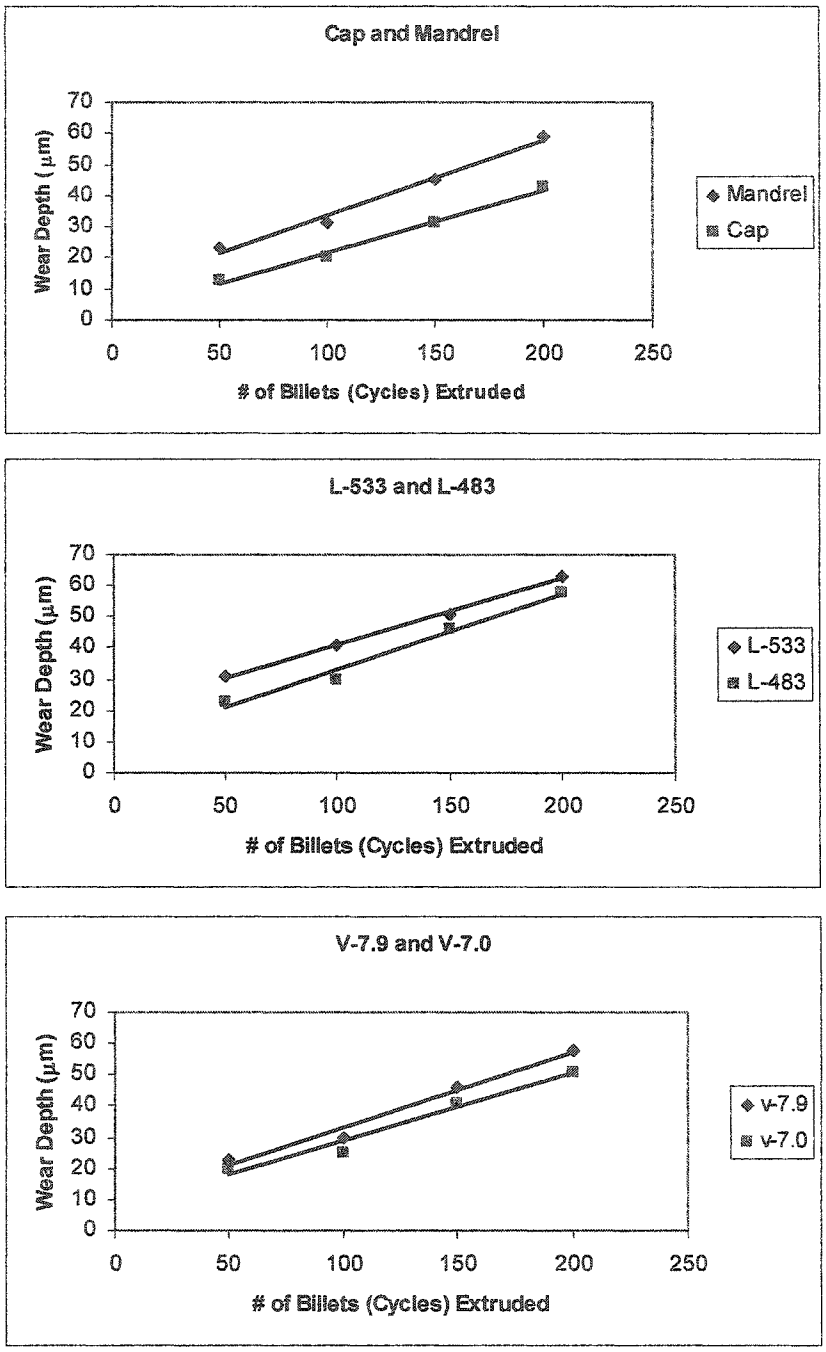

Figure 9.10 Increasing wear depth at mandrel and cap of a hollow die for varying billet length and ram speed (billet temperature is 460°C); variation suggests linear behavior; data source Saha [2000]

progressive wear behavior. As a new die is perfectly smooth, with no wear at the bearing surface, we have $W = 0$ at $t = 0$. The intercept would thus be zero. The model would then simplify to

$$W_f = mt_f. \tag{9.23}$$

W_f signifies the limiting amount of wear leading to die failure, and t_f is the number of billets extruded before reaching W_f.

9.3.1 Parameter Determination

Actual die failure data (due to wear at the die land) has been collected from ALUPCO for the box profile shown in Fig 9.6. Wear failures include the categories bearing washout, oversize, overweight, and dimension change, as described in chapter-5. The average die life (*MTTF*) was 508 extrusion cycles (number of billets extruded).

Die failure data (number of billets extruded before die was rejected due to excessive wear) are given in Table 9.2. Based on the tolerance for the minimum wall thickness, it was determined that a failure wear of $W_f = 75$ μm on the bearing surface of the die or the mandrel would lead to rejection. This means that each time a die failure occurred, wear had reached this limiting value. Slope (m) of the wear line was evaluated for each die rejection from the cycles (billets) to failure and limiting wear data. Mean and standard deviation values of this parameter (m) came out to be 0.169 mm and 0.035.

9.3.2 Monte Carlo Simulation — Wear

Monte Carlo simulation based on the wear model developed above was carried out for the same hollow die (simple tube) whose fracture simulation was presented above. It was assumed that the distribution (mean and standard deviation) of the slope m characterizing wear behavior remains the same for all H13 steel dies used in hot aluminum extrusion. 10,000 standard normal random numbers were generated as before, and were transformed to random values of the slope m, based on its μ and σ values determined above. A limiting wear value of 125 microns was used, determined from the tolerances shown in Fig 9.5. Wear life of the die was then evaluated for each simulated instance of m, using equation (9.23). Compared to an actual *MTTF* value of 722 billets, the simulated average life

Table 9.2 Various instances of number of billets to failure for the die studied; limiting wear was 75 microns for the die profile.

Failed Die	# of Billets	Surface Wear (μm)
1	392	75
2	642	75
3	598	75
4	713	75
5	576	75
6	335	75
7	340	75
8	548	75
9	480	75
10	725	75
11	559	75
12	611	75
13	295	75
14	341	75
15	525	75
16	402	75
17	356	75
18	282	75
19	227	75
20	658	75
21	1050	75

(based on wear failures only) came out to be 767 cycles. We know from the actual failure history of this die that wear was not a dominant failure mode. This fact is confirmed by the 3-parameter Weibull fit to the simulated data (Fig 9.11), yielding a relatively low correlation coefficient of 95.6% (as against $r^2 = 97.8\%$ for fracture failure). The Weibull parameters are $m = 2.89$, $\theta = 809$ kg, and $t_0 = 400$ kg.

9.4 Combined Fracture and Wear

As explained in section 5.8 earlier, various failure mechanisms are operating simultaneously on the die during its operative life. Fracture and wear are thus competing against each other. Final die failure takes place either when a preexisting crack (a_o) reaches the critical crack size (a_c), or wear on the die land reaches the limiting value (W_f). It is assumed here that the new failure modes progress independently of each other, until one of them becomes dominant and takes over. However, in reality, the failure modes may be inter-dependent in a rather complicated manner.

The number of cycles to failure under the competing fracture-wear mode was determined from the relation

$$t = \min (t_F, t_W), \tag{9.24}$$

where t_F is the simulated fracture life, t_W is the wear life, and t is the final predicted life, representing the failure (fracture or wear) that occurs earlier. The *MTTF* of this simulated fracture-wear die life was 717 billets. In comparison with the actual average life of 722 billets, this is a very close prediction.

Weibull distribution was once again found to be the best fitted to the simulated die life data, with a coefficient of correlation value of $r^2 = 98.5\%$, as shown in Fig 9.12. This combined fracture-wear model is obviously the best representation of die failure, yielding a shape parameter $m = 4.99$ and a scale parameter $\theta = 786$ kg.

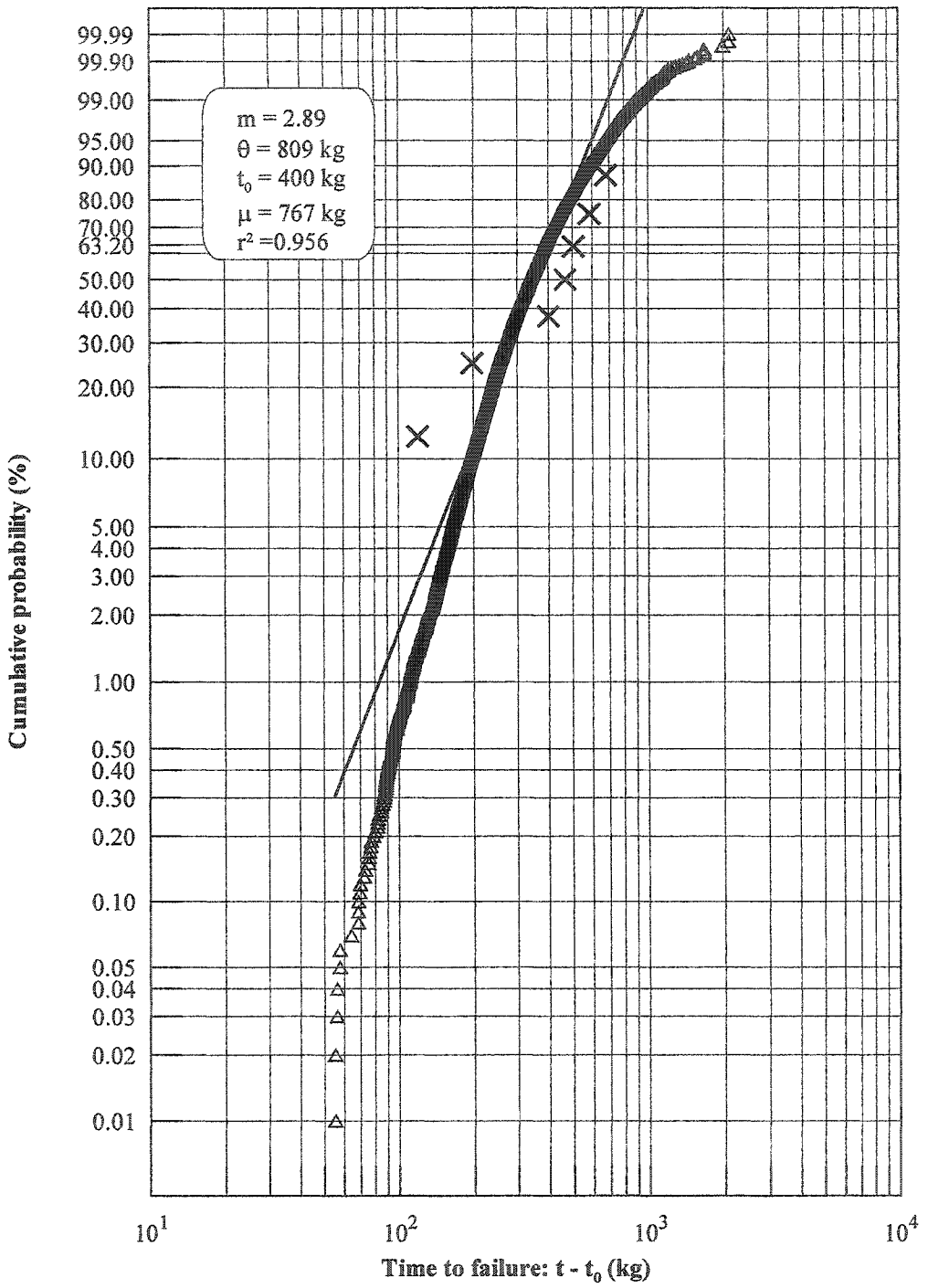

Figure 9.11 Plot showing simulated wear life data and the fitted 3-parameter Weibull line

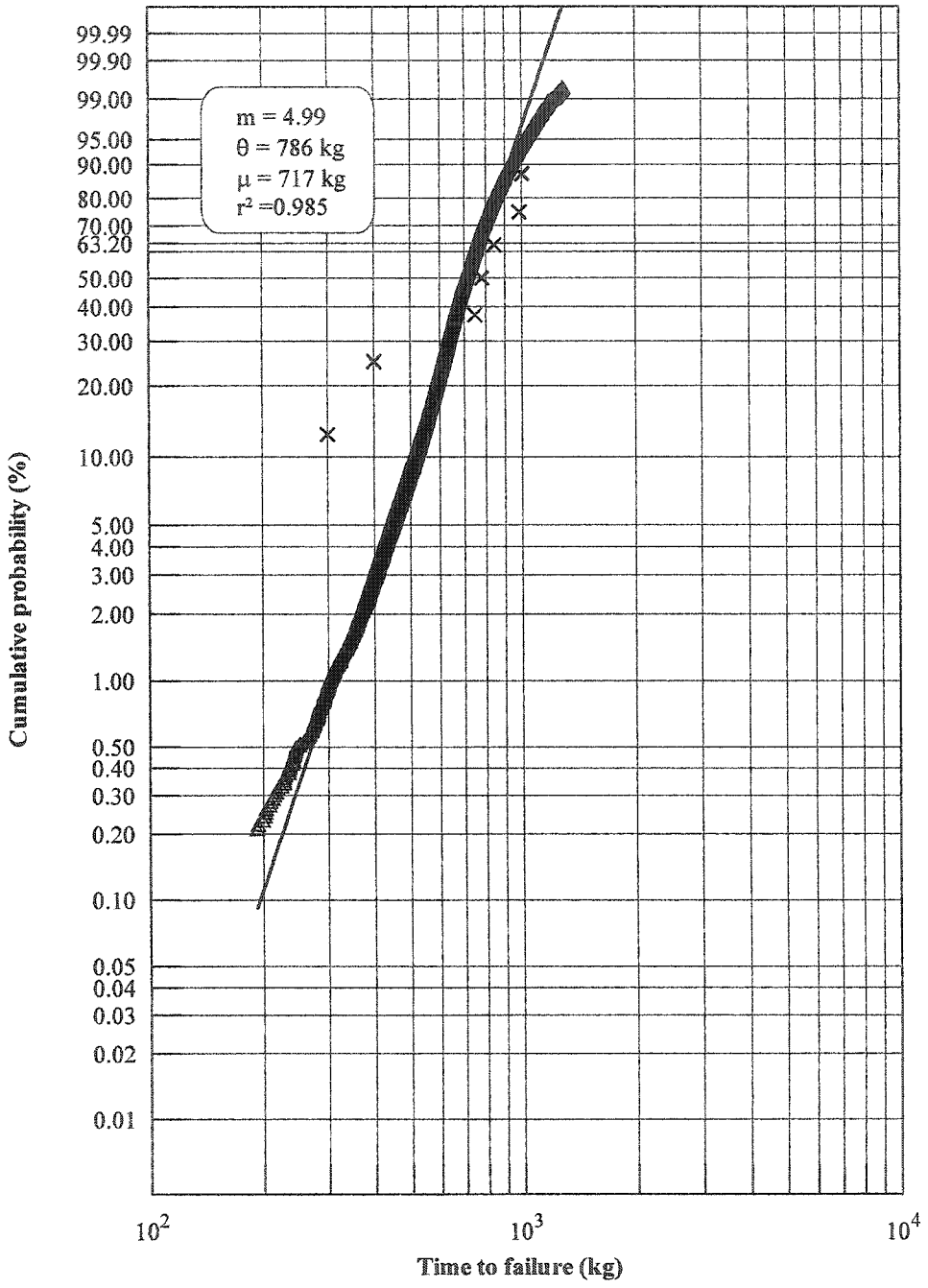

Figure 9.12 Plot showing simulated combined life data (fracture-wear competing mode)

9.5 REMARKS

A simulation is as good as the underlying model. One of the simplifications we have made in this study is to use the model of an edge crack in a flat plate whereas the actual die is a hollow cylinder. K_{IC}-CVN correlations need more experimental work and refinement. Paris equation parameters C and m need more precise estimation, especially for H13 tool steel. With these refinements, the model can be used for accurate simulation of failures of dies of simple geometry. The simulation strategy outlined here (simple shapes) could then be used to forecast failures of more complex dies by employing the complexity-pressure models developed earlier by the authors. A relatively sound replacement strategy for dies and related tooling can thus be formulated.

CHAPTER 10
EXTRUSION PRODUCT DEFECTS: CLASSIFICATION, CAUSES AND REMEDIES

10.1 INTRODUCTION

As outlined in Fig 1.2, commercial hot extrusion of aluminum involves different operations, such as billet preheating and shearing, loading and deformation, stretching and roll correction, age hardening, painting and anodizing. Because of the high tool and equipment investment involved, it is vital to understand the relationship between the condition of the extrusion press and ancillary equipment and their performance measured in terms of productivity and recovery. This in turn necessitates an understanding of the contributing and controlling factors related to product defects in extrusion. General reasons leading to rejection of an extruded product have been described earlier in section 1.9.

10.1.1 Current Work

The work presented in this chapter covers description of various types of product defects in commercial aluminum extrusion, a look into the mechanical and metallurgical factors that cause these defects, and suggestions (wherever possible) for viable corrective and preventive measures. Some defects have been described that have not been covered in earlier works, exhibits of actual defects from the industry have been presented that are not available in published literature, a complete category-wise defect classification has been carried out that has not been attempted in any previous study, some preventive/remedial measures prevalent in the industry are elucidated that cannot be found in earlier studies.

Some researchers have attempted to analyze a few of the process defects encountered in extrusion. However, no exhaustive and systematic study has yet been reported in this area. That is why many defects do not have a unique name, different workers coining different terms for the same flaw from time to time. Also, very few references are available on properly categorizing extrusion related flaws. Moreover, only a handful of researchers have come up with appropriate preventive or corrective measures for these defects. Some of the salient features that differentiate the current work from hitherto published material are:

1. Exhaustive definition, together with visual exhibits in most of the cases, of all defects arising in aluminum extrusion.
2. Scientific and systematic classification of extrusion related defects into logical categories.
3. Probe into the causes (mechanical, metallurgical, equipment or process related) of all the defects.
4. Description of practical remedies and precautionary measures generally carried out in the industry.

Defects have been classified into the following broad categories:

(a) Metal flow related defects
(b) Surface defects
(c) Weld defects
(d) Metallurgical defects
(e) Temperature and speed related defects
(f) Equipment and tooling related defects
(g) Anodizing defects
(h) Painting defects.

Wherever a reference has not been cited, visual exhibits are photographs of actual defect samples collected over time from the industry.

10.2 Metal-Flow Related Defects

These extrusion defects are the result of nonuniformity and nonhomogeneity of metal flow in the container. Extrusion is usually carried out as a discontinuous process: billets can be loaded into the container only one at a time. A *nonsteady* state of flow is thus caused by temperature variations in the billet and the limited billet length, as well as by friction between the container and the billet, and between the dummy block and the billet. Various investigators using different experimental methods have detected a variety of metal flow patterns in extrusion. The two most dominant factors influencing extrusion flow pattern are billet-container-die *friction*, and billet *thermal gradients*. The four characteristic patterns in direct extrusion using a square die were described in section 1.4 and shown in Fig 1.8, classified according to the increasing order of nonuniformity of flow.

10.2.1 Funnel Formation

Movement of the peripheral zones of the billet close to the die and die holder surfaces, independent of the nonuniform flow in the container caused by friction, results in shearing. Material in the axis region flows more rapidly towards the die orifice than at the edge. A funnel-shaped hollow, as shown in Fig 10.1 (a), is thus formed in the rear portion of the billet [Pearson and Parkins 1961]. A funnel can also occur in indirect extrusion [Thomsen et al. 1954], because shearing at the die is not prevented; Fig 10.1 (b).

10.2.2 Pipe Formation

Also called ***extrusion defect***, ***fishtailing***, or ***back-end defect***, this is the most common flaw encountered during aluminum extrusion, especially in the 6xxx series alloys. An annular separation in the cross section (due to division into an inner core and an external zone) is formed in the rear third of the extrusion. Billet-container friction results in the billet surface layers remaining stationary at the container wall while the billet core is sheared past. The region of dead metal that exists in the center directs the flow forwards giving rise to a cone shaped defect [Sheppard 1999] as shown in Fig 10.2.

(a)

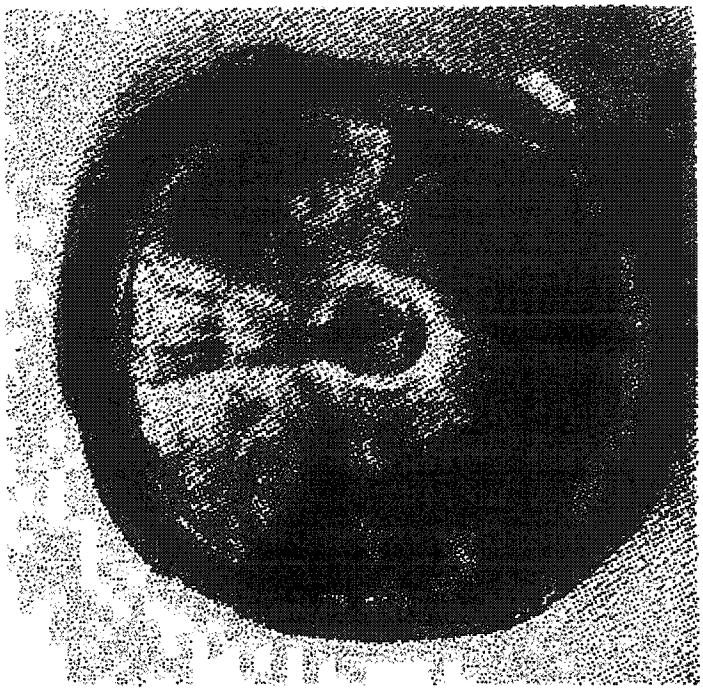

(b)

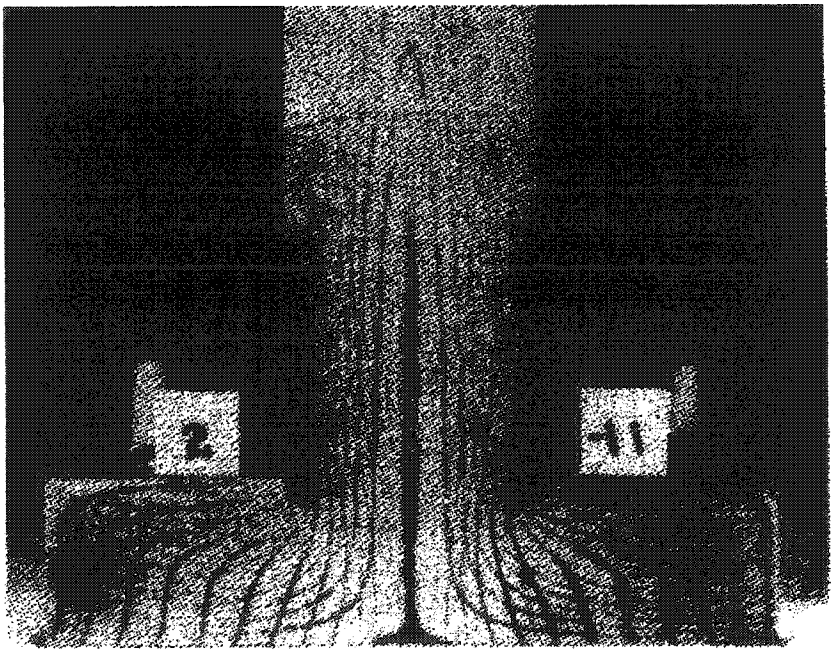

Figure 10.1 Funnel formation, as seen in the discard after extrusion of a solid rod (a), and in indirect extrusion (b) [Laue & Stenger 1981]

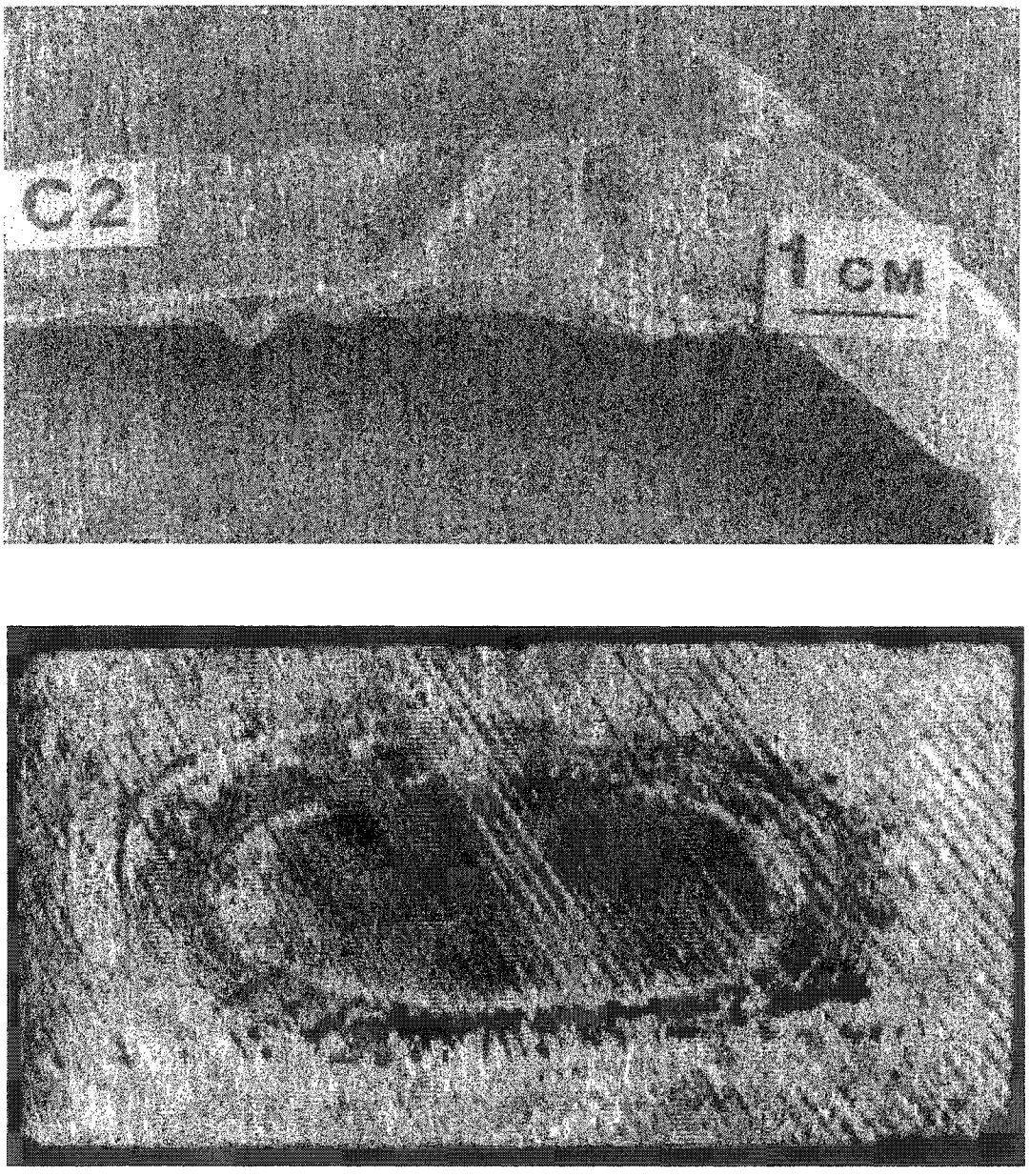

Figure 10.2 Pipe or extrusion defect, also known as back-end condition [Sheppard 1999, Aluminum Association 1993]

10.2.3 Internal Cracking

The center of an extruded product can develop cracks, variously known as **centerburst**, **center cracking**, **arrowhead fracture**, or **chevron cracking** [Kalpakjian 2003], as shown in Fig 10.3. These cracks are attributed to a state of *hydrostatic tensile stress* (also called *secondary tensile stress*) at the centerline of the deformation zone in the die. The situation is similar to the necked region in a uniaxial tensile test specimen.

Experimental results indicate that, for the same reduction, as the *die angle* becomes larger, the deformation across the product becomes more inhomogeneous. Another factor is the *die contact length*; the smaller the die angle, the longer the contact. Size and depth of the deformation zone increases with increasing contact length. Yet another parameter is the *aspect ratio* (*h/L*); the higher this ratio, the more inhomogeneous the deformation. Thus the center of the billet is not in a fully plastic state (it is rigid) since the plastic deformation zones under the die contact lengths do not reach each other. This defect is primarily observed in cold extrusion of small products (Fig 10.3).

10.2.4 Internal Defects in Hollow Extrusions

During extrusion of hollow shapes, friction between the mandrel and the internal billet surface can give rise to a significant distortion of the material flow at the internal surface. Alloys that tend to weld to steel during hot working (including pure aluminum and some aluminum alloys) deform in a manner similar to type *C* flow (Fig 1.8): shear zones occur below the internal surface of the billet, and material separation can occur in extreme cases. The result is a blotchy, torn internal surface, and material welded to the mandrel is difficult to remove.

10.2.5 Scale and Blister Formation

When lubricant traces are present in unlubricated extrusion (through some shear blade lubricant sticking to the billet, for instance), or lubrication breaks down in lubricated extrusion, a partial dead metal zone is formed. Lubricant trapped at the boundary of the dead metal zone extrudes into the product to form **subsurface defects**. Upon subsequent heating, escaping gases cause blistering at these locations. These defects, close to the

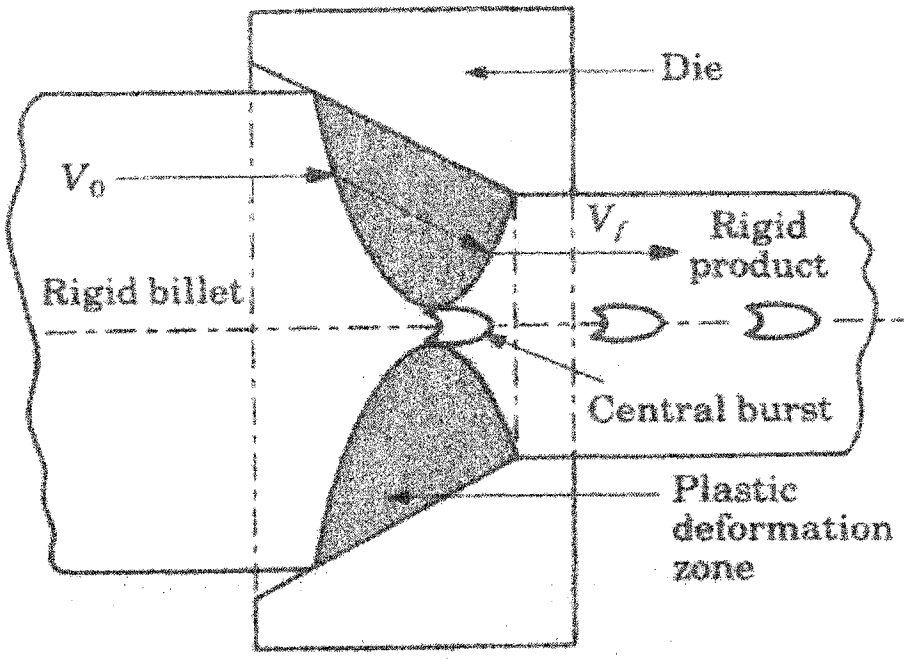

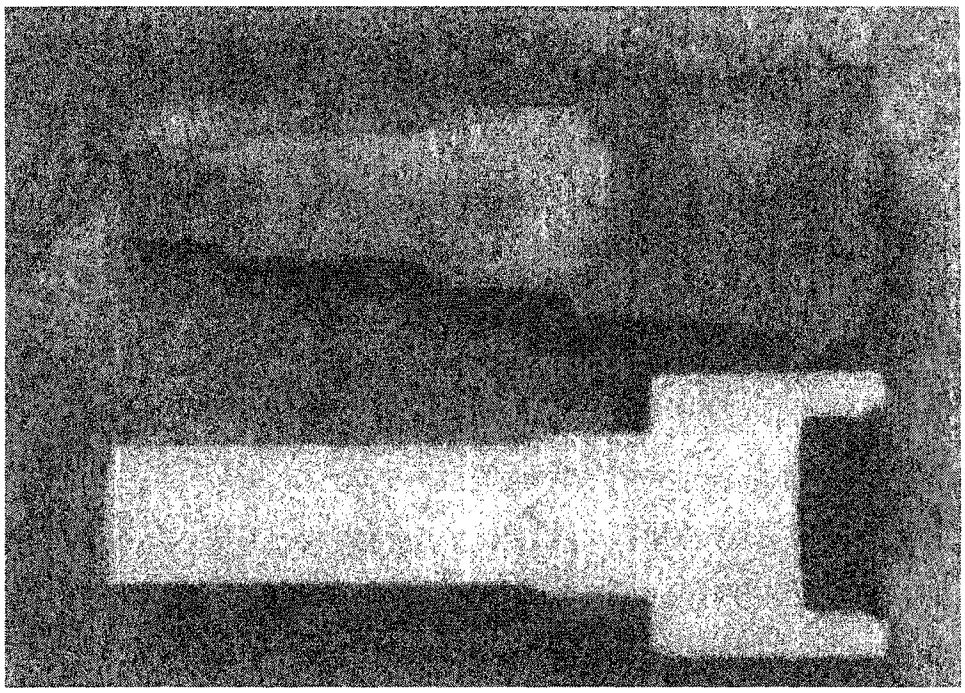

Figure 10.3 Centerburst defect, also called center cracking, arrowhead fracture, or chevron cracking [Kalpakjian 2003]

extrusion surface, result from the formation of **scales** or **blisters** and can develop in flow patterns of type *A* or *B* (Fig 1.8). Sometimes blisters do not appear immediately after extrusion but become noticeable during subsequent heat treatment. A **blow hole** is a blister that has ruptured and may produce a viod.

Blisters and blow holes, shown in Fig 10.4, can occur virtually at any position along the extruded length. **Front end blistering** is probably the most common form of this type of defect and can necessitate a scrap allowance being taken. Its cause is mainly due to *air entrapment* during loading and upsetting the billet. This can be exaggerated by factors such as a rough sheared surface on the back of the die or the shear, or a billet end that is not perfectly flat, pulling metal out of the welding chamber.

10.3 Surface Defects

Various defects mar the surface appearance of extrusion, including die lines, scoring, pick-up, and tearing. Pick-up and die lines are the most serious surface defects observed in common aluminum alloys such as 6063. Present evidence suggests that during extrusion a thin film of extrudate material adheres to the die land surface, and it is this interaction that results in the formation of these defects. The exact mechanism of this adhesion has not been formulated [Sheppard 1999].

10.3.1 Pick-Up Defect

This defect is observed as intermittent **score lines** of varying lengths between 3 mm and 12 mm and often terminates in a fleck of aluminum debris referred to as *pick-up* deposit; Fig 10.5. The problem is usually thought to be enhanced by inclusions in the cast billet, inadequate homogenization treatment [Langerweger 1982] and die deflection. The defect is also temperature sensitive.

10.3.2 Die Lines

The Aluminum Association defines **die lines** as "longitudinal depressions or protrusions formed on the surface of the drawn or extruded material due to imperfections on the die

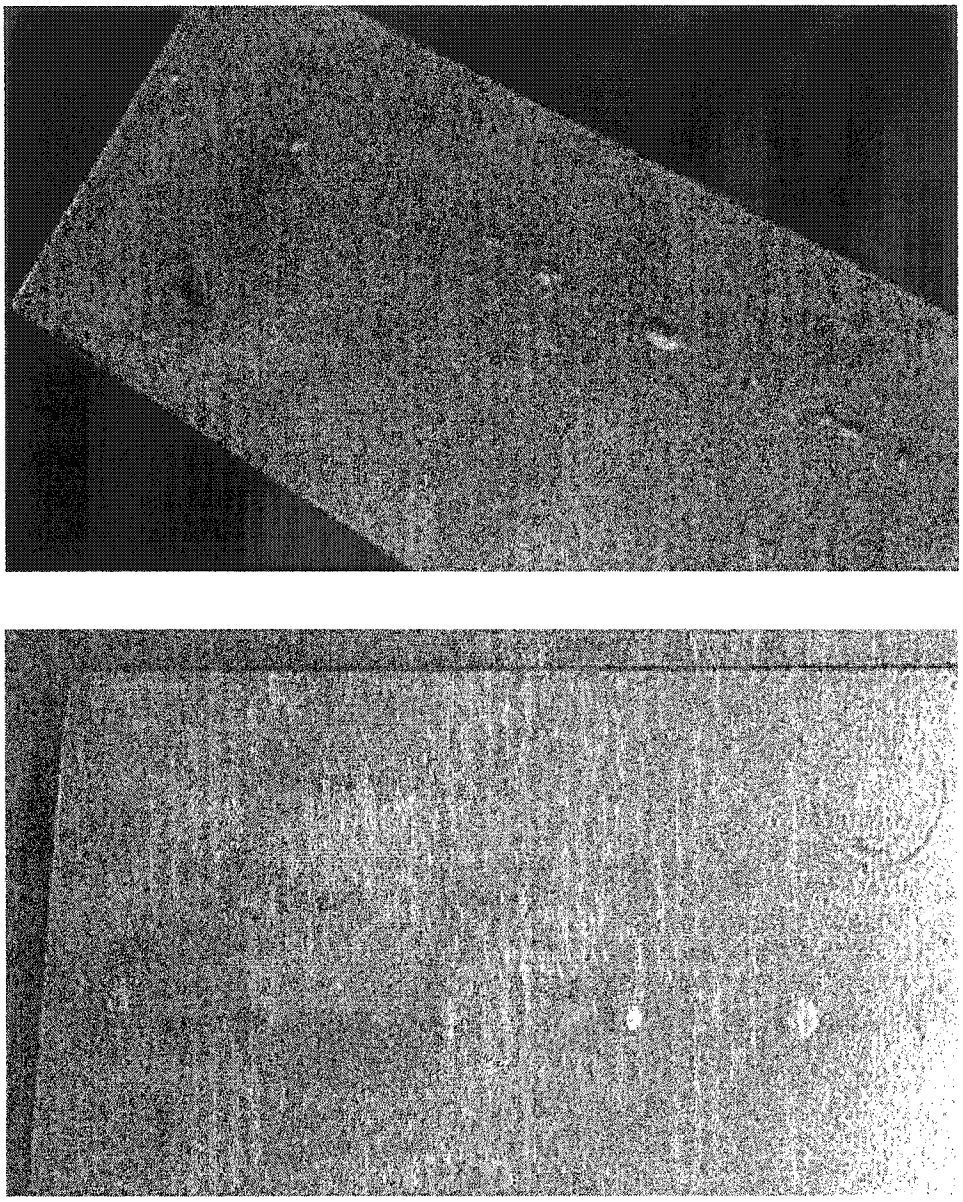

Figure 10.4 Blisters (above) and blow holes (below) are raised areas on the surface of an extruded product caused by subsurface gas expansion [ALUPCO].

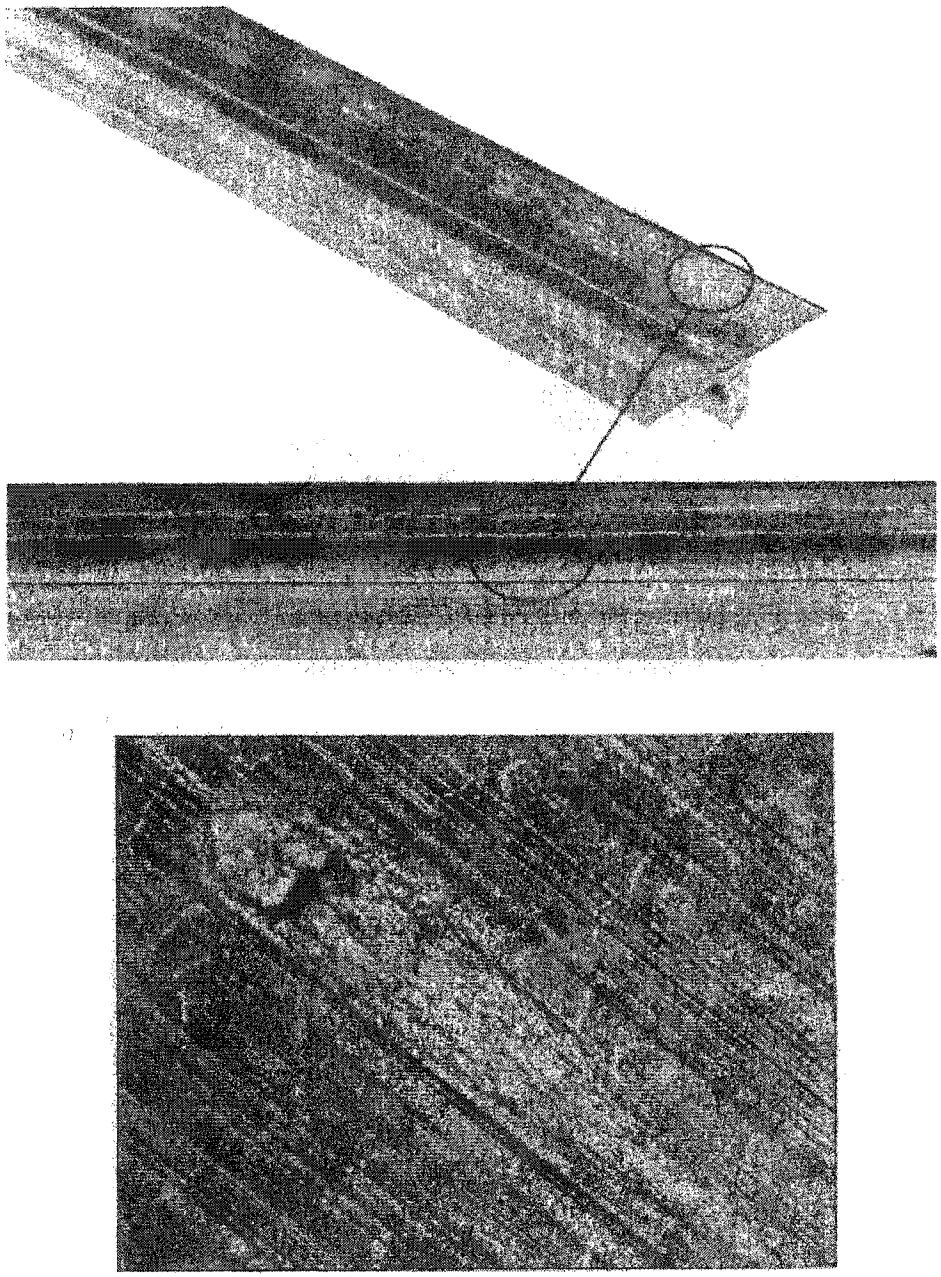

Figure 10.5 Pick-up is the name given to the surface defect caused by metal and oxide particles adhering to the surface of the product at different intervals [Aluminum Association 1993].

surface". Die lines, shown in Fig 10.6, are also believed to be caused by the interaction of the die land area, although this must involve a different area of the die land to that causing pick-up.

9.3.3 Micro Die Lines

Even with an optimum die land length and extrusion temperature, together with highly polished die lands, die lines are still observed to occur. These die lines are finer and shallower and are termed *micro die lines*. These may be a particular inconvenience when the extrudate is to be anodized following extrusion.

10.4 Weld Defects

It is now common practice to extrude billet on billet using a welding chamber or feeder ring to hold the back of the previous billet in the die and provide a surface for the next billet to weld on to. This can lead to defects known as *weld defects*.

10.4.1 Transverse Weld

If the mating surfaces of the billets were perfectly clean, there would be no weld problem. In practice, the billet ends are always oxidized, and the sheared face is often contaminated by stray lubricant and oxidized metal from the shear blade. As a result, the **billet-to-billet weld** or **transverse weld** is usually defective and represents a discontinuity in the extruded product; Fig 10.7.

10.4.2 Longitudinal Weld

Whereas in a solid section the transverse weld merges into the section surface, in a hollow it also merges into the **longitudinal weld** line. The presence of transverse weld and its associated contamination in close proximity to the seam weld constitutes a line of weakness. Thus *longitudinal weld* defects take the form of either low weld strengths or streaking on anodizing. Weld lines can also be formed in hollow sections due to insufficient temperature causing inadequate metal flow in the mandrel, resulting in poor coalescing in the welding chamber.

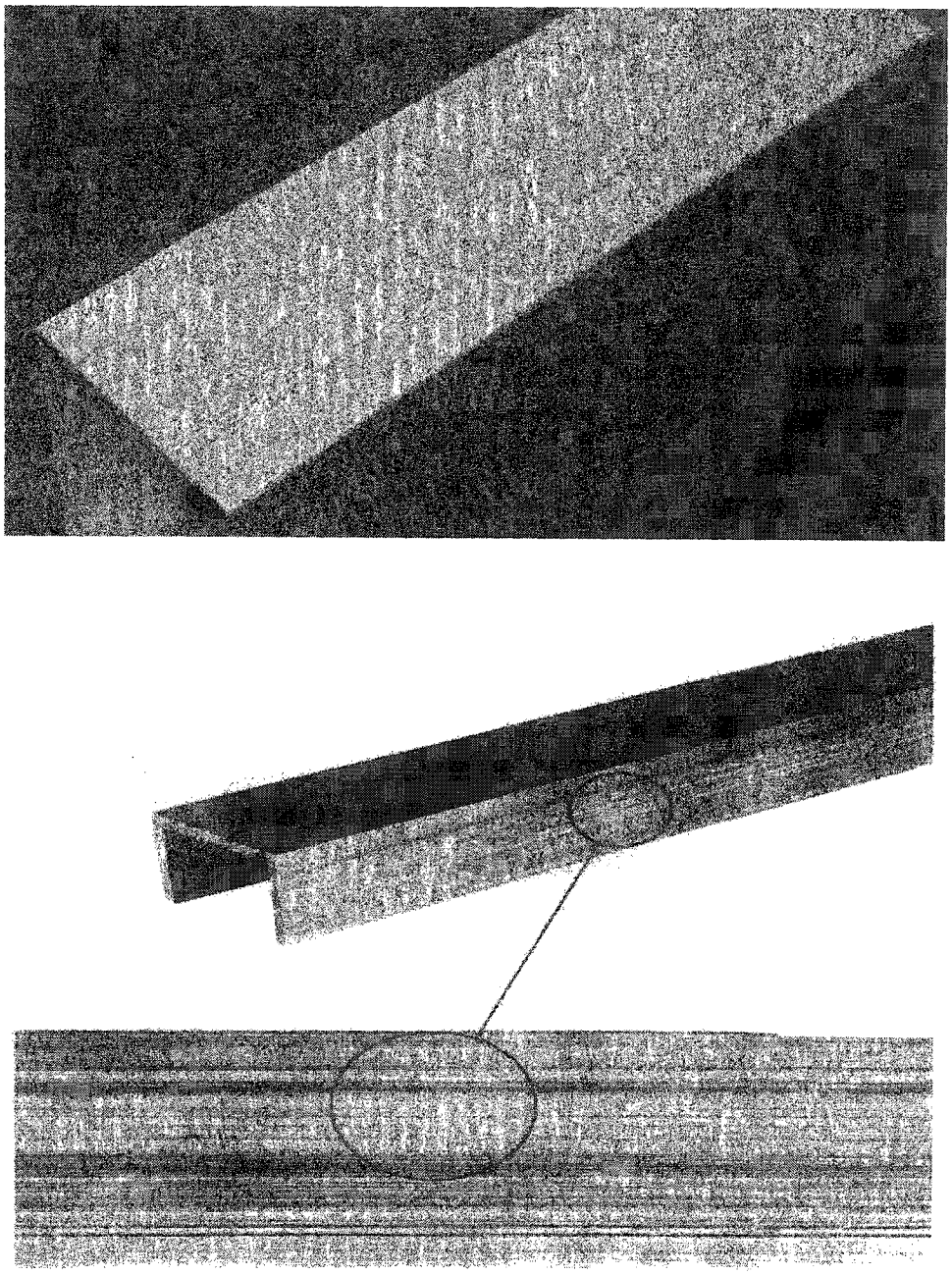

Figure 10.6 A die line is a longitudinal indentation or protuberance formed on the extruded surface, and is caused by a roughening of the die bearing known as bearing washout [ALUPCO, Aluminum Association 1993]

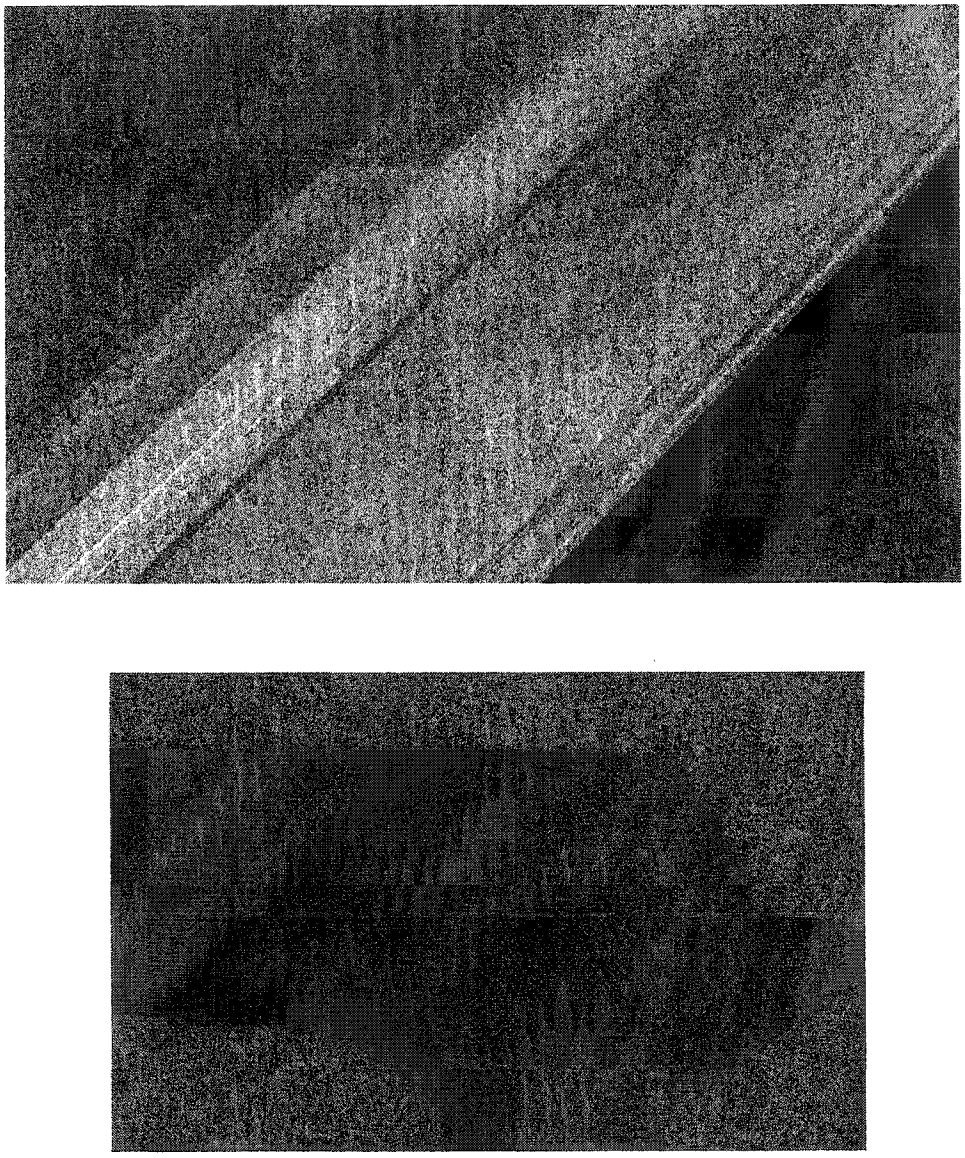

Figure 10.7 A weld line may be due to an imperfect billet-to-billet joint (above) [ALUPCO], or due to a transverse weld (below) [Sheppard 1999].

10.5 METALLURGICAL DEFECTS

Most of the metallurgical defects in aluminum extrusion can be divided into three major categories.

10.5.1 Streaking

These defects on the surfaces of anodized extrusions consist of bands or lines appearing darker or lighter, brighter or duller, in color and tone than the remainder of the surface. The basic cause of this streaking is a difference in microstructure between the streaked portion of the extrudate surface and the remainder, which leads to a difference in response in etching and anodizing [Cote et al. 1969]. *Ingot structure streaking* originates in the structure of the ingot or billet, and is a result of surface segregation or a shell zone present in the ingot. *Die design streaks*, also known as *pressure streaks*, occur due to large changes in wall thickness as a result of uneven cooling. The two streaking defects are shown in Fig 10.8 (top, middle).

10.5.2 Non-Uniform Appearance

These defects originate from occasional irregularities of the etching, anodizing and/or coloring process. Two subcategories are more important.

(a) **Hot spots** characteristically appear as dark (gray or black) rough patches, at regular or random intervals along the extruded length; Fig 10.8 (bottom). Not visible on the as-extruded surface, they appear readily after caustic etching as a heavy black smut. Completely removed by nitric acid de-smut, it sometimes reappears on anodizing in paler shades. Originating due to localized coarse precipitation resulting from different cooling rates of adjacent parts of the section, this can happen when a section has been in localized contact with a carbon support block on the run-out table and is momentarily cooled very rapidly in this localized region before being reheated from the adjacent mass.

(b) **Spangle** appears as a pronounced *grainy surface*. The cause of this defect is a preferential grain attack, visually emphasized by a *stepwise* appearance of

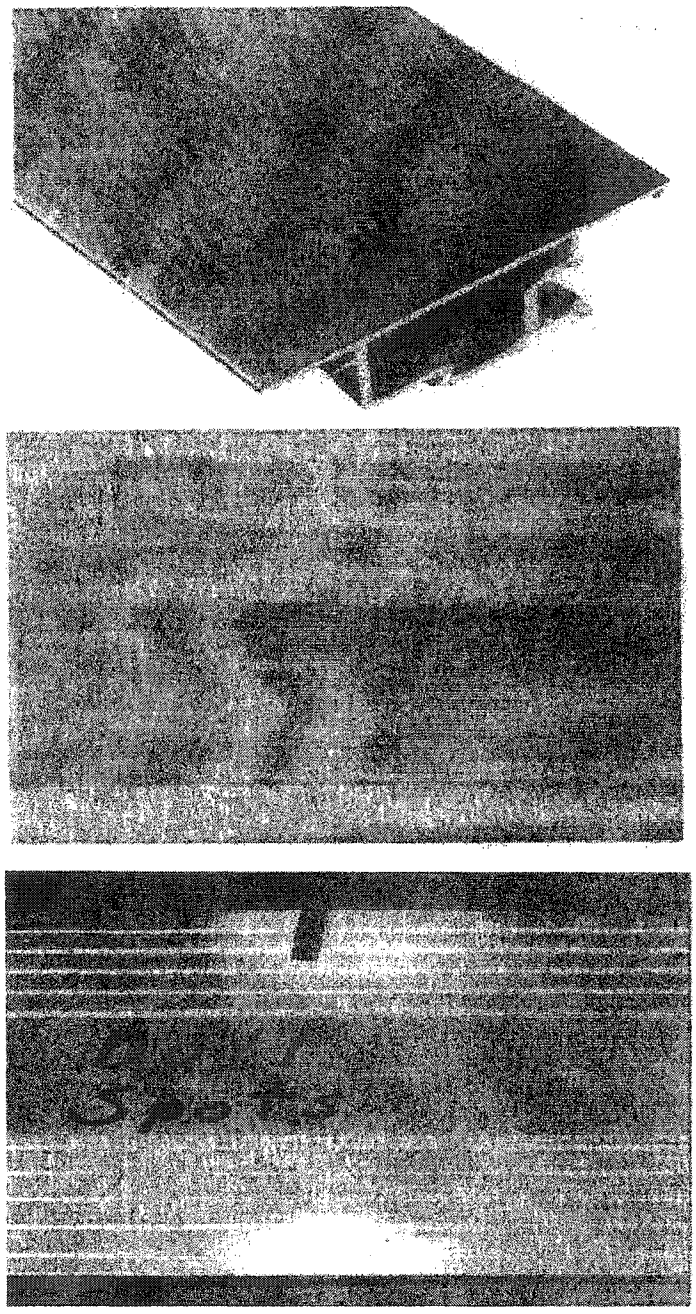

Figure 10.8 Surface appearance due to die design or bearing streaking (top), ingot or billet structure streaking (middle), and hot spots (bottom) [Aluminum Association 1993]

adjacent grains owing to the dependence of the rate of attack on the orientation of the crystallographic planes of individual grains. It is enhanced by the presence of zinc, either as an impurity in the alloy (particularly if from a remelt source), or dissolved in the caustic etch solution. It can also be intensified by higher etch temperatures.

10.5.3 Silicon Marks

These are black burn marks formed on the section surface during extrusion due to inclusions of very hard particles such as Si or Mg in the billet material, creating very high local friction and temperatures.

10.6 Defects Related to Temperature and Speed

The onset of mill finish (no subsequent surface treatment) surface defects is related to the temperature rise generated at the surface of the product as it is deformed. The level of temperature rise increases rapidly with exit speed due to the greater rate of work input and reduced heat loss to tooling. At a high enough exit speed local melting might occur. This condition gives rise to the classic **hot shortness** or **U-shaped cracking** defect.

Surface cracking occurs by local tensile failure at areas of melting due to the tensile stress state present at the edge of the die bearing. If the exit temperature or speed is too high, **tearing** initially starts at the edges of the extrusion and then develops over the remainder of the surface, giving rise to what is commonly called **fir-tree cracking** or **speed cracking** (circumferential surface cracks), as shown in Fig 10.9.

10.7 Equipment and Tooling Related Defects

The billet preheat ovens, billet shearing and transfer stations, die preheat ovens, extrusion press and die set, extrudate conveyors, and the post-extrusion correction stations, can all contribute to defects that can lead to rejection. Some of these equipment and tooling generated defects are briefly described below.

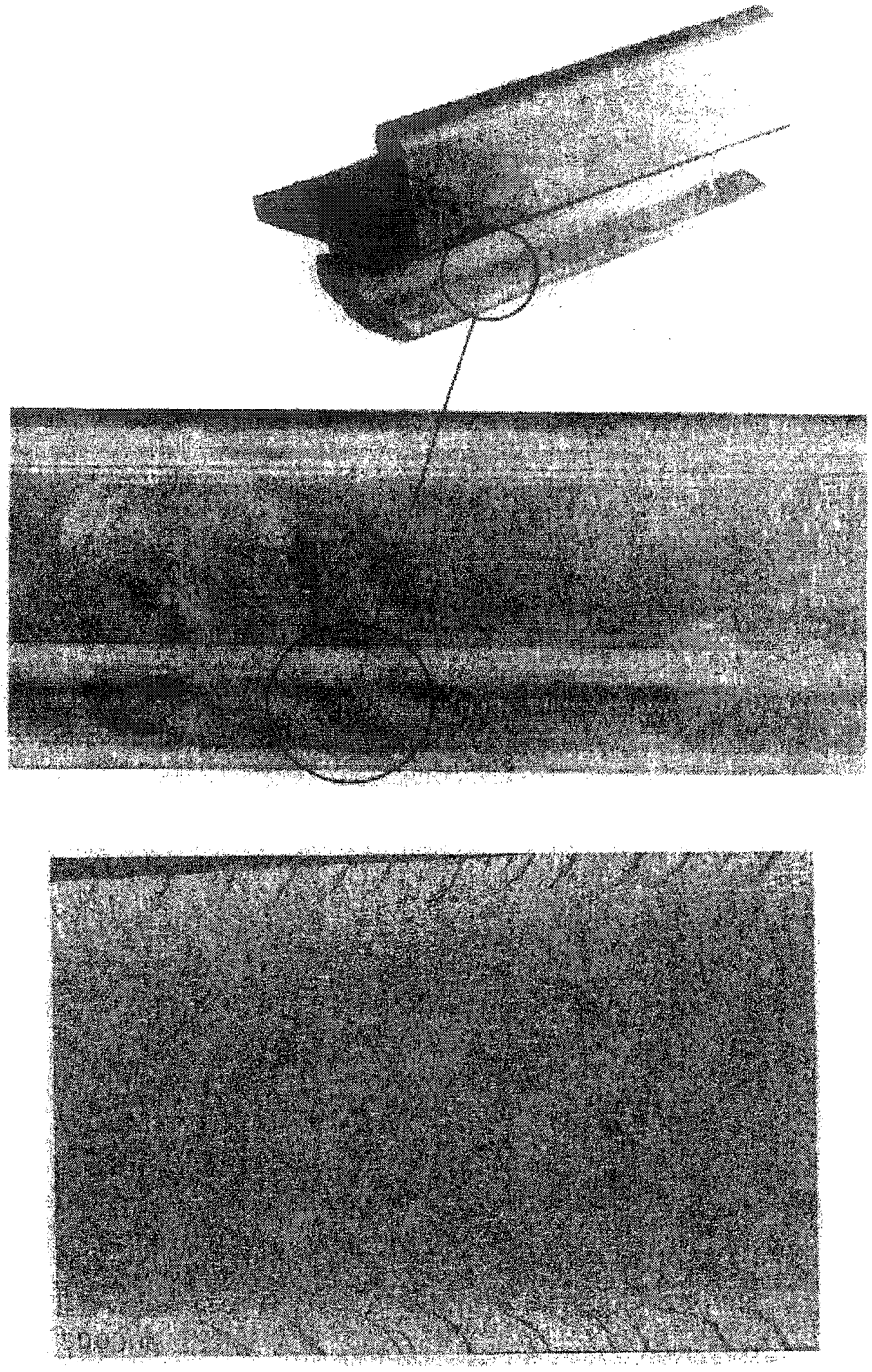

Figure 10.9 Cracking or speed tearing is a series of surface cracks perpendicular to the extrusion direction, normally occurring in corner radii or extremities, and is caused by localized high temperature [Aluminum Association 1993, Sheppard 1999].

10.7.1 Black Lines

These are burnt surfaces on the extrudate due to a local high pressure in the extrusion press; Fig 10.10. This can happen in the welding chamber for hollow dies, or at any aberration in a solid die that results in a localized high pressure. The defect generally becomes visible after etching.

10.7.2 White Lines

Nonuniform heating in any of the billet preheat ovens (due to local malfunction, deposits, etc) can cause localized high temperatures. The resulting alloy segregation may cause streaks of pure (whitish) aluminum in certain locations, appearing as *white lines* after extrusion.

10.7.3 Runout Marks

Also called **graphite lines**, these defects appear on the extruded surface (especially for heavy sections) due to friction of the hot section against conveyor rollers made of graphite; Fig 10.11.

10.7.4 Die Stop Marks

Whenever, due to a malfunction of a furnace or press component, the extrusion is temporarily stopped, *die stop marks* are formed on that particular section; Fig 10.11.

10.7.5 Stains/Oil Patches

Oil splashes during saw cutting (to get required section lengths after extrusion) spread on the extruded sections and burn because of high temperature; Fig 10.12. These stains can further deteriorate in the aging furnaces.

10.7.6 Twists and Bends

Several factors can cause dissimilar metal flow in the cavities of a multi-hole die: die openings (cavities) not being perfectly aligned (centered) with respect to the container; different wall thicknesses in the section design, etc. Material flow is thus faster on one side, resulting in bending or twisting; Fig 10.13. Similar problems can arise if the billet is

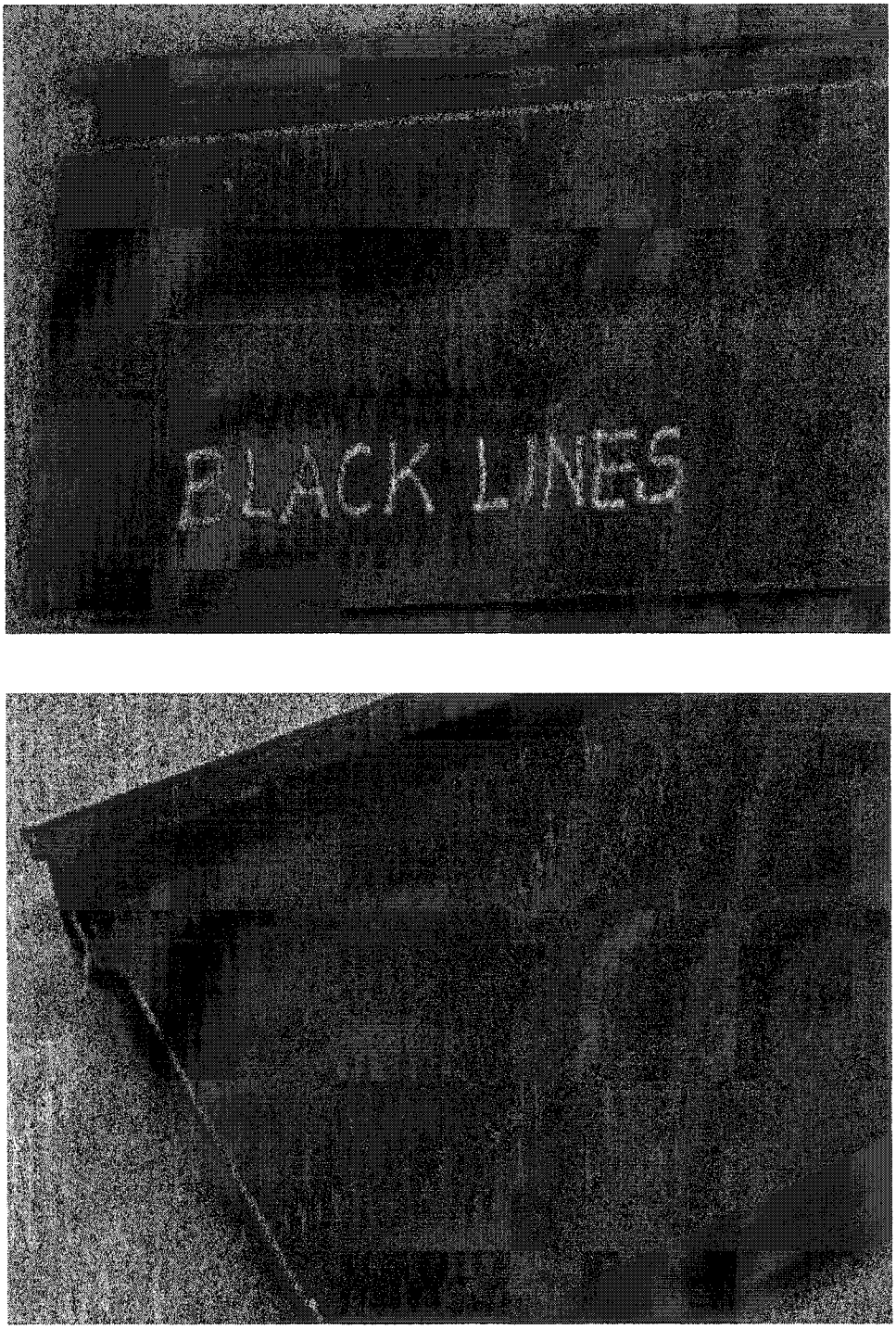

Figure 10.10 Black lines show as burnt surfaces on the extrudate due to local high pressures/temperatures [ALUPCO].

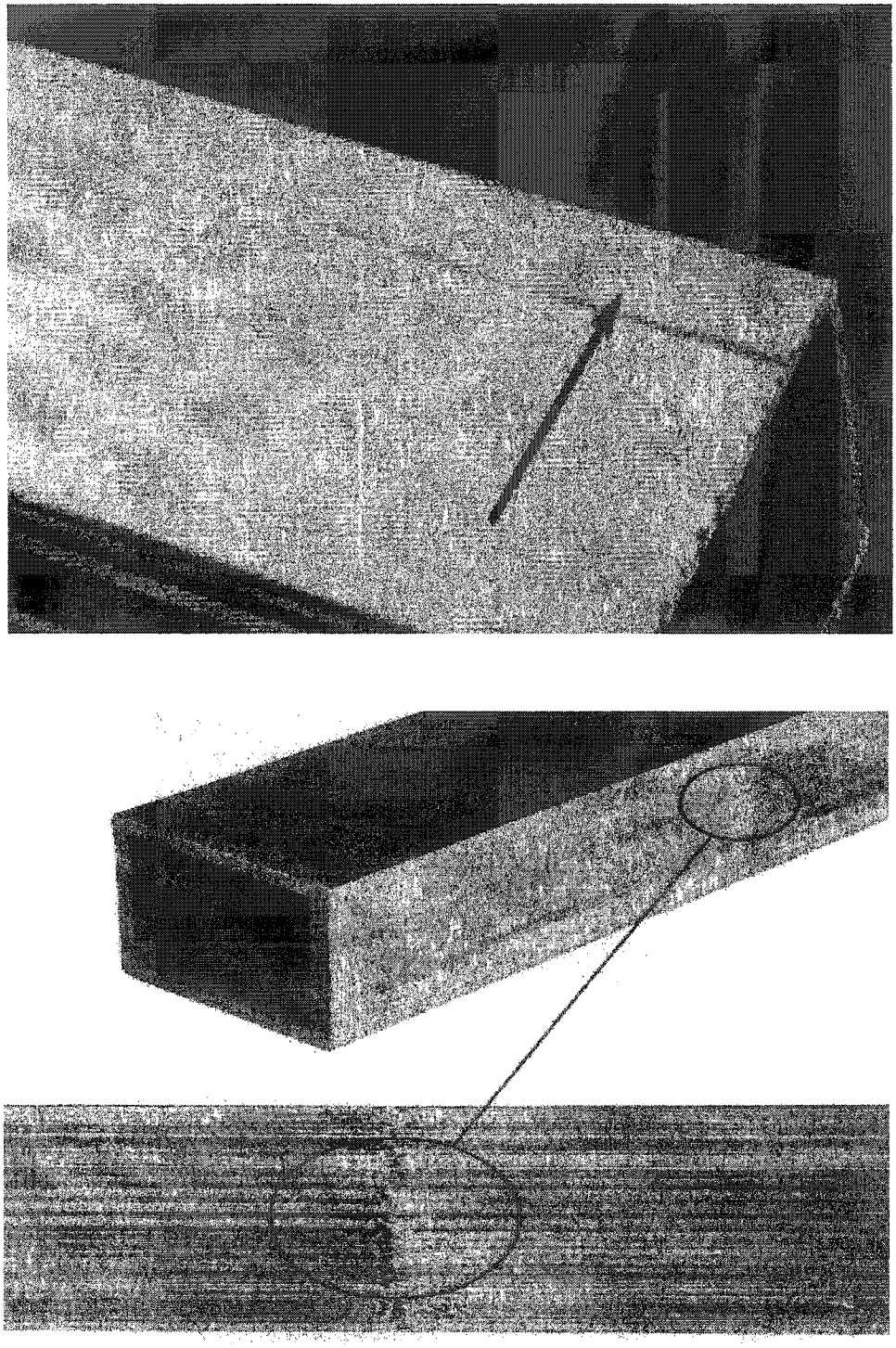

Figure 10.11 Runout marks (above) are usually longitudinal and can be either "carbon marks" or "roll marks", while a stop mark (below) is a band-like pattern perpendicular to the extruded length [Aluminum Association 1993].

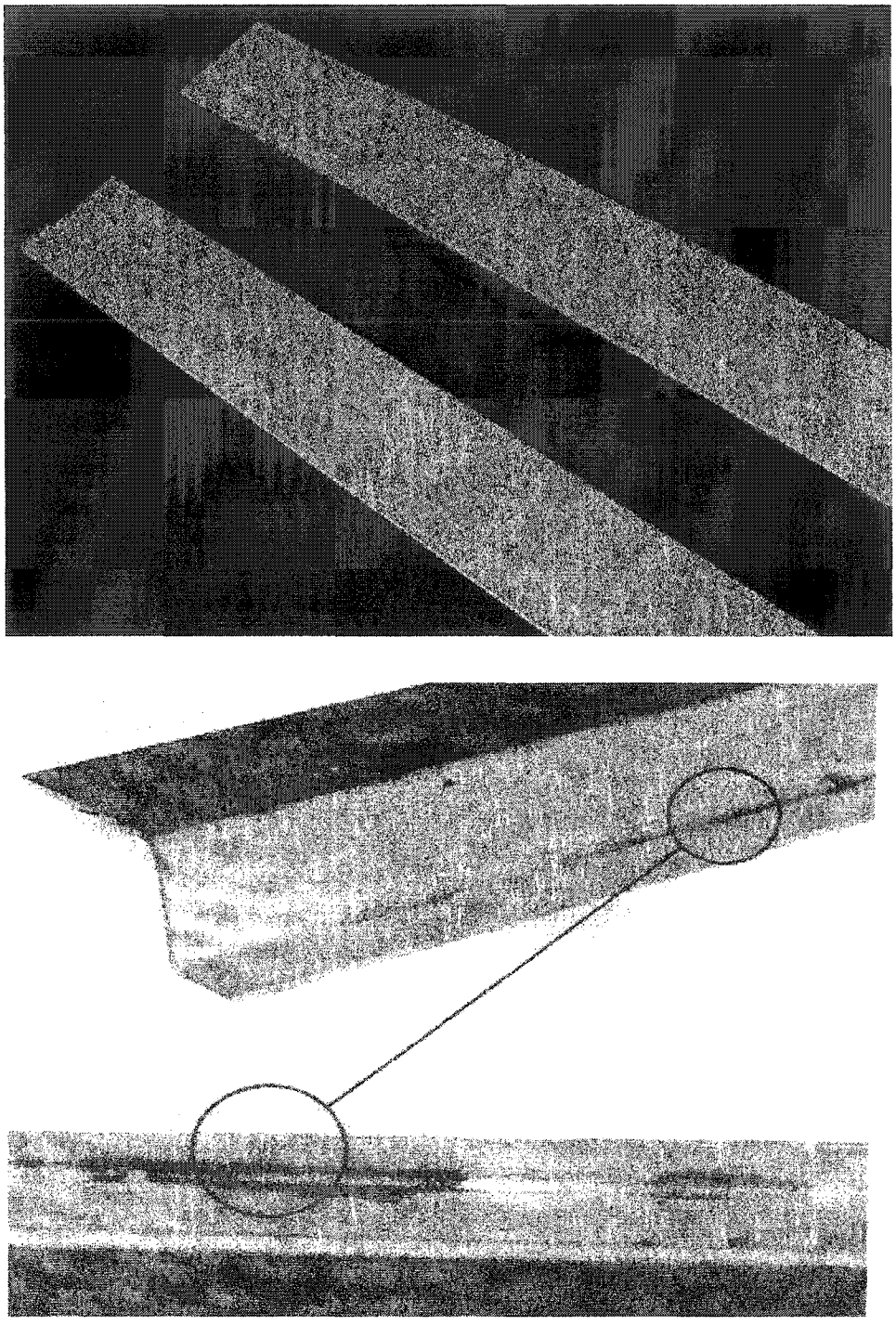

Figure 10.12 Stains and oil patches show as a yellow to brown area of surface discoloration [ALUPCO, Aluminum Association 1993].

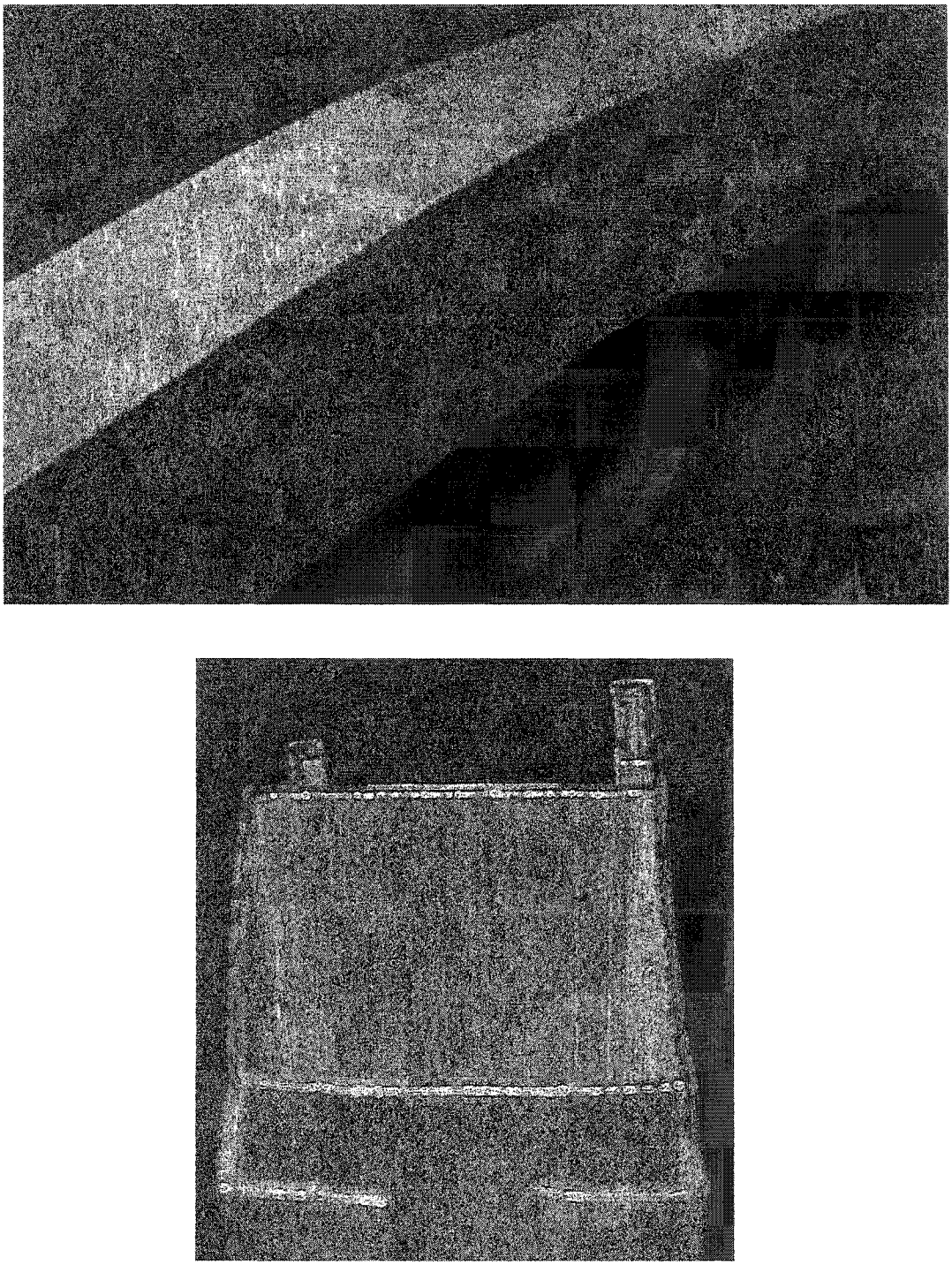

Figure 10.13 A section can deviate from straightness in the form of twists and bends (above), or it can be out of angle (below) due to nonuniform metal flow in the die [ALUPCO]

not uniformly heated on all sides, resulting in a nonuniform temperature distribution. Some bending can also occur due to improper support during stacking.

10.7.11 Dimensional Problems

The extrusion industry has various standards prescribing dimensional tolerances for acceptable architectural and other extruded products. A section can be **out of angle** (Fig 10.13) due to nonuniform metal flow in the die, or because of problems on the die-bearing surface. A **concave** or **convex** or **uneven surface** is another die related problem. It can also occur due to over-stretching of a critical surface in the correction area. A section is termed **off dimensions** if it is out of shape, or it has **uneven wall thickness**. It can happen, for instance, if the mandrel in hollow extrusion is not properly centered.

10.7.7 Scratches / Damages

If the die surface is not smooth enough (due to wear, lack of hardness, hard inclusions on die surface) or if the conveyor belts are damaged, *scratches* might appear on the extruded surface. There can also be general *damages* such as ends not being smoothly cut off by saw cutting, or sections being damaged by falling down or collision during movement by overhead cranes, etc. Damages can also occur during the stretching/straightening and roll correction stages; Fig 10.14.

10.7.8 Dents

Dents, as shown in Fig 10.14, can occur during transferring long extruded sections from one place to another by moving rollers or overhead-cranes.

10.7.9 Hot Rub Marks

In multicavity dies, extruded sections may rub against each other while coming out of the die openings. This chafing of hot extruded sections creates *hot rub marks*.

10.7.10 Rough Surface

Whenever the surface quality is below a specified industry standard, due to excessive die lines or any other surface problem, the unacceptable defect is termed *rough surface*.

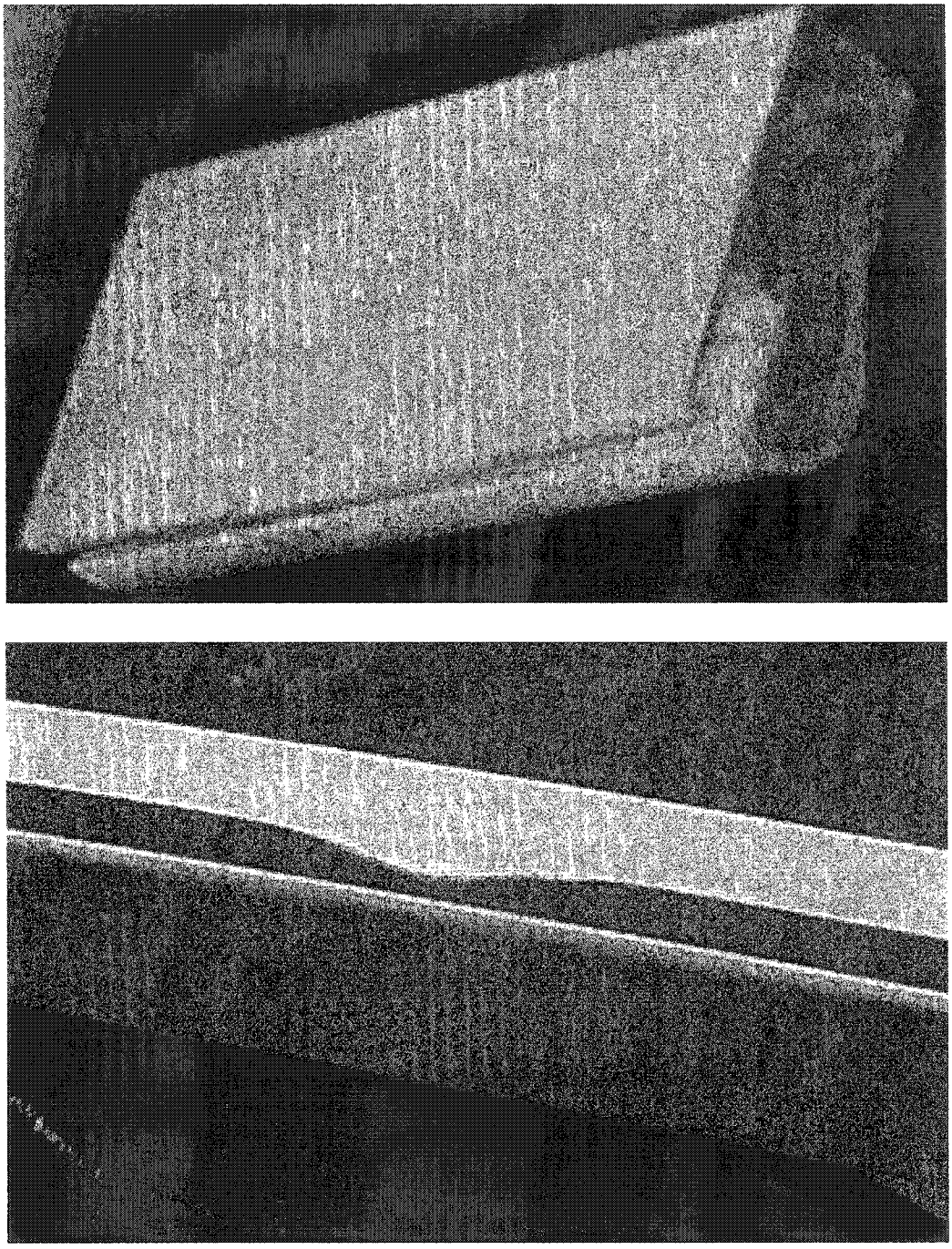

Figure 10.14 Damages (above) and dents (below) are categories of handling and traffic defects. [ALUPCO]

10.7.12 Low Hardness

As-extruded aluminum is quite soft and is therefore heat-treated by age hardening in furnaces for prescribed temperature-time cycles, depending on the aluminum alloy. Due to any number of malfunctions or problems in the furnaces, the aging process may produce *low hardness*.

10.8 Anodizing Defects

After extrusion, stretching, roll correction, and age hardening, some of the product is ready for delivery (mill-finish), while other orders may require anodizing or painting. Defects encountered during these stages are described below.

10.8.1 Black Pits

When there are small contaminations in the water in rinse tanks, and the sections are left immersed for more time than necessary, small local corrosion spots called *black pits* are formed. This is not a frequently occurring defect and is a result of rinse water not being replenished often enough.

10.8.2 Corrosion

This can sometimes happen due to damp or salty atmosphere, especially in certain geographical locations. Mostly occurring before the aging process, it can also be a result of contaminants in the cutting fluids used at saw-cutting stations and is thus usually found near the section ends. The defect is highlighted after anodizing. Figure 10.15 shows a surface marred by pitting and corrosion.

10.8.3 Dull Finish

When the sections are left in the caustic/etching tanks longer than required, a more than optimal surface layer is removed. The result is a grainy appearance, giving a *dull finish*.

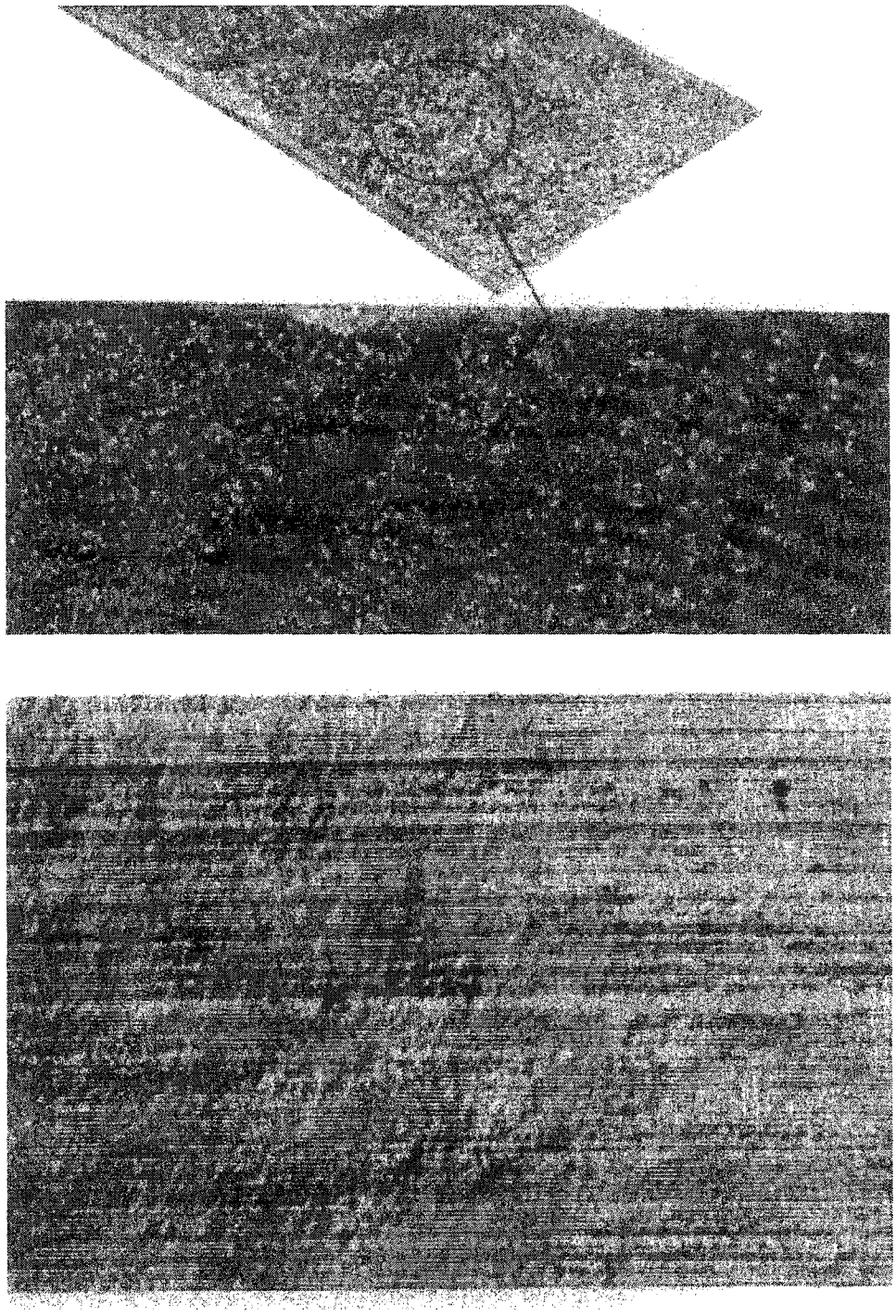

Figure 10.15 Pitting corrosion (above) is caused by chemical or electrochemical action, while orange peel (below) is a rough surface texture associated with large grains in the metal [Aluminum Association 1993].

10.8.4 Caustic Patches

If sections are left too long without rinsing after the caustic tanks, the caustic solution sticks locally and does not come off after rinsing. Also, due to bubbling and vaporization, some caustic vapors float up and deposit on the ceiling beams. When sections are carried high on the cranes, some of this caustic solution drips onto them and deposits. These spots show up after anodizing and are known as *caustic patches*.

10.8.5 Reduced Wall Thickness

Sometimes, when the anodizing quality is not good after completion of the process, the whole cycle has to be repeated. This repeated etching can result in more material removal than permitted. The result has to be scrapped due to *reduced wall thickness*.

10.8.6 Nonuniform Etching

If the etching/anodizing cycle is to be repeated, may be several times, the previous anodizing layer has to be removed. If this is not done correctly, then there is *nonuniform etching* that leads to rejection.

10.8.7 Process Scrap

These are miscellaneous rejects due to bad clamping resulting in sections falling into tanks, or falling down and bending/twisting, or dents and damages during handling and transportation.

10.9 Painting Defects

Some of the critical painting parameters are current, pressure, and nozzle size. Any or all of these can contribute to painting defects.

10.9.1 Less Microns

If any of the painting parameters (such as current, pressure, and nozzle size) are inappropriately set, or due to a combination of these, there can be an insufficient layer of paint.

10.9.2 Dust Particles

These can obviously give an unacceptable painting quality and appearance. Reasons might be contaminated paint powder, or dust particles in the painting oven.

10.9.3 Orange Peel

An improper current or pressure setting can have the consequence of more powder in certain locations. This leads to a porous appearance very much like the skin of an orange having minute projections and depressions. This *orange peel* defect is shown in Fig 10.15.

10.9.4 Blisters

If *blisters* caused during extrusion are not removed before painting, or if they become visible only after anodizing/painting, the only usual recourse is to scrap the product.

10.9.5 Overlapping

Due to currents of hot air in the oven, two sections might sometimes collide and stick together. After drying off, they cannot be pried apart without excessive damage and are thus scrapped.

10.10 Recommended Preventive and corrective Measures

Some of the defects described above cannot be avoided due to the nature of the process and existing circumstances. However, as most of the flaws originate in controllable process and tooling features, they can either be prevented or mitigated. Many of the following recommendations are heuristic in nature, based on tried and tested industrial practice.

10.10.1 Metal Flow Related Defects

A **funnel** defect can extend into the rear of the extrusion; hence, the billet should not be extruded completely. The optimum length of the discard must be determined

experimentally and must be greater for lower extrusion ratios (as in the production of thick rods), because the defect develops at an earlier stage in this case.

One or more of the following methods can be used to reduce the **pipe/extrusion** defect:

(a) *Extrusion with a shell*: This method is based on keeping the diameter of the dummy block 3 to 5 mm less than that of the container. The shell sheared off by the dummy block during extrusion remains, together with all impurities, as a cylinder and is pushed out after each extrusion [Laue 1981].

(b) *Machined billets*: Surface impurities and oxide skins can be removed to a certain extent by machining off the dirty, uneven, as-cast surface of the billet. High quality and clean billets do not need this treatment. The oxide layer may form again during billet heating [Laue 1981].

(c) *Extrusion with a long discard*: A successful but expensive method, it involves interrupting the process before the defect appears, leaving a correspondingly large discard (up to 30% of billet length). Extrusion with smaller discards and the use of fracture tests to determine the defect starting point are thus preferable [Laue 1981].

(d) *Similar billet and container temperatures*: When type *C* flow is caused by a temperature gradient resulting in heterogeneous deformation, altering the container temperature to that of the billet can reduce or prevent the danger of pipe formation.

To avoid **internal defects in hollow extrusion**, a lubricant can be used to improve the flow, helping to obtain a better inner surface. In many cases, however, a lubricant is dangerous, because it can easily be trapped under the tube surface during extrusion, resulting in blistering at high temperatures.

There are four possible ways to prevent **scales and blisters**:

(a) *Extrusion without a lubricant and with a flat die* not only removes the possibility of lubricant inclusions but also increases friction between the billet and the container. This restricts the billet surface along the container wall to such an extent that it cannot flow into the extrusion. The material therefore flows beneath

the surface of the billet by shearing and the residual surface layer containing the impurities collect in front of the dummy block.

(b) *Extrusion with a shell*: If scales and blisters still appear even when no lubricant is used, extrusion with a shell (method described above to prevent pipe formation) can be used.

(c) *Extrusion with a lubricant and with a conical die*: An alternative approach is to reduce the dead metal zone to such an extent that there is virtually no possibility of billet surface flowing into the extrusion. This can be done by using a good lubricant in the container and on the die, resulting in flow type *S* or *A*. Use of conical dies further increases the desired homogeneity of flow.

(d) To avoid air entrapment during upsetting, a *burp cycle* is sometimes employed, removing the ram pressure momentarily after upsetting to allow the air to escape.

10.10.2 Surface Defects

Apart from improved casting procedures and homogenization practices, attempts at eliminating **pick-up** defect have focused on modifications to tooling and improved extrusion practices including die modifications by nitriding, use of die materials less prone to aluminum build up, employment of an inert atmosphere [Kobayashi and Okinawa 1977], and the use of die cooling [Bischel et al. 1981].

There is a minimum die land length for successful surface operation (least visible **die lines**). At this optimum condition the entire land length is choked, preventing the introduction of oxygen to the virgin surface. The result is prevention of an oxide film that generally scores the surface. Polishing the die land is also an improving factor.

10.10.3 Weld defects

If dies are designed in such a way that welds occur on non-visible surfaces in the finished product, **weld defect** can be minimized.

10.10.4 Metallurgical Defects

Die-design streaks and **weld streaks** cannot be generally removed by mechanical treatment of the section. However, a discard of appropriate dimensions normally eliminates extrusion-defect streaks.

Hot spots cannot be generally eliminated after they have formed. The only possible solution is to avoid contact between the hot extrusions and the run-out table for more than the shortest time necessary to carry out their removal to the lateral transfer table, where cooling to below the critical temperature range should be effected as fast as possible with fan assisted air cooling.

As the defect called **silicon marks** is related to billet composition, which is very difficult to control, and since the problem is rare, defective parts of this type are scrapped.

10.10.5 Temperature and Speed Related Defects

These defects can be avoided by using lower temperatures and speeds (thus reducing the strain rate). However, this would slow down the output and reduce productivity. It is therefore a general practice to run a few test extrusions with each new die to determine the maximum speed that can be used without causing any defects.

10.10.6 Equipment and Tooling Related Defects

Runout marks may disappear (if not too dark) during anodizing and painting. Otherwise, graphite rollers must be properly maintained or replaced after optimum service life. As **die stop** marks cannot be removed once formed, the portion including the mark is discarded. To avoid **stains** and **oil patches**, the saw should optimally be placed far enough from the press to give extruded sections time to cool down so the oil will not burn.

For prevention of **twists and bends**, die cavities should be properly centered to obtain equal metal flow for all sections. Sometimes, if desired symmetry is unattainable, an additional cavity can be introduced. Also, minor bending/twisting can be corrected on the *stretching* machine. To avoid **dents** and general **damages**, care must be taken during

conveyor and overhead-crane transport as well as during packing. Defective parts of this type are few and have to be scrapped.

Preventive measure against **scratches** is periodic cleaning, polishing and nitriding of the die surfaces. Beyond a certain amount of surface erosion, the die should be replaced. **Hot rub marks** can be prevented by the use of separators (generally graphite blocks) placed upstream of the multi-cavity die to make sure that no contact or rubbing takes place between the exiting sections. If not beyond repair, **out of angle** defect can be removed on the *roll correction* machine. To avoid **uneven wall thickness**, the extrusion process must be stopped and the mandrel must be re-aligned properly.

CHAPTER 11
EXTRUSION PRODUCT DEFECTS: STATISTICAL ANALYSIS

11.1 INTRODUCTION

The previous chapter was given over to a detailed description of all the different types of product defects encountered in aluminum extrusion, their scientific classification into logical groups, discussion of their causes and mechanisms, and presentation of preventive and remedial measures prevalent in the industry. Attempt has been made in this chapter to statistically analyze the product defects generally encountered in commercial aluminum extrusion. The treatment can be used as a benchmarking tool for medium to large sized aluminum plants.

Aluminum extrusion is primarily a hot working process with high productivity and low rejection rates. From the typical operational setup outlined in Fig 1.2, six functional groups can be readily identified in the layout:

(a) Material preparation (billet preheating and sizing, die and die set preheating)
(b) Extrusion (billet deformation into the desired section profile)
(c) Product size and shape correction (stretching/straightening, roll correction, saw cutting to final size)
(d) Age hardening (to improve hardness and strength of the relatively soft aluminum product)
(e) Anodizing
(f) Painting

For ease of quality assurance and costing activities, the entire setup has been divided into three major cost centers: *press* (all activities up to and including age hardening furnaces), *anodizing*, and *painting*.

11.1.1 Current Work

Technical and economic viability of an extrusion plant depends on the minimization of defects that lead to product rejection. Attempts at improvement of extrusion quality and productivity thus translate straightaway into an analysis of product defects. Real world rejection data from ALUPCO (spanning nine years) have been collected and categorized, plant activities being divided into the three major cost centers mentioned above: press, anodizing, and painting. A statistical analysis of defects has been performed from three different viewpoints:

1. Plant-wise defects breakdown
2. Annual rejection behavior
3. Breakdown of defects at each cost center.

Rejection and acceptance probabilities at each cost center have been worked out relative to individual cost center production, and in relation to total plant production. Distribution of the defects has then been analyzed to lend some insight into their interrelationships and other issues.

ALUPCO is one of the largest aluminum extrusion facilities in the region, having a 3-press plant in Dammam (2000, 2500, and 3500 ton capacity), and one more 3-press plant and a die manufacturing facility in Jeddah. All the plants are ISO-qualified. Dammam plant has an annual average output in the range of 18,000-20,000 tons, and has about 12,000 dies of different profiles. The establishment can thus be treated as a representative medium-to-large size extrusion facility, and the work presented in this chapter can be used as a benchmarking tool for evaluating product defects and plant performance of a plant operating at high quality standards.

11.2 Data Collection, Classification and Formulation

It is practically impossible to treat each defect separately in conducting a defects analysis. Classification of these defects into categories with similar attributes (as described in the previous chapter) facilitates a much better understanding of their causes and remedies. Table 11.1 lists the defects commonly encountered in the aluminum extrusion industry, together with symbols assigned to each in this study. The defects are categorized into the three *cost centers* mentioned above: press, anodizing, and painting.

11.2.1 Probability of Rejection

If P_i is the amount of extrusion produced and R_i is the amount of rejection at the i^{th} cost center, then the *cost-center probability of rejection*, relative to cost center production, is

$$p_{ci} = \frac{R_i}{P_i}. \tag{10.1}$$

The *cost-center probability of acceptance* will then be

$$\overline{p}_{ci} = 1 - \frac{R_i}{P_i}. \tag{10.2}$$

From another viewpoint, *plant probability of rejection* at a certain cost center, in relation to total plant production, is

$$p_{pi} = \frac{R_i}{\Sigma P_i}. \tag{10.3}$$

Once again, the consequent *plant probability of acceptance* at that cost center will be

$$\overline{p}_{pi} = 1 - \frac{R_i}{\Sigma P_i}. \tag{10.4}$$

ΣP_i represents the total plant production, while ΣR_i stands for total plant rejection.

11.3 Results and Discussion

11.3.1 Overall Defects Breakdown

Figure 11.1 gives us the overall production and rejection picture (in metric tons of extrusion) with cumulative figures for the entire nine-year period. Out of the 153,226 ton

Table 11.1 Taxonomy of extrusion product defects

DEFECT SYMBOL	DEFECT CATEGORY	DEFECT SYMBOL	DEFECT CATEGORY
Press		**Anodizing**	
B/WL	Black/White Lines	BP	Black Pits
S/OP	Stains/Oil Patches	DF	Dull Finish
SM	Silicon Marks	C	Corrosion
B/DSM	Blisters/Die Stop Marks	PS	Process Scrap
LH	Low Hardness	CP	Caustic Patches
C/C	Concave/Convex	FiT	Fallen in Tank
T/B	Twists/Bends	RWT	Reduced Wall Thickness
GM/RM	Graphite Marks/Runout Marks	S/DA	Scratches/Damages (Anodizing)
OoA	Out of Angle	**Painting**	
OD	Off Dimension	LM	Less Microns
RS/BH	Rough Surface/Blow Holes	DP/OP	Dust Particles/Orange Peel
S/DPr	Scratches/Damages (Press)	B/O	Blisters/Overlapping
ODPr	Other Defects (Press)	S/DPn	Scratches/Damages (Painting)
		ODPn	Other Defects (Painting)

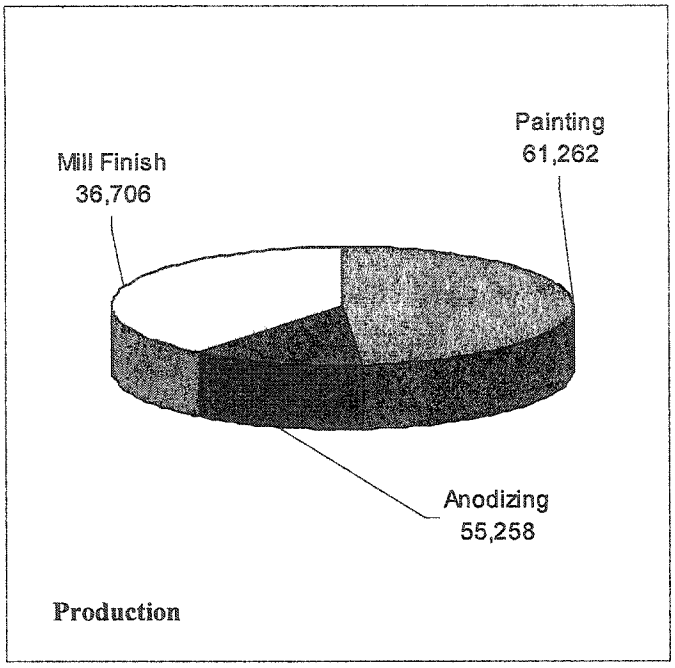

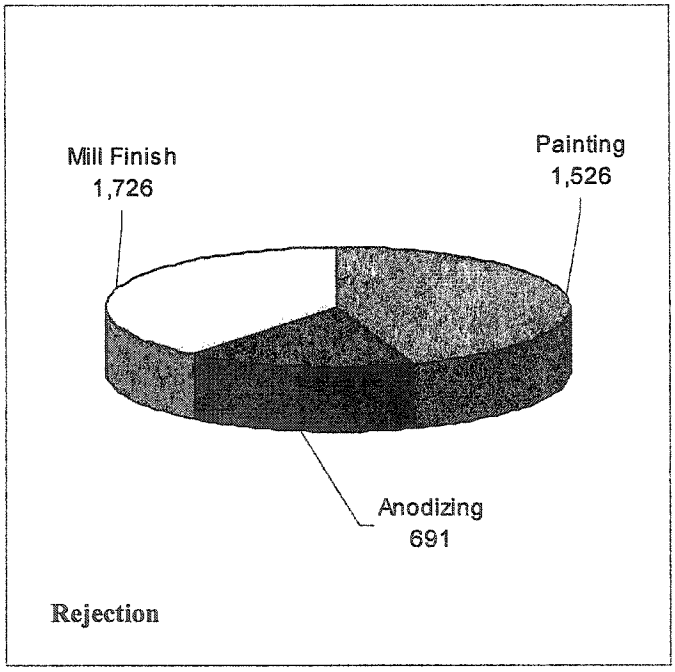

Figure 11.1 Total production (above) and total rejection (below) in tons extruded at each cost center, over a 9-year period

total plant production, 39,020 ton were *mill finish* orders (not requiring any anodizing or painting), 55,258 ton were anodized, and 61,262 ton were sent for painting. Mill finish rejects were 1,726 ton, anodizing defects were 691 ton, and painting discards were 1,526 ton.

Table 11.2 and Fig 11.2 illustrate the same scenario in terms of probabilities. Based on total output of each cost center (e.g., painting defects relative to painting production only), there was 1.13% rejection in the press area, 1.25% defectives in the painting section, and a sizeable 2.49% discards in the painting department. Total overall rejection probability was 2.57%. In addition to common problems such as equipment and tooling malfunction, inconsistencies in manpower expertise and efficiency, and material (paint powder and mixing agents etc) deficiencies, the painting section can also be seriously affected by some additional and somewhat uncontrollable external factors. Some of these are atmospheric heat (up to 50°C or more in summers in the region), humidity (reaching 95% or more during certain months), unpredictable wind velocities and sand/dust storms. Some or all of these may cause the relatively large rejection percentage in the painting section.

Based on total plant production (e.g., painting defectives relative to total plant output), the largest rejection of 1.13% was in the press area, followed by 0.996% painting rejects and 0.45% anodizing discards. Overall rejection for the whole plant of course remains the same at 2.57%. With possible problems in the billet and die/tooling preheat ovens, deformation chamber, stretching and roll correction stations, age hardening furnaces, together with design and maintenance troubles, the maximum amount of defective extrusion is intuitively expected to be in the press area. Also, as the number of controlling factors in the anodizing section is smaller than that in the painting sector (as mentioned above), percentage of anodizing defects is considerably less than that of painting rejects.

Table 11.2 Probabilities of rejection and acceptance at various cost centers

Cost Center (i)	P_i (ton)	R_i (ton)	p_{ci} (%)	$\overline{p}_{ci}$ (%)	p_{pi} (%)	$\overline{p}_{pi}$ (%)
Press	153,226	1,726	1.13	98.87	1.13	98.87
Anodizing	55,258	691	1.25	98.75	0.45	99.55
Painting	61,262	1,526	2.49	97.51	0.996	99.004

ΣP_i	ΣR_i	$\Sigma R_i / \Sigma P_i$	$1 - \Sigma R_i / \Sigma P_i$
153,226	3,942	2.57	97.43

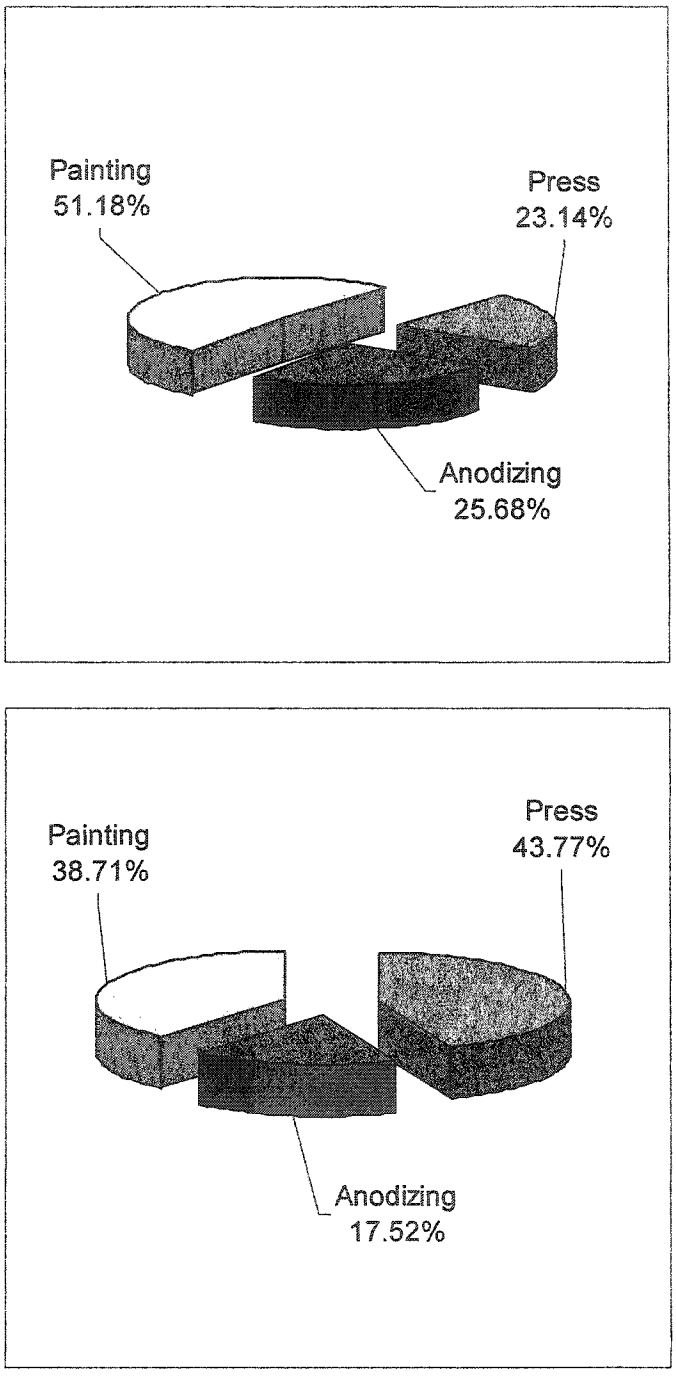

Figure 11.2 Relative probability of rejection at each of the three cost centers, based on production at each cost center (above), and as percentage of total plant production (below)

11.3.2 Annual Rejection Behavior

A summary of annual rejection due to uncorrectable defects for the whole plant and for each of the cost centers is presented in Fig 11.3 and Fig 11.4. Total annual rejection fluctuates around an average of about 438 tons of extrusion, while the average overall probability of rejection is 2.57%; Fig 11.3. In terms of tons of defective product (Fig 11.4), press defects are generally the highest, painting defects are the next, while anodizing defects are generally the smallest. This strengthens the observation made in the preceding section. Annual rejection pattern is given in terms of the rejection probability at each cost center, e.g., ratio of anodizing defectives to total anodizing product in that year. It can be seen that occurrence of painting defects is by far the highest, press flaws being generally the second, followed closely by anodizing rejects, though anodizing yields more discards than the press area in some years. This overall behavior is also in line with the conclusions drawn in the previous section.

As far as the yearly trends are concerned, rejection probabilities can give us a better insight than rejection amounts as they cancel out the effect of fluctuation in the annual production tonnage. We observe a healthy general progression of lower press rejects (percentage) from years 1 to 5, and again from years 7 to 9. Gradual fine-tuning of quality assurance procedures, better design and maintenance of dies and other tooling, improved manpower expertise due to increasing familiarity with process and equipment can all be the contributing factors. The upwards jump from year-6 to year-7 is due to a major breakdown at that time in one of the presses. Though the press was soon functional, getting back to standard quality levels took about a year. Apart from an excessively high painting-defects peak in the first year (Fig 11.4), anodizing and painting defects do not show a large amount of fluctuation over the years. This is understandable, as there was no major technological improvement in these two cost centers compared to the press section (such as breakthroughs in material, manufacturing, heat treatment and surface hardening of dies and other tooling).

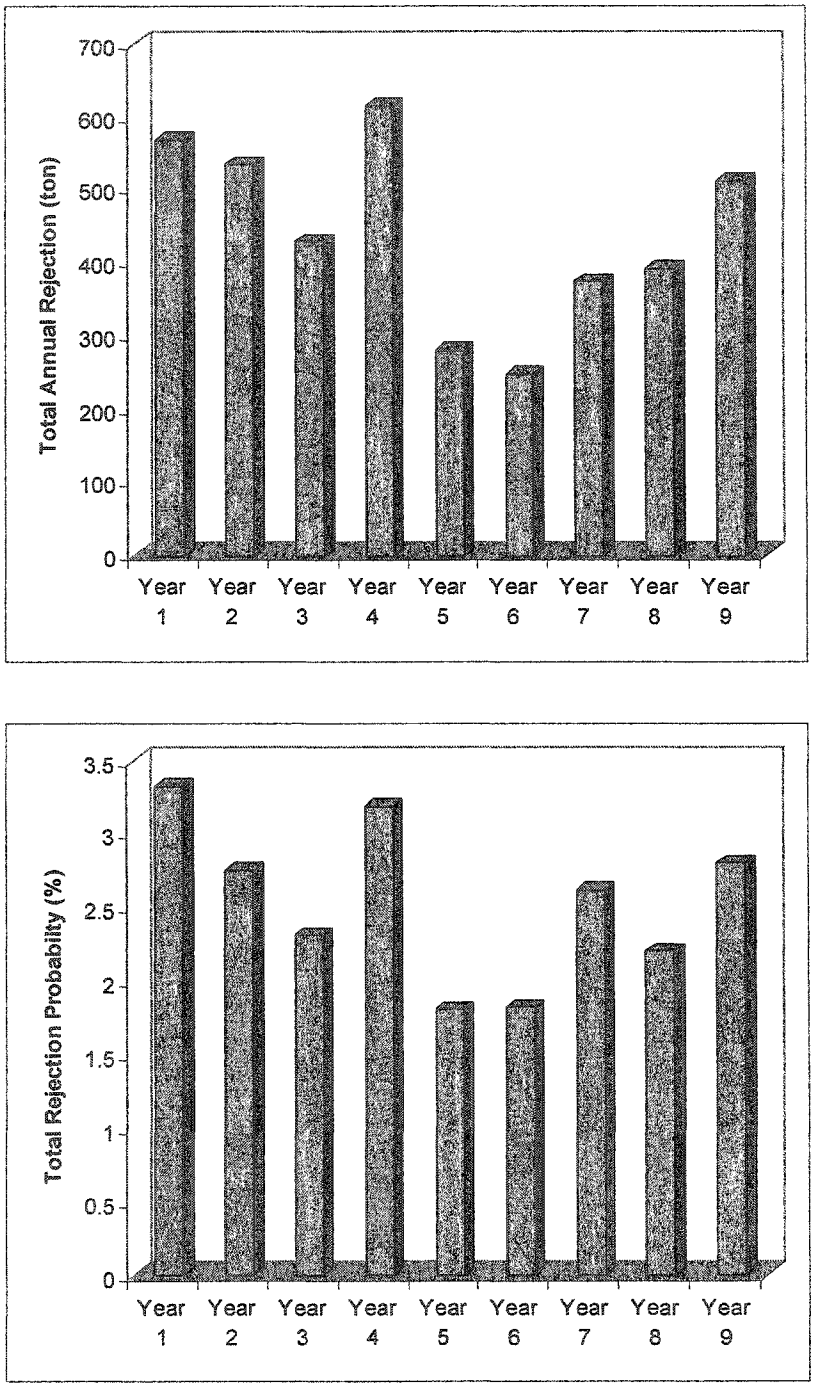

Figure 11.3 Total annual rejection amount in tons (above), and total annual rejection probability (below)

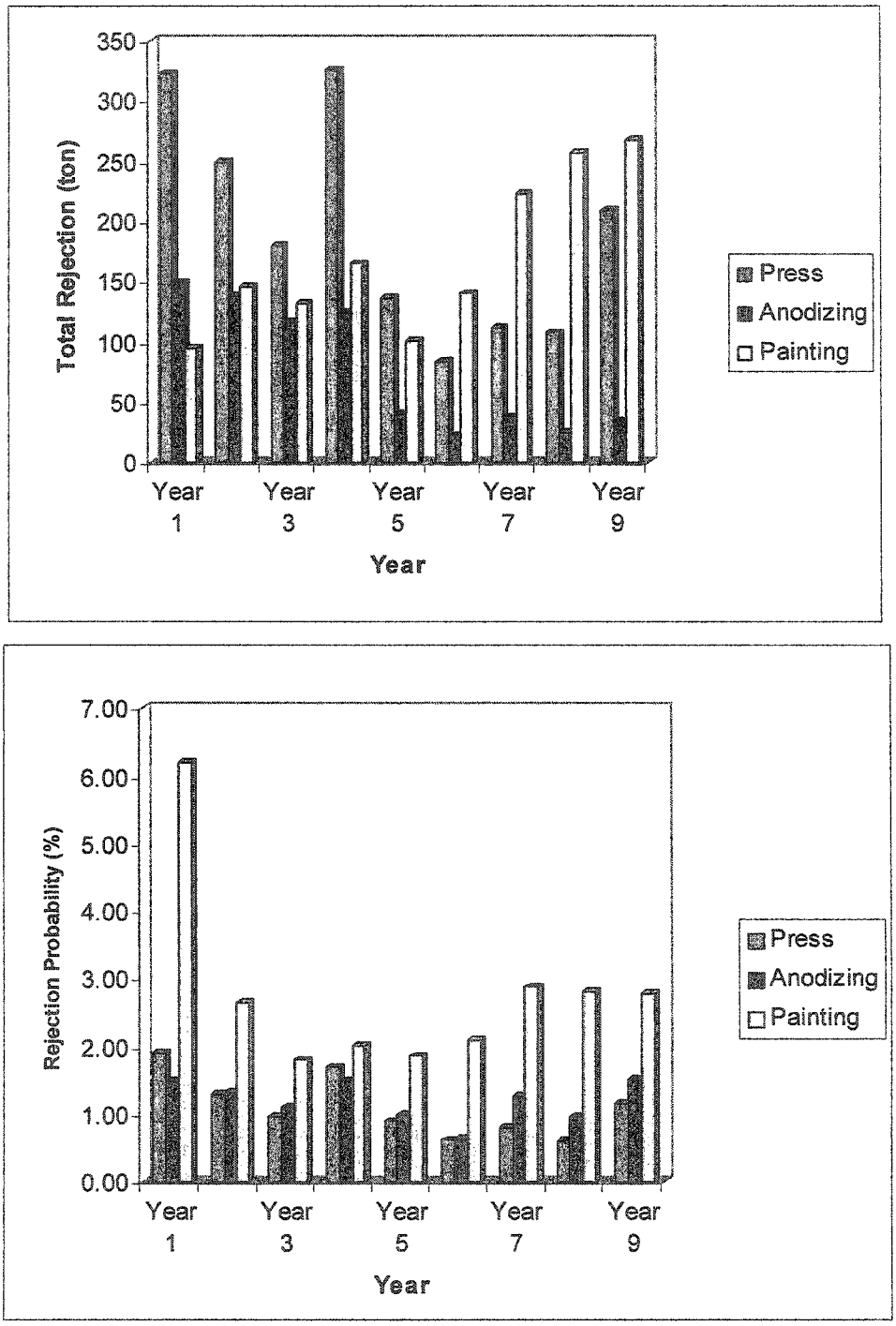

Figure 11.4 Annual rejection amount at each cost center in tons of product (above), and as rejection probability relative to cost center production (below)

11.3.3 Breakdown of Press Defects

As can be seen from Fig 11.5, the largest contributing class of rejections in the press area was *black/white die lines* (39.76%). Leaving aside *other press defects* (10.94%), which represents miscellaneous rejection causes, the only other significant defect category is *scratches/damages* (15.38%).

Pick-up and die lines are considered to be the most serious surface defects in common aluminum alloys such as Al-6063, as described in the previous chapter. Though the exact mechanism is not very clear, evidence suggests that a thin film of extrudate material adheres to the die land surface during extrusion, and this interaction results in the formation of these defects. Even with an optimum die land length and extrusion temperature, together with highly polished die lands, die lines are still observed to occur. These die lines are finer and shallower and are termed *micro die lines*. Any inclusions on the billet surface or on the die land aggravate the problem.

Scratches and damages, as described earlier, cover a wide variety of defect mechanisms. One of these is minor surface roughness on the die land (due to insufficient hardening during nitriding and heat treatment, excessive gradual wear of the bearing surface, hard surface inclusions during die manufacture or subsequent maintenance, etc). Another source is scrapes or grazes sustained through the material handling system such as conveyor belts, rollers, overhead cranes, etc. Yet another reason is scratches generated at the various saw-cutting stations. General damages during stretching, straightening and roll-correction add to the list.

11.3.4 Breakdown of Anodizing Defects

Apart from *process scrap* (27.56%) and *scratches/damages* (25.71%), which are general rejection categories covering miscellaneous defect sources, the most significant contributors to anodizing rejects were *corrosion* (22.66%) and *black pits* (10.39%), as shown in Fig 11.6. Other defect types are relatively insignificant.

Both of these categories belong to the *pitting/corrosion* defect group. Interestingly, they are not really caused by equipment malfunctions or lack of manpower skill. Rather,

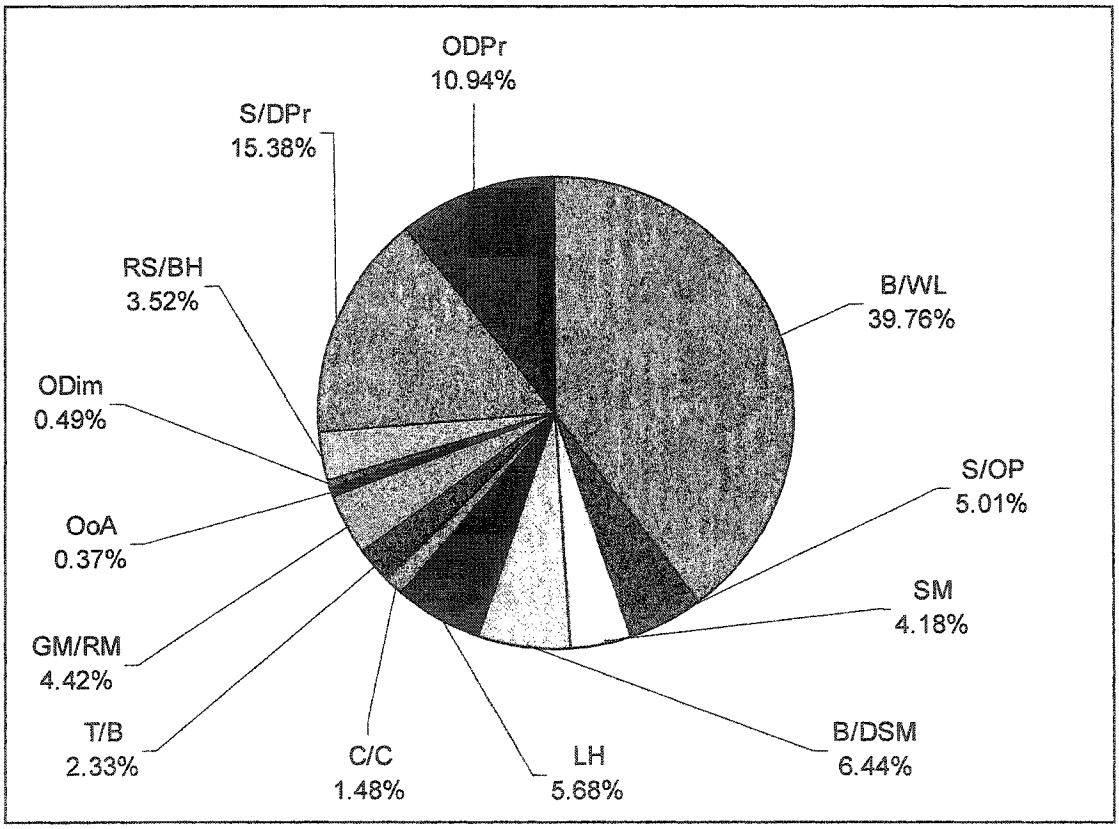

Figure 11.5 Cost center wise rejection breakdown: press area

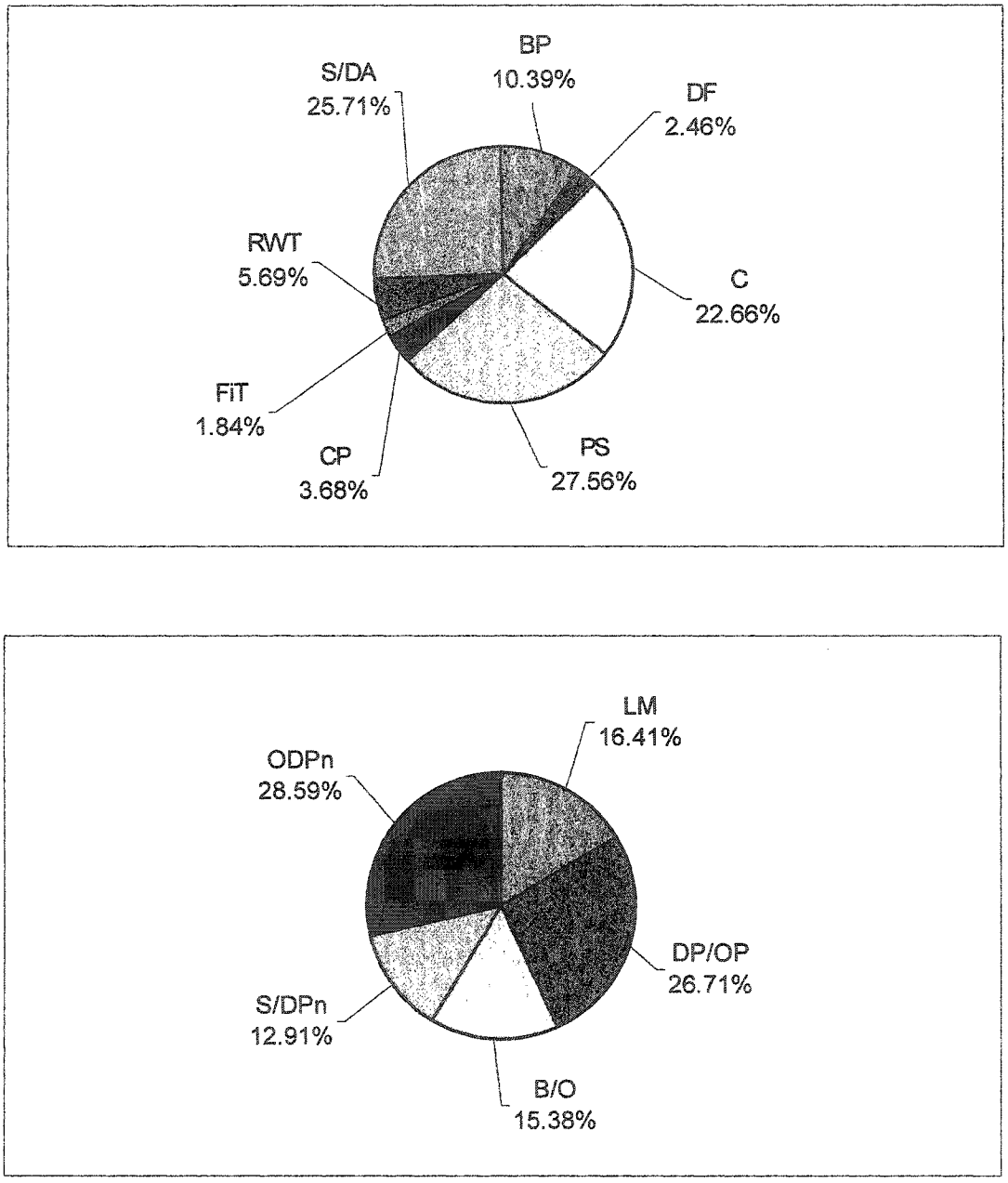

Figure 11.6 Cost center wise rejection breakdown: anodizing area (above) and painting area (below)

in this plant, these defects have roots in the climatic conditions of the region. Being in close proximity to a very salty sea, the moisture and salinity content of the air in the anodizing area is detrimentally high. Cordoning off and maintaining an artificial atmosphere in such a large area is rather cost-prohibitive and more uneconomical than sustaining the cost of rejection.

11.3.5 Breakdown of Painting Defects

If we ignore *other painting defects* (28.59%), which is a miscellaneous-type defect category, the most important source of painting rejections was *dust particles and orange peel* (26.71%), as revealed in Fig 11.6. Other rejection sources are not so critical.

Impurities in the paint powder are generally not as dominant a factor in dust particle inclusion in the painted surface as the geographical location of the plant. Even after partial atmospheric isolation of the paint area, intermittent dust and sand storms in the region do penetrate through.

CHAPTER 12
CONCLUSIONS

The heart of the entire extrusion plant is the *deformation chamber*, where the actual transformation of the billet material into the desired section shape takes place. The major aim of the work described in the previous chapters was to conduct a *thorough and in-depth investigation of the process going on in the extrusion chamber, and the interrelationships among the different process parameters and the various input and output entities involved.*

All the **solution methodologies** applicable to metal forming are prone to certain shortcomings. Any single method therefore does not provide a satisfactory tool for investigation of all the aspects of aluminum extrusion. That is why the approach adopted in the **current work** was to utilize all the useful methods together for a better understanding of the multitude of issues involved: *experimental-empirical*, *statistical-probabilistic*, and *2D-3D FEM* methods. This multi- methodology approach proved to be a great help in a comprehensive understanding of the field of aluminum extrusion.

Due to a variety of reasons, most of the research work available in the published domain is restricted to specific individual aspects of extrusion. A major contribution of the current work is the **comprehensive research approach** adopted. *The process, the tooling, and the product* were *simultaneously investigated*, the global view providing the opportunity to understand the entire process of extrusion, rather than isolated issues.

Elaborate experiment facilities are costly and difficult to establish and manage, and access to industrial data is generally very limited. Hence a major shortcoming of published works has been lack of experimental data. Owing to collaboration with local die manufacturing and aluminum extrusion facilities, **extensive amount of experimental**

work was carried out related to *hot and cold extrusion*, and *heat treatment and material testing*. A large amount of *industrial data* about *failure of dies and tools, and product defects* was also obtained from the same sources.

12.1 Pressure Variation

A number of experiments were conducted in the industry to record pressure variation against ram advance during hot extrusion of solid, hollow and semi-hollow dies of varying complexity, and at different ram speeds. Major conclusions and suggestions were:

1. Disregarding the start-up area, pressure generally dropped down quite smoothly with ram advance along the container. The partially fluctuating behavior of some curves could be due to automatic machine adjustments or process discontinuities.
2. When the ram speed was kept constant, pressure curves for more complex profiles were generally higher than less complex ones. A couple of cases not following this trend could be due to experimental anomalies or due to inadequate and inconsistent complexity definitions.
3. When extruding the same profile at different ram speeds, the trend was of higher-pressure curves for higher ram speeds, apart from one or two exceptions. The inconsistency could be due to die symmetry problems or due to deficient complexity definitions.
4. In all the cases, curves for solid shapes were clustered together and hollow ones together, with a notable gap between the two groups. This separation increased with increasing ram speed.

12.2 Pressure Prediction and Complexity

The basic premise for this study was that extrusion pressure for a complex profile can be expressed in terms of the pressure for a standard simple profile (solid circular) and the complexity index of the complex profile. Attempt was made to come up with a new and

more coherent definition of complexity for extrusion dies. Experimental runs in hot aluminum extrusion were carried out for a number of dies of different profiles (from simple solids and hollows to quite complex ones). Extrusion environment (die material, billet material, billet and die preheat temperatures, container temperature, etc) was the same for all runs. Various regression strategies were tried out (exponential, logarithmic and power law formats). The model giving the most consistent and relatively accurate results came out to be

$$C_5 = 0.95 + 0.05\left(\frac{P_s}{P_0}\right)^{1.5}.$$

In comparison with the four existing definitions, the new definition followed the actual pressure behavior most closely, and yielded the smallest average error in prediction of maximum extrusion pressure. The next best definition, yielding results not too far from the new definition, was the Altan formula (C_4).

12.3 Deformation Behavior

Cold extrusion experiments (at room temperature) were performed on split billets of lead, aluminum, and Al-6063. Dies of three different profiles, made of H13 steel, were used. Extrusion runs were carried out at four different ram speeds. Photographs of extruded billets studied under a microscope, and numerical simulations of the extrusion experiments, were used to investigate the regions and patterns of metal flow. Finite element simulations (using ANSYS and ANSYS-LSDYNA) carried out for materials, speeds, and extrusion ratios not covered by the experiments performed, further extended the scope of the study.

Consistent with the findings of recent studies, four regions of metal flow were identified: dead metal zone, shear zone, general deformation zone, and un-deformed zone. As extrusion progressed from an initial transient state to a steady state, the dead metal zone also evolved to a stable size and shape. Compared to hard and strong materials, flow lines in softer and weaker materials were sharper and more deeply gouged, with a smaller

and narrower dead metal zone. For constant shape complexity, and with increasing ram speed, the dead metal zone became narrower and somewhat smaller in size, but the metal flow got increasingly distorted. With changing complexity of the die profile, variation in the behavior of the dead metal zone and the metal flow pattern was somewhat erratic. This may be partly due to variation in the profile symmetry situation, and partly due to inconsistent and incomplete complexity definitions. As expected, due to the reduction of the die opening and the increased blockage of material flow, size of the dead metal zone increased with increasing extrusion ratio. Variation of DMZ size and extrusion pressure against extrusion ratio, for different materials and different ram speeds, showed a linear trend. DMZ curves were generally higher for tougher materials and lower extrusion speeds. Extrusion pressure yielded higher curves for tougher materials, and also for higher extrusion velocities.

More experiments need to be conducted, together with more simulated runs (especially 3D), to further corroborate these observations and to provide information about situations and materials that cannot be easily experimented on.

12.4 Die Failure Modes and Mechanisms

The study covered 17 different die profiles, and 616 die failures in commercial extrusion of Al-6063. There were 288 failures due to fatigue fracture, 158 owing to gradual wear, 116 because of plastic deformation and deflection, 25 mixed-mode type, 12 miscellaneous ones (not attributable to any distinct failure mode), and 17 breakdowns related to the mandrel. Total number of failures belonging to the solid category was 271, hollow type failures were 241 in number, and the remaining 104 were for semi-hollow shapes.

Important terms related to attributes of an aluminum extrusion die were discussed. Some characteristic features of extrusion profiles commonly and repeatedly used in the construction sector were identified. Mechanisms of die failure were classified into broad groups, including the three major modes of fatigue fracture, gradual wear, and plastic deformation or deflection.

On an overall basis (all types of dies considered together), the predominant failure mode was fracture (46%), followed by wear (26%), deflection (19%), mixed-mode (4%), mandrel-related (3%), and miscellaneous (2%). The major fracture-type failure was due to cracking or breaking of the brush path, the main wear-related one was of the dimension-change variety, and the notable deflection failure was located at the bearing. Bearing damage was also the primary cause of miscellaneous breakdowns.

Considering solid dies alone, fracture (77%) was the dominant failure mode, followed by some wear (15%) and a small fraction of deflection (3%). For hollow dies, wear (36%) and deflection (33%) were the major failure contributors, fracture being just 17%. In the semi-hollow shape category, all failure classes played almost equal parts, 34% fracture, 29% wear and 29% deflection.

Looking at each failure mode separately, fracture was found to be mostly in solid dies (74%), followed by a 14% share in hollow dies and 12% in semi-hollow ones. Of the breakdowns related to wear, 56% were in hollow dies, 25% in solid ones, and 19% in semi-hollow dies. Out of the dies scrapped due to plastic deformation, 68% were hollow, 26% were semi-hollow and only 6% were solid. Mixed-mode failures were mostly in hollow dies (69%), miscellaneous ones in solids (58%) and mandrel breakdowns predominantly in hollow dies (82%).

Analysis of the graphs leads to some interesting conclusions. Fatigue fracture was the principal failure mode for solid dies. Wear and deflection were almost equally responsible for hollow die failures. All the three major failure modes contributed almost evenly to breakdowns of semi-hollow dies. Most of these conclusions appear to have a sound basis in the mechanics of hot aluminum extrusion. However, more failure data can be collected to include a wider range of shape complexities within each profile type (solid, hollow and semi-hollow), and to have a large enough failure database to generalize the conclusions listed above.

12.5 Probabilistic Study of Die Life

A probabilistic analysis of die reliability was carried out, based on the die failure data discussed in chapter-5. In describing die life probabilities, the best overall *goodness of fit* was observed for the Weibull distribution, followed quite closely by normal and lognormal distributions. Minimum extreme value distribution does not appear to be a good representation of die reliability. Shape and scale parameters for the Weibull distribution (m and θ) were evaluated from die failure data for each die profile. Profile perimeter based complexity definitions (C_1, C_2, C_4, and C_5) exhibited a much closer relationship with θ as compared to definition C_3 (based on minimum wall thickness). The new definition (C_5) developed in chapter-3 yielded the best correlation, next best being definition C_4. All the graphs suggested a definite relationship between die complexity and die life, though the correlation (maximum of around 48% for C_5) was not very strong. However, all the definitions exhibited a counter-intuitive trend of an increase in die life with increasing shape complexity. The rather weak correlation, and this unreasonable trend, both strongly reinforced the earlier conclusion that conventional (extrusion pressure based) definitions of shape complexity are inadequate, and do not include many significant geometrical features of the die profile.

12.6 Complexity Based Die Life Prediction

Existing definitions of extrusion shape complexity (including the new definition C_5 proposed in chapter-3) were critically reviewed. Real world data covering form features and average life (*MTTF*) of a variety of simple and complex hot aluminum extrusion dies, covering a period of over 10 years, was collected and used for required calculations. Variation of *MTTF* and extrusion ratio (R) against available complexity indices were studied and analyzed. Linear and logarithmic models were generated for prediction of the mean time to failure of any given die, based solely on the form features of the die. New, more comprehensive and robust definitions of complexity index were developed in terms of form features of a die profile, based on the linear and logarithmic models. New

definitions satisfied the expected natural trend of decreasing die life with increasing die complexity, and yielded a much higher coefficient of correlation with *MTTF* than any of the existing definitions.

12.7 Fracture Toughness of Hot Work Tool Steels

A comprehensive and exhaustive literature search was conducted (covering published sources and tool steel manufacturers) to collect K_{IC}, *CVN*, *HRC*, and σ_Y data for AISI H13 tool steel, at various tempering and testing temperatures. Published data was augmented by data generated through in-house heat treatment and mechanical testing of H13 samples. Various linear, power law, logarithmic, and polynomial curve fitting techniques were judiciously used to interpolate and extrapolate for missing data points. Behavior of K_{IC}, *HRC* and *CVN* against tempering and operating temperatures was closely studied. Two linear and two power-law correlations were developed to predict K_{IC} values from available *CVN* values, both at room and elevated temperatures, and applicable to different heat treatments. The power law models yielded a higher correlation with experimental data than the linear models in the range of tempering and operating temperatures generally applicable to hot aluminum extrusion. More experiments need to be conducted to obtain elevated-temperature yield strength and fracture toughness (K_{IC}) values of tool steels, for further corroboration and validation of these models.

12.8 Life Prediction using Monte Carlo Simulation

Assuming die life and related material and geometrical parameters to be random variables, Monte Carlo simulation was carried out to predict the life of an extrusion die. Paris law was used as the model to estimate fatigue life of the die in terms of number of cycles to failure (number of billets extruded). Prediction model developed earlier (chapter-8) was utilized to obtain the value of fracture toughness (K_{IC}) of H13 hot work die steel under typical tempering and operating temperature conditions. Failure history of an actual simple hollow die from the aluminum extrusion industry was used as a case

study. The resulting (simulated) die life observations were adequately represented by a Weibull probability model with shape parameter m = 4.3 and scale parameter θ = 837 cycles (billets), an average die life of 759 kg (as against the actual *MTTF* of 722 kg), and a correlation coefficient of r^2 = 97.8%. A wear failure model (linear) was also developed, using actual wear data of a hollow box die. Monte Carlo simulation was then carried out, based on this model, to predict die life of the tube die. The simulation yielded a 3-parameter Weibull fit with m = 2.89, θ = 809 kg, *MTTF* = 767 kg, and r^2 = 95.6%. This lower goodness of fit for wear matched well with failure records, as the die studied seldom failed due to wear in actual practice. The combined fracture-wear failure model yielded the best simulation, with m = 4.99, θ = 786 kg, *MTTF* = 717 kg, and r^2 = 98.5%. The strategy outlined here could be easily adapted to forecast life of extrusion dies using tool steels subjected to different tempering routines and used at different operating temperatures.

12.9 Defect Classification, Causes and Remedies

All the defects typically encountered in the industry were described and explained with the help of visual illustrations. Flaws were categorized into metal-flow related, surface, weld, metallurgical, temperature and speed related, equipment and tooling related, anodizing, and painting defects. Causes and mechanisms of defect formation were discussed on the basis of mechanics and metallurgy in most of the cases. Various defects, categories, and mechanisms were described that have not been reported in published literature. Preventive and corrective measures, based on prevalent industrial practice, were discussed for most of the defects.

12.10 Statistical Analysis of Defects

Real world rejection data from a medium-to-large size commercial extrusion setup (covering a period of nine years) was collected, classified, and tabulated. Defect data were statistically analyzed based on plant-wise (overall) defects breakdown, annual rejection behavior, and individual breakdown of defects in the Press, Anodizing, and

Painting areas. The work can be used as a benchmarking tool for evaluation of plant performance and quantitative analysis of defects of a medium-to-large size extrusion facility operating at high quality standards.

REFERENCES

- AEC (2004), **Aluminum Extrusion Manual**, Aluminum Extruders Council (AEC), http://www.aec.org/extrusion/extrusion.html
- Ahn et al. (Nov 1997) "Study on the Prediction of Fatigue Life in an Axi-Symmetric Extrusion Die," *Journal of Materials Processing Technology*, **71** (3), p 343-349
- Altan T, Oh S-I, Gegel HL (1983) **Metal Forming: Fundamentals and Applications**, American Society for Metals, Metals Park, Ohio
- Alum Assoc (1993) **Visual Quality Characteristics of Aluminum Extrusions**, The Aluminum Association, Washington, DC
- Anderson TL (1991) **Fracture Mechanics: Fundamentals and Applications**, CRC Press, Boca Raton
- Arif AFM, Sheikh AK, Qamar SZ (May 2004) "An Investigation into Metal Flow and Dead Metal Zone in Extrusion," *3rd International Conference on Advanced Manufacturing Technology (ICAMT 2004)*, May 2004, Malaysia, p 941-947
- Arif AFM, Sheikh AK, Qamar SZ, Al-Fuhaid KM (Feb 2001) "Effect of Ram Speed and Tool Complexity on the Extrusion of Al-6063," *Proceedings of the International Conference on Aluminum Production and Processing: APPA-2001*, February 2001, Bahrain
- Arif AFM, Sheikh AK, Qamar SZ, Al-Fuhaid KM (Jul-Aug 2001) "Modes of Die Failure and Tool Complexity in Hot Extrusion of Al-6063," *Proceedings of the 16th International Conference on Production Research: ICPR-16*, July-August 2001, Prague, Czech Republic

- Arif AFM, Sheikh AK, Qamar SZ, al-Fuhaid KM (Mar 2003) "A Study of Die Failure Mechanisms in Aluminum Extrusion," *Journal of Materials Processing Technology*, 134 (3), p 318-328
- Arif AFM, Sheikh AK, Qamar SZ, al-Fuhaid KM (Sep 2001) "Variation of Pressure with Ram Speed and Die Profile in Hot Extrusion of Aluminum-6063," *Materials and Manufacturing Processes*, 16 (5), p 701-716
- Arif AFM, Sheikh AK, Qamar SZ, Raza MK, Al-Fuhaid KM (Dec 2002) "Product Defects in Aluminum Extrusion and Their Impact on Operational Cost," *Proceedings of the 6th Saudi Engineering Conference*, 14-17 December 2002, Dhahran, Saudi Arabia, p 137-154
- ASM (1975), **Source Book on Cold Forming**, American Society for Metals (ASM), Metals Park, Ohio, p 155
- ASM (1986) **Metals Handbook Vol-11: Failure Analysis and Prevention**, 9th edition, American Society for Metals (ASM), Metals Park, Ohio
- ASM (1990) **Metals Handbook Vol-2: Properties and Selection: Nonferrous Alloys and Special Purpose Materials**, 10th edition, American Society for Metals, Metals Park, Ohio
- ASM (1996) **ASM Handbook Vol-19: Fatigue and Fracture**, ASM International, Materials Park, Ohio
- Ault RT, Wald GM, Bertola RB (1971) "Development of an Improved Ultrahigh Strength Steel for Forged Aircraft Components," *AFML TR 71271*, Airforce Materials Lab, Wright-Patterson Airforce Base, Ohio, USA
- Axman C, Mannl V (Mar 1998) "Investigation of Metal Extrusion and Axial Compression of Compressible Media by means of a Modified Slab Method," *Archive of Applied Mechanics*, **68** (2), p 137-146
- Barsom JM, and Rolfe ST (1970) "Correlations Between K_{IC} and Charpy V-Notch Test Results in the Transition-Temperature Range," *Impact Testing of Metals, ASTM STP 466*, American Society for Testing and Materials, Philadelphia, p 281-302

- Basavaraju Ch (1998) "Estimated Upper Bound Extrusion Pressures and Experimental Results," *Proc 1998 ASME/JSME Joint Pressure Vessels and Piping Conf*, San Diego, California
- Berezhnoy VL, Hahn K-H, Chang J-Y (1999) "Extrusion Defects: Conditions of Formation and Methods of Prevention," *Light Metal Age*, **57** (3), p 6
- Bischel M, Reid A, Langerweger J (1981) *Aluminium*, **57**, p 878
- Björk T, Westergard R, Hogmark S (2001) "Wear of Surface Treated Dies for Aluminum Extrusuion — a Case Study," *Wear*, **249**, p 316-323
- Björk T, Westergard R, Hogmark S, Bergström J, Hedenqvist P (1999), *Wear*, **225**, p 1123-1130
- Bryant AJ, Dixon W, Fielding RAP (1999) "Prevention of Metallurgical Defects in Medium and High Strength Aluminum Extrusions," *Light Metal Age*, **57** (5), p 13
- Bryson B (1997) **Heat Treatment, Selection, and Application of Tool Steels**, Hanser Gardner Publications, Cincinnati
- Callister WD (2000) **Materials Science and Engineering: An Introduction**, 5th edition, John Wiley, New York
- Caloska J, Lazarev J, Nospal A, Stojkovski V (2002) "Exit Velocity Profile at the Extrusion Process of Aluminum of Square Pipe," *Southeastern Europe FLUENT Users Group Meeting*, 31 Oct-01 Nov 2002, Thessaloniki, Greece
- Chanda T, Zhou J, Duszczyk J (2000) "3D FEM Simulation of Thermal and Mechanical Events Occurring During Extrusion Through a Channel-Shaped Die," *Proc 7th Intl Aluminum Extrusion Technology Seminar: Vol 1*, 16-19 May 2000, Chicago, Illinois, p 125-134
- Chitkara NR, Butt MA (1999) "Axisymmetric Tube Extrusion Through a Smooth Conical or Cosine Die and over a Conical or Ogival Mandrel: Numerical Construction of Slip-Line Fields and Associated Velocity Fields," *Int J Mech Sciences*, **41** (10), p 1191-1215

- Chitkara NR, Butt MA (Apr 1997) "Combined Rod and Tube Extrusion: Numerical Solution of Axisymmetric Slip-Line Fields and Associated Velocity Fields," *Int J Mech Sciences*, **39** (4), p 435-454
- Chitkara NR, Butt MA (Mar 1997) "Axisymmetric Tube Extrusion through a Flat-Faced Circular Die: Numerical Construction of Slip-Line Fields and Associated Velocity Fields," *Int J Mech Sciences*, **39** (3), p 341-366
- Choi S, Lee Y-S, Oh H-K (February 1998) "Ductile Fracture in Axisymmetric Extrusion," *J Materials Processing Technologies*, **74** (1-3), p 263-267
- Chung JS, Hwang SM (Dec 1997) "Application of a Genetic Algorithm to the Optimal Design of the Die Shape in Extrusion," *J Materials Processing Technology*, **72** (1), p 69-77
- Cosenza C, Fratini L, Pasta A, Micari F (2004) "Damage and Fracture Study of Cold Extrusion Dies," *Engineering Fracture Mechanics*, **71**, p 1021-1033
- Cote J, Howlett EE, Wheeler MJ, Lamb HJ (1969) Plating, **356**, p 11
- Domblesky JP (August 2001) "Analysis od Fie Failures in Cold Heading using Finite Element Simulation," *Wire Journal International*, **34** (8), p 82-88
- Dougan JR (1982) "Relationship between Charpy V-Notch Impact Energy and Fracture Toughness," NUREG/CR-2362, ORNL/TM-7921, Oak Ridge National Laboratory, Oak Ridge, TN
- Dwight J (1999) **Aluminum Design and Construction**, E & FN Spon, London
- Elkholy A (1997) "Parametric Optimization of Power in Hydrostatic Extrusion," *Intl J Materials & Product Technology*, **12** (4-6), p 379-388
- Elkholy A (Oct 1997) "Parametric Optimization of Power in Hydrostatic Extrusion," *J Materials Processing Technology*, **70** (1-3), p 111-115
- Flitta I, Sheppard T (2000) "Material Flow and Prediction of Extrusion Pressure When Extruding Through Bridge Dies Using FEM," *Proc 7th Intl Aluminum Extrusion Technology Seminar: Vol 1*, 16-19 May 2000, Chicago, Illinois, p 125-134

- Gadal M S, Wang J (April 1999) "Simulation of Metal Forming Processes with Finite Element Methods," *Int J Numerical Methods in Engineering*, **44** (10), p1397-1420
- Gasiorczyk J, Richert J (2000) "Application of FEM Modeling to Simulate Metal Flow Through Porthole Dies," *Proc 7th Intl Aluminum Extrusion Technology Seminar: Vol 1*, 16-19 May 2000, Chicago, Illinois, p 195-202
- Geiger M, Haensel M (Sep 1993) "Energy-Based Approach to the Simulation of Fatigue Crack Initiation in Metal Formiing Tools," *Wire*, **43** (4), p 271-277
- Gotovskaya J, Solberg JK, Lange HI, Andersen LH (2004) "Wear of Inconel 718 Die During Aluminum Extrusion — A Case Study," *Wear*, **256**, p 126-132
- Gouveia B P P A, et al. (1999) "Finite Element Modeling of Cold Forward Extrusion," *J Materials Processing Technology*, **94**, p 85-93
- Groover KP (1999) **Fundamentals of Modern Manufacturing: Materials, Processing, and Systems**, John Wiley, New York
- Guobin L, Xiangzhi L, Jianjun W (1998) "Study of the Thermal Fatigue Crack Initial Life of H13 and H21 Steels," *J Materials Processing Technology*, **74** (1-3), p 23-26
- Hambli R, Badie-Levet D (200) "Damage and Fracture Simulation during the Extrusion Process," *Comp Methods Appl Mech Engg*, **186**, p 109-120
- Hsiang S-H, Liao C-S (Jan 1997) "Study on Hot Extrusion of Tubes," *J Materials Processing Technology*, **63** (1-3), p 254-259
- International Mold Steel, Inc (2003) "Premium H13," http://www.moldsteel.com
- Iwama T, Morimoto Y (Nov 1997) "Die Life and Lubrication in Warm Forging," *Journal of Materials Processing Technology*, **71** (1), p 43-48
- Jeong DJ, et al. (June 2001) "Effects of Surfac eTreatments and Lubricants fior Warm Forging Die Life," *Journal of Materials Processing Technology*, **113** (1-3), p 544-550
- Joun MS, Hwang SM (Jan 1998) "Die Shape Optimal Design in Three-Dimensional Shape Metal Extrusion by the Finite Element Method," *Intl J for Numerical Methods in Engg*, **41** (2), p 311-335

- Kalpakjian S (2003) **Manufacturing Processes for Engineering Materials**, 4th edition, Addioson-Wesley, Menlo Park, California
- Kim DK, Cho JR, Bae WB, Kim YII, Bramley AN (Nov 1997) "Upper Bound Analysis of the Square-Die Extrusion of Non-Axisymmetric Sections," *J Materials Processing Technology*, **71** (3), p 477-486
- Ko D-C, Kim B-M (2000) "Prediction of Central Burst Defects in Extrusion and Wire Drawing," *J Materials Processing Technology*, **102** (1), p 19-24
- Kobayashi Y and Okinawa S (1977) *Proc 2nd Intl Extrusion Technology Seminar*, Atlanta, Aluminum Assoc, Washington DC, **1**, p 129
- Kortmann W A (2000) "Failure in Extrusion Tooling: Causes and Methods of Avoiding Failures," *Proc Aluminum 2000: 2nd Intl Congress of Aluminum*, p 219-231
- Kusiak J, Libura W, Pietrzyk M, Misiolek WZ (1996) "Application of the Finite Element Technique to the Simulation of the Aluminum Extrusion Process," *Proc 6th Intl Aluminum Extrusion Technology Seminar: Vol 1*, 14-17 May 1996, Chicago, Illinois, p 361-367
- Kussmaul K, Roos E (1984) "Statistical Evaluation of Post-Yield Fracture Mechanics Properties on the Basis of the Notched Bar Impact Test," *Safety and Reliability of Pressure Components with Special Emphasis on Fracture Exclusion: 10th MPA Seminar*, Staatliche Materialprufungsanstalt Universitat Stuttgart, Vol 1, paper 12
- Lange K (1985) **Handbook of Metal Forming**, Society of Manufacturing Engineers
- Lange K and Stecke, "Some Recent Results of Investigations in Rod, Hooker and Can Extrusion and Upsetting," *Sheet Metal Ind*ustry, **43** (467), p 205, 1966
- Langerweger J (1982), *Aluminium*, **58** (2), p107
- Laue K and Stenger H (1981) **Extrusion: Processes, Machinery, Tooling**, American Society for Metals, Metals Park

- Lee G-A, Im Y-T (May 1999) "Finite Element Investigation of the Wear and Elastic Deformation of Dies in Metal Forming," *J Materials Processing Technologies*, **89-90**, p 123-127
- Lee G-A, Kwak D-Y, Kim S-Y, Im Y-T (May 2002) "Analysis and Design of Flat-Die Hot Extrusion Process 1. Three-Dimensional Finite Element Analysis," *Int J Mechanical Sciences*, **44** (5), p 915-934
- Lee R-S, Kwan C-T (Apr 1997) "Upper-Bound Analysis for Backward Extrusion of Generally Non-Axisymmetric Hollow Shapes," *J Chinese Society Mech Engrs*, Transactions of the Chinese Institute of Engineers, **18** (2), p 163-173
- Lewis EE (1996) **Reliability Engineering**, Addison-Wesley Longman
- Li H, Pugh D, Witkins MT and McKenzie J, "Design Considerations Arising from Cold Extrusion Research," *International Journal of Machine Tool Design & Research*, **2** (2), p 165, 1962
- Lin YT, Wang JP (Nov 1997) "New Upper-Bound Elemental Technique Approach," *Computers and Structures*, **65** (4), p 601-611
- Liu Z et al. (1999) "Finite Element Simulation of the Stress Distribution of Equal Cross Section Lateral Extrusion," *Materials Science and Engineering* A: Structural Materials: Properties, Microstructure and Processing, **262** (1), p137-140
- Lo S-W (Sep 1996) "Efficient Method of Designing Controlled Strain Rate Dies for Extrusions," *J Chinese Institute Engrs*, Transactions of the Chinese Institute of Engrs, **19** (5), p 623-631
- Lof J, Huetnik J, Nilsen KE (2000) "FEM Simulations of the Material Flow in the Bearing Area of the Aluminum Extrusion Process," *Proc 7th Intl Aluminum Extrusion Technology Seminar: Vol 1*, 16-19 May 2000, Chicago, Illinois, p 211-222
- Lof J, Huetnik J, Nilsen KE (2000) "FEM Simulations of the Material Flow in the Bearing Area of the Aluminum Extrusion Process," *Proc 7th Intl Aluminum Extrusion Technology Seminar: Vol-1*, 16-19 May 2000, Chicago, Illinois, p 211-222

- Lotzenheiser C (June 2001) "Learning the Extrusion Process Part II: Trouble Shooting and Fine Tuning," *Light Metal Age*, **59** (5-6), p 28-32
- Lu J, Saluja N, Riviere AL, Zhou Y (Jul 1998) "Computer Modeling of the Continuous Forming Extrusion Process of AA6061 Alloy," *J Materials Processing Technology*, **79** (1-3), p 200-212
- Lu Y H, Lo S W (Feb 1999) "Optimally-Controlled Strain-Rate Dies for Plane-Strain Extrusion," *J materials processing Technology*, **86** (1-3), p 56-66)
- METAOR (2003) "Metal Injection Molding," http://www.metalor2000.com
- Mielnik EM (1991) **Metalworking Science and Engineering**, McGraw-Hill, New York
- Minoda T, Hayakawa H, Yoshida H (Oct 2000) "Effect of Iron Content on the Surface Quality of 6063 Aluminum Alloy Extrusion," *J Japan Institute of Light Metals*, **50** (10), p 491-494
- Misiolek WZ (1997) "Evolution and Characterization of Microstructure in the Aluminum Extrusion Process," *Proc 1997 TMS Annual Meeting*, Orlando, Florida, p 49-60
- Misiolek WZ (June 1996) "Material Physical Response in the Extrusion Process," *J Materials Processing Technology*, 60 (1-4), p 117-124
- Misiolek WZ, Kelly RM (1992) *Proc 5th Intl Aluminum Extrusion Technology Seminar: Vol-1*, Chicago, Illinois, p 315-318
- Misiolek WZ, Kialka J (1996) *Proc 6th Intl Aluminum Extrusion Technology Seminar: Vol- 2*, Chicago, Illinois, p 107-111
- Monaghan J (May 1998) "Investigation of plane Strain Lateral Extrusion to Form Components having Staggered Branches," *Int J Materials Processing Technology*, **77** (1-3), p 305-313
- Müller KB (2002) "Deposition of Hard Films on Hot-Working Steel Dies for Aluminum," *J Materials Processing Technologies*, **130-131**, p 432-437

- Navinšek B, Panjan P, Urankar L, Cvahte P, Gorenjak F (2001) "Improvement of Hot-Working Processes with PVD Coatings and Duplex Treatment," *Surface and Coatings Technology*, **142-144** (July), p 1148-1154
- Osgood CC (1982) **Fatigue Design**, 2nd edition, Pergamon Press, Oxford
- Pearson EC, Parkins RN (1961) **The Extrusion of Metals**, 2nd edition, London
- Pederson TO (Sept 2000) "Numerical Studies of Low Cycle Fatigue in Forward Extrusion Dies," *Journal of Materials Processing Technology*, **105** (3), p 359-370
- Pöhlandt K (1989) **Materials Testing for the Metal Forming Industry**, Springer-Verlag, Berlin
- Qamar SZ, Arif AFM, Sheikh AK (Jul 2003) "An Investigation of Shape Complexity in Metal Extrusion," *Proceedings of the International Conference on Advances in Materials and Processing Technologies*, 8-11 July 2003, Dublin, Ireland, p 1178-1183
- Qamar SZ, Arif AFM, Sheikh AK (Sep 2003) "Extrusion Product Defects: A Statistical Study," *8th International Symposium on Advanced Materials (ISAM-2003)*, 8-11 September 2003, Islamabad, Pakistan
- Qamar SZ, Arif AFM, Sheikh AK, Younas M (June 2004) "Fatigue Life Assessment of Extrusion Dies using Monte Carlo Simulation," *3rd International Conference and Exhibition on Design and Production of Dies and Molds*, June 2004, Bursa, Turkey
- Qamar SZ, Sheikh AK, Arif AFM (May 2004) "Die Life Prediction using a Form Feature Based Definition of Extrusion Shape Complexity," *3rd International Conference on Advanced Manufacturing Technology (ICAMT 2004)*, May 2004, Malaysia, p 777-783
- Reddy NV, Dixit PM, Lal GK (Dec 1995) "Die Design for Axisymmetric Extrusion," *J Materials Processing Technology*, **55** (3-4), p 331-339
- Reddy NV, Dixit PM, Lal GK (Nov 1997) "Die Design for Axisymmetric Hot Extrusion," *Int J Machine Tools & Manufacture*, **37** (11), p 1635-1650

- Roberts G, Krauss G, Kennedy R (1998) **Tool Steels**, 5th edition, ASM International, Materials Park, Ohio
- Rolfe ST, and Novak ST (1970) "Slow Bend K_{IC} Testing of Medium Strength High Toughness Steels," *ASTM STP 463*, American Society for Testing and Materials, Philadelphia, p 124-159
- Saha P K (1998) "Thermodynamics and Tribology in Aluminum Extrusion," *Wear*, **218**, p 179-190
- Saha P K (2000) **Aluminum Extrusion Technology**, ASM International, Materials Park, Ohio
- Saha PK (1996) "Influence of Plastic Strain and Strain Rate on Temperature Rise in Aluminum Extrusion," *Proc 6th Intl Aluminum Extrusion Technology Seminar*, Aluminum Association and Aluminum Extruders Council
- Saha PK (1997) "Factors Affecting Speed and Pressure in 6063 Aluminum Extrusion," *Aluminum 2000 3rd World Congress*, vol **3**
- Sahoo SK, Kar PK, Singh KC (1999) "A Numerical Application of the Upper-Bound Technique for Round-to-Hexagon Extrusion Through Linearly Converging Dies," *J Materials Processing Technology*, **91**, p 105-110
- Sahoo SK, Kar PK, Singh KC (1999), "Direct Upper Bound Solution to Rectangular-to-Polygonal Extrusion Through Square Die," *J Manufacturing Science & Engg*, Transactions of the ASME, **121** (2), p 195-201
- Sahoo SK, Kar PK, Singh KC (Mar 1998) "Upper Bound Analysis of the Extrusion of a Bar of Channel Section from Square/Rectangular Billets," *J Materials Processing Technology*, **75** (1-3), p 75-80
- Sanford RJ (2003) **Principles of Fracture Mechanics**, Pearson Education, Upper Saddle River, New Jersey
- Schey J A (2000) **Introduction to Manufacturing Processes**, 3/e, McGraw-Hill, New York

- Schruff I, Schindler A, Kortmann W (May-June 1998) "Adequate Testing and Heat Treatment of Hot-Working Tool Steels: The Basis of a Good Perfoprmance," *HTM: Haerterie-Technische Mitteilungen*, **53** (3), p 139-146
- Sheikh AK, Arif AFM, Qamar SZ (Dec 2002) "Determination of Fracture Toughness of Tool Steels," *Proceedings of the 6th Saudi Engineering Conference*, 14-17 December 2002, Dhahran, Saudi Arabia, p 169-182
- Sheikh AK, Arif AFM, Qamar SZ (Jul 2003) "Die Life Probability and Reliability in Hot Aluminum Extrusion," *Proceedings of the International Conference on Advances in Materials and Processing Technologies*, 8-11 July 2003, Dublin, Ireland, p 1184-1191
- Sheikh AK, Arif AFM, Qamar SZ (Sep 2003) "Predicting Fracture Toughness Values of Hot Work Tool Steels at Elevated Temperatures," *8th International Symposium on Advanced Materials* (*ISAM-2003*), 8-11 September 2003, Islamabad, Pakistan
- Sheikh AK, Qamar SZ, Arif AFM (June 2004) "Extrusion Die Complexity — A Feature Based Characterization," *3rd International Conference and Exhibition on Design and Production of Dies and Molds*, June 2004, Bursa, Turkey
- Sheljaskow S (2001) "Tool Lubricating Systems in Warm Forging," *Journal of Materials Processing Technology*, **113** (1-3), p 16-21
- Sheppard T (1999) **Extrusion of Aluminum Alloys**, Kluwer Academic Publishers, Dordrecht
- Sheppard T, Nisaratanaporn E, McShane HB (May 1998) "Material Flow and Pressure Prediction when Extruding Through Bridge Dies," *Materials Research and Advanced Techniques*, **89** (5), p 327-337
- Shigley JE, Mischke CR, Budynas RG (2004) **Mechanical Engineering Design**, 7th edition, McGraw-Hill, Boston
- Sibilla S, Baron A (2000) "Numerical Modeling of Three-Dimensional Aluminum Flow in Extrusion Dies," *Proc 7th Intl Aluminum Extrusion Technology Seminar: Vol 1*, 16-19 May 2000, Chicago, Illinois, p 203-210

- Sonsoz A, Tekkaya AE (May 1996) "Service Life Estimation of Extrusion Dies by Numerical Simulation of Fatigue Crack Growth," *International Journal of Mechanical Sciences*, **38** (5), p 527-538
- Stambler I (April 1997) "Extrusion Research Enabling Production of All-Aluminum Cars," *Research and Development*, **39** (5), p 39-42
- Sudhakar KV (2002) "Micromechanics of Fracture in Extrusion Die Punch," *Engineering Failure Analysis*, **9**, p 159-165
- TALAT (2004), "Aluminum Extrusion: Alloys, Shapes and Properties," TALAT Lecture 1302, *Training in Aluminum Application Technologies* (*TALAT*), http://www.aluminium.org/education/TALAT/
- Tekkaya AE, Sonsoz A, Lange K (1995) "Life Estimation of Extrusion Dies," *CIRP Annals: Manufacturing Twechnology*, **44** (1), p 231-234
- Thackray R, Dashwood R, McShane H (2000) "Simulation of the Effect of Tooling and Billet Condition on Bulk and Surface Metal Flow during Extrusion," *Proc 7th Intl Aluminum Extrusion Technology Seminar: Vol 1*, 16-19 May 2000, Chicago, Illinois, p 213-223
- Thedja W W, Muller B K, Ruppin D (1992) "Tribological Processes on the Die Land Area during Extrusion of AA6063," *Proc 5th Intl Aluminum Extrusion Technology Seminar*, Aluminum Association & Aluminum Extruders Council
- Thelning K-E (1984) **Steel and its Heat Treatment**, 2nd edition, Butterworths, London
- Thomsen EG, Young CT, Bierbower JB (1954), *Engineering*, **5** (4), p 89/144
- Timken Latrobe Steel (2003) "Data Sheet: H13 Tool Steel," http://www.timken.com
- Trong TY, Wirsching HP and Martin WS (1991) "Advanced Fatigue Reliability Analysis," *International Journal of Fatigue*, **13** (5), p 389
- Ulysse P, Johnson RE (Jan 1998) "Study of the Effect of the Process Variables in Unsymmetrical Single-Hole and Multi-Hole Extrusion Processes," *J Materials Processing Technology*, **73** (1-3), p 213-225

- Unterweiser PM, Boyer HE, Kubbs JJ (ed) (1982) **Heat Treater's Guide: Standard Practices and Procedures for Steels**, American Society for Metals, Metals Park, Ohio
- Van der Sluys WA, Seely RR, Schwabe JE (1983) "Determining Fracture Properties of Reactor Vessel forging Materials, Weldments and Bolting Materials," *EPRI NP-922*, Electric Power Research Institute, Palo Alto, California, p 5-22
- Van Geertruyden WH, Claves SR, Misiolek WZ (Mar 2002) "Electron Backscatter Diffraction Analysis of Microstructural Evolution in Hot-Deformed 6xxx Series Aluminum Alloys," *Metallurgical and Materials Transactions Part A: Physical Metallurgy and Materials Science*, 33A (3), p 693-700
- Van Rens BJE (1999) "Finite Element Simulation of the Aluminum Extrusion Process: Shape prediction for Complex Profiles," *PhD Dissertation*, Technische Universiteit Eindhoven, the Netherlands
- Venugopal S, Medina EA, Malas III JC, Medeiros S, Frazier WG, Mullins WM, Srinivasan R (Dec 1996) "Optimization of Microstructure Development;: Application to Hot Metal Extrusion," *J Materials Engineering & Performance*, **5** (6), p 743-752
- Wallin K (2000) "Low-Cost J-R Curve Estimation based on CVN Upper Shelf Energy," *Fatigue and Fracture of Engineering Materials and Structures*, 24, p 537-549
- Wang JP (Jul 1998) "New Approach to Viscoplasticity in Plane-Strain Extrusion," *J Materials Processing Technology*, **79** (1-3), p 144-154
- Wifi AS, Shatla MN, Abdel-Hamid A (Jan 1998) "Optimum-Curved Die Profile for the Hot Forward Rod Extrusion Process," *J Materials Processing Technology*, **73** (1-3), p 97-107
- Wilson R (1975) Metallurgy and Heat Treatment of Tool Steels, McGraw-Hill, London

- Witt FJ (1983) "Relationships Between Charpy Impact Shelf Energies and Upper Shelf KIC Values for Reactor pressure Vessel Steels," *International Journal of Pressure Vessels and Piping*, 11, p 47-63
- Xie JX, Ikeda K, Murakami T (Feb 1995) "UBA Analysis of Pipe Extrusion Through a Porthole Die," *J Materials Processing Technology*, 49 (3-4), p 371-385
- Yang Y-S, Yeh W-C (Apr 1997) "Experimental Verification of the VUB Method using Plane Strain Extrusion Tests for 6061 Aluminum Alloy," *J Materials processing & Manufg Science*, **5b (4),** p 267-282
- Yang Y-S, Yeh W-C (Feb 1997) "Variational Upper-Bound Method for Analysis of Plane Strain Extrusion Tests," *J Chinese Society of Mechanical Engineers*, Transactions of the Chinese Institute of Engineers, **18** (1), p 1-14
- Zhang JM, Wang XW, Ruan XY (1992) "Simulating the Formation and Development of Defects in Metal Extrusion Process," *Intl SAMPE Metals and Metals Processing Conf, Vol 3*, SAMPE, Covina, California, p 13-19
- Zhong H, et al. (2000) "Computer Simulationm of a Thin-Walled Cup using the Thermomechanically Coupled Elasto-Plastc FEM," *J Materials Processing Technology*, **102** (1), p 128-137
- Zhou J, Li L, Duszczyk (March 2003) "3D FEM Simulation of the whole Cycle of Aluminum Extrusion throughout the Transient State and the Steady State using the Updated Lagrangian Approach," *J Materials Processing Technology*, **134** (3), p 383-397
- Zuyan L, Zhongjin W (1999) "Finite Element Analysis of the Load of Equal Cross Section Lateral Extrusion," *J Materials Processing Technology*, **94**, p 193-196

VITAE

PERSONAL

Name: Sayyad Zahid Qamar
Birth: 10th December, 1962, Karachi, Pakistan

EDUCATION

M.S. (1993), Mechanical Engineering, Texas A&M University, College Station, Texas, USA
B.E. (1985), Mechanical Engineering, NED University of Engineering and Technology, Karachi, Pakistan

INDUSTRIAL EXPERIENCE

Manager, Research & Development (1994-96), Karachi Shipyard & Engineering Works Ltd, Karachi, Pakistan
Deputy Manager, Engineering Design (1993-94), Karachi Shipyard & Engineering Works Ltd, Karachi, Pakistan
Production Engineer (1987-88), Hidada Ltd, Jeddah, Saudi Arabia
Quality Control Engineer (1986-87), Hidada Ltd, Jeddah, Saudi Arabia

ACADEMIC/RESEARCH EXPERIENCE

Lecturer-B (1999 to date), Mechanical Engineering, King Fahd University of Petroleum and Minerals (KFUPM), Dhahran, Saudi Arabia
Research Associate (1996-99), Mechanical Engineering, Ghulam Ishaq Khan Institute of Engineering Sciences and Technology (GIKI), Topi, Pakistan
Research Assistant (1990-93), Mechanical Engineering, Texas A&M University, College Station, Texas, USA

CONTACT

Email: zahidqam2000@yahoo.com